LOW FREQUENCY INVESTIGATIONS OF DISCRETE RADIO SOURCES AND OF THE GALAXY

A study of sources with curved spectra
and low frequency observations of galactic radiation

by

Raymond F. Haynes, B.Sc.(Hons.)

A thesis submitted in fulfilment of the
requirements of the Degree of
Doctor of Philosophy
in the

UNIVERSITY OF TASMANIA

HOBART

June, 1970.

This thesis contains no material which has been accepted for the award of any other degree or diploma in any other University, and to the best of my knowledge and belief, contains no copy or paraphrase of material previously published or written by any other person, except when due reference is made in the text of the thesis.

R.F. Haynes.

ACKNOWLEDGEMENTS

I am extremely grateful to my supervisor, Professor G.R.A. Ellis for his advice and encouragement during this project. I worked with Dr. P.A. Hamilton, Dr. P.M. McCulloch and Mr. D.J. Cole on various phases of the work and their help and advice were very much appreciated.

Technical assistance was received from a large number of people at various times throughout the duration of this project. I would like to thank the staff of the Physics Department of the University of Tasmania for their help. Many of the observations reported in this thesis were obtained at the Australian National Radio Astronomy Observatory and I would like to thank Dr. E.G. Bowen and Mr. J.G. Bolton for permission to use the facilities of the C.S.I.R.O. Observatory.

During this project I was assisted financially by a C.S.I.R.O. postgraduate studentship, it is gratefully acknowledged.

I would also like to extend my sincere thanks to my wife and parents for their encouragement and moral support during this project.

SUMMARY.

This thesis presents the results of five low frequency source surveys and two"background"surveys of the southern sky. The source results permit an analysis of the curved spectra of some 70 sources.

The thesis begins with a review of the mechanisms that have been proposed to account for the continuum emission from cosmic radio sources. This work is included to summarize and illustrate the relations used extensively in the analysis of source spectra later in the thesis.

New measurements of some 350 discrete radio sources between 40 and 160 MHz are presented. The results were obtained from two "continuum surveys" of the southern sky at 10.02 MHz and 153 MHz and from five discrete source surveys using the 210ft. and 60ft. telescopes of the Parkes Observatory. The observing time was limited so that, with the exception of the 153 MHz survey measurements at this observatory were confined to those sources which possibly had curved spectra. The techniques used to overcome the problems of interference, ionospheric effects and confusion between nearby sources are discussed. The low frequency observations reported in this section provide data that was needed to define the spectra of many of the sources reliably.

The effects of *electron energy cut-offs*, the *synchrotron self-absorption* process, the *Tsytovich-Razin effect* and *thermal absorption* are considered to explain the emission from the sources with low frequency *convex* spectra. The parameters of each of these models and the theoretical spectra fitted to the available flux density data of each source are given. Estimates of the magnetic field strength and free electron density are determined from the parameters of the *self-absorption* and *thermal absorption* models (respectively) for those sources for which ~~angular~~ angular size data is available. Calculation shows that the relativistic particle energy density exceeds the stored magnetic field energy density in 70 % of the sources for which these quantities can be determined.

Concave and *complex* curved spectra are explained in terms of power-law and self-absorbed components of radiation from the different parts of these(probably)multi-element sources.

Finally, the results of two high resolution surveys of the southern sky at 10.02 MHz (4°x5° beamwidth) and 153 MHz (2.18° beamwidth) are presented. Maps of the sky brightness temperature are given in *new* galactic co-ordinates. The effects of absorption in ionized hydrogen are clearly seen in the 10.02 MHz map. The results of the 153 MHz survey agree well with other surveys at 85 MHz and 178 MHz that have been published.

NOTATION.

In this thesis reference if often made to a system of *new galactic co-ordinates*. The notation l^{II}, b^{II} is used to specify the galactic longitude and latitude respectively in this system. The co-ordinates are defined (at Epoch 1950) such that the galactic pole is at:

12 Hours 42 Minutes 24 Seconds Right Ascension

$+27^{o}$ 36' Declination

and the origin of the system is at:

17 Hours 42 Minutes 24 Seconds Right Ascension

-28^{o} 55' Declination

In the above notation the symbol "o" refers to an angle in degrees while the symbol " ' " refers to an angle in minutes of arc.

In the discussion of source spectra it is convenient to specify the *flux density* of a source in flux units (f.u.), where:

$$1 \text{ flux unit} = 1 \times 10^{-26} \text{ Watt metre}^{-2} \text{ Hertz}^{-1}$$

Other quantities will normally be specified throughout the thesis in the units usually used in the literature.

Reference will often be made to articles in the literature which deal with measurements of sources which are south of declination $+27^{o}$. Owing to the large number of such references it is convenient to summarize all the articles in tabular form (see appendix 2). Specific articles are then referred to in the text of the thesis by a table index number.

For example: (see page 206)

S19: refers to the 19th. article of table 1 of appendix 2; namely:

"The Parkes Catalogue of Radio Sources"

(ed.) Ekers, J.A. (1969) Aust. J. Phys. Astrophys. Suppl. No. 7, 1

Articles dealing with identification data are also summarized in table 2 (appendix 2). These will also be referred to by a table number. For example (see page 208)

I04: refers to the 4th. article of table 2 of appendix 2; namely:

"Identifications for Parkes Sources -20° to -30° Declination"

Bolton , J.G. and Ekers, J. (1966) Aust. J. Phys., 19(2), 275

The spectral data used in the analysis (section 3) was obtained from the results given in section 2 of this thesis and from the articles listed in table 1 of appendix 2.

CONTENTS.

SECTION 5:

APPENDICES:

SECTION 1.

ELECTROMAGNETIC RADIATION FROM DISCRETE RADIO SOURCES.

CHAPTER 1.

EMISSION, ABSORPTION AND PROPAGATION OF THE RADIATION FROM DISCRETE SOURCES.

Introduction.

The first part of chapter 1 discusses mechanisms that have been proposed to account for the continuum emission from cosmic radio sources. In part 2 we consider the effects on the emission from a source of the two propagation processes, absorption in ionized hydrogen and Faraday rotation. Although there is no original work in this chapter, it is included to summarize and illustrate the relations used extensively in the analysis of source spectra in section 3.

PART 1: Emission Mechanisms.

A. Thermal (Black-body) Radiation.

The brightness, B, of a perfect radiator [black-body] at a temperature, Te, and a frequency, ν, is given by Planck's law:

$$B(\nu) = \frac{2h\nu^3}{c^2} \times \frac{1}{e^{h\nu/kTe} - 1} \quad \text{Watt m}^{-2}\,\text{Hz}^{-1}\,\text{rad.}^{-2} \quad \ldots.(1.1)$$

where:

h = Planck's constant ($=6.63\times10^{-34}$ joule sec)

c = velocity of light ($\simeq 3 \times 10^{8}$ m sec^{-1})

k = Boltzmann constant (1.38×10^{-23} joule degK^{-1})

Te is in units of degK and ν is in Hertz. At radio wavelengths, equation (1.1) can be approximated by the Rayleigh-Jeans form: ($h\nu << kTe$)

$$B(\nu) = \frac{2\ k\ Te}{\lambda^2} = \frac{2\ \nu^2\ k\ Te}{c^2} \qquad ....(1.2)$$

where:

λ is the wavelength of the emission (metre). Substitution of the numerical values of the constants into equation (1.2) gives:

$$B(\nu) = 3.072 \times 10^{-28}\ Te\ \nu^2\ Watt\ m^{-2} Hz^{-1} rad.^{-2}$$

where the frequency, ν is in megahertz. If the source subtends an angle, Ω (radians^2), the source flux density, $S(\nu)$ at a frequency, ν, is given by:

$$S(\nu) = \frac{2\ \nu^2\ k\ Te\ \Omega}{c^2} \qquad ....(1.3)$$

In an ionized hydrogen medium "free-free" electron transitions produce electromagnetic radiation. Kraus(1966) shows that at metre and decametre wavelengths the flux density of the emissions from ionized hydrogen at a temperature of 10^4 degK varies inversely as the square of the wavelength. The emission from such a medium at these wavelengths is consistent with equation (1.2).

B. Synchrotron Radiation from Electrons moving in a Uniform Magnetic Field in Vacuo.

Relativistic electrons moving in a vacuum emit synchrotron radiation as they are accelerated in a magnetic field. For complete discussions of the synchrotron theory see Westfold(1959), LeRoux(1961), Jackson(1962), Kraus (1966) and Ginzburg and Syrovatskii(1964 and 1965).

(i). Synchrotron Radiation from a Single Electron.

In the general analysis of the synchrotron process [eg. Westfold,1959] we introduce the quantity, ν_c, known as the *characteristic* or *critical* frequency of the radiation:

$$\nu_c = \frac{3\ e\ B_\perp \varepsilon^2}{4\pi\ m^3\ c^5} \qquad \ldots.(1.4)$$

[Ginzburg and Syrovatskii,1965]

where: the constants e, m, c are the electronic charge and mass and the velocity of light respectively,

$B_\perp$ is the component of the magnetic field perpendicular to the direction of motion of the electron,

and: ε is the energy of the electron.

Substituting values for the constants we get:

$$\nu_c = 16.1\ B_\perp \varepsilon^2 \text{ MHz} \qquad \ldots.(1.5)$$

where $B_\perp$ is in micro-gauss and ε is in GeV [1 GeV = 10^9eV]. Using this relation it can be shown that the spectral power

(or power per unit bandwidth) radiated by an electron at an angle θ to the field direction is:

$$P(\nu,\varepsilon,\theta) = \frac{\sqrt{3}\, e^3\, B_\perp}{m\, c^2} \times \frac{\nu}{\nu_c} \int_{\nu/\nu_c}^{\infty} K_{5/3}(x)\, dx \qquad \ldots.(1.6)$$

where we introduce the function:

$$F(\nu/\nu_c) = \frac{\nu}{\nu_c} \int_{\nu/\nu_c}^{\infty} K_{5/3}(x)\, dx$$

and $K_{5/3}(x)$ is a modified Bessel Function of the second kind of order $5/3$. Other terms in the expression are defined by:

$B = B \sin(\theta)$,

θ = angle of emission of the radiation with respect to the magnetic field direction

[$\theta \simeq$ the electron pitch angle:

Ginzburg and Syrovatskii, 1964]

and ν = frequency of emission.

Substituting values for the constants into equation(1.6) we obtain:

$$P(\nu,\varepsilon,\theta) = 2.343 \times 10^{-35}\, B_\perp\, F(\nu/\nu_c)\ \text{Watt Hz}^{-1} \qquad \ldots.(1.7)$$

where $B_\perp$ is in micro-gauss, and ν and ν_c are in the same units. The numerical evaluation of the function $F(\nu/\nu_c)$ is discussed in appendix 1.

The radiation from a relativistic electron moving in a uniform magnetic field is polarized, with the electric vector normal to the magnetic field lines at the point of emission. For an observer not in the orbital plane of the electron, the radiation observed is elliptically polarized. In this case the electric vector has a maximum value in the direction of electron acceleration. Westfold(1959) gives for the degree of polarization of the synchrotron power emitted by a single electron:

$$\pi = \frac{Fn(\nu/\nu_c)}{F(\nu/\nu_c)}$$

where:

$$Fn(\nu/\nu_c) = \frac{(\nu)}{\nu_c} \times K_{2/3}(\nu/\nu_c)$$

and:

$K_{2/3}(\nu/\nu_c)$ is a modified Bessel Function of the second kind of order $2/3$. Figure 1.1 shows the function $F(\nu/\nu_c)$ for different values of ν/ν_c while figure 1.2 shows the degree of linear polarization of the radiation from mono-energetic electrons moving in a uniform magnetic field. Values of the two functions $F(\nu/\nu_c)$ and $F_n(\nu/\nu_c)$ are given in table 1.1.

Note that the frequency of maximum emission, ν_{max}, from an electron is given by:

$$\nu_{max.} \simeq 0.29\ \nu_c \qquad \ldots.(1.8)$$

[Ginzburg and Syrovatskii,1965]

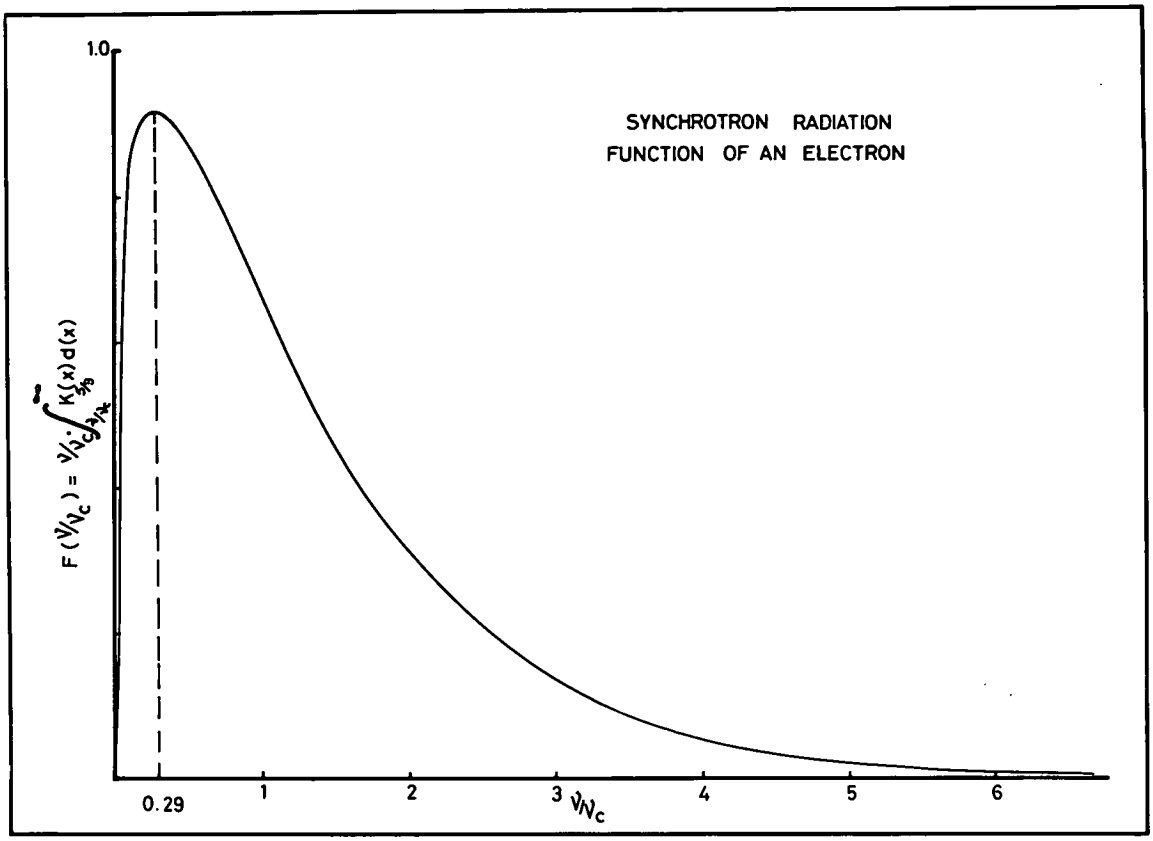

FIGURE 1.1.

The Behaviour of the Function

$$F(\nu/\nu_c) = \nu/\nu_c \int K_{5/3}(x)dx.$$

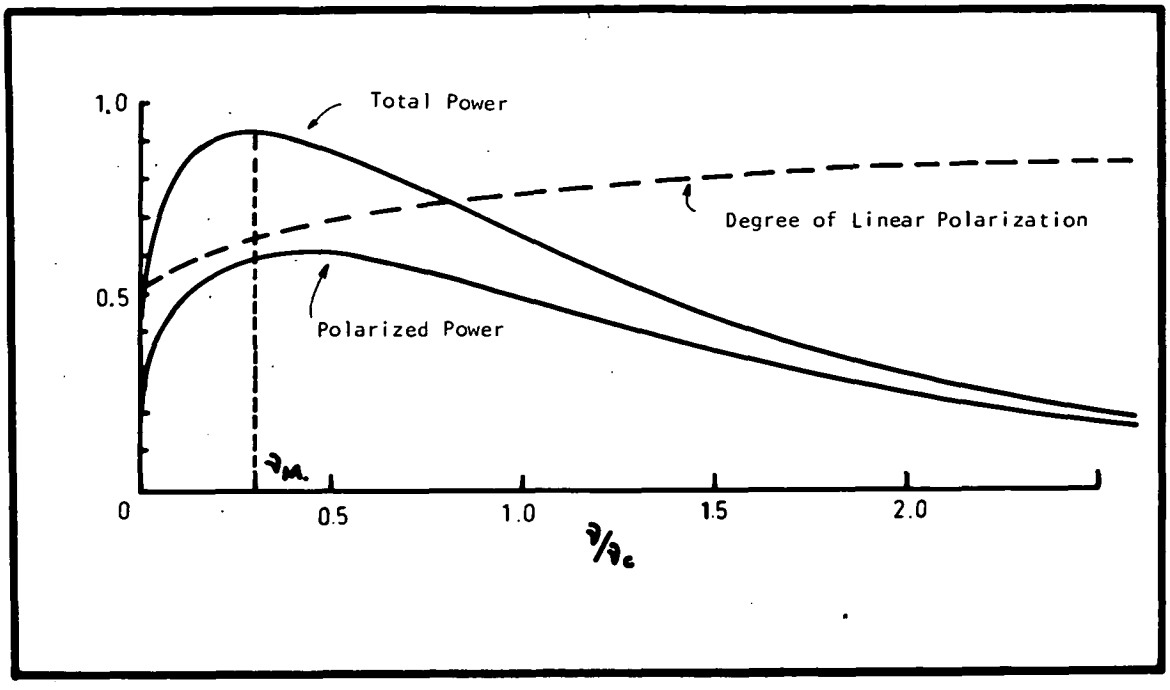

SYNCHROTRON RADIATION FROM MONOENERGETIC ELECTRONS WITH A UNIFORM DISTRIBUTION OF PITCH ANGLES

FIGURE 1.2

Degree of Linear Polarization of the Radiation from mono-energetic electrons Moving in a Uniform Magnetic Field.

TABLE 1.1

$$F(x) = x \int_{x}^{\infty} K_{5/3}(\eta)\, d\eta$$

$$F_n(x) = xK_{2/3}(x)$$

x	F	F_n	x	F	F_n
0....	0	0	1.0...	0.655	0.494
0.001..	0.213	0.107	1.2...	.566	.439
.005..	.358	.184	1.4...	.486	.386
.010..	.445	.231	1.6...	.414	.336
.025..	.583	.312	1.8...	.354	.290
.050..	.702	.388	2.0...	.301	.250
.075..	.772	.438	2.5...	.200	.168
.10...	.818	.475	3.0...	.130	.111
.15...	.874	.527	3.5...	.0845	.0726
.20...	.904	.560	4.0...	.0541	.0470
.25...	.917	.582	4.5...	.0339	.0298
.30...	.919	.596	5.0...	.0214	.0192
.40...	.901	.607	6.0...	.0085	.0077
.50...	.872	.603	7.0...	.0033	.0031
.60...	.832	.590	8.0...	.0013	.0012
.70...	.788	.570	9.0...	.00050	.00047
.80...	.742	.547	10.0...	0.00019	0.00018
0.90...	0.694	0.521			

[after Westfold, 1959]

and that most of the emission from an electron occurs at frequencies, ν, such that:

$$\frac{\nu}{\nu_c} \quad \text{is of the order of unity} \qquad \ldots.(1.9)$$

Thus, from equation (1.4) and equation (1.9), the radiation from an electron depends critically on the energy of the electron.

(ii). Synchrotron Radiation from Ensembles of Electrons.

The synchrotron radiation from an ensemble of electrons reflects the energy distribution of the radiating electrons. Suppose that in a uniform magnetic field of strength, B, the energy distribution of electrons at time, t, is $N(\varepsilon,\theta,t)\, d\varepsilon$. That is, the number of electrons with energy, ε, in the range ε to $(\varepsilon + d\varepsilon)$ is $N(\varepsilon,\theta,t)d\varepsilon$ at time,t. Suppose also that all the electrons in this distribution have a pitch angle θ. As mentioned previously, θ will be close to the angle between the direction of maximum radiation from the electron and the magnetic field direction. If the radiation from individual electrons is incoherent, the intensity of synchrotron emission from an ensemble of electrons at frequency, ν, angle θ, time,t, per unit frequency interval, per unit solid angle is: (from equation 1.6)

$$I_\nu(\theta,t) = \frac{L}{4\pi} \int_\varepsilon P(\nu,\varepsilon,\theta) \times N(\varepsilon,\theta,t)\, d\varepsilon \text{ Watt m}^{-2} \text{ Hz}^{-1} \text{rad}^{-2} \qquad \ldots.(1.10)$$

where: L is the line of sight thickness through the emitting region(metre)

and: $N(\varepsilon,\theta,t)d\varepsilon$ has the units of electrons metre^{-3} .

Many extragalactic radio sources emit polarized radiation [see, for example, Gardner et al.,1969 a]. This polarized emission can only be explained as synchrotron emission if there is large scale uniformity of the magnetic field within the source. If the field within the source is uniform then equation (1.10) can be rewritten:

$$I_\nu(\theta,t) = 2.343 \times 10^{-35} \frac{L\, B_\perp}{4\pi} \int_\varepsilon F(\nu/\nu_c)\, N(\varepsilon,\theta,t)\, d\varepsilon \quad \text{Watt m}^{-2}\ \text{Hz}^{-1}\ \text{rad.}^{-2} \qquad \ldots(1.11)$$

When the pitch angle of the electrons in the ensemble varies, the total emission observed, $I_\nu(t)$ will be the sum:

$$I_\nu(t) = \sum_\theta I_\nu(\theta,t) \quad .$$

(iii). Radiation from a power-law Distribution of Electrons.

The observed flux density, $S(\nu)$ of many discrete extragalactic radio sources is related to the frequency of observation, ν, by:

$$S(\nu) \propto \nu^\alpha \qquad \ldots.(1.12)$$

where α is a constant known as the spectral index. If the emission is produced by the synchrotron process, then the radiation from electrons with a differential energy spectrum of the form:

$$N(\varepsilon,\theta,t)\, d\varepsilon = K e\, \varepsilon^{-\gamma} d\varepsilon \quad \text{electrons metre}^{-3} \qquad \ldots(1.13)$$

will have an intensity (from equation 1.10) of:

$$I_\nu(\theta,t) = \frac{L}{4\pi} \int P(\nu,\varepsilon,\theta)\ Ke\ \varepsilon^{-\gamma} d\varepsilon \text{ Watt m}^{-2}\text{ Hz}^{-1} \qquad \ldots.(1.14)$$

where Ke and γ are constants and the other symbols have already been defined. Substitution of equation (1.5) into equation (1.14) gives:

$$I(\theta,t) = 2.343\text{x}10^{-35} \frac{L\ B_\perp}{4\pi} \int_\varepsilon Ke\ \varepsilon^{-\gamma} F\left[\frac{\nu}{16.1\ B_\perp \varepsilon^2}\right] d\varepsilon \qquad \ldots.(1.15)$$

Watt metre^{-2} Hz^{-1}rad^{-2}

where: $B_\perp$ is the component of the magnetic field in the direction perpendicular to the direction of motion of the electron [Micro-gauss];

L is the line-of-sight thickness of the source [metre];

ε is the energy of the electron in GeV;

ν is the frequency of emission in MHz;

and: Ke is a constant with units: (GeV)$^{-1}$ metre^{-3} .

The emissivity of the source per unit volume can be written as: (from equation 1.15)

$$E(\theta,t) = \frac{4\pi\ I_\nu(\theta,t)}{L} \text{ Watt metre}^{-3}\text{ Hz}^{-1} .$$

The differential electron energy spectrum within a source will, in general, be of the form:

$$N(\varepsilon,\theta,t)d\varepsilon = Ke\ \varepsilon^{-\gamma}d\varepsilon \quad \text{for } \varepsilon_1 \leq \varepsilon \leq \varepsilon_2$$
$$= 0 \quad \text{for } \varepsilon < \varepsilon_1 \text{ and } \varepsilon > \varepsilon_2 \qquad \ldots.(1.16)$$

where the two values of energy ε_1, ε_2 define the *cut-off* energies of the electron distribution. From the values of ε_1 and ε_2, the corresponding cut-offs in the synchrotron spectrum can be obtained from equation (1.5).

The integral in equation (1.15) can be determined explicitly provided the limits of integration in the equation can be extended to zero and infinity. If this is the case then, [see for example, Ginzburg and Syrovatskii, 1965]:

$$I_\nu(\theta,t) = \frac{\sqrt{3}\ M}{(\gamma+1)} \left[\frac{e^3}{mc^2} \left[\frac{3\ e}{2\pi\ m^3\ c^5} \right]^{\frac{1}{2}(\gamma-1)} Ke \right] B_\perp^{\frac{1}{2}(\gamma+1)} \nu^{\frac{1}{2}(1-\gamma)} \qquad \ldots.(1.17)$$

where: $M = \sqrt{\frac{(3\gamma-1)}{12}} \times \sqrt{\frac{(3\gamma+19)}{12}}$

$\sqrt{(x)}$ is the Euler γ-function

and all the other symbols have their usual meaning.

Thus, the radiation flux density, $S(\nu)$, is given by:

$$S(\nu) \propto B_\perp^{\frac{1}{2}(\gamma+1)}\ \nu^{\frac{1}{2}(1-\gamma)} \qquad \ldots..(1.18)$$

It follows that an observed spectrum of the form given by equation (1.12) can be adequately explained as synchrotron emission from an ensemble of electrons whose energy distribution is described by a power-law with index:

(facing page 13 et seq.)

Figures 1.3, 1.4, 1.5

Synchrotron spectra from power-law distributions of electrons. The lower and upper cut-off frequencies (Fc1, Fc2 respectively) are shown for each spectrum. [Magnetic field = 12 μgauss].

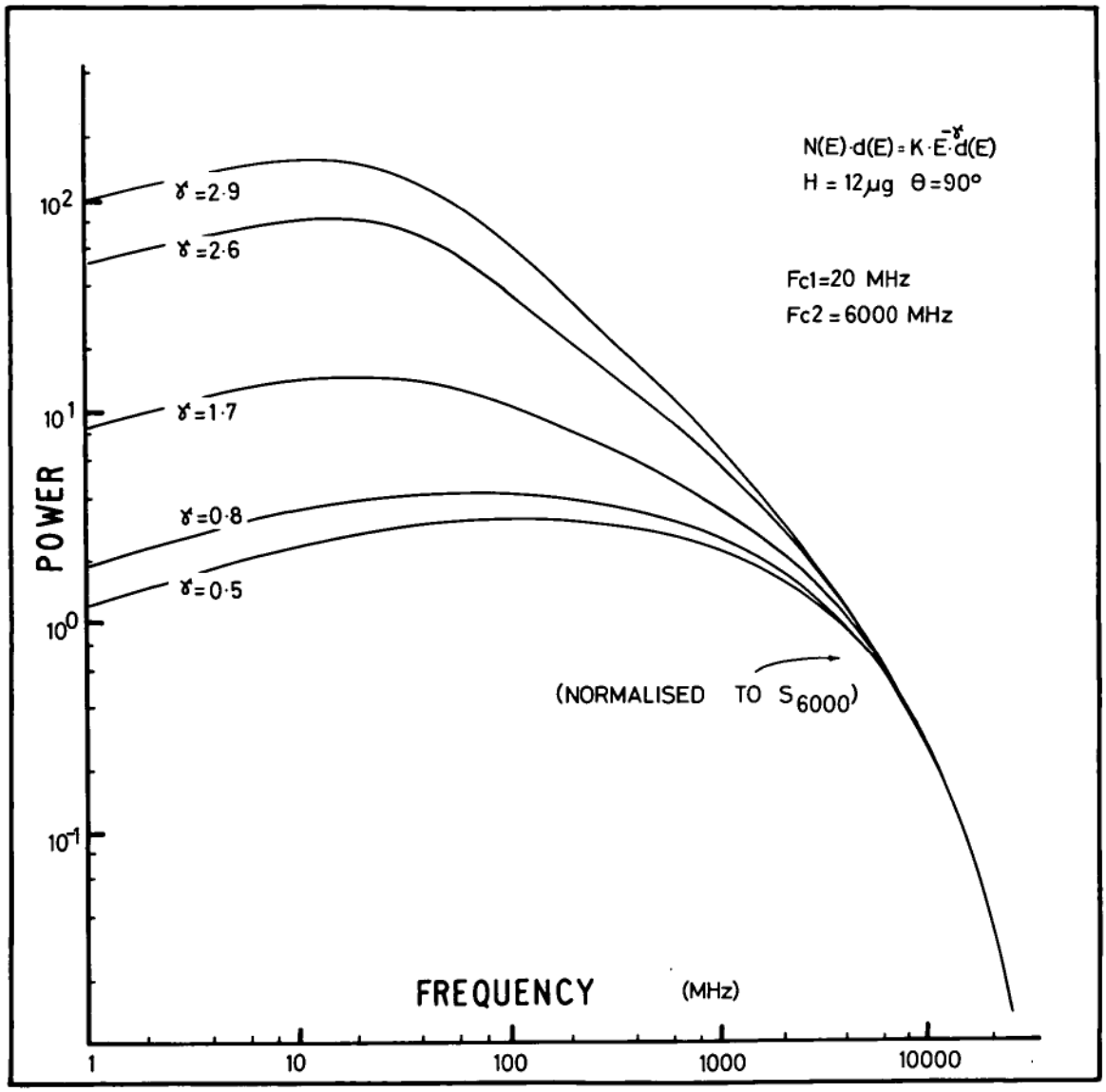
N(E)·d(E) = K·E^-γ d(E)
H = 12μg θ=90°
Fc1=20 MHz
Fc2 = 6000 MHz
γ=2·9
γ=2·6
γ=1·7
γ=0·8
γ=0·5
(NORMALISED TO S6000)
POWER
FREQUENCY (MHz)
10^2
10^1
10^0
10^-1
1
10
100
1000
10000

FIGURE 1.3.

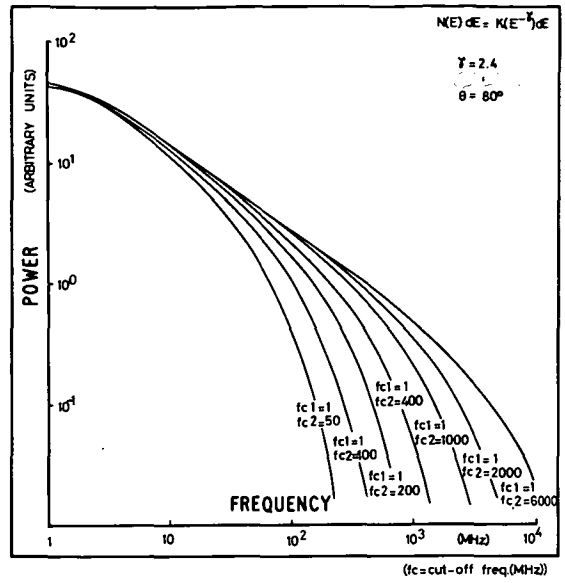
N(E) dE = K(E^-γ)dE
γ = 2.4
θ = 80°
POWER (ARBITRARY UNITS)
10^2
10^1
10^0
10^-1
fc1=1 fc2=50
fc1=1 fc2=400
fc1=1 fc2=200
fc1=1 fc2=400
fc1=1 fc2=1000
fc1=1 fc2=2000
fc1=1 fc2=6000
FREQUENCY
1
10
10^2
10^3
(MHz)
10^4
(fc=cut-off freq.(MHz))

FIGURE 1.4 .

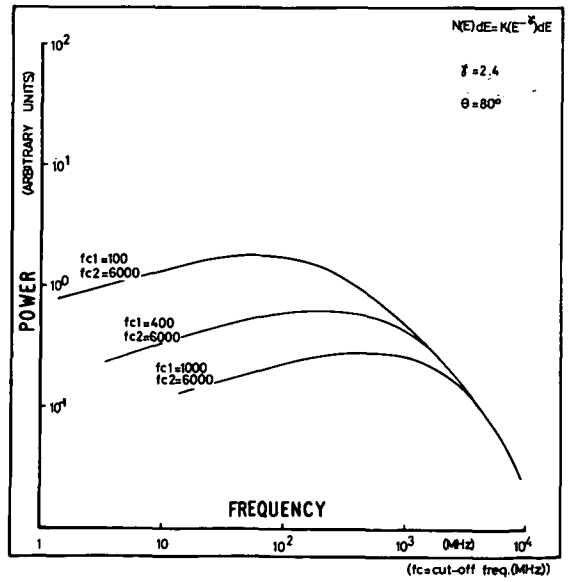
N(E) dE = K(E^-γ)dE
γ = 2.4
θ = 80°
POWER (ARBITRARY UNITS)
10^2
10^1
10^0
10^-1
fc1=100 fc2=6000
fc1=400 fc2=6000
fc1=1000 fc2=6000
FREQUENCY
1
10
10^2
10^3
(MHz)
10^4
(fc=cut-off freq.(MHz))

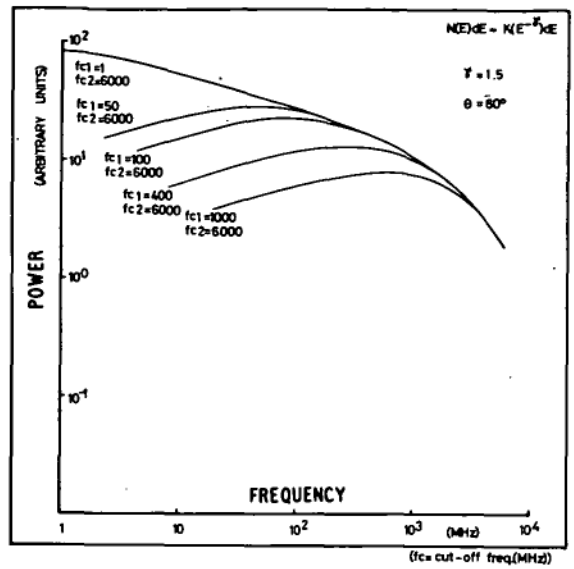
N(E)dE = K(E^-γ)dE
γ = 1.5
θ = 80°
POWER (ARBITRARY UNITS)
10^2
10^1
10^0
10^-1
fc1 =1
fc2=6000
fc1 =50
fc2 =6000
fc1 =100
fc2 =6000
fc1 =400
fc2 =6000
fc1 =1000
fc2=6000
FREQUENCY
1
10
10^2
10^3
(MHz)
10^4
(fc= cut-off freq.(MHz))

FIGURE 1.5 .

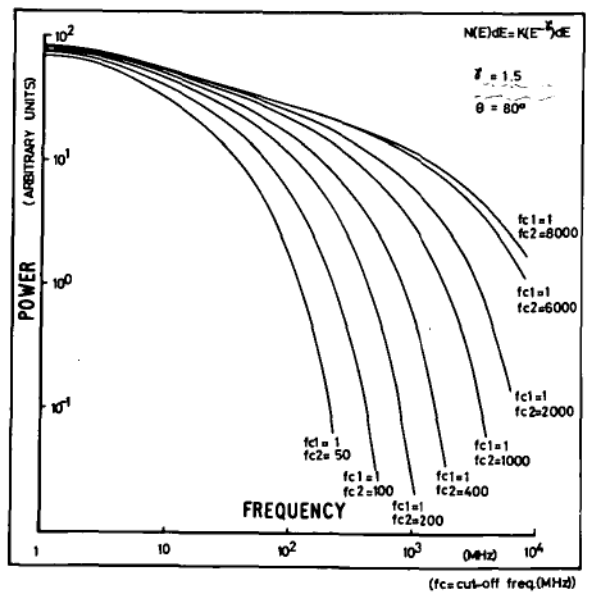
N(E)dE= K(E^-γ)dE
γ = 1.5
θ = 80°
POWER (ARBITRARY UNITS)
10^2
10^1
10^0
10^-1
fc1 = 1
fc2= 50
fc1 = 1
fc2 =100
fc1 =1
fc2=200
fc1 =1
fc2=400
fc1 =1
fc2=1000
fc1 =1
fc2=2000
fc1 =1
fc2=6000
fc1 =1
fc2=8000
FREQUENCY
1
10
10^2
10^3
(MHz)
10^4
(fc= cut-off freq.(MHz))

$$\gamma = 1 - 2\alpha \qquad \ldots.(1.19)$$

Synchrotron emission spectra produced by electron plasmas of the type defined by equation (1.16) are shown in figure 1.3 for values of γ in the range 0.5 to 2.9. The magnetic field in the emitting region is taken to be uniform and of strength 12 μgauss. The lower and upper cut-off frequencies, which by equation (1.5) define the cut-off energies of the electron distribution, are taken to be 20 and 6000 MHz respectively. Figures 1.4 and 1.5 show emission spectra for different values of the upper and lower cut-off frequencies. The computations were carried out using the method discussed in appendix 1.

(iv). Effects of the Medium on the Emission of Synchrotron Radiation.

The medium in the vicinity of a radiating electron exerts a strong influence on its emission. Two important processes, the Tsytovich-Razin effect and Synchrotron Self-absorption, will be considered.

The Tsytovich-Razin Effect.

Suppose that relativistic electrons are moving and radiating in a magneto-ionic medium in which the refractive index of the medium at the frequency of emission is less than unity. The relations discussed earlier in this chapter cannot

be used to determine the emission produced by the electrons. For low velocity electrons the effect of the medium is negligible, but not for those electrons moving with velocities of the order of the velocity of light [Tsytovich, 1951; Razin, 1960; Scheuer, 1965]. If the magnetic field strength within the medium is B, then the angular gyro frequency will be:

$$\omega_B = \frac{e\, B_\perp}{m c} \qquad \ldots\ldots(1.20)$$

where e,m, c and $B_\perp$ have already been defined above.

For the conditions appropriate to extragalactic radio sources:

$$B \sim 10^{-3} \text{ to } 10^{-5} \text{ gauss [Scheuer and Williams,1968]}$$

and hence:

$$\omega_B \sim 10^{4} \text{ Hz} \quad .$$

Then for a wave of angular frequency, ω, propagating in the medium we have:

$$\left[\frac{\omega_B}{\omega}\right]^2 \leq 10^{-6} \quad \text{for} \quad \omega \geq 10^{7} \text{ Hz} \ .$$

With these conditions, the refractive index, $n(\nu)$, of the medium, which is independent of the magnetic field [Ginzburg and Syrovatskii, 1964], is given by:

$$n(\nu) = \left[1 - \frac{Ne\, e^2}{m\pi\, \nu^2}\right]^{\frac{1}{2}} = \left[1 - \frac{8\times10^{7}\, Ne}{\nu^2}\right]^{\frac{1}{2}} \qquad \ldots.(1.21)$$

where: Ne is the free electron density within the medium, $[cm^{-3}]$;

e,m are the electronic charge and mass respectively;

and: ν is the frequency of the wave [Hz]

The synchrotron emission from a relativistic electron moving in a diffuse medium has been calculated by Razin (1960). If equation (1.21) holds then the emission per unit frequency interval is given by:

$$P(\nu,t,\theta) = \frac{\sqrt{3}\, e^3\, B_\perp}{m\, c^2} \left[1 + (1-n^2) \times \left[\frac{\varepsilon}{m\, c^2} \right]^2 \right]^{-\frac{1}{2}} F(\nu/\nu_c^*) \quad ....(1.22)$$

where:

n is the refractive index given by equation (1.21),

$$F(\nu/\nu_c^*) = \frac{\nu}{\nu_c^*} \int_{\nu/\nu_c^*}^{\infty} K_{5/3}(x)\, dx \quad ....(1.23),$$

c is the velocity of light,

ε is the energy of the electron

$$\nu_c^* = \nu_c \left[1 + (1-n^2) \left[\frac{\varepsilon}{m\, c^2} \right]^2 \right]^{-3/2} \quad ....(1.24)$$

and: e, m, θ, ν_c, ν, $B_\perp$ have their usual meanings.

The effect of the medium on the emission of synchrotron radiation can only be neglected provided: (from equations 1.21, 1.22):

$$\left[\frac{8 \times 10^7\, Ne}{\nu^2} \right] \times \left[\frac{\varepsilon}{m\, c^2} \right]^2 << 1 \quad ....(1.25)$$

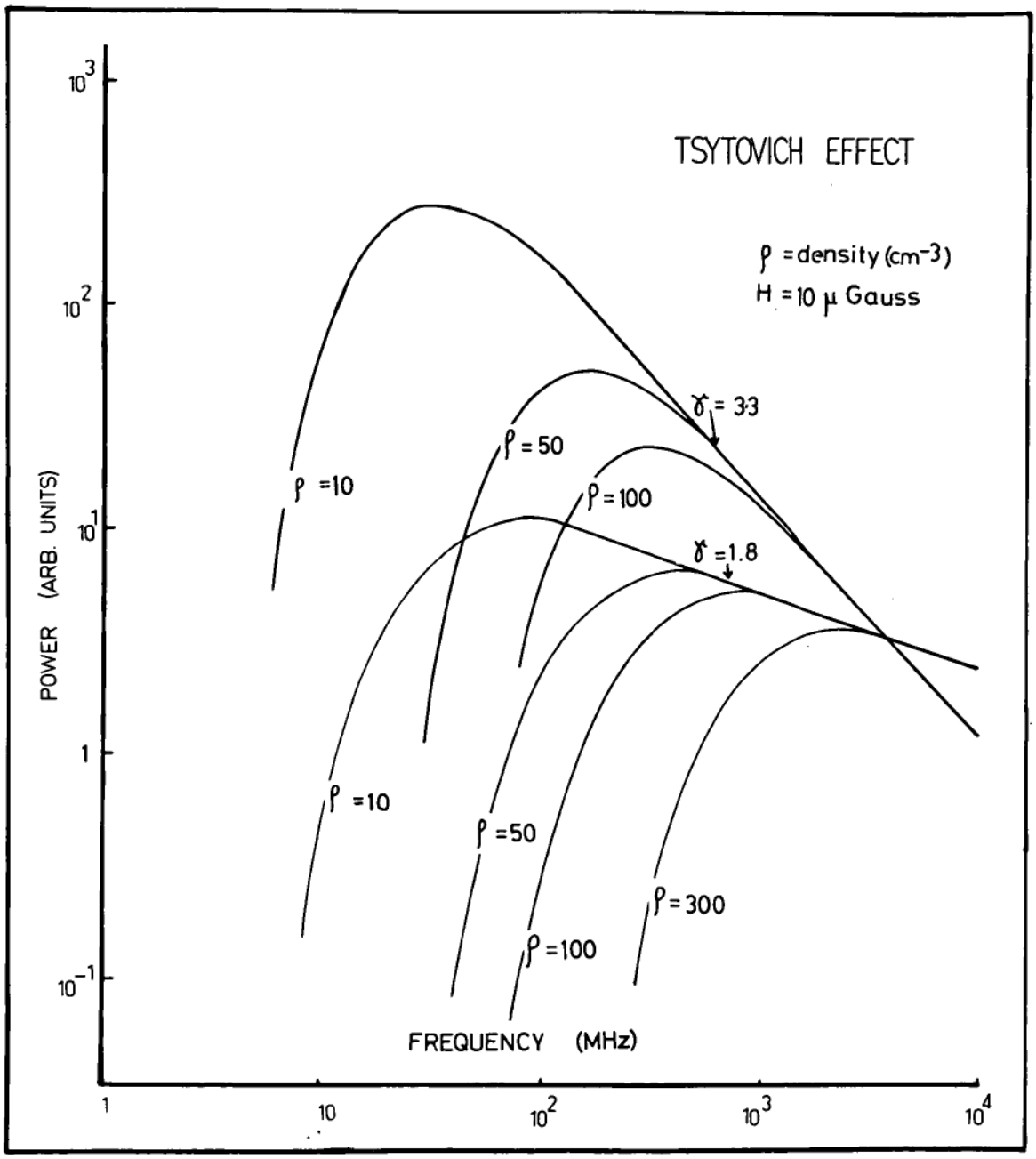

FIGURE 1.6.

Emission spectra from "power-law" distributions of electrons. The refractive index of the medium in the source is less than unity.

An alternative relation can be obtained from equations (1.5, 1.8, 1.25). The Tystovich effect is only important for frequencies of emission, ν, such that:

$$\nu \leq \frac{15\ Ne}{B_{\perp}} \text{ MHz} \qquad \ldots.(1.26)$$

where:

$B_{\perp}$ is in micro-gauss and Ne is in electrons cm^{-3}.

For example, in a medium in which Ne ~ 100 cm^{-3}, $B_{\perp} \sim 10^{-4}$ gauss, the Tsytovich effect is only important at frequencies less than 15 MHz.

The intensity of the radiation, I_{ν} at a frequency, ν, emitted by an ensemble of electrons in a magneto-ionic medium in which the refractive index is less than unity is given by equation (1.10) and equation (1.22). Figure (1.6) shows the shape of the emission spectrum from an electron energy distribution within the source of the form:

$$N(\varepsilon,\theta,t)\ d\varepsilon = Ke\ \varepsilon^{-\gamma} d\varepsilon \quad \text{for } \varepsilon_1 \leq \varepsilon \leq \varepsilon_2$$

$$= 0 \qquad \text{for } \varepsilon < \varepsilon_1 \text{ and } \varepsilon > \varepsilon_2$$

The curves were computed using equations 1.22 to 1.24 and the method outlined in appendix 1.

Synchrotron Self-absorption.(reabsorption)

Twiss(1954), Razin(1960) and LeRoux(1961) have shown that in an emission region in which the brightness temperature is of the same order as the kinetic temperature of the relativistic electrons, self-absorption of the radiation occurs. Slish(1963) and Williams (1963) have used the self-absorption theory to explain some source spectra. They found that sources with a high surface brightness and small angular size often exhibit high optical depths at low frequencies. The self-absorption theory is used extensively to explain the low frequency curvature of source spectra [eg. Scheuer and Williams, 1968] and to explain the secular variations observed in the emissions from some sources [eg. Kellermann and Pauliny-Toth, 1968].

The radiation observed from a region of combined emission and absorption can be expressed simply in the form:

$$S(\nu) = A \frac{E(\nu)}{\mu(\nu)} \left[1 - \exp[-\tau(\nu)] \right] \qquad \ldots.(1.27)$$

(Kraus, 1966-page 92)

where:

$S(\nu)$ is the observed flux density at frequency, ν;

$E(\nu)$ is the emissivity of the source region;

$\mu(\nu)$ is the absorption coefficient of the source;

A is a constant depending on the units;

and: $\tau(\nu)$ is the optical depth of the source medium at the frequency, ν.

If the radiating electrons have a power-law differential energy spectrum defined by equation (1.13), then from equation (1.18), the emissivity $E(\nu)$ of the source at frequency, ν, can be expressed as:

$$E(\nu) \propto \nu^{\frac{1}{2}(1-\gamma)} \quad .$$

The absorption coefficient, $\mu(\nu)$ at a frequency, ν, of the reabsorption process is obtained from the Einstein relations for spontaneous emission and absorption [eg. Wild, Smerd and Weiss, 1963]. This leads to the result:

$$\mu(\nu) \propto \nu^{-\frac{1}{2}(\gamma+4)} \quad .$$

It is convenient to introduce the quantity ν_0, the frequency at which the optical depth of the region is unity. The optical depth is:

$$\tau(\nu) = \int_0^L \mu(\nu)\, dl \qquad \ldots.(1.28)$$

Here L is the path length through the region in which self-absorption is occuring.

Substitution of the expressions for the absorption coefficient and the emissivity into (1.28) leads to the result that:

$$\tau(\nu) = [\nu_{0/\nu}]^{-\frac{1}{2}(\gamma+4)} \qquad \ldots.(1.29)$$

or: $= [\nu/\nu_0]^{\alpha-2.5}$ since the spectral

index, α, is related to γ by the relation:

$$\alpha = \tfrac{1}{2}(1-\gamma) \qquad \text{(from equation 1.19)}$$

The general expression describing the self-absorption becomes:

$$S(\nu) \propto \nu^{2.5} \left[1 - \exp\left[-\left\{\frac{\nu}{\nu_0}\right\}^{\alpha-2.5}\right]\right] \qquad \ldots.(1.30)$$

Equation (1.30) is obtained from equation (1.27) after substituting the expressions for the emissivity and absorption coefficient. Figure 1.7 shows the behaviour of equation (1.30) for various values of ν_0 .

Substitution of the full expressions for the absorption coefficient, $\mu(\nu)$, and the emissivity $E(\nu)$ into equation (1.27) leads to the relation:

$$\nu_0 \simeq 16\ B_\perp^{1/5}\ \theta^{-4/5}\ Se^{2/5}\ [1+z]^{1/5}\ \text{MHz} \qquad \ldots.(1.31)$$

[eg. Kellermann,1966]

where: $B_\perp$ is the component of the magnetic field perpendicular to the direction of motion of the electrons,(gauss)

θ is the angular size of the source emitting region (seconds of arc)

Se is the flux density [in units of 10^{-26} W m^{-2} Hz^{-1}] that would be observed from the source at the frequency, ν_0(MHz) in the absence of self-absorption.

The Function:

$$S(\nu) \propto \nu^{5/2}\{1 - \exp[-(\frac{\nu}{\nu_0})^{\alpha-2.5}]\}$$

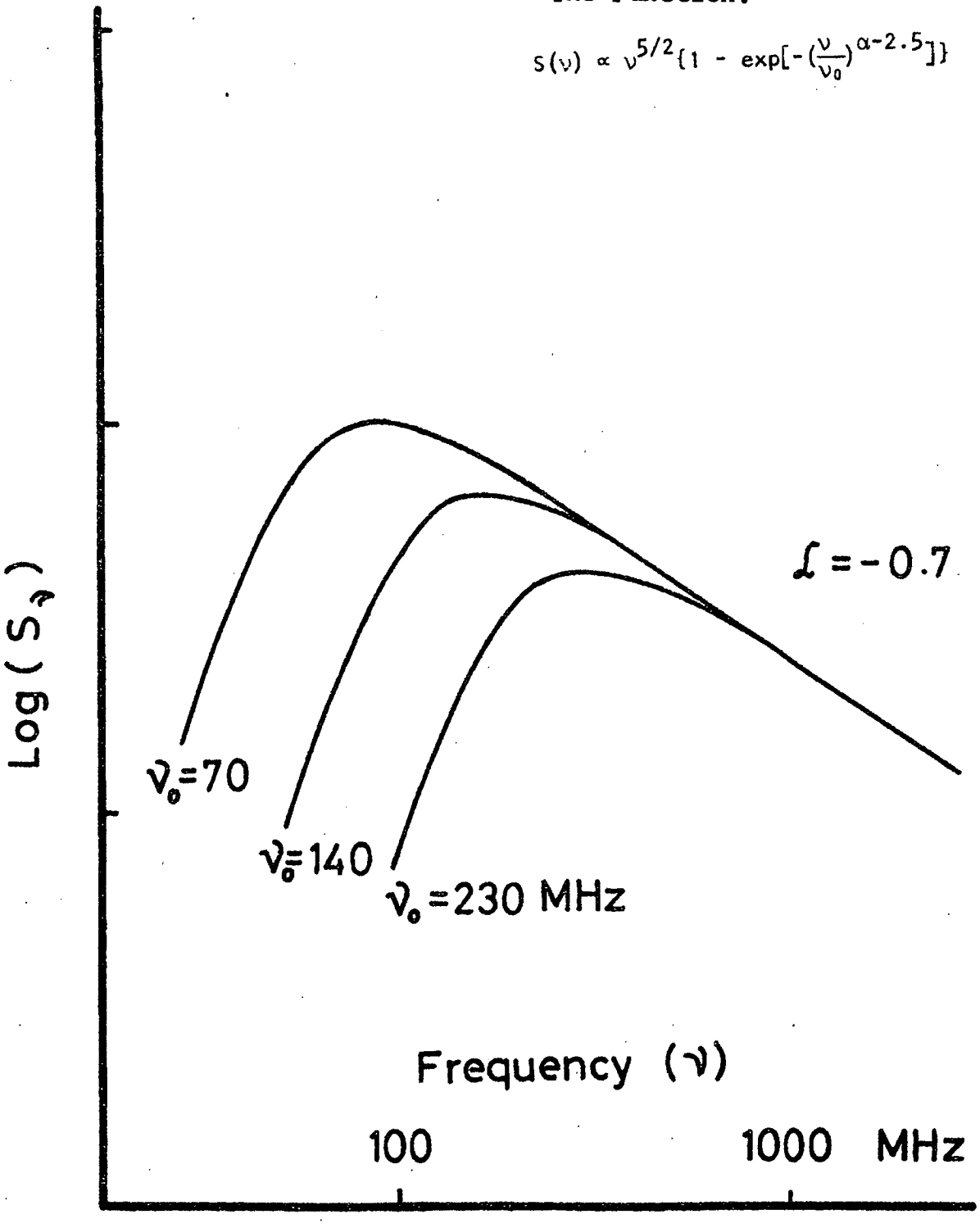

FIGURE 1.7.

and: z represents the optical redshift of the source.

The term (1+z) takes into account the cosmology of the universe.

Alternatively, if the maximum in the source flux density, S_m, occurs at a frequency, ν_m, we can use the relation given by Slish (1963) and later modified by Terrell (1967). Namely:

$$\theta = 8.84 \times 10^{8} \, [S_m]^{\frac{1}{2}} \, \nu_m^{-1.25} \, B^{\frac{1}{4}} (1+z)^{\frac{1}{4}} \, [f(\alpha)]^{\frac{1}{2}} \text{ sec.arc} \quad \ldots.(1.32)$$

where:

θ is the angular size of the source (sec.arc),

ν_m is in hertz, S_m is in flux units,

B is the <u>average</u> source magnetic field strength (gauss),

z is a parameter describing the redshift of the source.

α is the spectral index of the power-law radiation in the region of the source spectrum unaffected by self-absorption,

and: $f(\alpha) = 0.85 - 2.63\alpha + 0.33\,\alpha^2$.

The two results (1.31) and (1.32) are used extensively in the analysis of curved source spectra in section 3.

(v) <u>Energy Loss Mechanisms</u>.

The synchrotron theory of power-law emission is adequate to explain the non-thermal radiation observed from many sources at metre and decimetre wavelengths. However, new measurements at centimetre wavelengths [discussed by Kellermann and Pauliny-Toth, 1968], have shown that the high frequency spectra

of a significant number of sources are not of the power-law form. The processes that change the emission spectrum of a source from a simple power-law are therefore important for an understanding of the origin and physical conditions of a source. In this part of chapter 1 we consider the energy loss mechanisms of particular interest to the study of extragalactic radio sources. For a complete analysis of the various energy loss processes the reader is referred to articles by Kardashev(1962), van der Laan(1963) and Kellermann(1964 and 1966). Excellent reviews on this subject have been included in discussions by Ginzburg and Syrovatskii(1964 and (1965), Scheuer and Williams (1968) and Kellermann and Pauliny-Toth (1968).

To understand the energy loss processes we need first to consider the function describing the general distribution of electrons within the source. For simplicity we assume that the electrons of a source radiate in a vacuum and a uniform magnetic field, and also that the electron distribution within the source is isotropic. The electron energy distribution, $N(\mathcal{E},r,t)d\epsilon$ then completely specifies the "state" of the electrons within the source. Here ϵ is the energy of the electron, r specifies the position of the electron and t the time. The function $N=N(\epsilon,r,t)$, which gives the number of electrons <u>per unit volume</u> within a unit energy interval must satisfy the relation:

$$\frac{\partial N}{\partial t} - D.\Delta N + \frac{\partial}{\partial \varepsilon}[C(\varepsilon) N] + \frac{N}{T} = Q(r,\varepsilon,t) \qquad ....(1.33)$$

[Syrovatskii,1959]

where: D is the diffusion coefficient; $C(\varepsilon) = d\varepsilon/dt$ is the rate of change of electron energy due to radiation losses and collisions, Δ is the Laplace operator, T is the average lifetime of the electrons and $Q(r,\varepsilon,t)$ is the rate of injection of new electrons per unit volume, per unit energy interval into the source. Equation (1.33) can be written in the alternative form:

$$\frac{\partial N(\varepsilon,t)}{\partial t} = \alpha_1(t) \frac{\partial}{\partial \varepsilon}\left[\varepsilon^2 \frac{\partial N(\varepsilon,t)}{\partial t}\right] + \frac{\partial}{\partial \varepsilon}\left[-\alpha_2(t)\varepsilon+\beta(t)\varepsilon^2\right] N(\varepsilon,t)$$

$$+ Q(\varepsilon,t) - \alpha_3(t) N(\varepsilon,t) \qquad ....(1.34)$$

[Ginzburg,1957]

where the term containing:

$\alpha_1(t)$ - takes into account random acceleration of the particles by the Fermi mechanism;

$\alpha_2(t)$ - takes into account systematic acceleration by the Fermi mechanism and the changes in energy of the electron during an expansion of the source;

$\beta(t)$ - accounts for energy losses due to synchrotron radiation;

and: $\alpha_3(t)$ - accounts for electron capture by nuclei and the escape of electrons from the emitting region.

Energy losses by ionization and bremsstrahlung encounters are probably small in most extragalactic radio sources [Scheuer and Williams, 1968]. However, other processes such as energy losses by expansion of the source, the inverse Compton effect and synchrotron radiation are more important.

Energy Losses by Source Expansion.

If a source expands adiabatically [see Shklovskii (1960 a)], the energy distribution function of electrons is determined from equation (1.34) with $\alpha_1(t) = \alpha_3(t) = \beta(t) = 0$. Thus:

$$\frac{\partial N}{\partial t} = -\alpha_2(t) \frac{\partial}{\partial t} [\varepsilon N] \quad \ldots \text{(a)}$$

where for a uniform expansion: $\alpha_2(t) \simeq A/r \sim -\frac{1}{t}$ [Kardashev, 1962]. If the magnetic flux is conserved during the expansion, the magnetic field, B, is given by:

$$B = B_o(r_o/r)$$

where: r_o is the radius of the source at time, t_o;

B_o is the magnetic field at time, t_o;

A is the rate of expansion of the source;

and: r is the radius of the emitting region (spherical).

If the electron distribution within the source is a power-law with index γ at time, t_o, then at some later time, t, it will also be a power-law of the form: (obtained by solving (a) above)

$$N(\varepsilon, t)\, d\varepsilon = K e^{-\gamma}(\frac{t_o}{t})^{\gamma-1}\, d\varepsilon$$

where $N(\varepsilon, t)$ is the electron distribution function for the

whole source. The shape of the electron energy distribution curve remains unchanged as the source expands, and thus the shape of the emitted synchrotron spectrum also remains unchanged. From equations (1.17, 1.18) and from the relations given above it follows that:

$$I(\nu, t) \propto \left[\frac{t}{t_o} \right]^{-2\gamma} \nu^{\frac{1}{2}(1-\gamma)}$$

where: $I(\nu, t)$ is the observed intensity of synchrotron radiation at time, t, and frequency, ν;

t_o is the time when the expansion of the source commenced;

t is the present time;

and: γ is the index of the power-law distribution of electrons in the source.

A simple adiabatic expansion probably does not occur in "real" sources [Scheuer and Williams,1968]. However, such a model does give an approximation to the changes that are likely to occur in the emission spectrum of an expanding source. Other source expansion models have been discussed by van der Laan (1966), Rees and Simon (1968), Ryle and Longair (1967) and Kellermann and Pauliny-Toth (1968).

Loss of Electron Energy by the Inverse Compton Effect.

As a fast, charged particle passes through the alternating fields of an electromagnetic wave of frequency, ν, it radiates power at a rate:

$$\gamma^{-2} \sigma c U \quad [\text{erg sec}^{-1}] \qquad \ldots(1.35)$$

at a mean frequency of $\bar{\gamma}^2\nu$ [Hz] [Scheuer and Williams,1968]

Here: U is the energy density of the electromagnetic wave [erg cm^{-3}],

σ is the Thomson scattering cross section [= 6.65×10^{-25} cm^2],

$\bar{\gamma} = [1 - v^2/_{c}2]^{\frac{1}{2}}$,

c is the velocity of the light [cm sec^{-1}],

and: v is the velocity of the moving electron [cm sec^{-1}].

An alternative expression for the rate of energy loss has been given by van der Laan(1963).

$$\frac{d\varepsilon}{dt} = -7.59 \times 10^{-26} \bar{\zeta}\, \varepsilon^2 \text{ eV sec}^{-1} \qquad \ldots.(1.36)$$

where the energy of the electron, ε, is in eV and $\bar{\zeta}$ is the (thermal) photon energy density of the wave [eV cm^{-3}]. If the source expands uniformly, losses of electron energy by the inverse Compton effect are approximately proportional to r^{-10} [Kardashev,1962], where r is the radius of the source emission region. Compton losses are therefore only important in the early life of the radio source.

Loss of Electron Energy by Synchrotron Radiation.

As a relativistic electron moves through a uniform magnetic field of strength B it loses energy at a rate:

$$2\bar{\gamma}^2 U_{mag.} \sin^2(\theta) \text{ [erg sec}^{-1}\text{]} \qquad \ldots.(1.37)$$

by synchrotron radiation.

[Scheuer and Williams,1968]

where: $U_{mag.}$ is the energy density of the magnetic field,
$= B^2/8\pi$ [erg cm^{-3}] where B is in gauss;

θ is the pitch angle of the electron;

$\bar{\gamma} = [1 - v^2/_{c^2}]^{\frac{1}{2}}$;

v is the velocity of the electron [cm sec^{-1}];

c is the velocity of light [cm sec^{-1}];

m_0 is the rest mass of the electron.

In terms of the energy of the electron, ε ($= m_0c^2$), the rate of loss of energy is given by:

$$\frac{d\varepsilon}{dt} = -3.94 \times 10^{-15} B_{\perp}^2 \varepsilon^2 \text{ eV sec}^{-1} \quad \ldots.(1.38)$$

where $B_{\perp} = B \sin(\theta)$ [gauss]

From equations (1.36 and 1.38), losses by the inverse Compton effect will exceed those by synchrotron radiation provided:

$$\bar{\zeta} > 5.19 \times 10^{10} B_{\perp}^2 \text{ eV cm}^{-3} \quad \ldots.(1.39)$$

The radio photon energy density is given by:

$$\bar{\zeta} \simeq \frac{3L}{4\pi r^2 c} \quad \text{(a)}$$

[Kellermann and Pauliny-Toth,1968]

where L is the radio luminosity of a source resulting from synchrotron emission and r is the radius of the source.

If the power emitted by a radio galaxy ~ 10^{54} eV sec^{-1} and radius r ~ 30 kilo-parsecs, then $\bar{\zeta}$ ~ 10^{-3} eV cm^{-3} (from (a) above). Thus, since the magnetic field strength within most extragalactic radio sources ~ $10^{-4\pm1}$ gauss [Kellermann and Pauliny-Toth,1969] it follows that the conditions of equation (1.39) will not normally be satisfied in most radio galaxies. However, inverse Compton losses are important in young, compact, variable radio sources which have a high surface brightness temperature [see for example Kellermann and Pauliny-Toth,1969].

Changes in the Electron Energy Distribution resulting from Synchrotron Radiation.

Electrons emitting synchrotron radiation lose energy at a rate:

$$\frac{d\epsilon}{dt} = -\beta \epsilon^2 \qquad (\text{erg sec}^{-1}) \quad [\text{cf. equation 1.38}] \quad ...(b)$$

where: $\beta = 6.08 \times 10^{-21} B_{\perp}^2$ when the energy, ϵ is in GeV; $B_{\perp} = B \sin(\theta)$ is the magnetic field in micro-gauss, and θ is the electron pitch angle.

Substitution of (b) into the distribution equation (1.34), gives the relation defining the time-dependence of the electron energy distribution within the emitting region:

$$\frac{\partial N}{\partial t} = -\beta \frac{\partial}{\partial \epsilon} [\epsilon^2 N] \qquad ....(1.40)$$

[Kardashev, 1962]

If, at the initial instant of time, the distribution of electrons within the source is a power-law (all electrons with pitch angle θ), that is:

$$N(\varepsilon,\theta,t=0)\, d\varepsilon = K_e \varepsilon^{-\gamma} d\varepsilon \text{ for } \varepsilon_{01} < \varepsilon < \varepsilon_{02}$$

$$= 0 \qquad \text{for } \varepsilon < \varepsilon_{01} \text{ or } \varepsilon > \varepsilon_{02} \qquad \ldots\ldots(1.41)$$

and if no new electrons are injected into the source, then at some later time, t, synchrotron radiation losses will have changed the electron distribution within the source to: (obtained by solving (1.40))

$$N(\varepsilon,\theta,t)\, d\varepsilon = \frac{K_e\, \varepsilon^{-\gamma}\, d\varepsilon}{[1 - a\, B_\perp^2\, \varepsilon\, t]^{2-\gamma}} \qquad \ldots\ldots(1.42)$$

where: Ke , γ are constants and $a = \beta / B_\perp^2$

The cut-off energies, ε_{01}, ε_{02}, which define the initial electron energy distribution (1.41), will change so that at time, t the cut-off energies of the new electron distribution (1.42) will be:

$$\varepsilon_{1,2} = \frac{\varepsilon_{0\ 1,2}}{[1 + \varepsilon_{0\ 1,2}\, \beta t]} \qquad \ldots\ldots(1.43)$$

[obtained from (b)]

The characteristic life time of the radiating electron, T, is obtained from (1.43):

$$T = 1/\beta\varepsilon_0 = \frac{8.3 \times 10^9}{B_\perp^2\ \text{gauss}\ \varepsilon_{\text{GeV}}} \quad \text{years}$$

where the subscript zero denotes the conditions at time, t=0. From equation (1.42), the new electron energy distribution has a cut-off at the energy, ε_s given by:

$$\varepsilon_s = \frac{1}{\beta t} \qquad \ldots.(1.44)$$

The corresponding cut-off in the synchrotron radiation spectrum will occur at the frequency: [from equation (1.5)]

$$\nu^* = 1063\ B_\perp^{-3}\ \text{[gauss]} \times t^{-2}\ \text{[years]}\ \text{MHz} \qquad \ldots.(1.45)$$

[see, for example, Ginzburg and Syrovatskii, 1965]

Figures 1.8 and 1.9 show the behaviour of the distribution function (equation 1.42) with time for values of γ equal to 1.5 and 2.3. The field strength is 40 μgauss.

The particle spectrum slopes steeply downward at energies above ε_s when $\gamma > 2$. The corresponding synchrotron spectrum shows a steepening at frequencies above ν^*. The spectrum is given by:

$$S(\nu) \propto \left\{ \frac{\nu}{\nu_2} \right\}^{\frac{1}{2}} \exp\left[- \frac{\nu}{\nu_2} \right] \qquad \ldots.(1.46)$$

[Kellermann, 1966]

where ν is the frequency of emission, $S(\nu)$ is the flux density at frequency, ν, and ν_2 is the high frequency cut-off point in the radio spectrum calculated from equations (1.5 and 1.43). At frequencies less than ν^*, the radio spectrum is a power-law with spectral index, $\alpha = \frac{1}{2}(1-\gamma)$. The electron

(facing pages 35, 36.)

Figures 1.8, 1.9.

The behaviour of the electron distribution function, described by equation (1.42), with time for values of $\gamma = 1.5$ and 2.3 respectively.

Part B of each diagram illustrates the integrand in equation (1.10). Plots of the energy, ε, against the relation $N(\varepsilon) \times F(\nu/\nu_c)$ are shown at a time of 2.5×10^6 years after the energy loss process commenced. The curves with decreasing maxima correspond to increasing frequencies of emission as shown at the right of the curves.

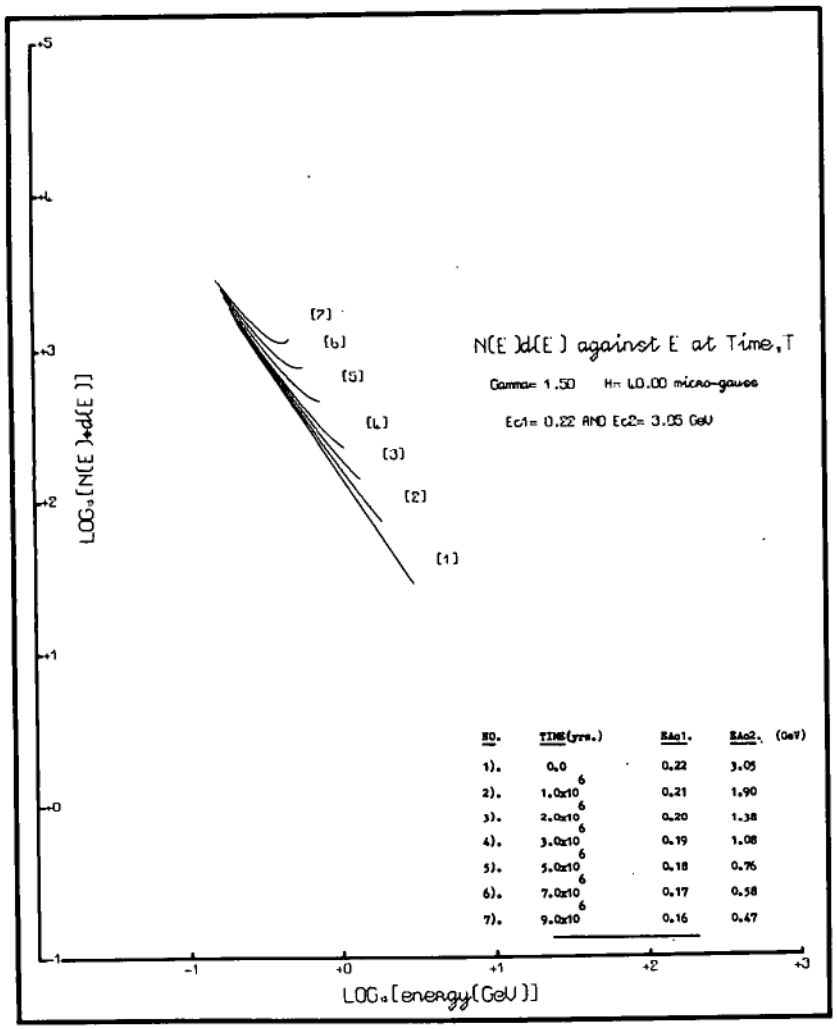
N(E)d(E) against E at Time,T
Gamma= 1.50 H= 10.00 micro-gauss
Ec1= 0.22 AND Ec2= 3.05 GeV
[7]
[6]
[5]
[4]
[3]
[2]
[1]
NO. TIME(yrs.) Ec1. Ec2. (GeV)
1). 0.0 0.22 3.05
2). 1.0x10^6 0.21 1.90
3). 2.0x10^6 0.20 1.38
4). 3.0x10^6 0.19 1.08
5). 5.0x10^6 0.18 0.76
6). 7.0x10^6 0.17 0.58
7). 9.0x10^6 0.16 0.47
LOG10[N(E)*d(E)]
LOG10[energy(GeV)]

A.

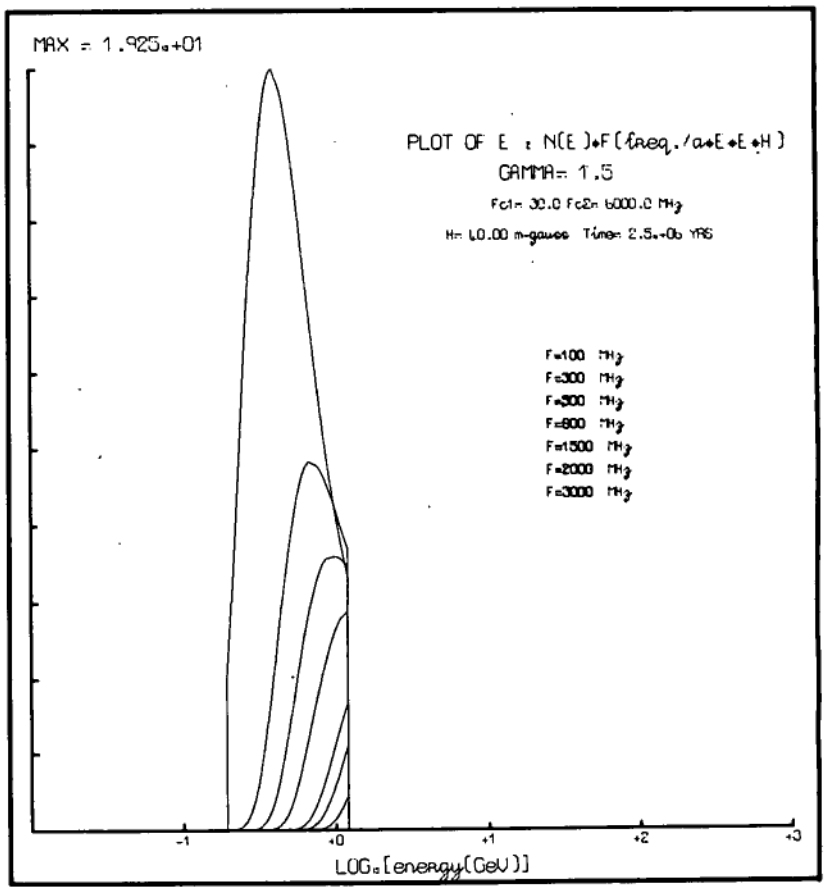
MAX = 1.925E+01
PLOT OF E : N(E)*F(freq./a*E*E*H)
GAMMA= 1.5
Fc1= 30.0 Fc2= 6000.0 MHz
H= 10.00 m-gauss Time= 2.5E+06 YRS
F=100 MHz
F=300 MHz
F=500 MHz
F=800 MHz
F=1500 MHz
F=2000 MHz
F=3000 MHz
LOG10[energy(GeV)]

B.

FIGURE 1.8.

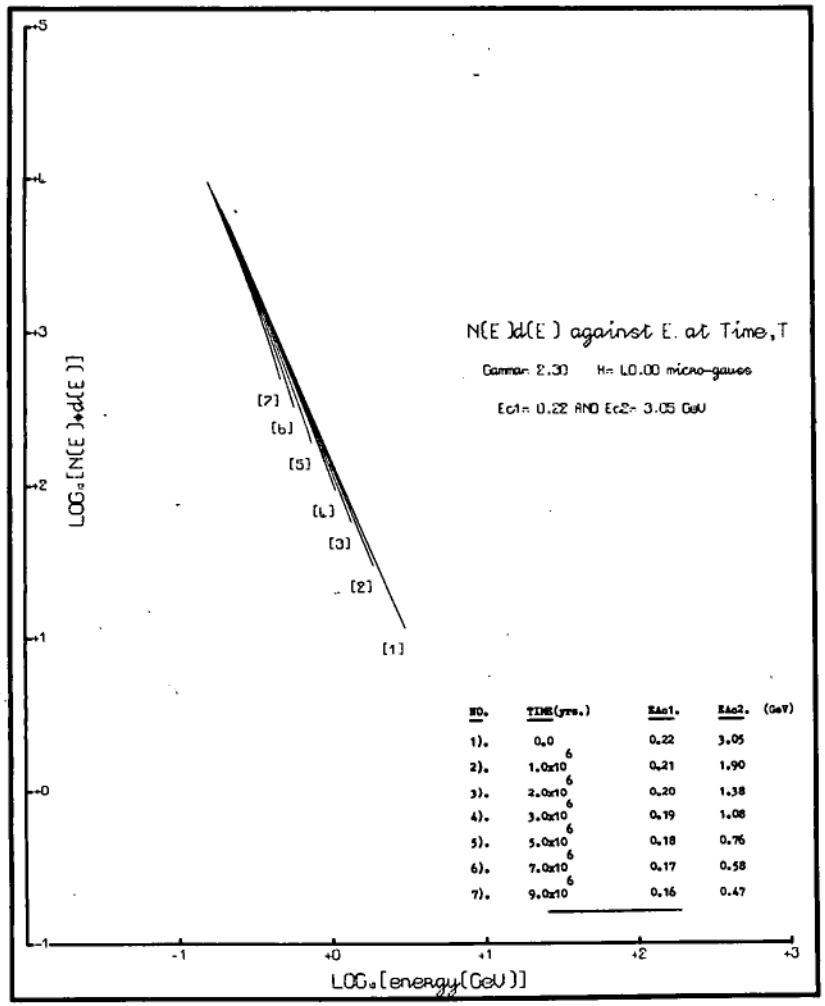
N(E)d(E) against E. at Time,T
Gamma= 2.30 H= 10.00 micro-gauss
Ec1= 0.22 AND Ec2= 3.05 GeV
[7]
[6]
[5]
[4]
[3]
[2]
[1]
NO. TIME(yrs.) Ec1. Ec2. (GeV)
1). 0.0 0.22 3.05
2). 1.0x10^6 0.21 1.90
3). 2.0x10^6 0.20 1.38
4). 3.0x10^6 0.19 1.08
5). 5.0x10^6 0.18 0.76
6). 7.0x10^6 0.17 0.58
7). 9.0x10^6 0.16 0.47
LOG10[N(E)*d(E)]
LOG10[energy(GeV)]

A.

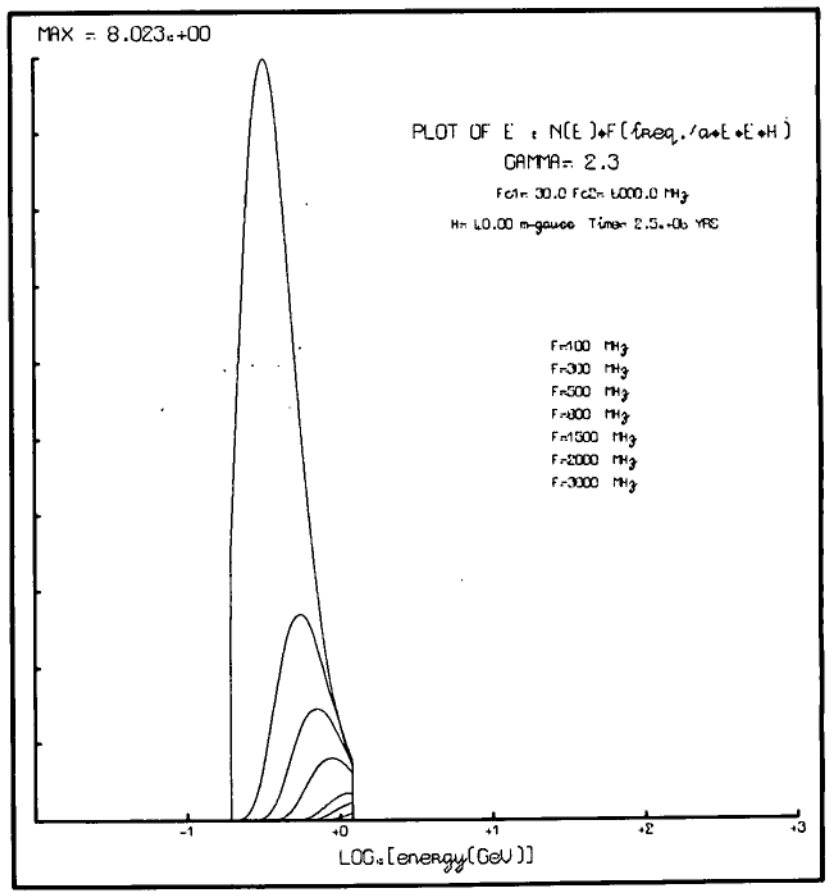
MAX = 8.023E+00
PLOT OF E : N(E)*F(freq./a*E*E*H)
GAMMA= 2.3
Fc1= 30.0 Fc2= 4000.0 MHz
H= 10.00 m-gauss Time= 2.5E+06 YRS
F=100 MHz
F=300 MHz
F=500 MHz
F=800 MHz
F=1500 MHz
F=2000 MHz
F=3000 MHz
LOG10[energy(GeV)]

B.

FIGURE 1.9.

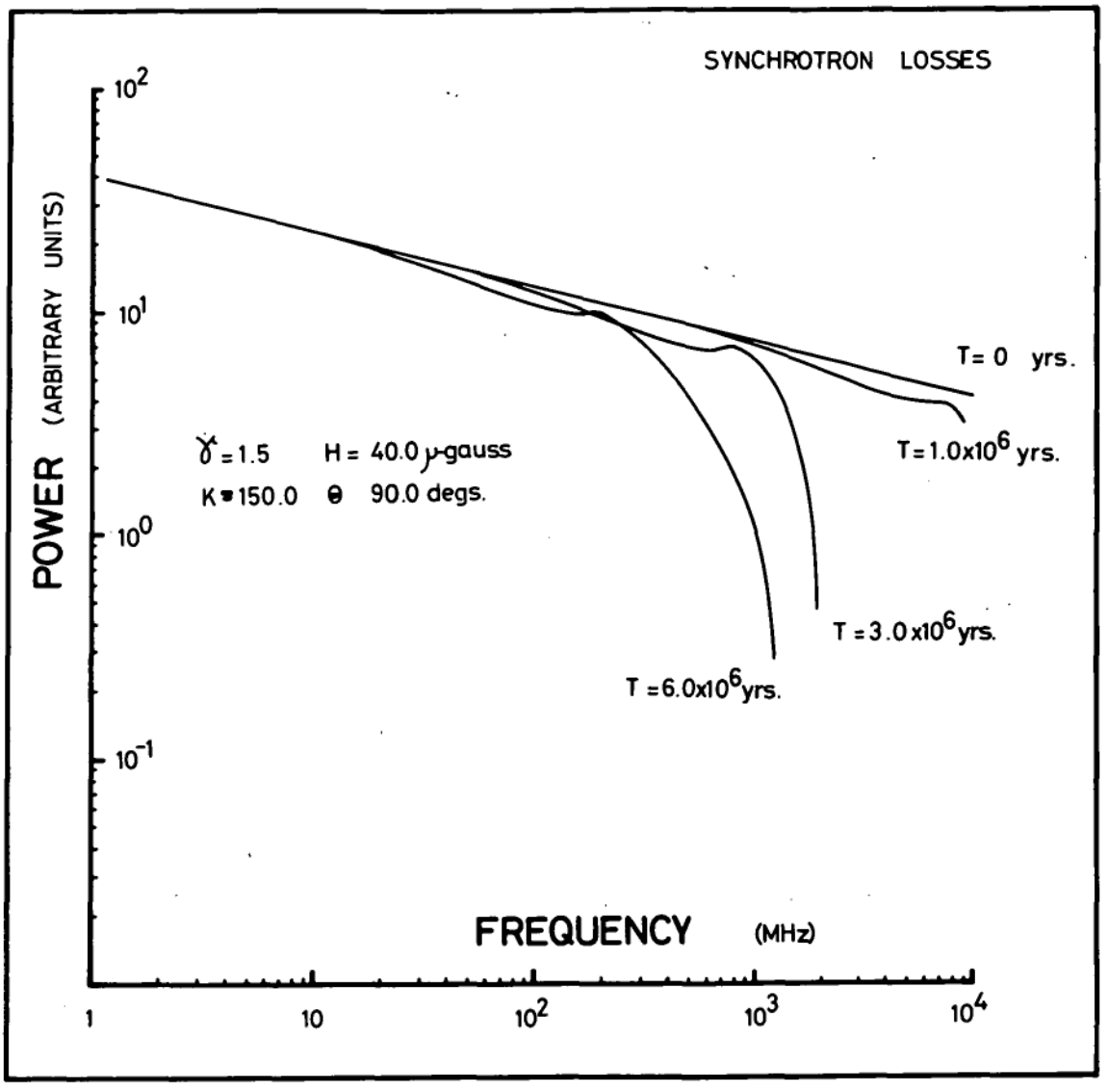

FIGURE 1.10.

Variations in the emission from a source with time when the electrons lose energy by synchrotron radiation. Note that (for $\gamma < 2$) enhancement of the radiation occurs near the cut-off frequency (see text).

spectrum rises rapidly with time for $\gamma < 2$ then falls abruptly to zero. If there is a sufficient concentration of electrons with energy near ε_s, (for $\gamma < 2$) there will be enhancement of the synchrotron spectrum near the frequency ν^*. This is illustrated in figure 1.10.

If the electron distribution within the source is isotropic, then θ can be eliminated from equation (1.42) by integration over all possible pitch angles of the electrons. There will be a "bend" rather than a "break" in the radio spectrum at a frequency ν^* with these conditions. The spectral index will be $\alpha = \frac{1}{2}(1-\gamma)$ below ν^*, while above ν^* the spectrum will also be a power-law with spectral index $\frac{(2\gamma+1)}{3}$ [Kellermann, 1966; Kardashev, 1962].

Kellermann (1966) suggested that synchrotron radiation losses together with periodic injection of new electrons could account for the high frequency steepening of source spectra. The spectrum of the injected electrons was taken to be a power-law (with index $\gamma = 1.5$). The spectral index of the emitted synchrotron spectrum was therefore $\alpha = \frac{1}{2}(1-\gamma) = -0.25$ in the early life of the radio source. Subsequent synchrotron radiation losses steepened this spectrum to one with spectral index $\alpha = -0.75$. This process possibly occurs in the early life of extragalactic radio sources [Scheuer and Williams,1968], or in old, extended sources with a high magnetic field.

For the majority of sources however, Kellermann's theory requires excessively high values of source age and/or magnetic field strength to satisfy the observations.

(vi). Injection of New Electrons into a source.

In the discussion above we have assumed that no new electrons are added to a source during its lifetime. Repeated outbursts of energy from variable radio sources [Kellermann and Pauliny-Toth,1968] indicate that catastrophic events do occur periodically in some sources. We consider two simple particle injection models:

(a) Q = constant

(b) $Q = q\epsilon^{-\gamma_B}$

where: Q is the rate of injection of new electrons per unit volume per unit energy interval.

q and γ_B are constants,

and: ϵ is the electron energy.

With these conditions the electron energy distribution function is defined by: (from equation 1.34)

$$\frac{\partial N}{\partial t} = -\beta \frac{\partial}{\partial \epsilon} [\epsilon^2 N] + Q \qquad \ldots.(1.47)$$

Model a.

If at the initial instant of time the electron distribution within the source is a power-law, then the

equilibrium solution of equation (1.47) is:

$$N(\varepsilon) = \frac{Ke\ \varepsilon^{1-\gamma}}{[\gamma+1]\ a\ B_{\perp}^{2}\ \varepsilon^{2}} \qquad \ldots.(1.48)$$

[Kellermann, 1966]

where:

all the symbols have already been defined.

The radio spectral index from this electron distribution will be $\alpha = -\frac{1}{2}\gamma$. If the injection of new electrons commenced at the initial instant of time, the spectral index of the synchrotron spectrum will evolve from a value α to a value $\alpha-\frac{1}{2}$ [Kellermann, 1966].

Model b.

If the electron distribution within the source at the initial instant of time is of the form:

$$N(\varepsilon,\ t=0)\ d\varepsilon = Ke\ \varepsilon^{-\gamma_A}\ d\varepsilon \quad \text{for } \varepsilon_1 \leq \varepsilon \leq \varepsilon_2$$

$$= 0 \quad \text{for } \varepsilon < \varepsilon_1 \quad \text{or} \quad \varepsilon > \varepsilon_2$$

and if the injection of new electrons into the source commences at time, t=0, then the solution of (1.47) is [Kardashev(1962)]:

$$N(\varepsilon,t) = Ke\ \varepsilon^{-\gamma_A}\ [1 - \beta t\varepsilon]^{\gamma_A-2} + \frac{q\ \varepsilon^{-(1+\gamma_B)}}{\beta(\gamma_B-1)} \left[1-(1-\beta t\varepsilon)^{\gamma_B-1} \right] \qquad \ldots.(1.49)$$

where: Ke,q are constants and γ_A, γ_B are spectral indices of the electron distributions.

Note that again, there is a cut-off in this electron distribution after a time, t, at an energy of $\varepsilon_s = 1/\beta t$. The synchrotron emission spectrum corresponding to equation (1.49) will have a "break" at a frequency, ν^* , given by equation (1.45). If at the initial instant of time, t=0, we have Ke=0 then after a time, t the spectral index of the radiation at frequencies below ν^* is $\alpha = \frac{1}{2}(1-\gamma_B)$. Above ν^* the spectral index will be $\alpha^* = -\frac{1}{2}\gamma_B$ [Kardashev, 1962]. Figure (1.11) shows the behaviour of the distribution function (equation (1.49)) with time.

Having discussed the synchrotron process it should be noted that a number of alternative theories have been proposed to account for some of the radiation from sources with unusual spectra: Compton emission [Rees, 1967], maser emission [Zheleznyakov, 1967 α and β ; McCray, 1966], proton synchrotron emission [Jukes, 1967] and a plasma oscillation process [Ginzburg and Ozernoy, 1966]. Although it will not be necessary to refer to these processes to account for the curvature in source spectra (section 3), they are mentioned here for completeness.

(facing page 42.)

Figure 1.11

Part A.

The behaviour of the electron energy distribution function, equation (1.49), with time. Note that enhancement of the number of electrons occurs near an energy of ε_s, calculated from equation (1.44). Plots (1) to (5) correspond to the following times after the beginning of electron injection:

PLOT NUMBER	TIME (years)
1.	0.0
2.	1.0×10^6
3.	2.0×10^6
4.	3.0×10^6
5.	4.0×10^6

Part B.

This illustrates the integrand in equation (1.10). Plots of the energy, ε, against the relation $N(\varepsilon) \times F(\nu/\nu_c)$ are shown at a time of 3.0×10^6 years after the commencement of electron injection. The curves with decreasing maxima correspond to increasing frequencies of emission as shown.

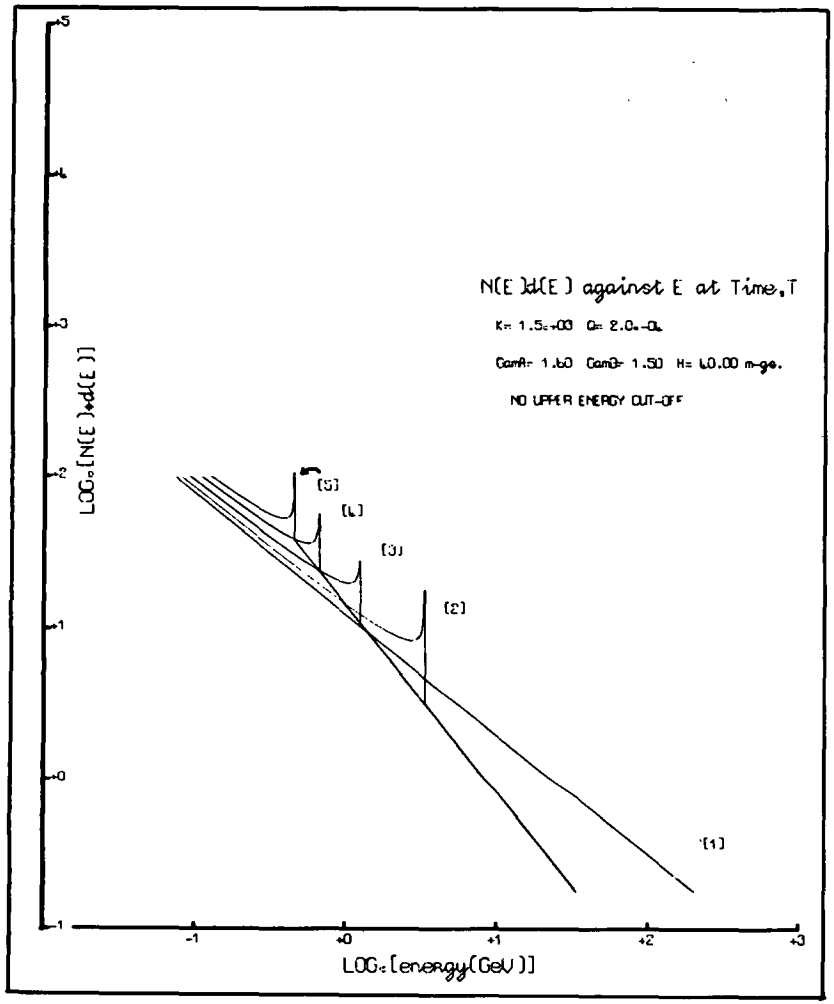

A.

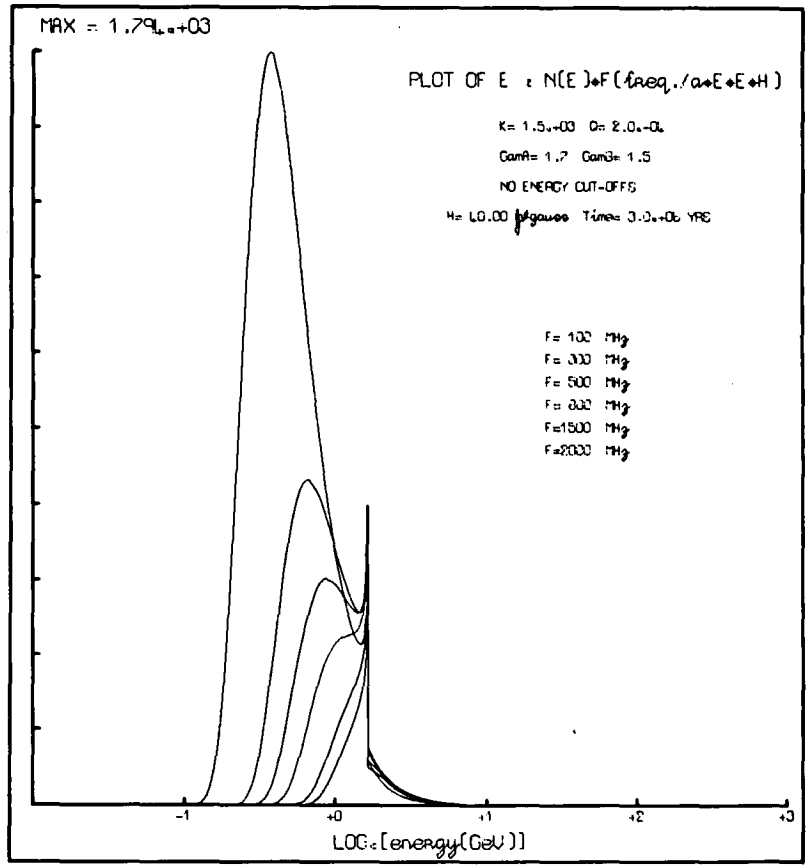

B.

FIGURE 1.11 .

CHAPTER 1(cont.)

PART 2. Absorption and Faraday Rotation in Ionized Hydrogen.

As an electromagnetic wave travels through a region of ionized hydrogen, [H II], it is partially absorbed. If there is also a magnetic field in the medium then the plane of polarization of the wave will be rotated [Faraday rotation]. Both of these processes depend on the frequency of the wave and the free electron density within the medium. The theory of absorption in ionized hydrogen has been discussed extensively by Shklovskii (1960), Ginzburg (1961), Ginzburg and Syrovatskii (1964) and Kraus (1966).

A. i. The Absorption Coefficient of an H II Region.

As an electromagnetic wave passes through an ionized medium, the energy of the wave is partially carried by free electrons moving coherently with the wave. However, during an electron-ion collision much of this energy will be lost as imparted kinetic energy to the ion. This is a result of the incoherent nature of the collisions with respect to the wave.

Ginzburg (1961) has derived the expression for the absorption coefficient in an ionized region in which "free-free" transitions occur. Consider a completely ionized, electrically neutral medium in which the following three

conditions hold:

(1). the angular frequency, ω, of the electromagnetic wave is much greater than the angular plasma frequency, ω_0, of the absorbing medium; ie. $\omega >> \omega_0$;

(2). the Rayleigh-Jeans relation holds:

[from equations 1.1, 1.2 $h\nu << kTe$]

and (3). $2\pi e^2/_{h\nu} >> 1$ [i.e. $Te << 3 \times 10^5$ degK]

[Ginzburg, 1961: Section 37]

where: k is the Boltzmann constant (1.38×10^{-16} erg $degK^{-1}$)

Te is the kinetic temperature of the ionized region (degK)

ν is the wave frequency in Hertz ($= \frac{\omega}{2\pi}$) ,

$\omega_0 = [\frac{4\pi N e^2}{m}]^{\frac{1}{2}}$,

h is Planck's constant ($=6.63 \times 10^{-27}$ erg sec),

N is the density of free electrons (cm^{-3}),

v is the velocity of the electron (cm sec^{-1})

and: e,m are the electronic charge and mass respectively.

With these conditions the absorption coefficient per unit distance becomes:

$$\mu(\nu) \simeq \frac{10^{-2} N^2 Te^{-3/2}}{\nu^2} [17.7 + \ln (\frac{Te^{3/2}}{\nu})] \quad \text{neper cm}^{-1} \quad ...(1.50)$$

The optical depth of the absorber is then defined by the integral of $\mu(\nu)$ over the absorbing path length, L (cm).

Hence:

$$\tau(\nu) \simeq \frac{10^{-2}\, Te^{-3/2}}{\nu^2} \left[17.7 + \ln\left(\frac{Te^{3/2}}{\nu}\right)\right] \int_0^L N^2 \, dl \text{ neper} \quad \ldots(1.51)$$

where in this case Te is assumed constant along the absorbing path.

The quantity $\xi \left[= \int_0^L N^2 dl\right]$ is called the *emission measure* ; for astrophysical calculations it is usually expressed in units of cm^{-6}parsec.

(ii). Absorption in a cloud of H II.

The observed brightness of a source seen through a cloud of ionized hydrogen is: (see figure 1.12-case I)

$$B(\nu) = B_1(\nu) \exp\left[-\int_0^L \mu(\nu,x)\, dx\right] \text{ Watt } m^{-2} \text{ Hz}^{-1} \text{ rad.}^{-2} \quad \ldots(1.52)$$

where:

$\mu(\nu)$ is the absorption coefficient per metre at the frequency, ν(Hz),

$B_1(\nu)$ is the "unabsorbed" brightness of the source [Watt m^{-2} Hz^{-1} $rad.^{-2}$],

L is the line-of-sight thickness of the absorber (metre).

From equation (1.51), the optical depth of the cloud is:

$$\tau(\nu) = \int_0^L \mu(\nu,x)\, dx \text{ neper}$$

and

$$B(\nu) = B_1(\nu) \exp[-\tau(\nu)] \text{ Watt } m^{-2} \text{ Hz}^{-1} \text{ rad.}^{-2} \quad \ldots.(1.53).$$

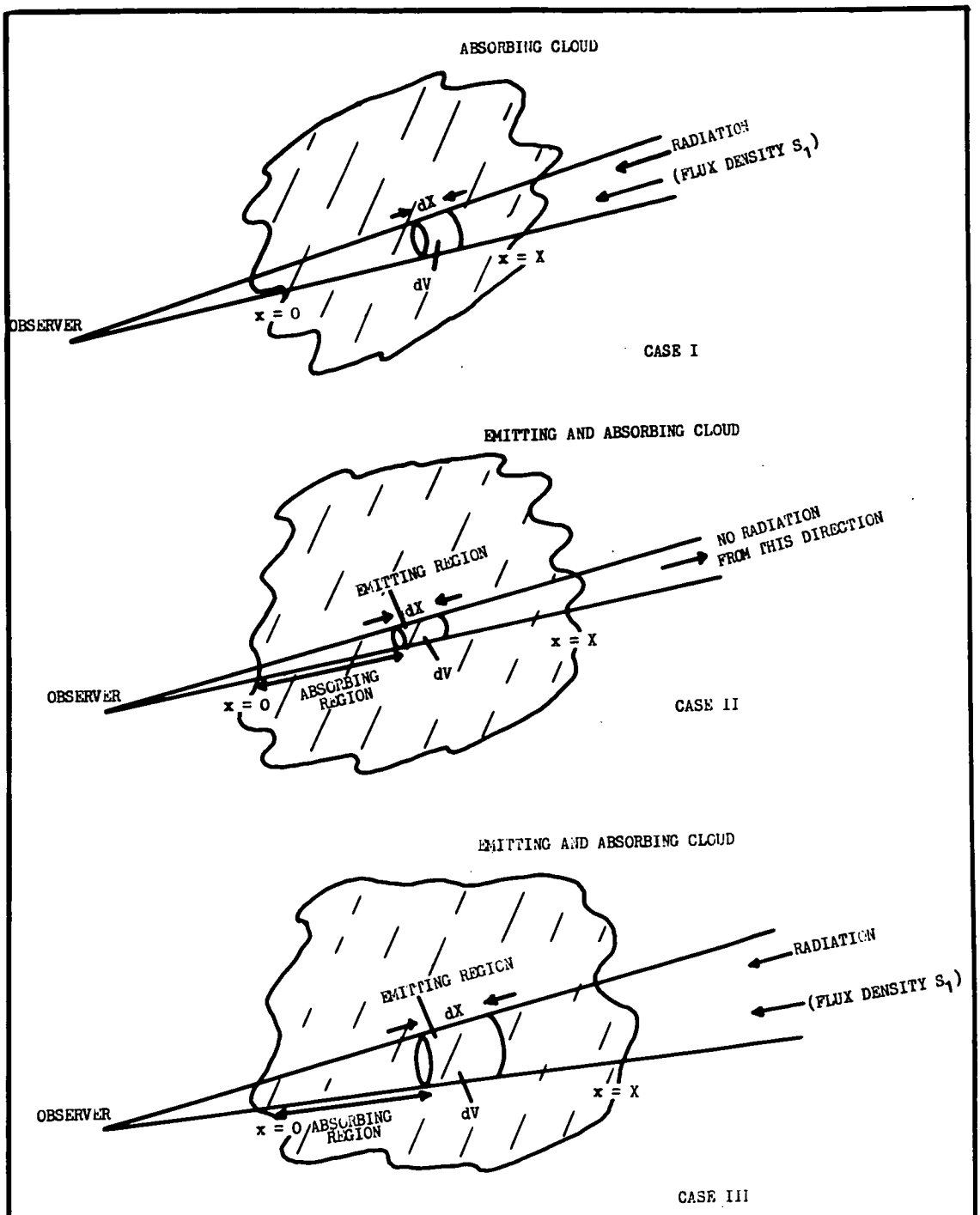

EMISSION AND ABSORPTION IN A CLOUD OF IONIZED HYDROGEN.

FIGURE 1.12 .

(iii). Emission and Absorption within a cloud of H II.

Consider a region in which there is both emission and absorption. Using equation (1.52), the apparent brightness of a volume element, dV of this region at a frequency, ν, is: (see figure 1.12-case II)

$$dB(\nu) = \frac{E(\nu,x)\ dx}{4\pi}\ \exp[\ -\tau(\nu)]$$

However, $\tau(\nu) = \int_0^x \mu(\nu,x)\ dx$

and hence:

$$d\tau(\nu) = \mu(\nu,x)\ dx$$

Substituting we have:

$$dB(\nu) = \frac{E(\nu,x)\ d\tau\ \exp[-\tau]}{4\pi\ \mu(\nu,x)}$$

where $E(\nu)$ is the emissivity of the region at frequency, ν and $\mu(\nu)$ is the absorption coefficient at frequency, ν. If the absorption and emission is uniform throughout the cloud then:

$$B(\nu) = \frac{E(\nu)}{4\pi\mu(\nu)}\ [1 - \exp(\ -\ \tau(\nu)]\ \text{Watt m}^{-2}\ \text{Hz}^{-1}\text{rad.}^{-2} \quad \ldots.(1.54)$$

The quantity:

$$B_1(\nu) = \frac{E(\nu)}{4\pi\mu(\nu)}$$

is the intrinsic brightness of the cloud.

(iv). Emission and Absorption within a cloud plus Emission from behind the cloud* [see figure 1.12 - case III]

From equations (1.53, 1.54), the apparent brightness of the radiation from the direction of the cloud will be:

$$B(\nu) = B_0(\nu)\exp[-\tau(\nu)] + B_1(\nu)\,[1-\exp(-\tau(\nu)]\ \text{Watt m}^{-2}\text{Hz}^{-1}\text{rad.}^{-2} \quad \ldots.(1.55)$$

where: $B_o(\nu)$ is the brightness of the source beyond the cloud at frequency, ν;

$B_1(\nu)$ is the intrinsic brightness of the cloud;

and: $\tau(\nu)$ is the optical depth (neper) of the cloud;

all at a frequency, ν(Hz).

Equations (1.53, 1.54) describe the two ionized hydrogen absorption models to be used in the source spectral analysis of Section 3.

(v). Adaption of the H II Absorption Models for numerical fitting to source spectra.

It is convenient to introduce the variable ν_0, the frequency at which the optical depth of the absorbing region becomes equal to unity. If the emission measure, ξ, is expressed in units of cm^{-6} parsecs; ν_0 in MHz and Te in degrees Kelvin, then from equation (1.51) we can write:

* This is the theoretical model used to explain the low frequency emission from the galaxy [Hamilton, 1969].

$$\nu_0 \simeq 630\ Te^{-3/4}\ \xi^{\frac{1}{2}}\ \text{MHz} \qquad \ldots.(1.56)$$

[ξ is the emission meature, Te the temperature]

We consider the following two absorption models.

(1). Suppose that ionized hydrogen *surrounds* the source of radiation which we will assume is a synchrotron source with a power-law emission spectrum.

The emitted flux density observed from outside the absorber is: (from equations 1.3, 1.53)

$$S(\nu) = A\ \nu^{\alpha} \exp[-(\nu_{0/\nu})^2] + \frac{2k\ \nu^2}{c^2}\ Te\ \Omega[1 - \exp[-(\nu_{0/\nu})^2]]$$

$$\text{Watt m}^{-2}\ \text{Hz}^{-1} \qquad \ldots.(1.57)$$

For non-thermal radio sources, the thermal emission from the ionized gas (that is the second term in equation 1.57) can be neglected.

Hence

$$S(\nu) = A\ \nu^{\alpha} \exp[-(\nu_{0/\nu})^2]\ \ \text{Watt m}^{-2}\ \text{Hz}^{-1} \qquad \ldots.(1.58)$$

In these relations:

Ω = solid angle subtended by the ionized gas portion of the source;

A = constant, α = spectral index of the synchrotron source;

ν = frequency (Hz), ν_0 = frequency when the optical depth equals unity;

k = Boltzmann constant, c = velocity of light.

(2). If the ionized hydrogen is *uniformly mixed* with the synchrotron source, and if the spectrum emitted by the non-thermal source is a power-law with spectral index, α, then from equations (1.3, 1.54):

$$S(\nu) = \left[\frac{A\nu^{\alpha+2}}{\nu_0^2} + \frac{2\,k\,\Omega\,\nu^2 Te}{c^2}\right] \times \left[1 - \exp\left[-(\nu_{0/\nu})^2\right]\right] \quad \text{Watt m}^{-2}\,\text{Hz}^{-1} \qquad \ldots.(1.59)$$

If the thermal emission from the ionized gas is neglected then:

$$S(\nu) = \frac{A\nu^{\alpha+2}}{\nu_0^2}\left[1 - \exp\left[-(\nu_{0/\nu})^2\right]\right] \quad \text{Watt m}^{-2}\text{Hz}^{-1} \qquad \ldots.(1.60)$$

Model fitting of equations (1.58, 1.59) to an observed source spectrum leads to a value for the quantity ν_0 or to the integral:

$$\int_0^L \frac{N^2\,dl}{Te^{3/2}} \qquad \ldots..(1.61)$$

If the linear size, L and the kinetic temperature of the absorbing region are known then we can estimate the free electron density, N within the absorber. In most extragalactic radio sources there is no way however, of determining the value of Te. A value commonly used in the literature is $Te \sim 10^4$ degK. Ginzburg (1961) states that complete ionization will exist within an HII region at this temperature.

To illustrate the above equations, suppose that in the H II medium of a source $Te \sim 10^4$ degK and L ~ 40 kparsecs. If model fitting of equations (1.58) or (1.60) to the spectrum

The Functions:

A: $S(\nu) \propto \frac{\nu^{\alpha+2}}{\nu_0^2} [1 - \exp(-\frac{\nu_0^2}{\nu^2})]$

B: $S(\nu) \propto \nu^{\alpha} \exp [-\frac{\nu_0^2}{\nu^2}]$

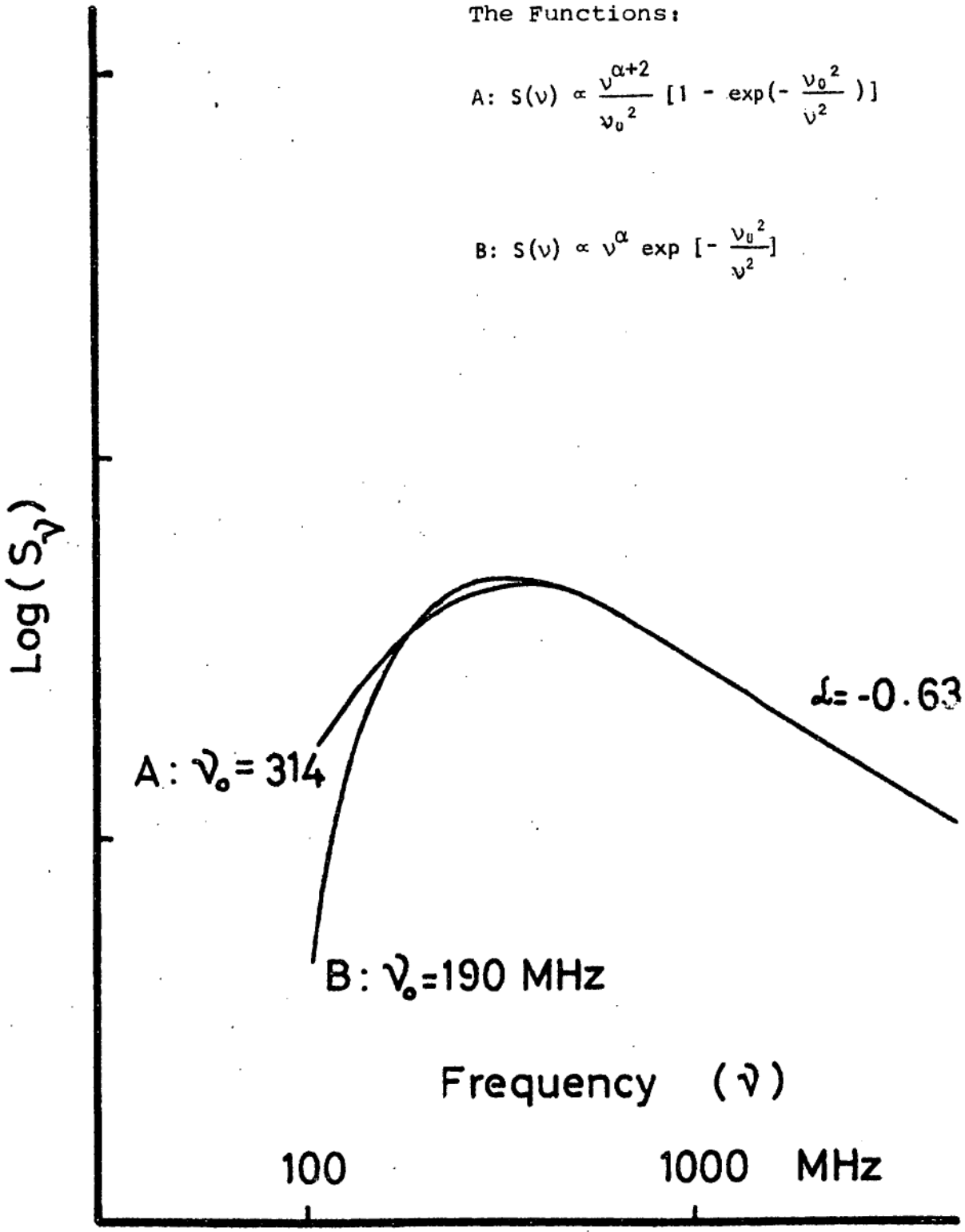

FIGURE 1.13 .

of the source shows that $\nu_0 \sim 110$ MHz, then the free electron density in the absorber is $N \sim 2\ cm^{-3}$ (from equation 1.61). Figure (1.13) shows spectra specified by equations (1.58),(1.60).

B. Faraday Rotation.

As polarized radiation propagates through a magneto-ionic medium the polarization angle of the emission changes because of Faraday rotation [Oort and Walraven, 1956; Ginzburg, 1961]. If the propagation is "quasi-longitudinal", then a wave of frequency, ν which travels a distance, L at an angle, θ to the magnetic field has its plane of polarization rotated by an amount:

$$\phi = \frac{e^3}{2\pi m^2 c^2 \nu^2} \int_0^L N B \cos(\theta)\, dl \qquad \ldots.(1.62)$$

[Ginzburg, 1961]

where: N is the free electron density,

B is the magnetic field strength,

c is the velocity of light,

and: e,m are the electronic charge and mass respectively.

The angle of the plane of linear polarization, ψ, can be expressed in terms of the *rotation measure*, R.M.

$$\psi = \psi_{intr.} + [R.M.]\ \lambda^2 \qquad \ldots.(1.63)$$

[Gardner and Whiteoak, 1963]

where $\lambda_{intr.}$ is the intrinsic polarization angle at the source and λ is the wavelength of the radiation. Substituting the

constants into (1.62) gives: [when λ is in metres]

$$\text{R.M.} = 8.1 \times 10^{5} \int_{0}^{L} N\, B \cos(\theta)\, dl \quad \text{radian metre}^{-2} \qquad \ldots.(1.64)$$

where:

B is in gauss, N in electrons per cubic centimetre,

and: L (parsecs) is the line-of-sight distance through magneto-ionic medium.

The observed degree of polarization of the emissions from a distant source will be a maximum if the magnetic fields in the source and medium are uniform.

Most of the Faraday rotation of emission from extragalactic sources occurs within our own galaxy [Hoyle and Ellis, 1963; Gardner and Davies, 1966]. If all the Faraday rotation is assumed to occur within the galaxy, then the term $\int N\, B \cos(\theta)\, dl$ in equation (1.64) may give an estimate of the mean line-of-sight magnetic field strength within the galaxy provided a value of N is known. However, magnetic field reversals over the propagation path make such estimates of field strength unreliable. Measurements of the polarization angles of the emission at a number of different wavelengths permit extrapolation to zero wavelength, giving an estimate of the intrinsic polarization angle, $\psi_{intr.}$ [Gardner and Whiteoak, 1963]. This may provide information about the magnetic field structure within the source.

SECTION 2

SOURCE OBSERVATIONS

Chapter 2.

A Review of Radio Source Observations in the Southern Hemisphere.

A. Introduction.

In this chapter we review the measurements that have been undertaken of discrete extragalactic radio sources south of declination $+27^{o}$. First we consider the calibration method usually used during the source surveys, then we discuss the surveys completed in three frequency ranges: below 45 MHz, 45 to 5009 MHz, and above 5009 MHz.

For more extensive discussions of source measurements the reader is referred to Ryle (1963); Howard and Maran (1965) Shakeshaft (1967) and Scheuer and Williams (1968).

B. Calibration.

Absolute intensity measurements of discrete radio sources are difficult [e.g. Findlay, 1966] and thus most source measurements are calibrated relative to the intensity of a few *standard* or *calibration* sources. The spectra of these sources are obtained by absolute measurements using small aerials of known gain. The flux density scale of Conway, Kellermann and Long (1963) has been used for calibrating many surveys. This scale was determined as follows. Measurements at nine different frequencies between 38 MHz and 3200 MHz were used to define a set of standard

source spectra. The flux density scale was based on absolute measurements of the flux density of Cassiopeia A at frequencies where they were available. At intermediate frequencies the spectra of seven sources were compared to define a new scale based on the mean flux density of the seven sources. The scale of Conway et al. has been modified by Kellermann (1964a) to include new observations and more calibration sources.

C. Source Flux Density Measurements Below 45 MHz.

Measurements of discrete radio sources in this frequency range are complicated by the effects of ionospheric absorption and refraction and by electrical interference. Insufficient resolving power of the telescope will also lead to unreliable estimates of the flux density of sources close together. These difficulties have been discussed extensively in the literature [e.g. Ellis, 1963; Ellis, 1965; Scheuer and Williams, 1968] and we will consider them only where appropriate to determine the reliability of source measurements in the next chapter.

There have been no extensive source surveys undertaken in the southern hemisphere below 45 MHz. Measurements at 4.7 MHz [Ellis et al., 1966] and near 45 MHz [Haynes and Hamilton, 1968 - reported in chapter 3] have been published, but these are limited surveys only. A number of low

frequency surveys made in the northern hemisphere include results for sources south of declination $+27^{\circ}$. These are summarized in table 1 of appendix 2. The most extensive was made at a frequency of 38 MHz [Williams et al., 1966].

D. Source Flux Density Measurements between 45 and 5009 MHz.

Most of the observations of discrete radio sources have been undertaken in this frequency range. Extensive surveys have been completed in the southern hemisphere at frequencies of 85.5 MHz [Mills, Slee and Hill, 1958]; 408, 1410, 2650 MHz ["The Parkes Catalogue of Radio Sources", Ed. J.A. Ekers, 1969]; 635, 1410, 2650 MHz [Shimmins et al., 1968]; 5000 MHz [Kellermann, 1966a] and 5009 MHz [Shimmins et al., 1969]. The Parkes Catalogue gives spectral data of 1800 sources between declination $+20^{\circ}$ and -90° (excluding the regions of the galactic plane and of the Clouds of Magellan). The source information at 1410 and 2650 MHz in this catalogue is complete to the limiting flux density of 4 flux units at the survey frequency of 408 MHz. It should be noted however that some source flux densities at 408 MHz given in the Parkes Catalogue may be overestimated owing to confusion effects [Murdoch and Large, 1968].

Most sources south of declination -20° have been measured at only four frequencies, (85.5, 408, 1410 and 2650 MHz). More data was needed before a detailed study of source spectra could be undertaken.

Northern hemisphere surveys that include results for sources south of declination $+27^{o}$ are given in table 1 of appendix 2.

E. Source Flux Density Measurements above 5009 MHz.

No systematic surveys above 5009 MHz have been undertaken in the southern hemisphere, although measurements by Dent and Haddock (1966), Medd et al. (1968) and Doherty et al. (1968) include results for some sources south of declination $+27^{o}$. Further measurements above 5009 MHz in the centimetre and millimetre wavelength range are needed.

F. Discussion.

Surveys have been undertaken in the southern hemisphere at frequencies of 85.5, 408, 1410, 2650, 5000 and 5009 MHz [see C. above]. Most of the measurements at 1410 MHz and higher frequencies have, however, been of sources discovered at low frequencies. The present data is therefore biassed against sources which are weak at low frequencies (flat spectra sources). Recent measurements at Parkes at 2650 MHz [J. Wall - private communication] indicate that many sources still remain to be found in the southern hemisphere.

A number of authors [Hornby and Williams, 1966; Kellermann and Pauliny-Toth, 1969] have discussed curvature in the spectra of northern hemisphere sources. A similar project has not been possible for sources south of declination 0^{o}, mainly because of the lack of spectral data.

Measurements above 1000 MHz are needed to study sources which are opaque or have cut-offs at centimetre wavelengths; Kellermann and Pauliny-Toth (1969) suggest that more than 50% of northern hemisphere sources are of this type. There is also a need for low frequency data since the only extensive survey completed below 408 MHz is that of Mills et al. (1958) at 85.5 MHz. An analysis of low frequency curved spectra is impossible with only this data.

Early in 1965 a decision was made by workers in Tasmania to build a large low frequency radio telescope to work in the range 3 to 20 MHz [beamwidth 1° at 20 MHz]. The instrument will be used to measure discrete sources and to investigate the distribution of ionized hydrogen in the galaxy. Assuming that source data would be obtained with this telescope, information between 20 MHz and 408 MHz was still required. The author commenced a series of source surveys in this frequency range early in 1967 (see chapter 3). The telescopes used were the 210 ft. and the 60 ft. paraboloids of the Parkes Observatory [geographic coordinates: latitude 32° 59' 55" south, longitude, 148° 15' 50" east]. The observing time available was limited so that, with the exception of the 153 MHz survey, measurements were confined to those sources which possibly have low frequency curved spectra. If the shape of each spectrum can be determined accurately it may be possible to differentiate between models proposed to account for the curvature.

CHAPTER 3.

Low Frequency Source Observations.

A. Introduction.

The results of a number of low frequency source surveys are presented in this chapter. The measurements are discussed under the following headings:

(B). Sources used as calibration standards.

(C). Source flux densities at 10.02 MHz.

(D). Source flux densities at 153 MHz.

(E). Observations of sources which possibly have curved spectra.

Part B outlines the method of calibration used to obtain the source flux densities and discusses the spectra of sources used as calibration standards. The distinction in presentation of the results in C,D and E is made only because the methods of observation and data reduction are different in each case.

B. Sources used as calibration standards.

The measurements reported in this chapter were all calibrated by a relative intensity method using the sources PKS 0915-11, 1648+05 and 1711-00 as calibration sources. The low frequency spectrum of each standard source was determined from the flux density scales of Conway, Kellermann and Long (1963) and Kellermann (1964 a). The spectra of seven other sources were used as secondary standards;

these were: PKS 0106+13, 1120+05, 1226+02, 1330+02, 1932-46, 2152-69 and 2310+05. The spectra of these sources have been determined relative to the primary calibration standards. Figures 3.1 to 3.5 show a compilation of the spectral data available for each calibration source. The data was obtained from the articles listed in table 1 of appendix 2. We have fitted a power-law spectrum to the data of each source (except PKS 1226+02) using a weighted least-squares method. This curve fit is accurate to within 4% in the frequency range 40 to 180 MHz; the results are given in table 3.1 and shown in figures 3.1 to 3.5.

C. Source flux densities at 10.02 MHz.

A high resolution survey of the southern sky has recently been completed [Hamilton and Haynes, 1968]. The map showing the distribution of sky brightness at 10 MHz is discussed in chapter 6; here we present the source results obtained from the survey.

(i) Difficulties of the observations.

Ground based observations of low frequency cosmic radiation are limited by the effects of the ionosphere and by interference. Difficulties may also be encountered in calibrating low frequency measurements. As an introduction to the 10 MHz results we shall briefly discuss these problems.

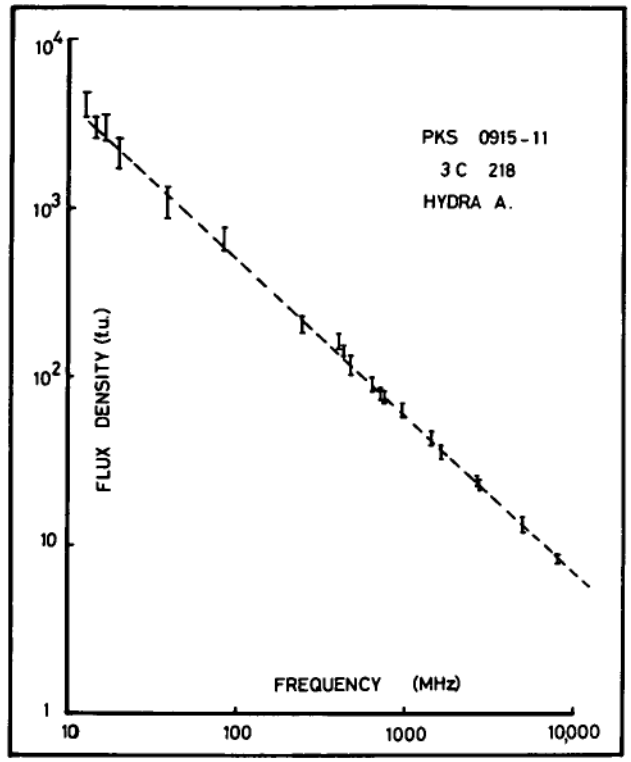
PKS 0915-11
3C 218
HYDRA A.
FLUX DENSITY (f.u.)
FREQUENCY (MHz)
10^4
10^3
10^2
10
1
10
100
1000
10,000

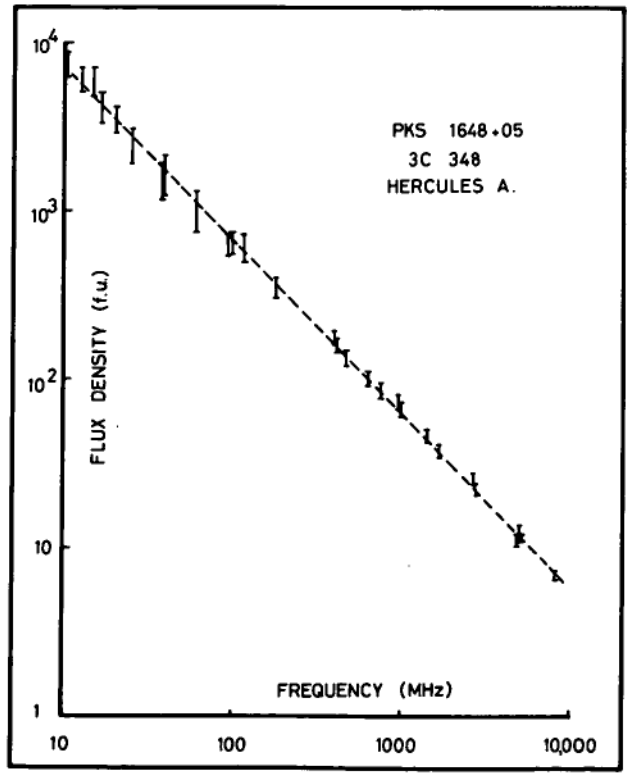
PKS 1648+05
3C 348
HERCULES A.
FLUX DENSITY (f.u.)
FREQUENCY (MHz)
10^4
10^3
10^2
10
1
10
100
1000
10,000

FIGURE 3.1 .

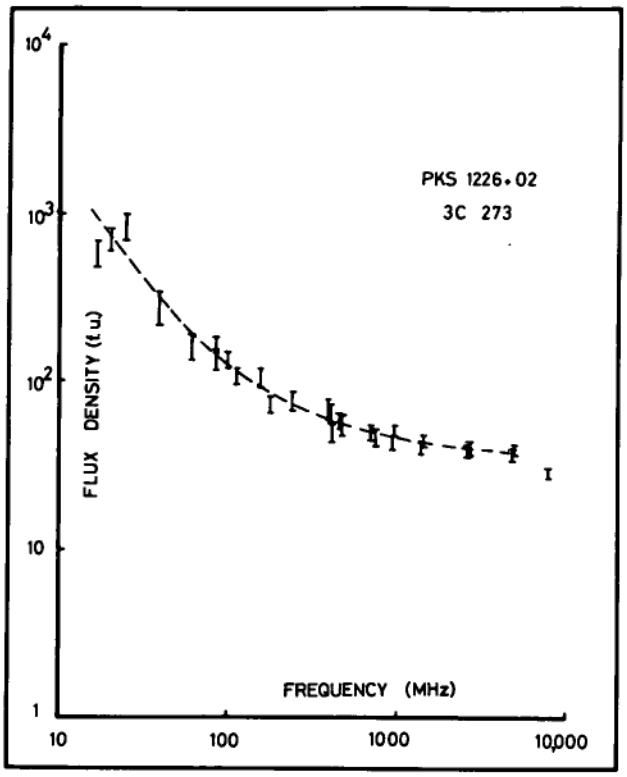
PKS 1226.02
3C 273
FLUX DENSITY (f.u.)
FREQUENCY (MHz)
10^4
10^3
10^2
10
1
10
100
1000
10,000

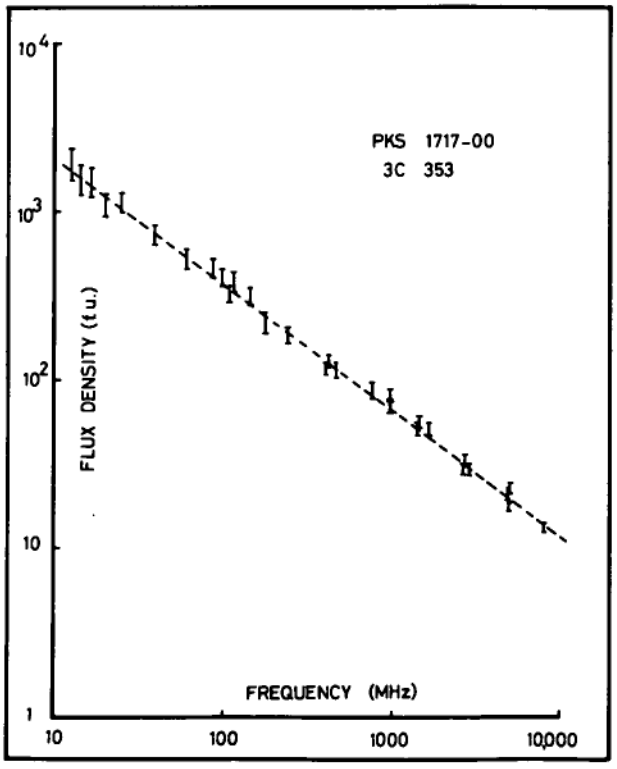
PKS 1717-00
3C 353
FLUX DENSITY (f.u.)
FREQUENCY (MHz)
10^4
10^3
10^2
10
1
10
100
1000
10,000

FIGURE 3.2 .

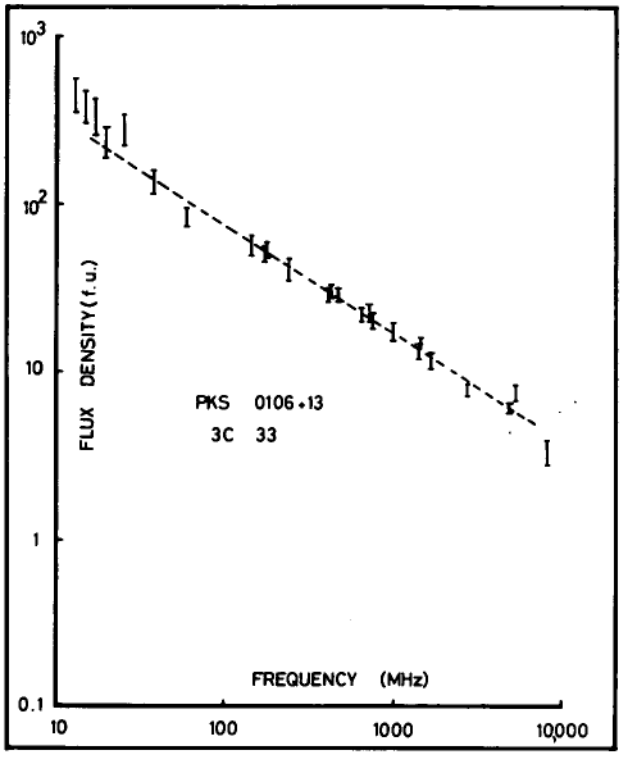
10^3
10^2
10
1
0.1
FLUX DENSITY (f.u.)
PKS 0106+13
3C 33
FREQUENCY (MHz)
10
100
1000
10,000

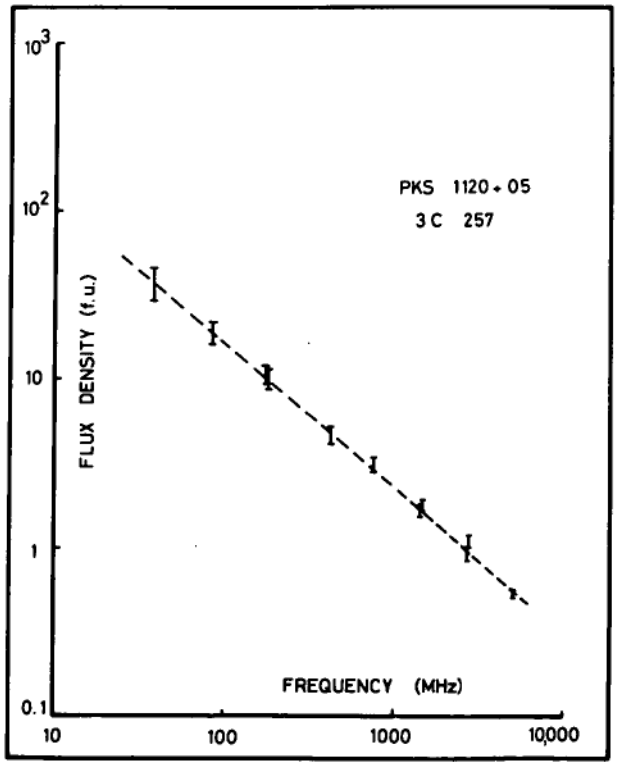
10^3
10^2
10
1
0.1
FLUX DENSITY (f.u.)
PKS 1120+05
3C 257
FREQUENCY (MHz)
10
100
1000
10,000

FIGURE 3.3.

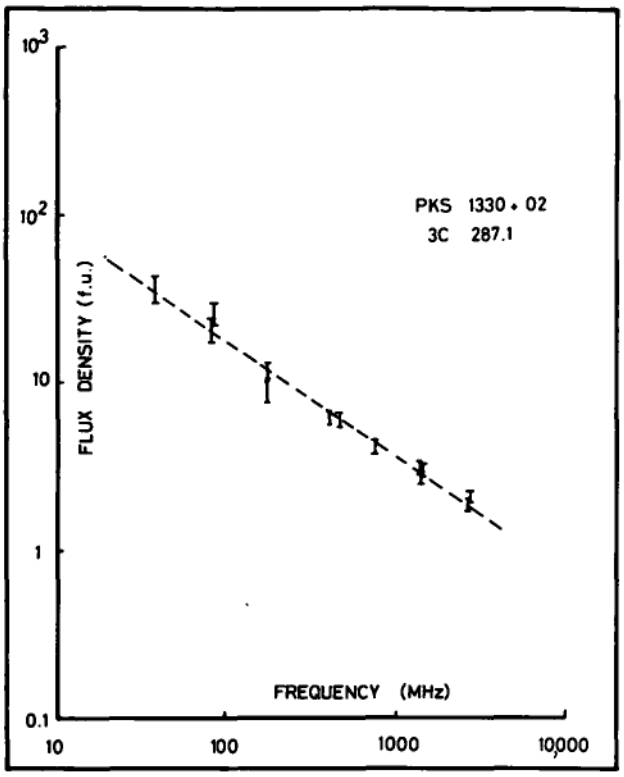
PKS 1330+02
3C 287.1
FLUX DENSITY (f.u.)
FREQUENCY (MHz)
10³
10²
10
1
0.1
10
100
1000
10,000

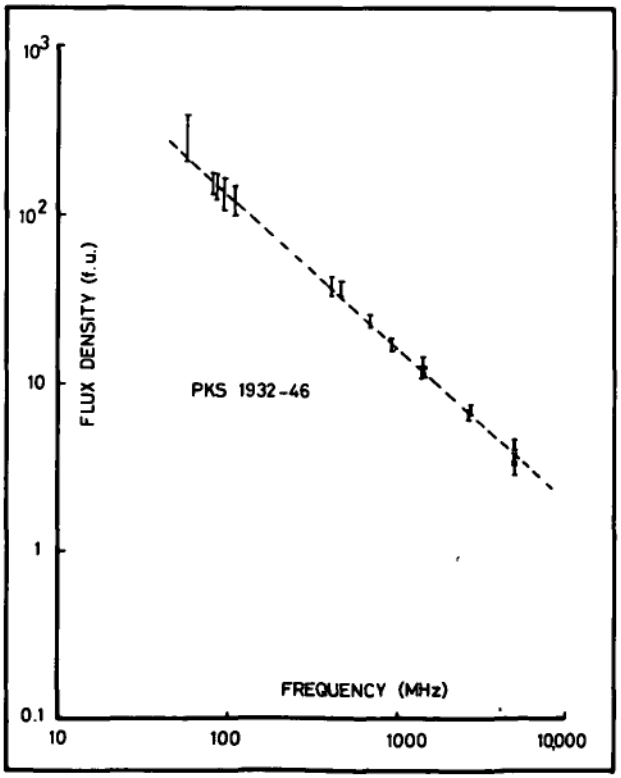
PKS 1932-46
FLUX DENSITY (f.u.)
FREQUENCY (MHz)
10³
10²
10
1
0.1
10
100
1000
10,000

FIGURE 3.4 .

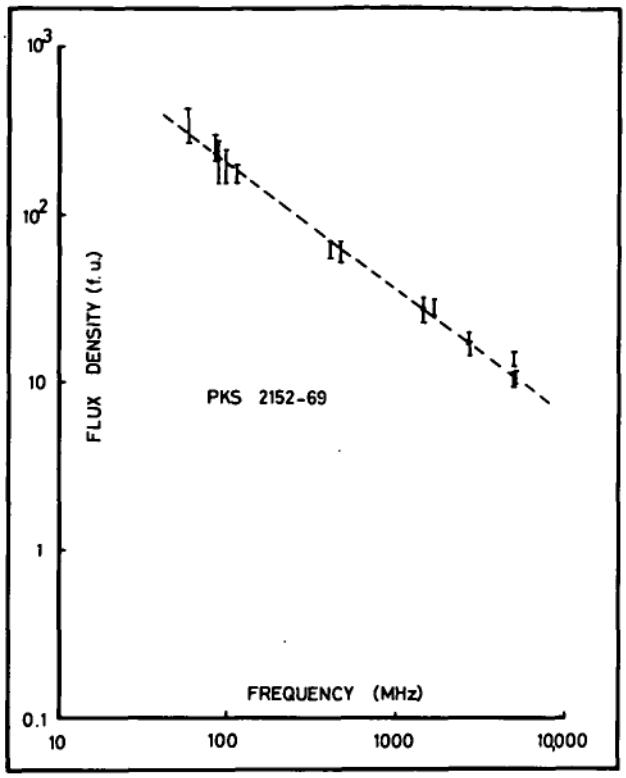
10^3
10^2
10
1
0.1
FLUX DENSITY (f.u.)
PKS 2152-69
FREQUENCY (MHz)
10
100
1000
10,000

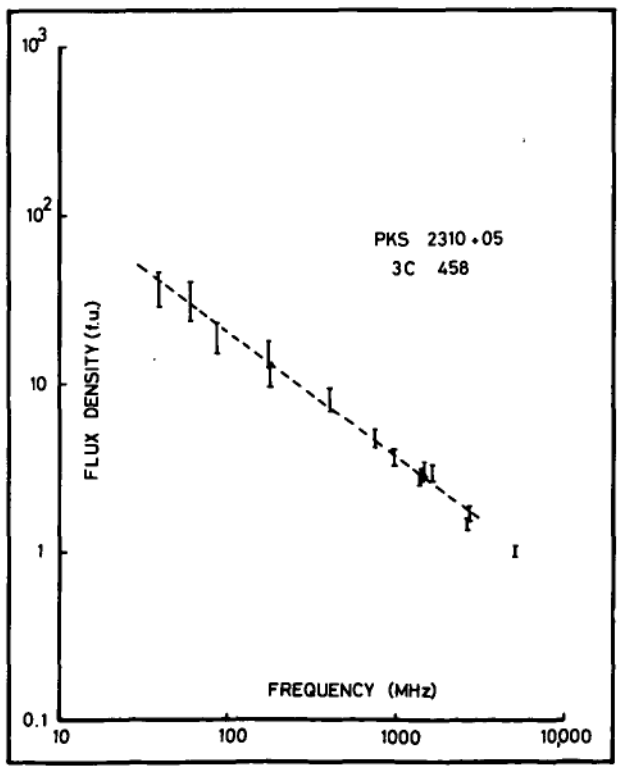
10^3
10^2
10
1
0.1
FLUX DENSITY (f.u.)
PKS 2310+05
3C 458
FREQUENCY (MHz)
10
100
1000
10,000

FIGURE 3.5

POWER-LAW CURVE FITTING RESULTS.

$S(\nu) = A\nu^{\alpha}$

TABLE 3.1

SOURCE (PKS) →	0915-11	1648+05	1717-00	0106+13	1120+05	1330+02	1932-46	2152-69	2310+05
A →	1.77×10^{-16}	1.09×10^{-15}	4.01×10^{-18}	1.40×10^{-19}	1.33×10^{-18}	5.33×10^{-20}	2.56×10^{-17}	2.37×10^{-18}	2.03×10^{-19}
α →	-0.94	-1.03	-0.75	-0.65	-0.86	-0.68	-0.91	-0.75	-0.75

FREQ(MHz)	INTERPOLATED FLUX DENSITIES (flux units*)								
75.0	674.2	852.7	467.9	90.6	20.7	21.1	169.3	254.3	24.7
76.0	665.9	841.2	463.3	89.8	20.5	20.9	167.3	251.7	24.5
79.0	642.0	808.3	449.9	87.6	19.8	20.4	161.5	244.5	23.8
80.2	633.0	795.9	444.9	86.7	19.5	20.2	159.3	241.7	23.5
81.2	625.6	785.8	440.7	86.0	19.3	20.0	157.5	239.4	23.3
82.0	619.9	777.9	437.5	85.5	19.2	19.9	156.1	237.6	23.1
84.0	606.0	758.8	429.6	84.1	18.8	19.6	152.7	233.3	22.7
85.0	599.2	749.6	425.8	83.5	18.6	19.4	151.0	231.3	22.5
132.0	395.8	476.5	305.6	62.4	12.7	14.3	101.1	165.6	16.2
200.0	267.6	310.6	223.5	47.5	8.8	10.8	69.2	120.9	11.8
300.0	182.6	204.6	164.6	36.3	6.2	8.1	47.8	88.9	8.7
400.0	139.2	152.1	132.5	30.0	4.8	6.7	36.8	71.4	7.0
600.0	95.0	100.2	97.6	23.0	3.4	5.0	25.4	52.5	5.2
800.0	72.5	74.5	78.6	19.0	2.6	4.1	19.5	42.2	4.1
1000.0	58.7	59.2	66.4	16.4	2.2	3.5	15.9	35.6	3.5
1200.0	49.4	49.1	57.9	14.5	1.8	3.1	13.5	31.0	3.0
1400.0	42.7	41.9	51.5	13.1	1.6	2.8	11.7	27.6	2.7

* 1 f.u. = 10^{-26} W $m^{-2}Hz^{-1}$

Ionosphere:

Measurements of cosmic radiation from beneath the ionosphere are only possible when the ionospheric critical penetration frequency, f_0F_2, is less than the observing frequency. An examination of world-wide contours of f_0F_2 shows that this quantity is minimal between geomagnetic latitudes of 50° and 60° during winter nights in years of low solar activity. Tasmania is thus ideally situated for low frequency radio astronomy. This can be seen from figure 3.6 which shows the number of hours per day for which f_0F_2 was less than 4 MHz in Hobart between 1961 and 1963 (after Ellis, 1965).

Even when the ionospheric penetration frequency is less than the observing frequency the cosmic radiation passing through the ionosphere undergoes attenuation by absorption and ionospheric screening. These effects have been discussed by Ellis (1965) and from his results it is possible to estimate the attenuation. Table 3.2 and figure 3.7 summarize Ellis' results. Ionospheric screening has also been investigated by Dr. Grote Reber and the author (Haynes, 1966). A high resolution antenna (beamwidth of 8° at 2.1 MHz) was used to investigate the relation between the rate at which the ionospheric "aperture" opened as f_0F_2 decreased at night and the increase in the observed

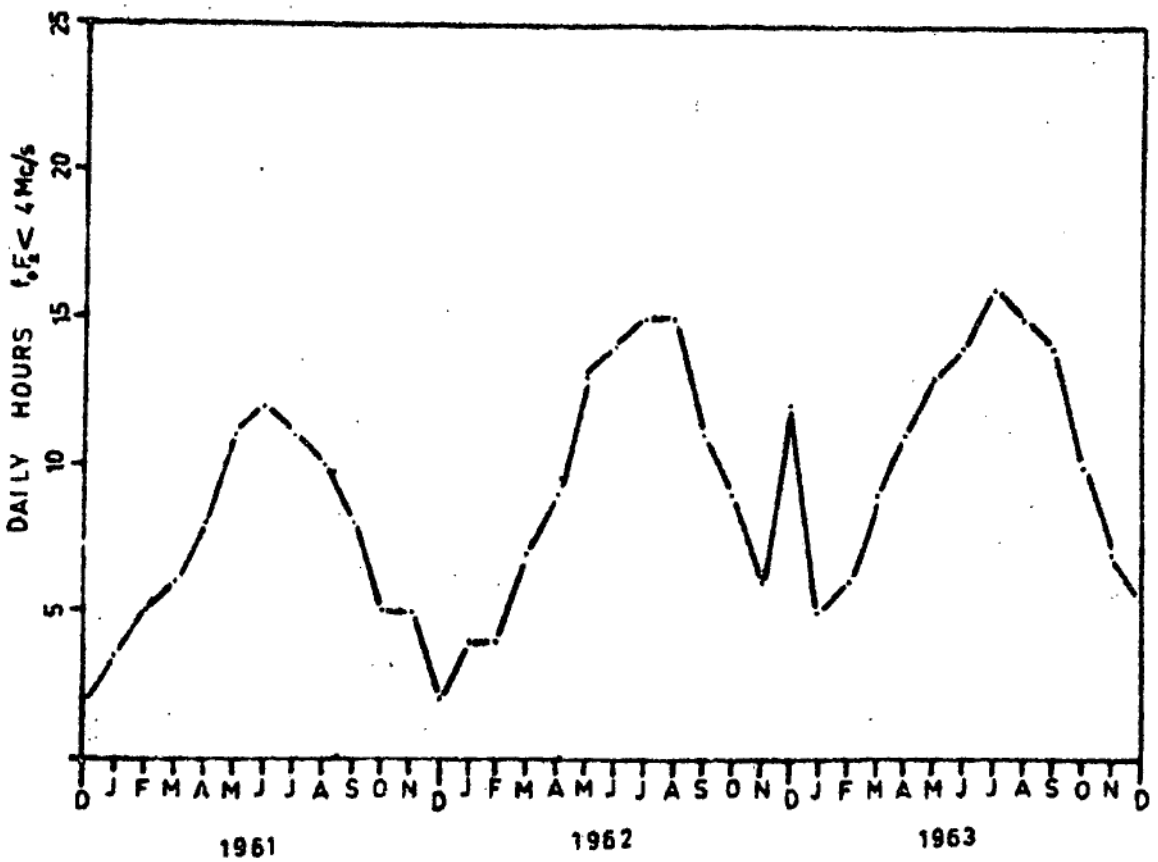

FIGURE 3.6

Number of hours per day that f_0F_2 was less than 4 MHz between 1961 and 1963 in Hobart.

(after Ellis, 1965)

TABLE 3.2

	ATTENUATION dB			
FREQUENCY Mc/s	1.65	2.3	4.8	9.6
	0 mode only			
D REGION	0.25	0.14	0.13	0.05
F REGION	0.1	0.05	0.05	-
F REGION SCREENING	0.6	0.25	0.05	-
GROUND	5.0	1.8	1.0	1.05
TOTAL	5.96	2.24	1.23	1.2

IONOSPHERIC ATTENUATION

(after Ellis, 1965)

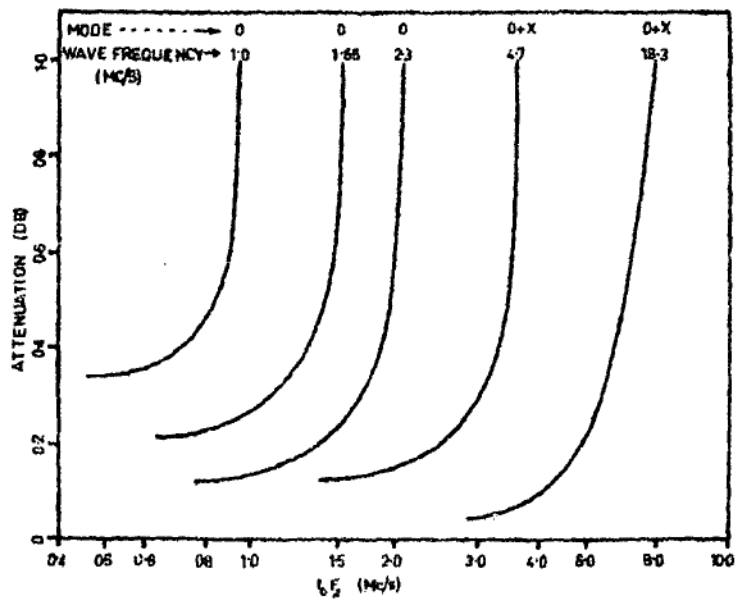

—Ionospheric attenuation as a function of f_0F_2 for different observing frequencies

FIGURE 3.7

(after Ellis, 1965)

intensity of galactic radiation. It was found, for example, that when f_0F_2 was ~ 1.8 MHz, that is 0.3 MHz less than the observing frequency, the ionospheric attenuation was ~ 0.2 dB and the reflectivity of the F layer of the ionosphere was ~ 30%. We would expect the reflectivity to be very small when no attenuation occured. It follows that a significant amount of "leakage" of cosmic radiation through the ionosphere occurs when f_0F_2 is only slightly less than the observing frequency. Observations at 2.1 MHz (Reber, 1968) and 4.7 MHz (Ellis and Hamilton, 1966) in fact, showed that the effects of ionospheric attenuation could be accounted for by a careful selection of the records obtained. The selection process used in the 10 MHz survey is discussed below.

Interference:

The most important problem encountered in low frequency surveys is that of interference, particularly "man-made" interference from transmitting stations, arc welders and the like. This type of radiation can propagate for large distances beneath the ionosphere. Intense interference can usually be identified and the receiver may be tuned to clearer channels. Low level interference is, however, harder to detect and the only reliable method of overcoming it is to repeat measurements a sufficient number of times to obtain reproducible records.

Calibration:

Difficulties may arise in the calibration of a low frequency survey. The equivalent temperature of the galactic radiation below 20 MHz is usually in excess of 10^5 degK and such temperatures are beyond the range of thermal loads and noise diodes. Two methods of calibration have been used by workers in Tasmania. Ellis (1965) used a noise diode and a wide-band amplifier to achieve temperatures similar to that of the sky. This method depends on knowing the characteristics of the amplifier reliably. An alternative method is to relate the low frequency survey to a strong source or a specific region of the sky. In this case the spectrum of the reference must be known. Both of these methods of calibration are subject to errors which, in general, will be greater than those introduced by calibrations at higher frequencies using thermal loads or noise diodes. However, there seems to be no way of overcoming this problem at the present time.

(ii). Equipment:

The 10.02 MHz survey was undertaken at Penna, near Hobart (latitude 42.9° south; longitude 147° east) at the same site as that used for the 4.7 MHz survey discussed by Ellis et al. (1963).

Antenna:

The antenna consisted of a filled rectangular aperture of 24x15 half-wave dipoles at a height of a quarter-wave above the ground. The primary beam response of the array was $4^{\circ}x5^{\circ}$ to the half-power points. Figure 3.8 shows a plan of the array and the computed aerial space factors for the system. Each dipole was connected via an impedance transformer (quarter-wave line) to transmission lines running the full east-west width of the array. The signal from each transmission line then independently passed through a transformer (balun) and a coaxial cable to the input of the receiver.

Receiver:

The total-power receiver has been described elsewhere by Hamilton (1968). It was a multi-channel instrument using a variable intermediate frequency and delay cables to produce six beams in the sky at fixed declinations. Figure 3.9 shows a block diagram of the receiver (after Hamilton, 1968). A similar system to this was used successfully at 4.7 MHz [Ellis et al., 1963; Ellis and Hamilton, 1966].

To help overcome the problem of interference the receiver centre frequency was swept over a frequency range of five to six times the pass band, that is, 10 KHz. A

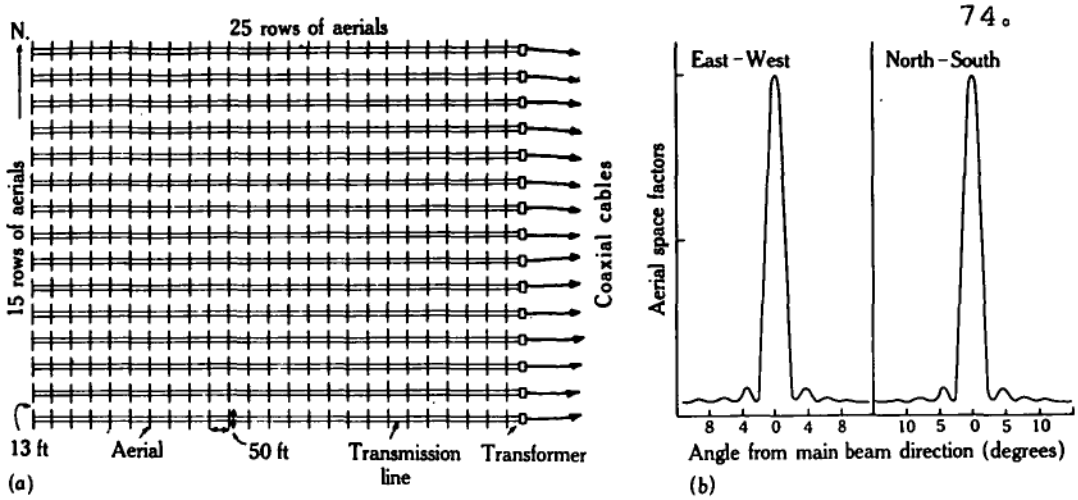

—Details of the receiving system showing (*a*) a plan of the dipole array and feeds and (*b*) computed aerial space power factors (normalized).

FIGURE 3.8.

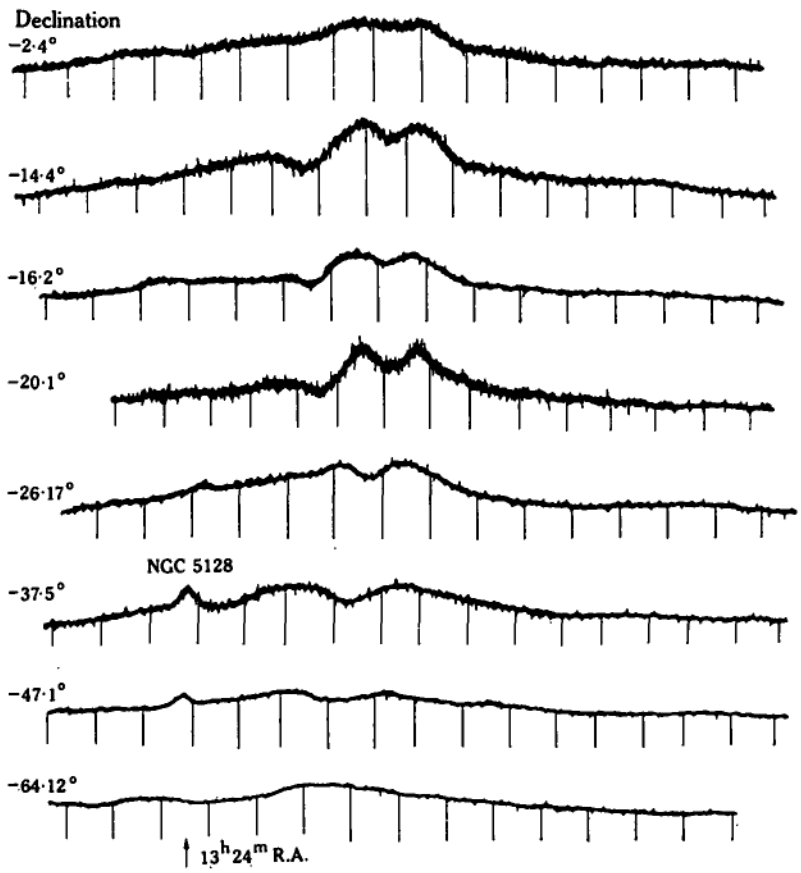

—Sample records at eight declinations.

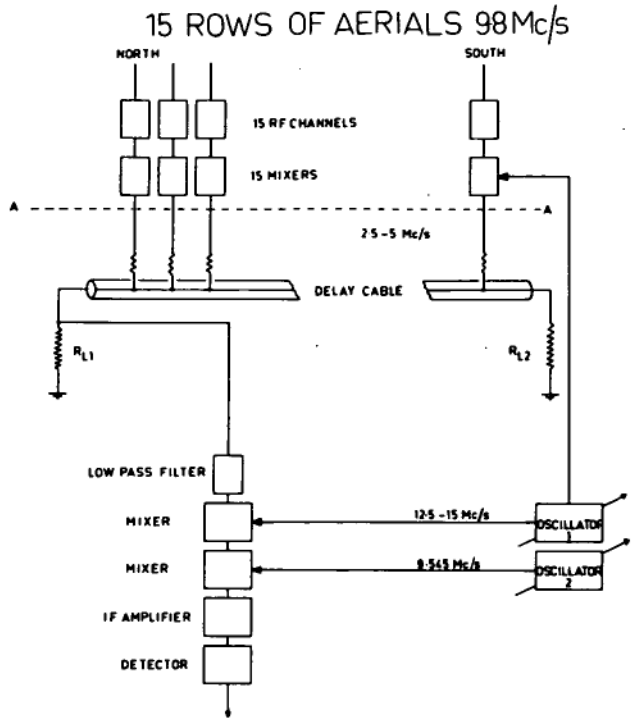

—Block diagram of single beam receiver. The signals from the 15 aerial lines are added in the delay line and the output from the resulting beam appears across R_{L1}.

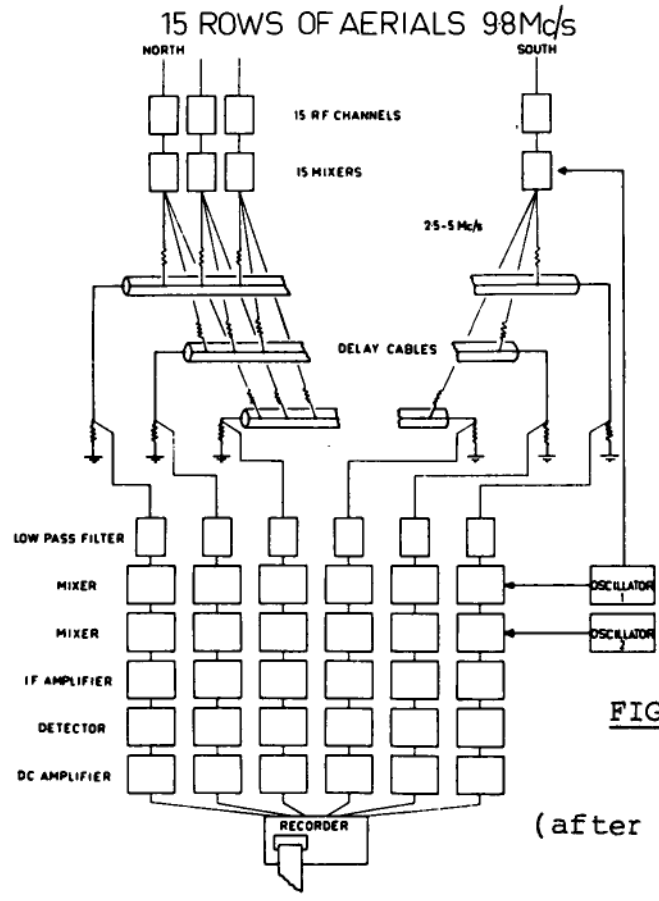

FIGURE 3.9

(after Hamilton, 1968)

—The complete six-beam receiver.

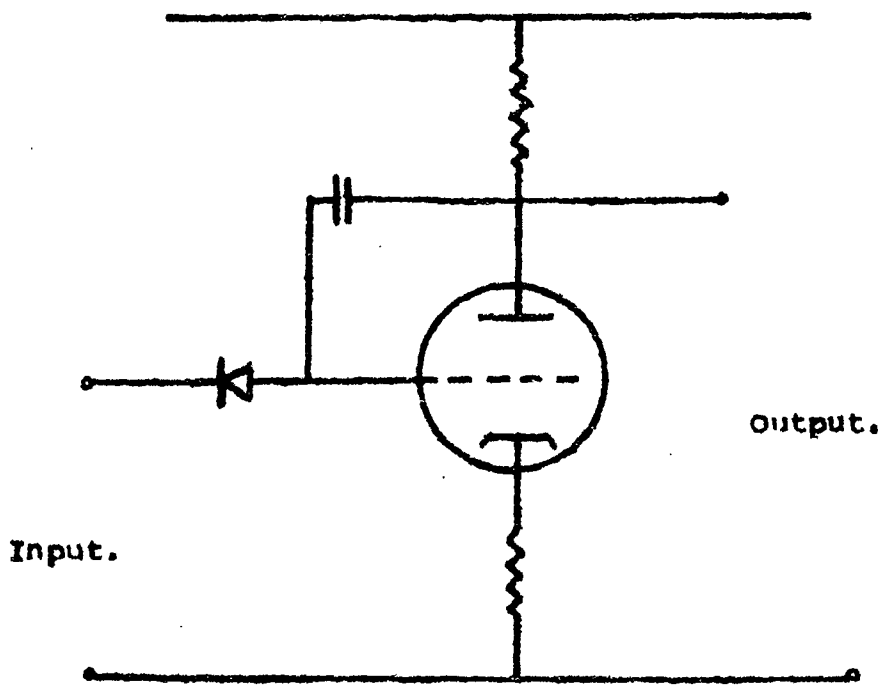

FIGURE 3.10

MINIMUM READING CIRCUIT.

transmitting station within the passband then appeared as a periodic impulse at the second detector of the receiver. A minimum reading d.c. amplifier of the type described by Ellis (1960) followed the detector. This circuit (see (figure 3.10)) ignored the impulse and only the galactic background radiation was recorded. The success of this method of interference-rejection depends on the separation of the stations being greater than the receiver bandwidth, which was 2.1 KHz (-6dB) determined by mechanical filters. Approximately two-thirds of the records were reasonably clear of interference.

(iii). Observing procedure:

The observations were obtained in 1966 and early 1967; the measurements being terminated in February, 1967 when the antenna was destroyed by a bush fire. The results of the 10 MHz survey are based on right ascension scans obtained at fixed declinations between -2.4° and -64°. Once per hour the aerials were disconnected and replaced by dummy loads at room temperature. This gave a check on the zero level and also put time marks on the records. The aerial phasing system required that all the r.f. amplifiers (see figure 3.8) be adjusted to have identical phase shifts and gains and hence the whole receiver was realigned twice weekly. The gain of the receiver was kept constant to within 5% by this means.

Throughout the observations much time was spent at the telescope endeavouring to find channels clear of interference. The only channel that remained clear for up to 6 or 8 hours a day between 9.7 MHz and 10.2 MHz was at 10.02 MHz.

(iv.) Data Reduction.

The results of the 10 MHz survey are based on observations obtained at night when the effects of the ionosphere are minimal. Profiles at each declination were selected for smoothness, reproducibility and absence of interference. The final profile at a given declination was obtained using the method of Ellis and Hamilton (1966). The records of highest intensity were averaged at intervals of 10 minutes in time. The highest records were used since ionospheric absorption, if present, would reduce the intensity. This procedure was not used in the vicinity of the trough observed on the records near 18 Hrs. right ascension. Scattered radiation may possibly reduce the depth of the trough. In this region we selected the records for greatest relative depth compared with the intensity outside the trough. These were the only corrections made to account for ionospheric attenuation since any remaining errors are thought to be less than the errors in reading the records.

Sample declination scans are shown in figure 3.8.

(v). Calibration of the Source Measurements:

The source results have been obtained from the declination scans of the background survey. The flux densities have been determined by taking the source HYDRA A [PKS 0915-11] as a standard. The flux density of this source at 10 MHz is 4,600 flux units (see B above).

(vi). Results:

The short time constant (~ 0.01 second) and the narrow bandwidth (2.1 KHz) required to overcome the problems of interference resulted in rather large fluctuations on the record levels. The measurement of discrete sources was therefore difficult. The minimum reading d.c. amplifier caused further difficulty if the source was scintillating owing to ionospheric irregularities. The minimum observable flux density was calculated to be in the range 800 to 1400 flux units depending on the background intensity (~ 10^5 to 10^6 degK). The flux density results given below are based on four to six reproducible profiles of each source.

The errors in the results are caused by the method of determining the flux density of Hydra A at 10 MHz and from fluctuations on the records. The reliability of each result is indicated in the table of results.

Seven sources were measured at this frequency (see table 3.3). The new observations corroborate the results of Ellis and Hamilton (1966 a) since they confirm that the sources

TABLE 3.3

Source Flux Densities at 10.02 MHz.

PKS Catalogue No.	Position(1950.0) R.A. H	M	S	Decl. °	'	New Results $S_{10.02}$	ERROR	Previous Measurements $S_{4.7}$	$S_{85.5}$	S_{408}	$S_{1410\ MHz}$	
0821-43 0834-46						2800	18%	3600	690 1100			Puppis A (not resolved)
1322-42	13	22	24	-42	45.0	43000	16%	51000	8700			Cent. A
1343-60	13	43	19	-60	10.0	1500	20%		795	242	130	IAU 13 S 6A
1549-56	15	49	01	-56	01.0	1400	20%	2000	270	144	130	Non-thermal
1648+05	16	48	42	+05	04.5	7800	16%		890	141.7	42.8	Herc. A
1711-38	17	11	18	-38	24.0	1600	21%	1500	300	196	77	Non-thermal

Flux Densities at 4.7 MHz are from Ellis and Hamilton, (S00 table 1, appendix 2;)
at 85.5 MHz, from Mills et al., (S15 table 1, appendix 2;)
at 408 and 1410 from the Parkes Catalogue, (S32 table 1, appendix 2;)
and Komesaroff, (S35 table 1, appendix 2;)

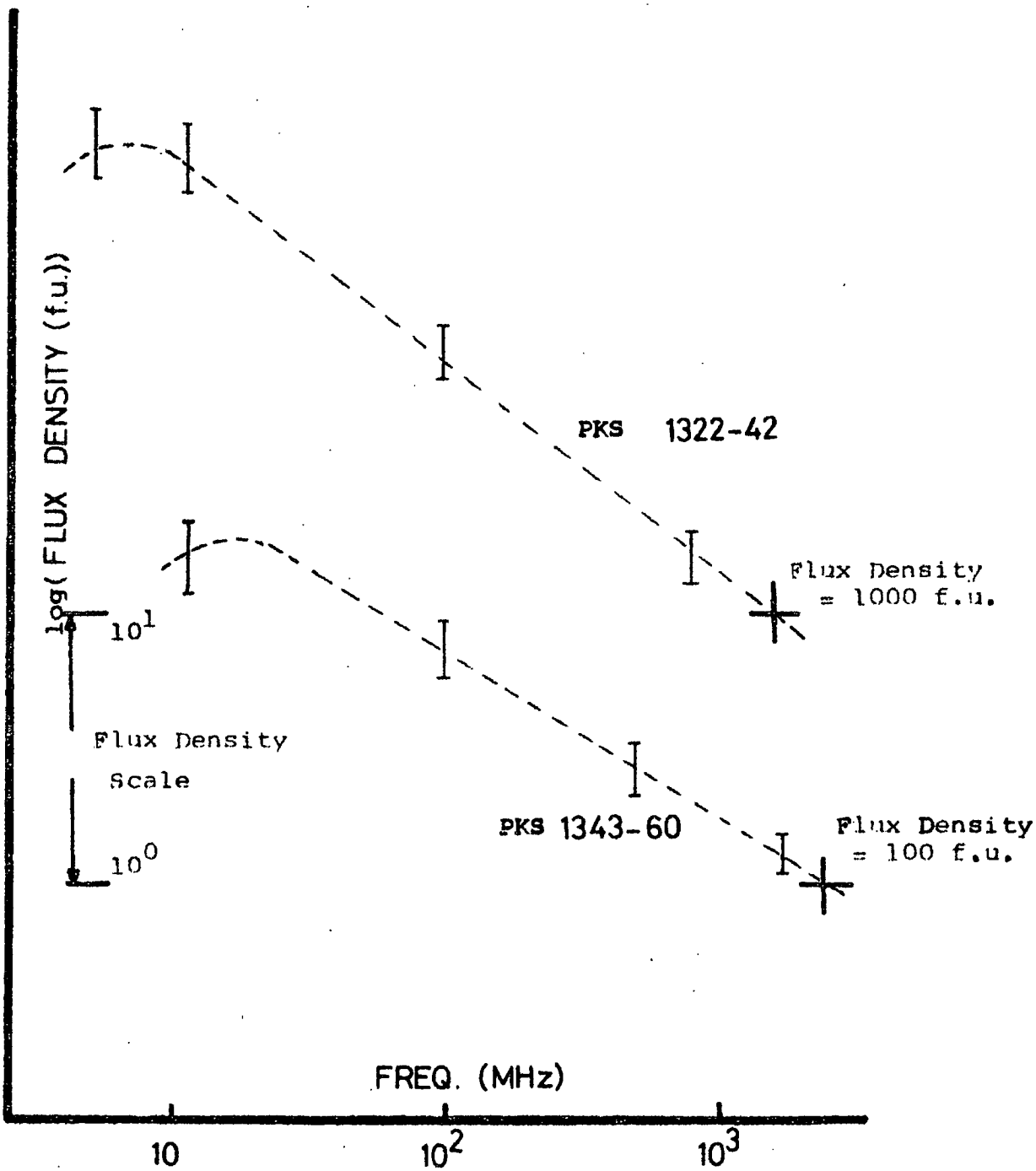

FIGURE 3.11 A

Sources measured at 10 MHz with curved spectra.

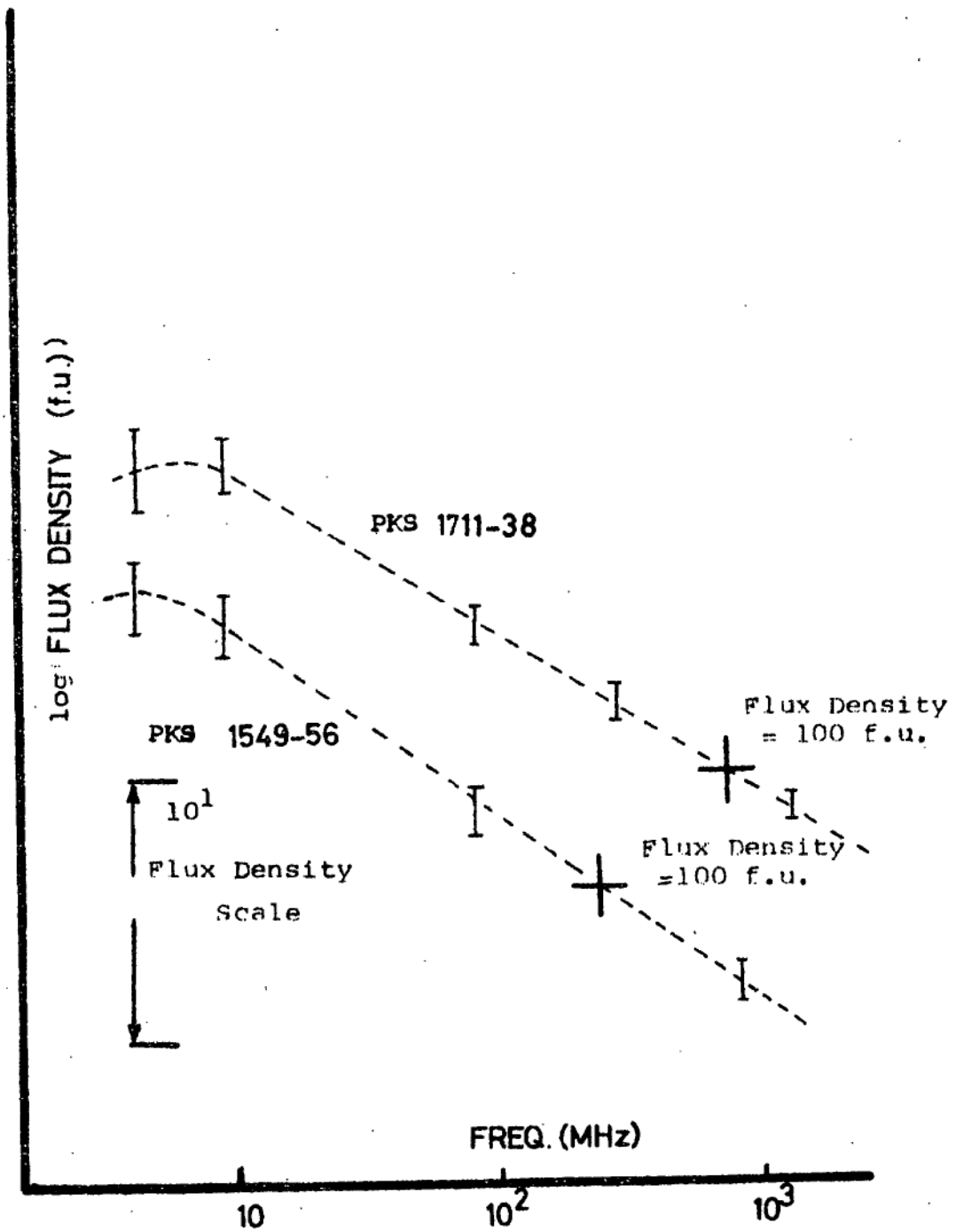

FIGURE 3.11 B

Sources measured at 10 MHz with curved spectra.

PKS 1322-42, 1549-56 and 1711-38 have low frequency curved spectra. The curvature may be attributed to absorption in ionized hydrogen in the galactic plane (see section 3). Figure 3.11 gives the spectra of the sources measured.

D. 153 MHz Source Measurement.

Source measurements were obtained during a galactic background survey at 153 MHz using the Parkes 210 ft. paraboloid. The results of the background survey are discussed in chapter 6; here we present the source results.

(i). Equipment:

The feed system consisted of a pair of half-wave dipoles mounted a quarter-wave above a secondary reflector at the focus of the telescope. Scans of a number of standard sources showed that the primary beam of the telescope at this frequency is close to circular with a Gaussian profile and a half-power beamwidth of 2.18°.

The 153 MHz solid-state, total-power receiver was a standard piece of equipment available at the observatory. It had one stage of conversion to an intermediate frequency of 30 MHz. The i.f. bandwidth was 3.8 MHz and with a second detector time constant of 1 second the peak-to-peak fluctuations on the records were about 1.5 degK.

(ii). Observing Procedure:

The method of scanning the sky consisted of driving the telescope in declination at a rate of 2.5 degrees per minute while keeping the right ascension fixed. Scans were spaced 12 minutes apart in right ascension and were 30° long in declination. The declination scans were tied together using right ascension scans at declinations of $+10^{\circ}$, 0°, -20°, -60° and -80° . For the tie-in scans, the telescope was driven at the maximum rate of 2.5 degrees per minute for 3 hours in right ascension, then pointed to the south celestial pole. This part of the sky was used as a reference for the entire survey. The declination scans were made at closer spacings of 6 minutes in right ascension near the galactic centre to check for fine detail in the emission structure.

Some difficulty was experienced during the survey from "man-made" interference; however this decreased at night and clear channels could be found.

(iii). Calibration:

The two sources Hydra A [PKS 0915-11] and Hercules A [PKS 1648+05] were used as calibration sources for this survey. The flux densities assumed were 340 and 420 flux units for Hydra A and Hercules A respectively (see β above). Scans of these standard sources were used to calibrate the signal from a temperature saturated noise diode used as a

secondary standard. This signal was also compared with hot and cold loads in the course of calibrating the background survey, and the two methods were found to give good agreement.

(iv). Data Reduction:

As a result of the type of scanning grid used, very few scans passed directly through discrete radio sources. The observations had to be corrected as follows to obtain the source flux densities. Charts of each declination scan were examined for sources and the position of each source determined to within the limits of the scanning grid. The Parkes Catalogue of sources [S32 table 1, appendix 2] was searched for sources within 0.6 degrees of the position of each source measured off the charts. Provided that only one source was catalogued within 0.6 degrees and, further, that no strong sources were catalogued within one beamwidth of the telescope position, the observed source was tentatively identified with the catalogued source. The measured flux density was then corrected using the source position given in the Parkes catalogue and by taking the aerial response pattern to be circular and Gaussian.

Some 1300 source profiles were measured from the chart recordings. However, only 312 of these were retained as reliable measurements free from confusion with strong nearby sources.

(v). Errors in the Measurements:

The overall accuracy of the 153 MHz source flux densities is 10% ± 0.8 flux units. The errors result from noise fluctuations on the records and from the calibration technique.

Comparison between corrected flux densities obtained from records on the scanning grid and "on-source" scans of a number of sources indicate that an error of not greater than 2% is introduced for the measurements selected as satisfactory. Fluctuations on the records caused an error of ± 0.8 flux units. Repeated measurements showed that the method of calibrating the noise diode signal and variations in this signal produced an error of 8% of the source flux density.

No attempt was made to keep the position angle of the feed constant during the observations and the effects due to polarization of the source or background radiation have been neglected. These errors, however, will be small compared with the other errors mentioned above.

Source confusion effects were removed by the selection process applied to the records.

(vi). Flux Density Results at 153 MHz:

Details of 248 sources are given in table 3.4, a further 64 measurements are shown in parentheses since the results for these sources may include effects due to a nearby weak source.

(facing page 87)

Explanation of Table 3.4

Column 1: Source catalogue number from the Parkes Catalogue.

Columns 2 and 3: Mean position for epoch 1950.0 (from the Parkes Catalogue).

Columns 4,5,6,7,8, and 9: Flux density in flux units at frequencies of 85.5, 153, 159(or 178, as indicated by an asterisk), 408, 1410 and 2650 MHz. Observations at 85.5 MHz are from the Mills, Slee and Hill (MSH) catalogue; at 159 and 178 MHz from the 3C catalogue and at 408, 1410 and 2650 MHz from the Parkes Catalogue.

Column 10: Spectral index as determined at 400 MHz (C, curved spectrum).

Columns 11 and 12: Catalogue numbers as given in the 3C and MSH catalogues.

References:

3C catalogue: S19 to S22 table 1, appendix 2;

MSH catalogue: S15 table 1, appendix 2;

Parkes Catalogue: S32 - table 1, appendix 2;

TABLE 3.4.

(1)	(2)			(3)		(4)	(5)	(6)	(7)	(8)	(9)	(10)	(11)	(12)
Parkes Cat. No.	Position (1950·0) R.A. h	m	s	Dec. °	′	Flux Densities at (MHz): 85·5	153	159	408	1410	2650	Spectral Index α_{400}	Other Cat. Nos. 3C	MSH
0000+00														
2357+00	23	57	22	+00	26·3		18·0		2·3	<0·5	0·3	1·1±0·2		
0003+00														
0000−17	00	00	48	−17	43·9		14·6		5·5	2·2	1·4	0·7±0·2		
0003−42	00	03	28	−42	52·3	17	14·3		4·6	1·7	0·9	0·8		00−42
0004−83	00	04	09	−83	22·5		24·7		7·9	2·5	1·3			
0007−44	00	07	58	−44	40·0	31	26·8		6·5	1·7	0·9	1·0		00−43
0008−42	00	08	22	−42	10·2		9·3		6·4	5·4	2·6			
0010+00	00	10	34	+00	35·2	20	11·4		5·1	1·6	0·9	0·9±0·1	5	00+02
0012−38	00	12	52	−38	21·1	19	12·8		4·9	1·6	0·7	0·9		00−35
0013−63	00	13	35	−63	27·6	27	13·8		7·4	1·9	0·7	0·8		00−61
0020−25	00	20	38	−25	19·3	21	11·0		4·8	2·4	1·4	0·9		00−27
0021−29	00	21	58	−29	45·7	33	19·9		8·2	3·3	1·6	0·9		00−29
0022−60	00	22	53	−60	46·6		10·9		3·5	1·4	0·7			
0023−13	00	23	32	−13	04·7		(37·1)		5·0	1·3	0·6	1·1±0·2		
0031+01	00	31	49	+01	05·3	20	(18·3)		(3·0)	0·5	0·3	1·2±0·1		00+06
0032−20	00	32	39	−20	20·7	19	7·1		5·9	2·4	1·0	0·7		00−216
0036−62	00	36	30	−62	48·2		8·4		3·1	1·4	0·8			
0036+03	00	36	45	+03	03·5	14	(22·3)		4·1	1·6	1·1	0·7±0·1		00+010
0037+04	00	37	18	+04	39·0		36·6		3·8	0·8	0·5	1·1±0·2		
0047−02	00	47	12	−02	59·8	18	14·6		4·2	1·3	0·8	0·9±0·1		00−014
0048−44	00	48	25	−44	45·1	16	15·6		4·2	1·6	0·7	0·9		
0053−01	00	53	39	−01	34·5		42·2		10·3	2·0	(0·9)	1·2±0·1		00−413
0055−01	00	55	01	−01	39·6	(72)	46·1	17·0	12·1	4·7	3·6	0·6±0·1	29	00−017
0056−17	00	56	38	−17	16·8	29	12·6		5·5	1·7	0·9	1·0±0·1		00−126
0057−18	00	57	42	−18	04·6		(18·5)		3·9	1·2	0·7	0·9±0·2		
0101−12	01	01	53	−12	51·6	18	16·6		4·4	1·8	1·3	0·7±0·1		01−11
0103−45	01	03	06	−45	22·0	41	17·2		7·5	2·8	1·5	1·1		01−41
0105−16	01	05	48	−16	20·4	53	30·1	20·0	12·3	3·8	2·2	0·9±00	32	01−12
0109+02	01	09	32	+02	40·7		8·6		1·9	0·6	0·3	1·0±0·3		
0110−69	01	10	01	−69	17·2		(24·2)		5·5	2·0	1·0			
0114−21	01	14	26	−21	07·7	18	(25·3)		11·6	4·1	1·9	0·3		01−26
0115+02	01	15	49	+02	42·9		13·0		(4·5)	1·5	1·0	0·6±0·3	(37)	
0116−19	01	16	07	−19	05·3	14	(16·7)		2·6	1·2	0·7	0·8±0·1		01−18
0118+03	01	18	29	+03	28·3	(16)	(8·1)		(5·0)	1·2	0·6	1·1±0·3	(39)	(01+03)
0122−25	01	22	26	−25	33·6	9	8·7		4·2	1·3	0·7	0·5		01−29
0123−01	01	23	28	−01	38·5	88	25·1	26·0	16·4	4·5	(1·9)	1·0±0·1	40	01−05
0125−14	01	25	03	−14	18·7	30	23·3		8·9	2·4	1·5	0·8±0·1		01−111
0126−53	01	26	29	−53	10·4	11	10·4		3·8	0·9	0·6	0·7		01−54
0124−40	01	24	12	−40	59·1		12·2			1·4	2·6			
0128+03	01	28	40	+03	58·6	18	(9·1)		5·3	2·2	1·0	0·8±0·1		01+06
0128−26	01	28	07	−26	25·5	18	10·7		5·7	1·2	0·6	0·7		01−211
0129−07	01	29	35	−07	10·8	19	9·3		(4·7)	1·2	0·7	0·9±0·1		01−06
0129−51	01	29	11	−51	18·5	8	(18·3)		3·1	1·0	0·5	0·6		01−55
0131−36	01	31	42	−36	44·6	56	31·7		16	7·1	3·4	0·8		01−311
0132+07	01	32	39	+07	56·2	15	10·7		6·8	2·4	1·3	0·8±0·1		01+08
0137−10	01	37	44	−10	12·3		4·4		(2·0)	1·2	0·6	0·9±0·4		
0139−14	01	39	17	−14	59·6		13·3		2·2	0·4	0·3	1·0±0·3		
0146+00	01	46	16	+00	07·2		19·0		2·6	(0·5)	(0·5)			
0146+06	01	46	08	+06	06·3	19	11·7		3·4	0·8	0·4	1·1±0·1		01+011
0148−29	01	48	20	−29	46·5		11·8		2·8	1·8				01−217
0150+00	01	50	15	+00	07·3		(20·6)		1·9	0·5	0·3	1·0±0·3		
0152−76	01	52	14	−76	29·8		9·3		3·9	0·8				
0157+01	01	57	38	+01	10·3	16	10·1		4·5	0·6	0·4	1·1±0·1		01+014
0157−31	01	57	57	−31	08·2	26	13·4		9·3	3·7	2·4	0·7		01−315
0202−76	02	02	00	−76	34·1	18	11·2		8·0	2·6	1·3	0·6		01−71?
0213−13	02	13	12	−13	13·4	(42)	(30·6)	(13)	11·9	5·0	2·7	0·7±0·1	(62)	02−15
0214−48	02	14	53	−48	03·4	31	18·5		9·5	2·4	1·3	0·8		02−43
0215+02	02	15	50	+02	44·1		24·7		3·5	0·7	0·3	1·3±0·2		
0216−25	02	16	29	−25	03·1	15	(19·3)		4·7	1·3	0·7	0·7		02−25
0218−02	02	18	21	−02	10·5	74	(73·8)	26	12·4	3·9	1·7	1·0±0·0	63	02−07
0220−42	02	20	21	−43	13·9	17	11·5		4·2	0·9	1·6	0·9		02−45
0222−23	02	22	49	−23	26·3	19	16·5		6·2	1·9	1·1	0·7		02−27
0235+09	02	35	46	+09	59·3		14·5		2·6	1·3	(0·4)	0·6±0·3		
0237+09	02	37	43	+09	44·6				(1·1)	<0·5	0·3			

TABLE 3.4. (cont.).

(1)	(2)			(3)			(4)	(5)	(6)	(7)	(8)	(9)	(10)	(11)	(12)
Parkes Cat. No.	Position (1950·0) R.A. h	m	s	Dec. °	′		Flux Densities at (MHz): 85·5	153	159	408	1410	2650	Spectral Index α_{400}	Other Cat. Nos. 3C	MSH
0241−51	02	41	52	−51	22·7		37	22·8		11·8	2·9	0·8	0·7		02−53
0245−55	02	45	27	−55	54·2		48	35·9		12·2	2·4	1·2	0·9		02−54
0246−13	02	46	15	−13	35·3		15	13·7		2·1	0·8	0·6	0·9±0·1		02−114
0255+05	02	55	04	+05	50·7		51	37·3	25*	16·2	5·9	3·3	0·8±0·0	75	02+010
0257−05	02	57	32	−05	44·3			12·0		2·9	0·4	0·3	1·2±0·3		
0304−12	03	04	34	−12	17·6			36·3		5·5	1·5	0·8	1·0±0·2		
0312−03	03	12	54	−03	27·3		20	15·3		4·0	1·2	0·8	0·9±0·1		03−01
0319−45	03	19	39	−45	21·8		19	12·3		9·5	3·4	1·7	0·5		03−43
0320−37	03	20	42	−37	25·0		950	474·2		249		89			03−31
0332−05	03	32	09	−05	44·8			(18·2)		3·3	1·6	1·0	0·6±0·2		
0331−01	03	31	42	−01	21·2		64	43·8	19·5	11·9	2·5	1·5	1·1±0·0	89	03−03
0332−39	03	32	17	−39	10·5		10	(18·7)		4·5	1·7	0·9	0·5		03−32
0336−01	03	36	59	−01	56·2			19·5		3·5	1·5	2·2	C		
0344−34	03	44	40	−34	31·5		33	18·9		9·3	3·0	1·7	0·8		03−36
0347+05	03	47	08	+05	43·0		15	(27·9)		9·0	3·3	2·0	0·7±0·3		03+010
0349−14	03	49	10	−14	38·3		44	16·6	(8·5)	11·6	2·9	(1·4)	0·9±0·4	(95)	03−19
0356+10	03	56	15	+10	17·7			44·2	44*	27·5	10·8	(5·8)	0·7±0·1	98	
0410−75	04	10	11	−75	15·3		87	55·3		40	13·5	7·5	0·5		04−71
0418−05	04	18	22	−05	44·6			(46·5)		3·8	0·8	0·6	0·9±0·2		
0424−26	04	24	41	−26	49·9			18·2		3·7	1·2	0·6			
0427−36	04	27	52	−36	37·5		35	15·2		7·2	2·1	1·1	1·0		04−36
0427−53	04	27	51	−53	56·1		50	39·5		14·6	5·6	2·7	0·8		04−54
0431−13	04	31	49	−13	29·0		(38)	17·9				0·4			04−112
	04	31	55	−13	17·0					(7·7)	1·4	0·8	1·1±0·1		
0442−28	04	42	38	−28	14·8		82	66·0		22	7·1	3·9	0·9		04−218
0446−20	04	46	25	−20	36·0		19	18·6		4·2	0·9	0·4	1·0		04−219
0448−04	04	48	30	−04	36·4		(23)	6·9		(5·0)	(0·7)	0·5	1·1±0·1		04−117
0452+10	04	52	20	+10	04·4			13·7		2·8	0·6	0·3	1·2±0·3		
0453−20	04	53	13	−20	40·5		18	(18·1)		9·3	4·7	3·1	0·4		04−222
0455−40	04	55	49	−40	29·9		13	9·5		3·7	1·0	0·6	0·8		04−410
0456−30	04	56	33	−30	10·8			28·2			2·7	1·6			
0458+01	04	58	08	+01	26·5		15	11·3		3·4	0·8	0·6	0·9±0·1		04+114
0502−10	05	02	30	−10	19·5		20	7·0		4·8	1·4	0·8	0·9±0·1		05−11
0503−28	05	03	42	−28	59·7		30	26·7		5·5	1·1	0·6	1·1		05−22
0508−07	05	08	37	−07	38·1			(21·4)		3·1	1·1	0·6	0·8±0·2		
0510−04	05	10	18	−04	0·18			25·5		3·1	0·6	0·5	0·9±0·3		
0511−30	05	11	44	−30	31·7		29	10·1		8·9	2·7	1·2	0·8		05−35
0511−48	05	11	35	−48	28·0		41	(43·8)		13·2	3·5	2·1	0·7		05−42
0514+10	05	14	05	+10	53·3			(21·3)		3·3	1·1	0·7	0·8±0·2		
0517−56	05	17	36	−56	16·3			30·7		4·6	1·2	0·8			
0518−45	05	18	24	−45	49·8		570	343·0		166	66	30	0·8		05−43
0521−36	05	21	14	−36	30·0		66	54·5		37	18·6	11·4	0·4		05−36
0532−05	05	32	51	−05	25·0		(69)	41·6	45	(213)	(289)	(49·0)	HII region	145	05−011
0604−20	06	04	29	−20	22·2		23	20·0		8·9	3·3	2·0	0·6		06−22
0611−74	06	11	36	−74	30·0			5·4		2·6	1·1				
0612−47	06	12	16	−47	26·1		27	12·2		5·8	1·2	0·7	1·0		06−43
0625−53	06	25	18	−53	39·3		113	73·3		26	6·7	3·5	1·0		06−55
0637−75	06	37	20	−75	14·4		20	13·0		9·7	6·7	4·9	0·4		06−71
0646−39	06	46	33	−39	53·1		26	23·6		7·0	2·6	1·5	0·8		06−312
0651−56	06	51	53	−56	38·3		18	8·6		4·9	1·1	0·7	0·8		06−57
0656−24	06	56	54	−24	12·5		59	50·3		13·0	3·1	1·3	1·0		06−216
0709−20	07	09	39	−20	37·3		33	26·8		8·7	2·0	1·1	0·8		07−23
0710+11	07	10	12	+11	52·1			21·8	17·2*	8·6	2·7	1·3	1·0±0·1	175	
0727−36	07	27	20	−36	34·3			8·3		4·9	2·0	1·3			
0748−44	07	48	08	−44	04·7		27	14·6		8·0	2·3	1·1	0·8		07−413
0800−09	08	00	15	−09	49·8			8·0		6·1	1·7	(1·1)	1·0±0·2		
0806−10	08	06	31	−10	19·1		40	25·4	21·0	13·7	3·4	2·3	0·8±0·0	195	08−14
0809−05·2	08	09	33	−05	10·9			25·1			0·6				
0809−05·7	08	09	35	−05	40·8		22			4·8	1·3	0·8	0·9±0·1		08−04
0812−02	08	12	56	−02	59·3		35	19·5		(9·4)	1·6	0·9	1·0±0·1	196·1	08−05
0812+02	08	12	51	+02	04·8		22	26·6		6·0	2·0	1·0	0·9±0·1		08+02
0818−74	08	18	57	−74	44·6			(47·2)			0·6				
0819+06	08	19	53	+06	06·9		60	(62·7)	17·8*	6·6	2·3	(0·8)	1·1±0·1	198	08+03
0825−20	08	25	07	−20	16·3		26	20·6		11·7	3·7	2·1	0·5		08−24
0832−07	08	32	36	−07	36·0		13	11·1		3·5	0·4		1·1±0·2		08−010

* Flux values measured at 178 MHz.

TABLE 3.4. (cont.).

(1)	(2)			(3)			(4)	(5)	(6)	(7)	(8)	(9)	(10)	(11)	(12)
Parkes Cat. No.	Position (1950·0) R.A. h	m	s	Dec. °	′	″	Flux Densities at (MHz): 85·5	153	159	408	1410	2650	Spectral Index α_{400}	Other Cat. Nos. 3C	MSH
0837−12	08	37	27	−12	04	1		27·9		5·7	1·8	1·0	0·9±0·2		
0842−75	08	42	12	−75	29	5	58	51·6		10·5	4·3	2·4	1·1		08−71
0843−33	08	43	10	−33	38	3	17	(26·6)		4·6	2·0	1·3	0·8		08−38
0850−20	08	50	47	−20	36	0	19	(11·9)		6·2	2·2	1·3	0·7		08−216
0850−03	08	50	56	−03	29	3		13·8		4·3	1·2	0·8	0·8±0·2		
0851−14	08	51	28	−14	16	7	24	(48·0)		6·1	1·6	0·9	0·9±0·1	209	
0853+03	08	53	00	+03	24	4		(84·5)		2·6	0·7	0·4	1·0±0·3		
0855−19	08	55	48	−19	39	3	17	(15·4)		3·4	1·3	1·0	0·8±0·1		08−119
0859−05	08	59	58	−05	04	4	18	13·9		5·0	1·0	0·6	1·0±0·1		08−015
0859−14	08	59	55	−14	04	0	12	8·6		5·4	3·1	2·6	0·4±0·1		09−11
0859−25	08	59	37	−25	44	2	54	51·0		16·4	5·8	3·3	0·8		08−219
0905+04	09	05	17	+04	26	8		12·2		2·9	0·6	0·3	1·2±0·3		
0905−68	09	05	59	−68	16	9		18·0		6·1	1·7	0·9			
0906+01	09	06	27	+01	33	7		(66·7)		2·6	1·3	1·2	0·3±0·2		
0909+08	09	09	30	+08	23	8	13	7·2		2·3	0·8	0·4	1·0±0·1		09+01
0912−16	09	12	53	−16	18	9		13·4		2·7	0·8	0·4	1·0±0·3		
0933+04	09	33	51	+04	36	9	24	(24·3)	9·7*	5·1	0·9	0·3	1·2±0·1	222	09+03
0941+10	09	41	34	+10	00	0	32	17·7	14·6*	8·7	2·3	1·0	1·0±0·0	226	09+05
0943−76	09	43	25	−76	06	7		48·1		6·6	2·1	1·2			
0944−13	09	44	58	−13	32	5		12·2		3·2	0·6		1·2±0·3		
0945+07	09	45	06	+07	39	9	89	41·0	30·0*	22·1	7·8	4·3	0·8±0·0	227	09+07
0949+00	09	49	26	+00	11	8	(36)	33·6	23·0*	(12·0)	(3·2)	1·5	1·0±0·1	230	} (09+08)
0950+00	09	50	13	+00	14	4	(36)	37·0		(12·0)	(3·2)	0·5			
0955−28	09	55	50	−28	50	2	18	(27·3)		6·0	1·4	0·7	0·7		09−212
0955+03	09	55	33	+03	39	7	18	7·8		4·4	0·9	0·4	1·1±0·1		09+010
0957+00	09	57	42	+00	19	5		10·7		3·1	1·0	0·6	0·9±0·2		
1002−21	10	02	52	−21	33	3	48	33·1		7·7	1·8	0·7	1·2		10−21
1005+07	10	05	20	+07	46	1	30	22·3	26*	16·4	6·2	3·5	C	237	10+01
1008+06	10	08	19	+06	40	0	39	24·0	14·0*	12·3	3·1	1·3	C	238	10+02
1011+31	10	11	33	−31	37	6	10	9·1		3·7	1·4	0·9	0·6		10−33
1015−31	10	15	55	−31	28	5	14	14·1		5·5	3·5	3·0	0·6		10−35
1023+06	10	23	54	+06	44	4	35	13·0		5·2	0·9	0·4	1·3±0·1	243	10+06
1027+00	10	27	35	+00	51	9		11·2		2·1	1·0	0·9	0·4±0·3		
1030−34	10	30	58	−34	03	4	20	13·7		6·2	1·4	0·8	0·8		10−38
1031−40	10	31	13	−40	48	2		14·0		4·2	1·2	0·4			10−410
1031+11	10	31	23	+11	30	0		(49·5)		5·1	1·3	(0·5)	1·1±0·2		
1056+09	10	56	59				19	17·6		3·2	0·5	0·3	1·2±0·1		10+011
1108+03	11	08	48	+03	25	5	15	12·8		4·7	1·2	0·5	1·0±0·1		11+02
1110−01	11	10	59	−01	56	8	18	10·2	8·0	4·6	1·4	0·9	0·8±0·1	253	11−05
1116−02	11	16	51	−02	46	7	31	19·5	15·0	10·2	1·6	0·6	C	255	11−08
1116−46	11	16	05	−46	17	9		21·4		7·3	2·4	1·6			
1122−37	11	22	56	−37	06	0	7	9·1		4·9	1·3	0·7	0·2		11−32
1123−35	11	23	28	−35	06	7	17	17·7		7·2	2·6	1·6	0·5		11−33
1131−17	11	31	51	−17	12	1	(19)	11·3		4·7	1·5	0·9	0·8±0·1		(11−17)
1131−19	11	31	08	−19	37	9	32	18·0		4·6	1·2	0·5	1·1±0·1		11−16
1134+01	11	34	53	+01	34	1		15·5		3·6	1·1	0·6	1·0±0·2	(262)	
1136−13	11	36	38	−13	34	1	44	42·6		12·8	4·1	2·8	0·8±0·0		11−18
1136−32	11	36	48	−32	05	8	28	23·8		5·8	2·5	1·2	1·0		11−38
1138+01	11	38	37	+01	30	1	15	(17·9)		7·2	2·1	1·6	0·7±0·1	(262)	11+08
1138−26	11	38	02	−26	12	9	28	8·9		4·1	0·9	0·4	1·2		11−27
1143−48	11	43	04	−48	19	3	28	30·1		9·3	3·3	1·8	0·7		11−46
1146+05	11	46	17	+05	12	4	11	7·6		(3·0)	0·6	0·3	1·0±0·1		11+012
1146−11	11	46	36	−11	48	1	17	13·8		4·2	1·4	0·7	0·9±0·1		11−113
1148−00	11	48	10	−00	07	2		7·8		3·5	2·9	2·6	0·1±0·2		
1152+04	11	52	23	+04	40	4	12	(13·7)		4·0	0·8	0·3	1·1±0·1		11+013
1211−41	12	11	39	−41	43	2	18	(21·2)		5·1	1·6	1·0	0·8		12−41
1215−45	12	15	28	−45	45	2	19	11·3		10	5·4	3·2	0·4		12−43
1226+02	12	26	34	+02	19	1	167	(150·1)	72*	55·1	41·2	37·3	C	273	12+08
1232−41	12	32	59	−41	36	5	11	7·3		7·1	2·2	1·0	0·3		12−44
1245−19	12	45	45	−19	43	0		19·1		7·9	5·1	3·5	0·4±0·1		
1245−41	12	45	54	−41	01	7	45	34·6		10·3	4·1	2·4	1·0		12−45
1246+09	12	46	17	+09	33	1	14	8·7		4·2	0·8	0·4	1·1±0·1		12+010
1247−19	12	47	41	−19	29	7		14·3		4·3	1·2	0·7	0·9±0·2		
1249+09	12	49	11	+09	12	2		7·2		5·1	1·8	1·0	0·9±0·1		
1252−12	12	52	00	−12	17	1	53	37·9	42·0	17·6	6·8	4·5	0·7±0·0	278	12−118
1259−44	12	59	38	−44	30	4		8·2		4·2	1·7	0·9			

* Flux values measured at 178 MHz.

TABLE 3.4. (cont).

(1)	(2)			(3)			(4)	(5)	(6)	(7)	(8)	(9)	(10)	(11)	(12)
Parkes Cat. No.	Position (1950·0) R.A. h	m	s	Dec. °	′		Flux Densities at (MHz): 85·5	153	159	408	1410	2650	Spectral Index α_{400}	Other Cat. Nos. 3C	MSH
1306−09	13	06	01	−09	34·5		19	(21·1)		10·0	4·4	2·8	0·6±0·1		13−02
1307−001	13	07	14	−00	03·7		(25)			2·7	1·5	0·7	0·9±0·1		(13−03)
1307+00								20·8							
1307−00·7	13	07	51	−00	43·4		(25)				0·7				
1309−22	13	09	00	−22	00·9		61	31·1		22	5·4	2·6	0·7		13−23
1312−18	13	12	24	−18	42·6		22	12·8		(6·4)	1·2	0·6	1·0±0·1		13−14
1313−13	13	13	46	−12	11·0			(26·4)		(4·1)	1·2	0·6	1·0±0·3		
1331−09	13	31	14	−09	52·5		18	(14·0)		(6·7)	(1·6)	0·6	0·9±0·1		13−16
1332−33	13	32	58	−33	37·9		70			32	7·0	3·2			
1333−33	13	33	44	−33	43·0		70	(78·3)		32	7·0	1·4			13−33
1334−33	13	34	47	−33	54·2		70			32	7·0	2·3			
1334−29	13	34	11	−29	36·3		36	22·1		8·5	2·6	1·3	0·9		13−25
1335−06	13	35	31	−06	11·9		35	19·3		10·1	3·2	1·9	0·8±0·1		13−011
1348−12	13	48	09	−12	57·4			20·0		4·2	1·3	0·6	1·0±0·2		
1355−41	13	55	56	−41	38·0		35	22·0		13·2	4·6	2·6	0·7		13−45
1358−11	13	58	58	−11	22·0		13	22·1		5·0	2·0	1·0	0·7±0·1		13−117
1400−33	14	00	58	−33	48·0		57	34·4		10·3	0·8	0·3	1·1		14−32
1401−05	14	01	16	−05	11·6			7·1		3·4	0·6	0·3	1·3±0·3		
1411−30	14	11	44	−30	12·4			17·3		4·2	1·4	0·7			
1416−15	14	16	14	−15	41·9		(22)	12·1		(5·1)	1·7	1·2	0·8±0·1		14−14
1420−27	14	20	06	−26	14·2		40	32·4		8·9	2·6	1·3	1·0		14−28
1424−11	14	24	55	−11	50·9		22	(31·0)		4·4	1·4	0·6	1·0±0·1		14−110
1424+03	14	24	57	+03	29·3			7·5		3·0	0·7	0·4	1·1±0·2		
1425+04	14	25	42	+04	33·3		13	(14·6)		3·1	0·8	(0·3)	1·0±0·2		14+07
1434+03	14	34	24	+03	27·2		31	22·7		8·1	2·7	1·8	0·8±0·1		14+010
1445−16	14	45	30	−16	08·0			11·8		3·0	1·2	1·2	0·4±0·2		
1446+00	14	46	10	+00	30·2			8·7		3·1	1·7	1·0	0·7±0·2		
1446+04	14	46	28	+04	13·8			(23·4)		2·4	0·8	(0·4)	0·9±0·4		
1451−36	14	51	21	−36	28·8		41	(47·4)		11·5	2·9	1·5	0·8		14−38
1459−41	14	59	11	−41	54·3		55	32·9		17·4	4·7	1·4	0·7		14−415
1508−05	15	08	13	−05	31·8		8	(17·2)		8·9	3·9	2·5	C		15−05
1510−08	15	10	09	−08	54·9			(9·7)		3·0	3·0	3·0	−0·0±0·2		
1514+00	15	14	14	+00	26·1		16	(17·7)		4·4	2·5	1·8	0·6±0·1		15+06
1514+07	15	14	18	+07	12·6		140	43·0	46*	26·4	5·6	2·2	1·2±0·0	3·7	15+05
1523+03	15	23	23	+03	19·2			14·8		5·0	2·2	1·2	0·8±0·1		
1539−09	15	39	26	−09	18·3			7·3		2·4	1·2	1·0	0·4±0·3		
1547−79	15	47	45	−79	32·6			33·0			4·0	2·8			
1549−79	15	49	36	−79	06·3			(20·1)			6·2	4·9			
1603+00	16	03	42	+00	08·6		35	30·5		(7·9)	2·2	1·4	0·9±0·1		16+03
1609−14	16	09	17	−14	12·0			(33·6)		2·3	1·2	(0·4)			
1621−11	16	21	13	−11	34·0		20	21·3		8·6	2·2	1·3	0·8±0·1		16−18
1635−14	16	35	55	−14	10·0			9·2		(4·3)	1·2	1·0	0·6±0·3		
1640−15	16	40	59	−15	20·2		30	(27·7)		5·7	1·2	0·5	1·1±0·1		16−117
1648+05	16	48	42	+05	04·5		890	424	350*	161	46·0	24·6	1·0±0·0	348	16+010
1644−10	16	44	43	−10	39·0			(42·9)		6·9	2·2	1·4	0·8±0·1		
1701+05	17	01	08	+05	06·1			5·5		3·1	0·6	0·3	1·2±0·2		
1712−03	17	12	25	−03	17·7		21	(53·0)		8·3	1·5	0·5	C		17−04
1712−12	17	12	51	−12	03·0			(10·0)		3·1	1·0	0·6	0·8±0·2		
1717+00	17	17	56	−00	55·9		475	324·7	180*	138	50·2	27·5	0·8±0·2	353	17−06
1754−59	17	54	35	−59	46·3		25	44·4		15	3·9	1·5	0·4		17−51
1802+11	18	02	44	+11	01·3			(169·9)	15*	4·3	1·1	0·7	1·1±0·1	368	
1914−45	19	14	04	−45	36·5		13	28·1		3·5	0·8	0·4	0·8		19−42
1928−34	19	28	25	−34	01·7			13·1		3·1	1·2	0·4			
1932−46	19	32	20	−46	28·2		141	(157·2)		39	13·4	6·9	0·8		19−46
1933−58	19	33	18	−58	45·9		17	25·4		6·8	3·5	1·8	0·6		19−56
1951−50	19	51	25	−50	09·9		14	(23·2)		4·0	1·5	0·9	0·8		19−42
1954−55	19	54	21	−55	17·8		54	21·6		14·8	7·0	4·0	0·8		19−57
1955−35	19	55	43	−35	43·3		45	17·5		9·6	2·4	1·2	1·0		19−35
2006−56	20	06	31	−56	37·8		81	(87·3)		12·2	1·9	0·4	1·2		20−52
2019+09	20	19	43	+09	52·0		27	15·8	15*	9·4	3·4	1·4	0·9±0·0	411	20+031
2030−23	20	30	18	−23	02·8		22	13·1		8·2	3·0	1·6	0·6		20−28
2032−35	20	32	35	−35	05·1		41	19·9		12·8	6·4	3·7	0·7		20−37
2044−02	20	44	34	−02	47·5			9·6	9·5	7·2	2·3	1·5	0·7±0·1	422	
2045+06	20	45	40	+06	50·1		22	41·6	13·4*	(9·8)	2·6	1·1	0·9±0·1	424	20+010
2049−36	20	49	08	−36	51·8		19	11·4		4·3	1·4	0·6	1·0		20−38
2058−13	20	58	57	−13	30·6		14	9·1		3·7	1·3	0·6	0·9±0·1		20−119

* Flux values measured at 178 MHz.

TABLE 3.4. (cont.).

(1)	(2)			(3)		(4)	(5)	(6)	(7)	(8)	(9)	(10)	(11)	(12)
Parkes Cat. No.	Position (1950·0) R.A. h	m	s	Dec. °	′	Flux Densities at (MHz): 85·5	153	159	408	1410	2650	Spectral Index α_{400}	Other Cat. Nos. 3C	M8H
2059−09	20	59	38	−09	33·3		15·1			0·4	0·3	0·6±0·7		
2101−49	21	01	41	−49	01·5		7·3			1·1	0·7			
2104−25	21	04	23	−25	39·0	100	54·1		31	12	7·3	0·8		21−21
2105−48	21	05	24	−48	59·1		8·4		3·1	1·2	1·0			
2107−34	21	07	44	−34	03·6	14	15·2		3·8	1·3	0·7	0·8		21−32
2119−16	21	19	18	−16	54·6	(30)	(17·2)			0·6	0·3			21−19
2120−16	21	20	14	−16	40·8	(30)	(14·5)		(9·0)	1·3	0·6	0·8±0·4		
2123+00	21	23	14	+00	42·4		17·8		1·9	0·7	0·4	0·8±0·3		
2126+07	21	26	34	+07	19·8	27	19·9	10·3*	6·6	2·4	1·1	0·9±0·0	435	21+04
2141−81	21	41	14	−81	46·6		14·2		10	3·1	1·7			
2146−13	21	46	46	−13	18·6	(13)	12·3		5·6	1·5	0·9	0·9±0·1		21−119
2149−20	21	49	04	−20	00·4	18	10·7		6·5	2·1	1·4	0·7±0·1		21−121
2149−28	21	49	12	−28	43·0	12	8·3		5·4	3·2	1·9	0·5		21−214
2150−52	21	50	51	−52	04·6	28	14·6		10	4·2	2·1	0·7		21−58
2152−69	21	52	58	−69	55·8	253	113·7		80	32	17·5	0·8		21−64
2154−11	21	54	03	−11	41·2	28	20·1		6·5	1·1	0·5	1·1±0·1		21−114
2154−18	21	54	12	−18	28·3	25	22·2		8·8	3·6	0·9	C		21−123
2201−55	22	01	44	−55	32·8		8·4		4·9	2·1	1·0			
2203−18	22	03	26	−18	50·3	16	(18·7)		7·8	6·2	4·9	0·3±0·1		22−11
2207−43	22	07	57	−43	48·4	13	(14·6)		4·0	1·1	0·7	0·8		22−42
2207−45	22	07	15	−45	57·7		17·0		5·9	1·6	0·9			
2210−25	22	10	12	−25	43·3		5·4		3·2	1·3	0·9			
2211+08	22	11	12	+08	59·6	31	(29·0)		2·5	0·8	0·5	1·2±0·1		22+03
2213−45	22	13	49	−45	36·4		13·6		5·6	2·3	1·3			
2216−03	22	16	16	−03	50·6	(18)	8·5		2·8	0·9	1·0	C		22−06
2216−28	22	16	56	−28	12·1		16·1		6·8	2·6	1·0			
2218−50	22	18	05	−50	33·8		7·2			2·0	0·8			
2219−15	22	19	49	−15	01·5		(20·2)			0·4	0·3	0·6±0·7		
2220−15	22	20	00	−15	26·2		(40·1)		(3·3)	0·6	0·3	1·2±0·4		
2220−50	22	20	26	−50	32·6		7·7			1·2	0·7			
2221−02	22	21	16	−02	21·9	60	19·6	(20·5)	17·5	5·3	(2·3)	0·8±0·1	445	22−09
2226+08	22	26	36	+08	58·8	19	17·2		5·0	0·6	0·5	1·1±0·1		22+06
2226−38	22	26	52	−38	39·7		13·1		8·4	2·6	0·9			
2226−41	22	26	25	−41	07·3	28	13·1		8·9	3·2	1·6	0·7		22−43
2250+03	22	50	07	+03	29·1	11	16·1		1·7	0·5	0·3	1·0±0·1		22+011
2252−53	22	52	48	−53	01·4	22	23·5		7	3·5	1·7	0·7		22−54
2253−52	22	53	48	−52	14·9	28	27·2		7·8	3·1	1·3	0·8		22−55
2258+08	22	58	59	+08	22·5		4·9		2·3	0·6	0·4	0·9±0·3		
2304+00	23	04	13	+00	38·7		(40·1)		1·6	<0·5	0·3	0·9±0·3		
2305−41	23	05	06	−41	49·3		11·4		4·4	1·9	0·9			
2307+10	23	07	59	+10	39·7		12·8		3·1	0·7	0·7	0·7±0·2		
2309+09	23	09	55	+09	03·5	29	23·4	14*	8·8	2·6	1·5	0·9±0·0	456	23+03
2310−41	23	10	07	−41	43·0		11·4		4·4	1·8	0·9			
2313+03	23	13	59	+03	48·3	57	26·9	24*	14·8	4·6	2·3	0·9±0·0	459	23+05
2313−18	23	13	09	−18	17·1		20·1		4·7	1·3	0·9	0·8±0·2		
2317−27	23	17	19	−27	44·5	23	22·7		9·2	3·3	1·8	0·7		23−24
2319−55	23	19	14	−55	02·5		12·3		4·5	2·2	1·0			
2322−05	23	22	44	−05	14·2		27·4		4·3	1·5	0·8	0·9±0·2		
2323−40	23	23	51	−40	44·3	15	8		8·0	3·9	2·2	0·5		23−43
2325−15	23	25	55	−15	11·2	14	12·7		6·1	2·0	1·3	0·7±0·1		23−113
2331−41	23	31	45	−41	42·8	50	24·9		15·6	5·7	2·9	0·9		23−44
2331−09	23	31	11	−09	20·9		22·9		6·0	1·2	0·5	1·3±0·2		
2332−66	23	32	15	−66	54·4	26	11·0		7·8	2·5	1·3	0·8		23−63
2334−35	23	34	14	−35	01·8	24	13·6		4·5	1·3	0·6	1·1		23−34
2335+03	23	35	30	+03	11·6		4·7		3·4	1·4	1·1	0·6±0·2		
2337−06	23	37	13	−06	21·0		11·2		3·4	1·3	0·8	0·7±0·2		
2338+04	23	38	27	+04	14·0		7·4		5·4	1·6	1·0	0·9±0·1		
2338+03	23	38	55	+03	02·2		6·8		3·8	1·0	0·4	1·2±0·2		
2338−16	23	38	37	−16	37·8		17·2		4·2	1·4	0·8	0·8±0·2		
2338−58	23	38	31	−58	32·4	25	11·6		7·4	3·3	1·8	0·6		23−52
2354−35	23	54	27	−35	02·4	39	23·5		5·9	1·3	0·5	1·2		23−37

* Flux values measured at 178 MHz.

Table 3.5

Comparison of the 3C survey measurements with results at 153 MHz in Table 3.4.

Source. [PKS]	Flux Densities (flux units) 3C value	153 MHz value
0055-01	17.0	46.2
0105-16	20.0	30.2
0331-01	19.5	43.8
0349-14	8.5	16.6
0806-10	21.0	25.0
1008+06	14.0	24
1717-00	180	324.7

Twenty-seven of the sources listed in table 3.4 are common to the 3C catalogue of sources [S19 - table 1, appendix 2]. There is good agreement between the new survey results and the 3C measurements at 159 MHz for 20 of these sources, but flux densities given here for the remaining 7 sources are consistently higher than the values in the 3C catalogue. The measurements for these 7 sources are compared in table 3.5. Sources observed at 153 MHz which have curved spectra are discussed in section 3.

E. Observations of Sources which possibly have Curved Spectra.

The results of a series of low frequency surveys of extragalactic radio sources are presented here. The measurements were undertaken in five different surveys between August, 1967, and July, 1969, using the 210ft. and 60 ft. paraboloids of the Parkes Observatory. The aim of the observations was to obtain accurate spectral data between 40 and 140 MHz for those sources suspected of having low frequency curved spectra.

(i). Difficulties in the measurements:

The beamwidth of the 210 ft. telescope is greater than 2 degrees below 150 MHz and hence low frequency measurements of sources with this instrument are limited by confusion effects. Source positions and flux densities given in the Parkes Catalogue were used to compute the background

intensity due to confusing sources within one beamwidth of the sources to be measured. Sources which possibly have curved spectra were measured provided the confusion effects were small.

Source observations using total-power receivers may be limited by the effects of galactic radiation, especially within 10 to 15 degrees of the galactic plane. Thus, sources in regions of high galactic background radiation were not measured using this technique. Two of the surveys discussed below were undertaken using a multiplying interferometer and such a system helps to overcome this problem although background irregularities may still be interpreted as discrete sources.

Considerable difficulty was experienced in finding channels free from interference below 100 MHz. This problem was overcome during the surveys reported here by observing mainly between 2300 Hrs. and 0800 Hrs. local time (Parkes), when transmitting station interference was minimal, and by using tunable receivers with a narrow bandwidth. The receivers and feed-systems built by the author are discussed below.

(ii). Equipment:

Aerials:

Various feed systems including broad-band dipoles, tunable folded (half-wave) dipoles and contra-wound helices were built and tested by the author for these

observations. The properties of the aerials finally used are summarized in appendix 3.

Receivers:

The total-power receivers were fully transistorized with one r.f. stage(gain 15 dB) followed by one stage of conversion (single-sided) to an intermediate frequency of either 10 or 30 MHz. The i.f. amplifiers (gain ~ 70 dB) had a bandwidth of not greater than 1.5 MHz. A power-law second detector and d.c. amplifier followed the i.f. stages. The receivers could be tuned remotely using synchronous motors geared (5000 : 1) to variable capacitors in the r.f. and local oscillator stages of each system.

The lay-out of the Parkes interferometer is discussed in appendix 3; here we describe the receivers built by the author for the source observations using this instrument.

Two similar receiver systems tuning over the frequency ranges 43 to 85 MHz and 122 to 180 MHz were constructed. Figure 3.12 shows a block diagram of one of the receivers. The components above the horizontal dashed line were contained in two thermally insulated focus packages mounted immediately behind the feed systems at the foci of the 210 ft. and 60 ft. telescopes. (Pictures of the packages are given in appendix 3). Each receiver had two low noise r.f. amplifiers (gain ~ 30 dB) followed by one stage of conversion (single-sided) to an intermediate frequency of 10 MHz. The receiver could be

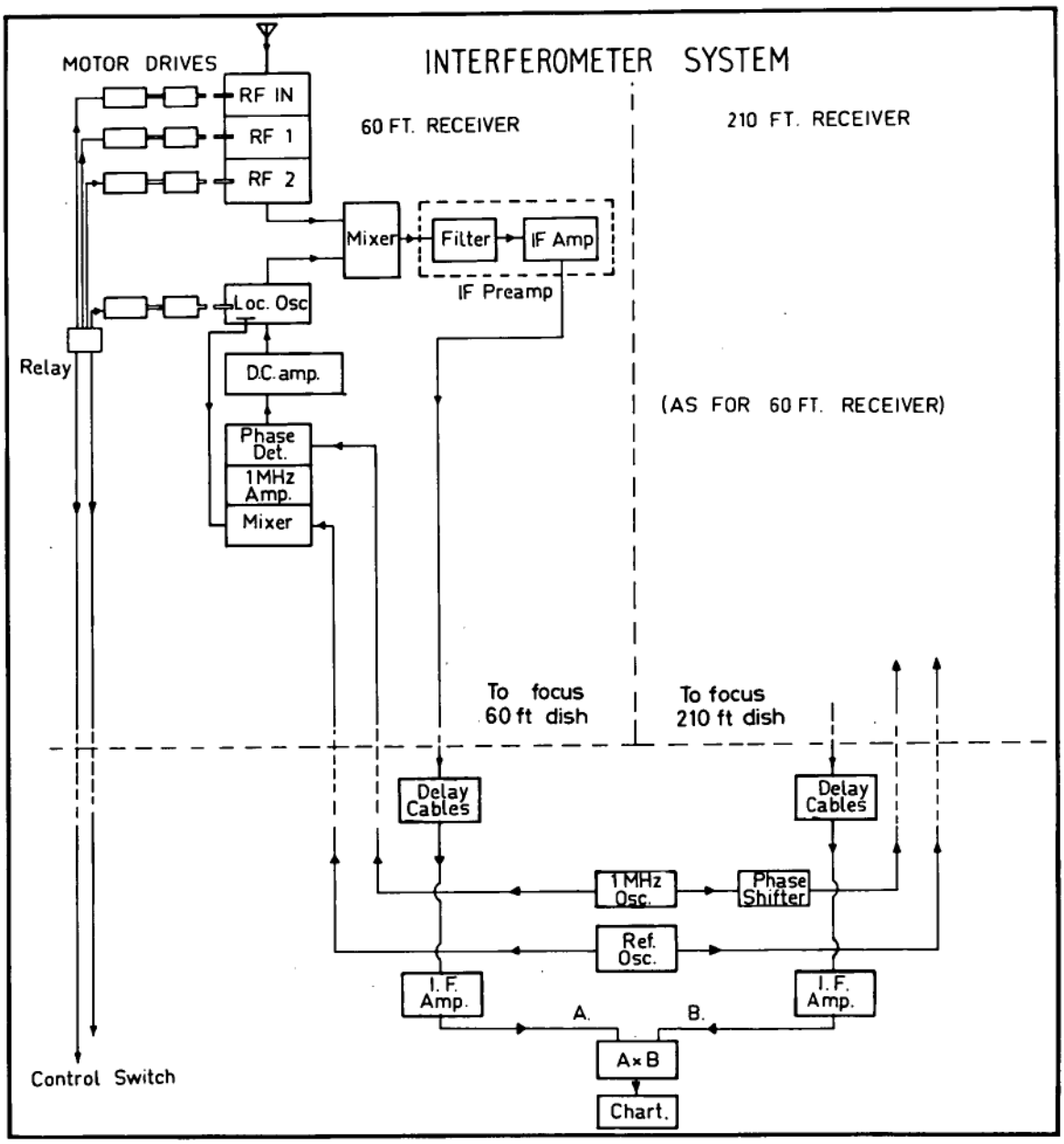

FIGURE 3.12.

Block Diagram of the low-frequency Parkes Interferometer Receiver.

tuned remotely using small D.C. motors geared (2500 : 1) to the variable capacitors in the r.f. and local oscillator stages (see figure 5 appendix 3). A pre-i.f. amplifier (gain ~ 55 dB) was required in each focus package to overcome signal losses in the long coaxial cables from the focus of each telescope to the i.f. amplifiers in the tower of the 210 ft. telescope. The main i.f. amplifiers had a gain of 70 dB at bandwidths of 1.5 MHz, 230 KHz, 180 KHz, or 108 KHz. The bandwidth used could therefore be varied to overcome the problems of interference at any one time. The i.f. signals from each telescope receiver were corrected for path differences (see discussion, page 219 appendix 3) in a cable-switching network and continuously multiplied in a ring modulator of the type described by Blum (1959). The product output was amplified and recorded.

The multiplying interferometer uses the principle of observing a source at two "phase-related" observing stations, in this case, the foci of the 210 ft. and 60 ft. telescopes. Phase coherence at the input to each receiver was achieved by phase locking the local oscillator of each receiver to two reference signals fed out to each focus package from the tower of the 210 ft. telescope. The phase locking system was basically the same as that described by Read (1961) except that the operating frequency of the receiver could be varied. Other characteristics of the receivers are given in table 3.6.

TABLE 3.6

Observing Period.	Receiver Type.	Tuning Range. [MHz]	Bandwidth Available.	Receiver Noise temp. etc.	Feed System.
August,1967	Total Power	43 to 63	1.8 MHz	Noise * Fluctuations of 1.5 degK	Pair of broad-band cage dipoles 50% efficient from 42 to 160 MHz
"	Total Power	84 to 125	2.1 MHz	Noise * Fluctuations of 2.2 degK	"
January,1968	Total Power	50 to 70	1.2 MHz	630 degK	2 wire helix: 20in. diameter, 8ft. long
January,1969	Interferometer System	40 to 85	1.5MHz, 230kHz 180kHz, 108kHz	178 degK	Variable length folded dipoles tuning from 74 to 150 MHz.
July,1969	"	122 to 180	"	356 degK	

* Noise fluctuation on the records with a time constant of 3 secs.

Properties of receivers used for source measurements.

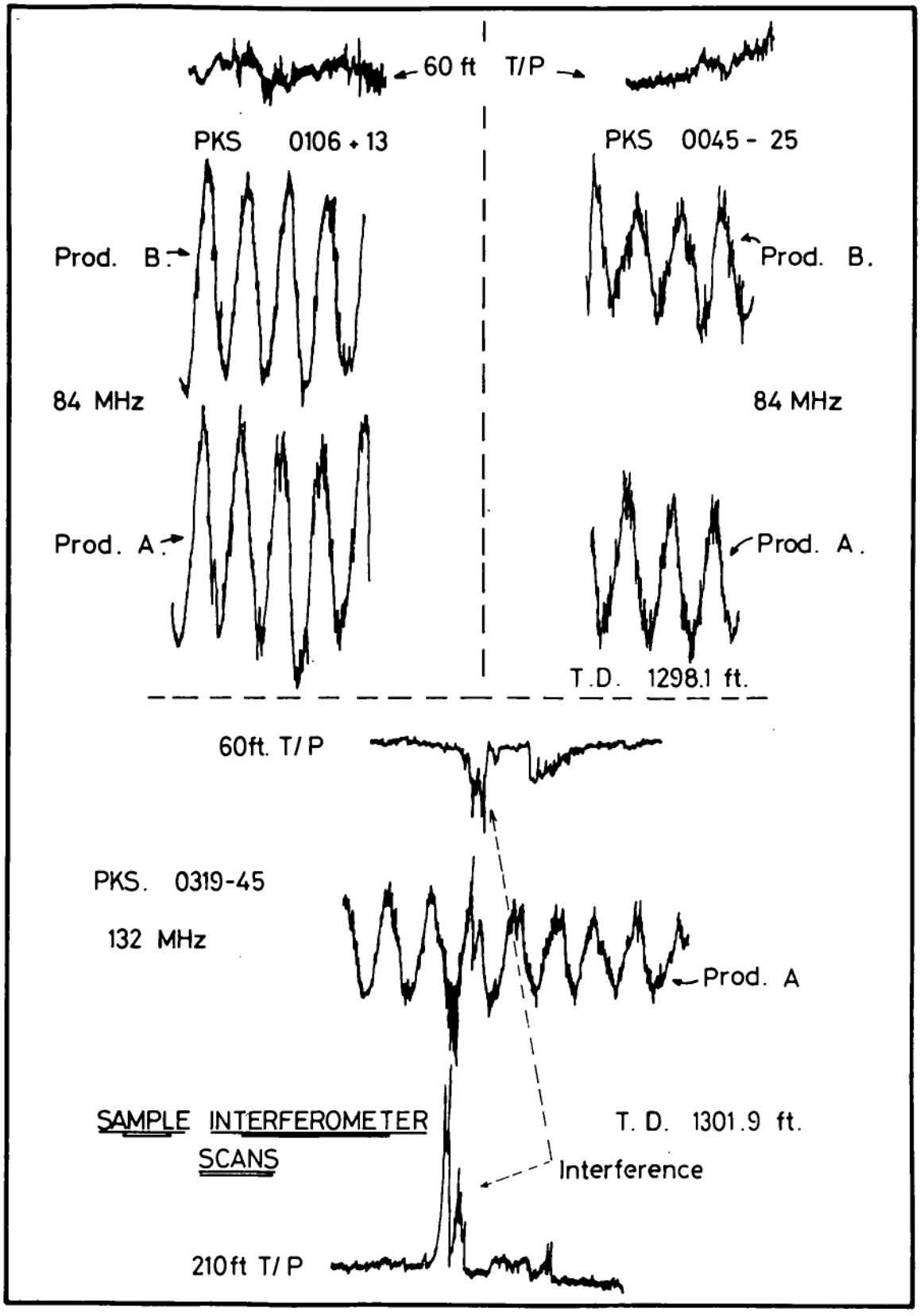
60 ft
T/P
PKS 0106 + 13
PKS 0045 - 25
Prod. B
Prod. B.
84 MHz
84 MHz
Prod. A
Prod. A.
T.D. 1298.1 ft.
60ft. T/P
PKS. 0319-45
132 MHz
Prod. A
SAMPLE INTERFEROMETER SCANS
T. D. 1301.9 ft.
Interference
210ft T/P

FIGURE 3.13.

(iii). Observing Procedure:

The total power observations consisted of scans in right ascension and declination through the centroid of each source. The drive rate was 0.5 degrees per minute. When a channel free from interference was found, twelve or more sources were measured before the observing frequency was changed.

The observations with the interferometer were obtained with the telescopes separated by 1000 or 1300 feet on an east-west baseline orientation. The fringe pattern was held stationary to the ground and hence sources passed through the fringes as they moved across the sky. This observing method helped to overcome problems of transmitting station interference since such "sources" remain stationary with respect to the aerial response. Both in-phase and quadrature phase products were recorded and the amplitude of the fringe pattern of a given source was found by averaging the results of five to eight good fringes. It should be noted that the Parkes interferometer has insufficient resolution below 180 MHz to study the structure of extragalactic radio sources. Thus all the sources measured were "point-sources" in relation to the fringe pattern of the system. Figure 3.13 shows sample interferometer scans of the sources PKS 0045-25, 0106+13, and 0319-45.

(iv). Calibration:

The source Hydra A [PKS 0915-11] was taken as

the standard of flux density for the total power measurements (see B above). Scans of this source were used to calibrate the output from a temperature saturated noise diode which was then used as a secondary standard.

The ten sources discussed in B above were taken as standards of flux density for the interferometer survey. A calibration source was measured every fourth or fifth interferometer scan to keep a close check on the gain and phase stability of the receiver.

(v). Errors in the Measurement:

The reliability of the total power measurements is shown in table 3.7. The errors result from variations in the noise diode signal, fluctuations in the records and errors in determining the flux density of Hydra A. Sources confused with nearby sources were not measured using total-power receivers.

The errors in the interferometer measurements result from the method of calibration, noise fluctuations on the records and from confusion effects. The method of determining the flux density of each calibration source is accurate to within 4 percent (see B above). Noise fluctuations on the records varied from scan to scan, probably as a result of low-level interference not detected at the time. The errors of this type have been calculated in flux units and are given for

TABLE 3.7

ERRORS IN THE TOTAL-POWER MEASUREMENTS

Observing Period	August, 1967.	August, 1967.	January, 1968.
Receiver Frequency.	43 to 63 MHz	84 to 125MHz	50 to 70 MHz
Errors in Measuring Hydra A.	10 %	6 %	small
Errors from variations in the noise diode signal.	7 %	7 %	8 %
Errors from fluctuations on the records.	±6 f.u.	± 2 f.u.	± 4 f.u.
Errors in determining the flux density of Hydra A at the observing frequency. [see part B above]	4 %	4 %	4 %
Total Error.	21% ± 6 f.u.	17% ± 2 f.u.	12% ±4f.u.

each source in the table of results. The method of determining the errors due to confusion effects is discussed in appendix 3; errors of this type are given for each source in the table of results.

Errors in the measurements due to polarization of the source or background radiation have been neglected since they are probably small.

(vi). Flux Density Results Between 40 and 140 MHz:

Flux density results for sources are given in table 3.8. The reliability of each measurement is indicated. The results preceded by an asterisk were obtained using total-power observations; the remainder were obtained from interferometer scans. The table is described in the "Notes on table 3.8".

(vii). Source Spectra:

More than 70 sources have been observed during this investigation. The new low-frequency measurements have provided information that was necessary to define the spectra of many of the sources accurately. These results, together with previous measurements (see table 1, appendix 2) show that 62 of the sources have curved spectra. (See figures 3.14 to 3.21). Some of these were suspected or known to have curved spectra but the low frequency data available was limited. Others were previously thought to have straight spectra [PKS: 0702-10(?), 0704-23, 0841+15, 1044+15, 1140-11, 1232-41, 1827-36].

(facing page 104)

Notes on Table 3.8.

Column 1. Source catalogue number taken from the Parkes catalogue [S32, table 1, appendix 2].

Columns 2,3. Source right ascension [Hours, minutes, seconds] and declination [Degrees, minutes].

Columns 4,5. Source flux density at 85.5 MHz [S15, table 1, appendix 2] and 408 MHz [S32, table 1, appendix 2].

Columns 6,7. Number of sources within 6^{o} of the measured source and the integrated flux density of confusion sources.

Column 8. Frequency of new observation.

Column 9. Measured flux density.

Column 10. Errors in the results.

Columns 11,12. Source position in *new* galactic co-ordinates.

Column 13. Other catalogue numbers [3C from S19 - S22, table 1, appendix 2; MSH from S15, table 1, appendix 2].

TABLE 3.8. SOURCE RESULTS.

1.	2.			3.		4.	5.	6.	7.	8.	9.	10.		11.	12.		13.
PARKES CAT.NO. (PKS)	RIGHT ASCENSION (RA) (1950.0)			DECLINATION (DECL)		$S_{85.5}$	S_{408}	CONFUSION No. in 6°	SOURCES BACKGROUND AT 408 MHz	NEW FREQ.	RESULTS FLUX DENSITY	ERRORS		ℓ^{II}	b^{II}	3C	OTHER CAT. NOS. MSH
	(H	M	S)	(°	')	(f.u.)	(f.u.)		(f.u.)	(MHz)	(f.u.)	(f.u.	%)	(°)	(°)		
0002+12	00	02	19	+12	32		6.3	7	3.6	76.0	25.2	±1.6	± 13%	105.7	-48.5		
										81.2	19.4	1.6	22%				
										84.0	23.8	1.2	21%				
0008-42	00	08	22	-42	10		4.5	4	4.1	84.0	14.8	3.4	32%	329.6	-73.1		
0023-26	00	23	18	-26	19	17.0	14.2	4	3.4	81.2	17.2	1.9	15%	42.3	-84.2		00-210
										132.0	21.4	2.5	9%				
0036+03	00	36	44	+03	03		3.6	11	2.8	81.2	15.3	0.9	28%	117.0	-59.4		00+010
										84.0	12.0	1.7	25%				
0045-25	00	45	05	-25	34	29.0	10.7	3	0.04	84.0	39.2	2.3	4%	97.4	-88.0		00-222
0049-43	00	49	56	-43	23	23.0	5.2	6	>10.0	84.0	18.9	1.7	32%	302.4	-74.0		00-414
0109+14	01	09	25	+14	27			10	>10.0	76.0	<25	3.0	35%	130.4	-47.8		
0123-01	01	23	28	-01	38	88.0	13.6	16	3.5	81.2	51.3	2.3	4.7%	142.2	-62.9	40	01-05
										*82.7	59.6	2.0	17%				
										*84.0	69.3	2.0	17%				
										*88.2	63.0	2.0	17%				
										*94.0	61.2	2.0	17%				
										*99.2	71.7	2.0	17%				
										*112.9	54.1	2.0	17%				
										*113.0	56.6	2.0	17%				
										132.0	38.9	1.9	4.1%				
0157+01	01	57	38	+01	10	16.0	4.0	14	1.7	84.0	12.3	0.7	17%	155.8	-57.0		01+014

TABLE 3.8. (cont.).

1.	2.	3.	4.	5.	6.	7.	8.	9.	10.		11.	12.	13.
0252-71	02 52 19	-71 17	7.0	10.4	9	2.4	84.0	7.5	0.5	28%	290.0	-42.9	02-72
							*86.1	11.1	2.0	17%			
							*99.0	9.1	2.0	17%			
0319-45	03 19 42	-45 21	19	6.7	0	0	132.0	17.60	2.0	4%	254.2	-55.2	03-43
0320-37	03 20 42	-37 25	950	176.8			*42.7	1255	6.0	21%	240	-57	03-31
							*46.3	1532	6.0	21%			
							*54.2	1022	4.0	12%			
							*58.0	1309	6.0	21%			
							*67.4	985	4.0	12%			
0320+05	03 20 42	+05 24		6.1	9	0.9	81.2	<14	0.9	30%	177.0	-40.8	
0340+04	03 40 52	+04 48	35.0	7.1	6	4.8	81.2	33.5	2.5	16%	181.9	-37.5	93 03+08
0349-27	03 49 33	-27 53	53	11.2			*86,5	50.1	2.0	17%	225	-50	03-212
							*91.0	42.0	2.0	17%			
							*95.0	47.0	2.0	17%			
							*103.0	44.0	2.0	17%			
							*108.0	42.6	2.0	17%			
							*112.5	41.7	2.0	17%			
0358+00	03 58 33	+00 28	19.0	4.8	10	1.1	81.2	15.2	1.1	25%	190.1	-36.9	99 03+012
							84.0	<26	3.8	28%			
0408-65	04 07 59	-65 53	36.0	33.3	9	3.3	84.0	34.2	1.4	18%	278.6	-40.9	04-62
							*49.2	33.0	6.0	21%			
							*87.5	32.5	2.0	17%			
							*108.5	35,9	2.0	17%			
							*109.0	43.2	2.0	17%			

TABLE 3.8. (cont.).

1.	2.	3.	4.	5.	6.	7.	8.	9.	10.		11.	12.		13.
0442-28	04 42 37	-28 15	82	15.6			*82.8	129.8	2.0	17%	228	-39		04-218
							*86.2	95.5	2.0	17%				
							*91.5	86.1	2.0	17%				
0518-45	05 18 18	-45 50	570	117.9			*44	774.2	6.0	21%	252	-35		05-43
0602-31	06 02 23	-31 56	17.0	4.6	4	2.5	132.0	9.6	0.7	12%	238.2	-23.3		06-32
0624-05	06 24 43	-05 51	120.0	43.2	*	*	132.0	82.5	2.4	4%	215	-8	161	06-04
0634-20	06 34 25	-20 34	67	21			*88.0	71.8	2.0	17%	230	-12		
							*93.8	67.7	2.0	17%				
							*105.0	54.0	2.0	17%				
0702-10	07 02 06	-10 23		13.3	*	*	132.0	8.3	0.7	30%	224	-2		
0704-23	07 04 28	-23 07	6.0	5.1	4	5.0	132.0	7.3	0.7	6%	235.4	-7.2		07-21
0709-20	07 09 39	-20 38	8.7	6.2	4	0.7	132.0	11.3	0.6	4.3%	233.7	-5.0		07-23
0741-06	07 41 55	-06 22		12.8			132.0	8.9	0.8	6%	225	+9		
0827+07	08 27 24	+07 55		3.9	7	2.5	132.0	7.7	0.3	9%	217.3	+25.4		
0841+15	08 41 06	+15 59		3.4	13	3.4	132.0	5.1	0.5	18%	210.5	+31.9		
0909+16	09 09 16	+16 31		4.0	13	8.1	132.0	10.9	0.9	20%	213.1	+38.3		
0933+04	09 33 56	+04 36	24.0	4.5	11	1.8	132.0	17.7	1.5	6%	230.1	+38.3	222	09+03
0957+14	09 57 49	+14 15		2.7	7	3.5	132.0	7.6	0.5	20%	222.4	+48.1		
1044+15	10 44 01	+15 59		4.8	3	0.1	132.0	8.8	1.2	3%	228.0	+58.9		
1049-09	10 49 00	-09 02		4.8	2	0.04	132.0	13.9	0.2	3%	260.2	+43.4		10-019
1055+01	10 55 55	+01 50	14.0	4.7	8	1.0	84.0	12.8	0.5	32%	251.5	+52.8		10+010
							132.0	6.5	1.0	18%				
1116-02	11 16 51	-02 47	31.0	8.5	4	2.0	132.0	19.4	1.7	9%	263.0	+52.5	255	11-08
1120+05	11 20 35	+05 47	19.0	4.6	6	5.0	132.0	14.8	0.9	8%	254.8	+59.8	257	11+05

TABLE 3.8. (cont.).

1.	2.	3.	4.	5.	6.	7.	8.	9.	10.	11.	12.	13.
1136-13	11 36 38	-13 34	44.0	10.6	7	6.0	132.0	27.4	0.7 12%	277.5	+45.4	11-18
1140-11	11 40 03	-11 26	14.0	4.8	6	6.4	84.0	18.2	0.8 28%	277.4	+47.7	11-111
							132.0	11.3	0.4 15%			
1232-41	12 32 48	-41 36	11.0	5.0	6	2.8	84.0	13.9	1.6 30%	299.8	+20.9	12-44
1239-04	12 39 45	-04 30	25.0	9.5	9	1.1	84.0	24.5	1.7 24%	298.7	+58.0 275	12-013
							132.0	18.9	1.4 17%			
1253-05	12 53 35	-05 31	37.0	11.2	6	1.6	132.0	21.4	0.4 12%	305.1	+57.1 279	12-020
1302-49	13 02 33	-49 12	20	9.9			*59.2	19.2	4.0 12%	305	+13	13-41
1330+02	13 20 21	+02 16	19.0	6.1	9	0.7	79.0	20.2	0.9 22%	326.2	+63.0 287.	113+07
							84.0	21.4	1.7 18%			
1345+12	13 45 06	+12 33		7.7	4	1.9	132.0	5.0	0.5 24%	347.2	+70.2	
1355-41	13 55 57	-41 38	35	9.4			*59.2	64.2	4.0 12%	316	+19	13-45
1414+11	14 14 28	+11 02		7.3	4	2.0	85.0	16.5	2.6 26%	358.0	+64.1 296?	
							132.0	13.3	0.9 11%			
1416+06	14 16 38	+06 42	114.0	21.5	11	2.4	76.0	100.4	3.8 20%	352.2	+60.7 298	14+05
							*100.0	96.2	2.0 17%			
							*116.0	91.0	2.0 17%			
1427-50	14 27 08	-50 29	15.0	4.2	2	2.0	132.0	14.4	0.2 10%	318.5	+9.1	14-56
1434+03	14 34 26	+03 37	47.0	7.1	11	1.5	84.0	34.9	2.0 5%	354.3	+55.4	14+010
							132.0	14.7	0.5 10%			
1449-13	14 49 52	-12 59	19.0	(7.0)	7	2.6	132.0	12.5	1.0 18%	342.9	+40.1	14-119
1459-41	14 59 06	-41 54	55	12.4			*59.2	76.0	4.0 12%	327	+14	14-415
							*87.0	60.9	2.0 17%			
							*105.2	40.7	2.0 17%			

TABLE 3.8. (cont.)

1.	2.	3.	4.	5.	6.	7.	8.	9.	10.		11.	12.	13.
1508-05	15 08 13	-05 32	8.0	7.4	7	2.8	84.0	<12.5	1.8	35%	353.9	+42.9	15-05
1514+07	15 14 17	+07 12	140.0	23.2	10	8.7	76.0	112.3	5.4	12%	9.0	+50.1 317	15+05
							132.0	77.8	1.6	12%			
1514+18	15 14 43	+18 41		5.5	4	2.6	79.0	16.9	1.1	14%	26.3	+55.5 316	
							132.0	10.8	2.8	4%			
1523+03	15 23 18	+03 19		4.4	12	4.0	84.0	<9.4	0.9	29%	6.7	+46.0	
							132.0	6.4	1.3	8%			
1550+20	15 50 12	+20 15			*	*	76.0	28.3	0.4	30%	33.0	+48 326	
							79.0	22.5	0.6	30%			
							132.0	13.7	1.7	15%			
1602-63	16 02 14	-63 24		10.8			*109.0	36.5	2.0	17%	323	-08	
							*112.0	35.7	2.0	17%			
1617-04	16 17 24	-04 12		4.0	4	0.04	84.0	12.5	0.8	9%	9.2	+30.7	
							132.0	5.4	1.5	4%			
1618+17	16 18 07	+17 44		5.5	2	0.04	85.0	27.6	1.8	4%	33.2	+41.1 334	
							132.0	16.9	2.2	3%			
1637-77	16 37 03	-77 10		10.0	5	6.7	132.0	23.1	1.4	14%	314.4	-20.0	
1645+17	16 45 28	+17 25		3.8	4		132.0	4.1	0.7	30%	35.9	+34.9	
1712-03	17 12 24	-03 18	21.0	6.9	6	3.6	132.0	17.6	1.3	25%	18.3	+19.6	17-04
1732+16	17 32 26	+16 03		3.5	3	1.3	84.0	22.1	3.8	15%	39.3	24.0	
							132.0	11.9	0.4	10%			
1754-59	17 54 37	-59 46	25.0	11.1	6	1.5	82.1	35.0	5.3	28%	333.8	-17.0	17-51
							132.0	26.2	2.4	8%			
							*93.2	39.1	2.0	17%			

TABLE 3.8 (cont.)

1.	2.	3.	4.	5.	6.	7.	8.	9.	10.		11.	12.		13.
1801+01	18 01 44	+01 01		4.8?	3	1.7	132.0	<1.5	0.3	25%	28.4	+11.0		
1802+11	18 02 44	+11 01		3.8	5	3.5	84.0	38.1	3.9	5%	37.7	+15.2	368	
1814-51	18 14 09	-51 59	27.0	10.2	1	0.04	84.0	36.0	1.2	6%	342.3	-16.2		18-52
							*113.2	28.4	2.0	17%				
							132.0	25.1	2.0	4%				
1814-63	18 14 45	-63 47	71.0	25.2	9	0.2	81.2	64.5	2.7	5%	330.9	-20.8		18-61
							*59.2	76.0	4.0	12%				
							*94.0	74.6	2.0	17%				
							*108.0	80.0	2.0	17%				
							*113.2	86.4	2.0	17%				
1827-36	18 27 37	-36 05		16.3	2	0.1	132.0	24.6	2.4	6%	358.3	-11.8		
							*111.8	35.9	2.0	17%				
							*112.0	42.2	2.0	17%				
1836+17	18 36 13	+17 10		14.0			* Flux @ 80 MHz				47	+11	386	
							<40 f.u.							
1934-63	19 34 49	-63 49		3.7	3	2.5	132.0	<2.1	0.3	30%	332.8	-20.4		
							159	1.7	0.2	28%				
1936-15	19 38 25	-15 32	(39)	(13.7)			*93.2	44.4	2,0	17%	24	-18		
1949+02	19 49 44	+02 23	64.0	13.6	*	*	80.2	56.2	4.1	5%	42	-12	403	19+010
1954-55	19 54 20	-55 18	54	10.5			*93.2	54.7	2.0	17%	343	-31		19-57
							*113.2	62.3	2.0	17%				
2012+23	20 12 18	+23 26			*	*	80.2	178.2	6.0	5%	63	-6	409	
							84.0	171.9	6.1	5%				
							132.0	106.2	4.8	2%				

TABLE 3.8 (cont.).

1.	2.	3.	4.	5.	6.	7.	8.	9.	10.	11.	12.	13.
2048-57	20 48 06	-57 15	12.0	4.4	6	0.8	80.2	22.1	0.4 30%	340.0	-38.7	20-57
							132.0	16.8	1.4 14%			
2104-25	21 04 25	-25 39	100	22.0			*99.0	109.0	2.0 17%	21	-40	21-21
2116+18	21 16 10	+18 05		4.7	5	4.6	81.2	22.9	1.2 26%	68.2	-21.3	
2127+04	21 28 03	+04 49		2.6	8	1.1	132.0	<7.6	1.7 15%	58.6	-31.8	
2137-06	21 37 35	-06 59		3.2	4	0.1	132.0	6.3	0.8 5%	48.1	-40.3	
2145+06	21 45 36	+06 44		3.0	11	1.5	132.0	7.1	1.3 9%	63.6	-34.0	
2211-17	22 11 41	-17 17	127.0	26.0	7	1.9	81.2	172.1	4.8 6%	40.2	-52.4 444	22-17
							132.0	90.4	2.5 6%			
							*85.0	147.1	2.0 17%			
							*101.0	126.4	2.0 17%			
							*106.0	113.2	2.0 17%			
							*112.9	95.8	2.0 17%			
2216-03	22 16 16	-03 51	(33.0)	2.3	7	8.0	132.0	12.1	1.0 25%	59.1	-46.7	22-06
2226-38	22 26 53	-38 40		6.0	3	1.5	80.2	30.7	1.4 24%	3.0	-58.4	
							132.0	17.3	1.3 7%			
2230+11	22 30 07	+11 28		6.2	15	1.5	81.2	6.9	0.9 18%	77.4	-38.6	
							132.0	5.5	0.5 11%			
2251+15	22 51 29	+15 53		13.9	20	5.8	84.0	18.1	4.9 24%	86.1	-38.2 454.3	
2318-16	23 18 24	-16 39	23.0	8.2	11	6.8	80.2	30.9	2.5 25%	55.4	-66.5	23-18
							132.0	17.0	0.9 18%			
2322-12	23 22 43	-12 24	30.0	6.6	12	1.4	80.2	26.1	1.5 10%	65.3	-64.8	23-112
2335+26	23 35 57	+26 44			*	*	80.2	71.5	6.3 4%	103	-33 465	
2356-61	23 56 24	-61 12	296	48.8			*54.2	364.0	4.0 12%	314	-55	23-64
							*84.0	254.8	2.0 17%			
							*98.0	214.2	2.0 17%			
							*99.0	208.4	2.0 17%			
							*115.0	165.0	2.0 17%			

(facing pages 111 et seq.)

Figures 3.14 to 3.21

Sources measured at low frequencies (see table 3.8) which have curved spectra.

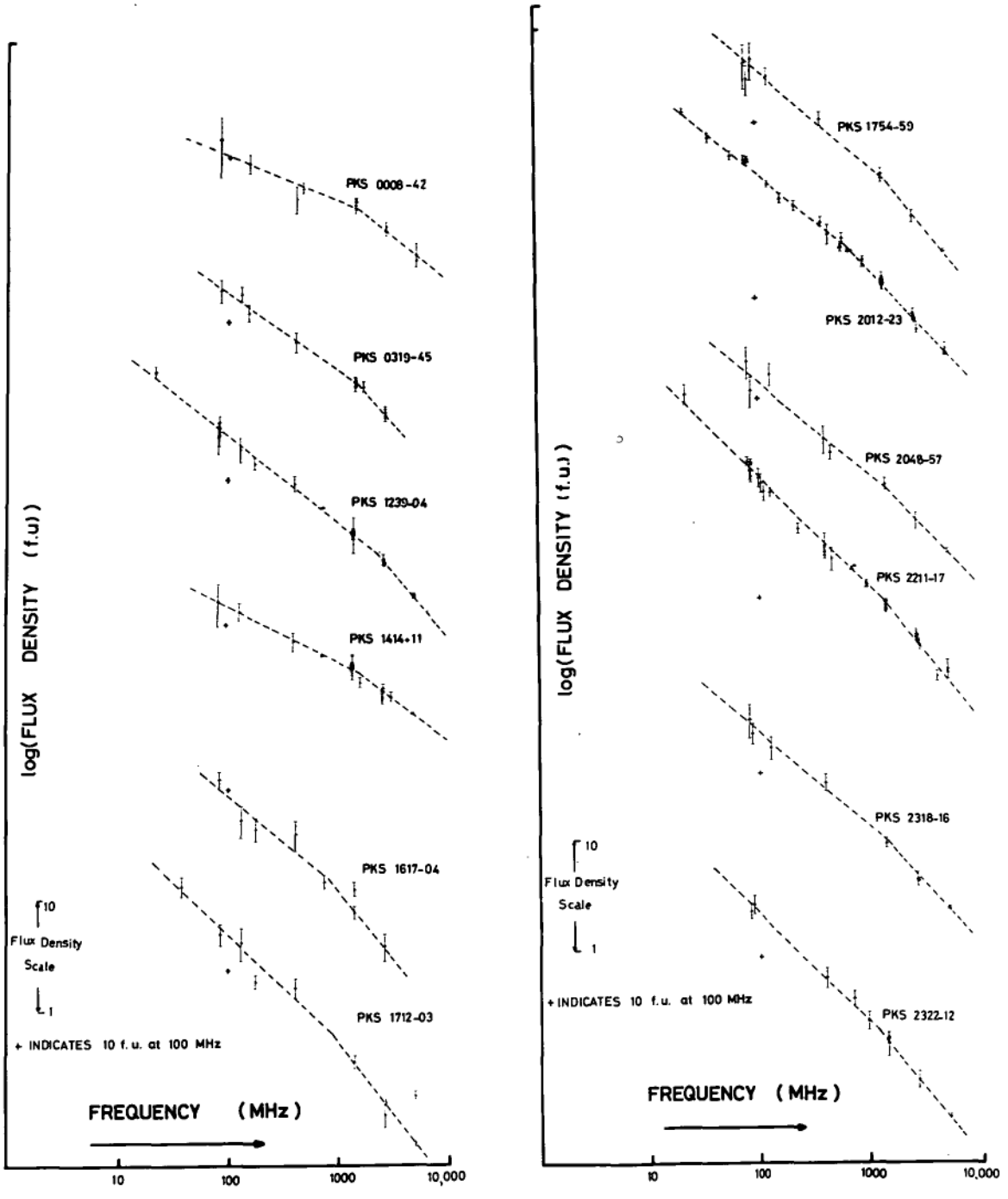
log(FLUX DENSITY (f.u.))
PKS 0008-42
PKS 0319-45
PKS 1239-04
PKS 1414+11
PKS 1617-04
PKS 1712-03
10
Flux Density
Scale
1
+ INDICATES 10 f.u. at 100 MHz
FREQUENCY (MHz)
10
100
1000
10,000
log(FLUX DENSITY (f.u.))
PKS 1754-59
PKS 2012-23
PKS 2048-57
PKS 2211-17
PKS 2318-16
PKS 2322-12
10
Flux Density
Scale
1
+ INDICATES 10 f.u. at 100 MHz
FREQUENCY (MHz)
10
100
1000
10,000

FIGURE 3.14.

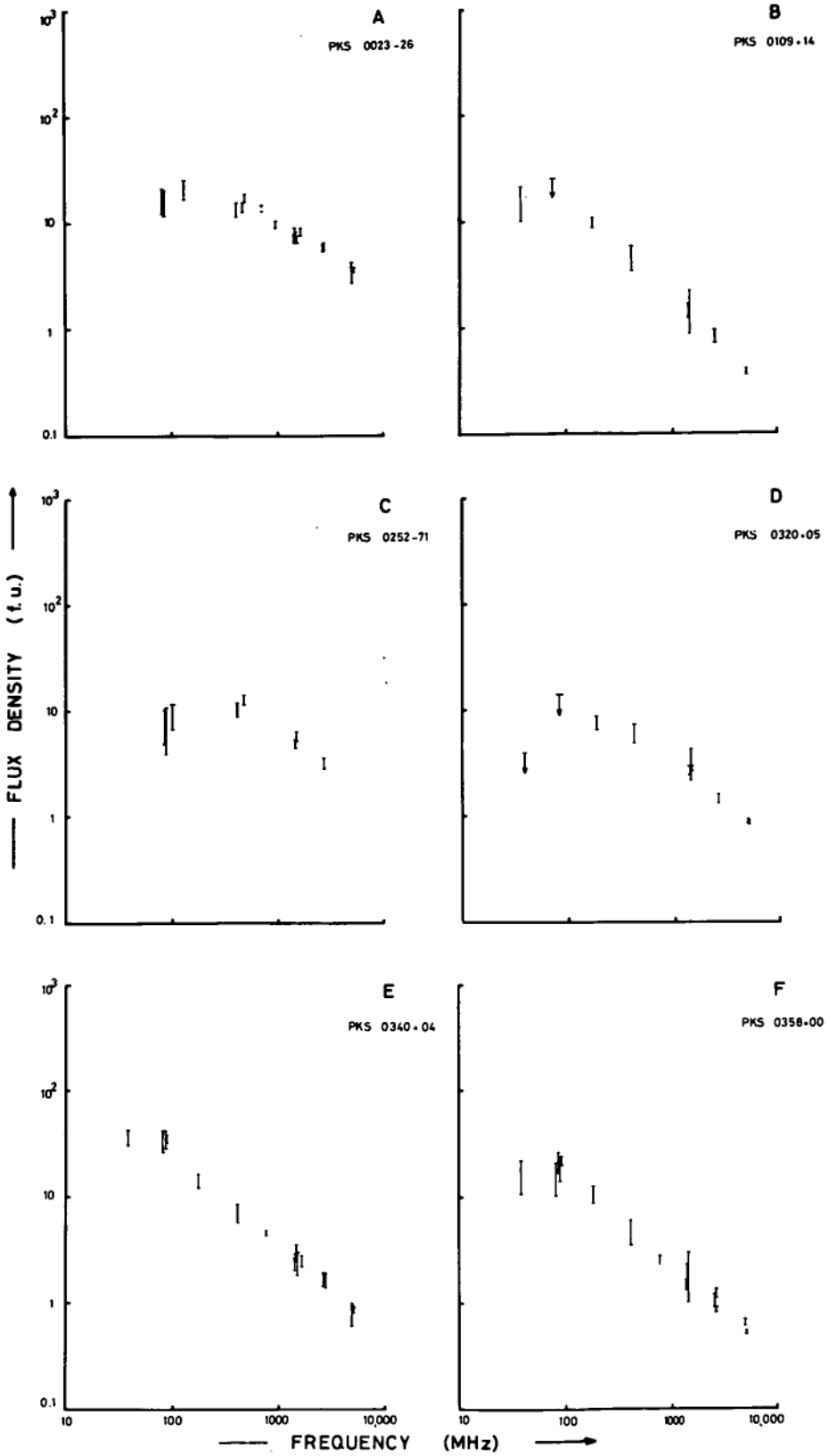
A
PKS 0023-26
B
PKS 0109+14
C
PKS 0252-71
D
PKS 0320+05
E
PKS 0340+04
F
PKS 0358+00
FLUX DENSITY (f.u.)
FREQUENCY (MHz)
10
100
1000
10,000
0.1
1
10
10^2
10^3

FIGURE 3.15

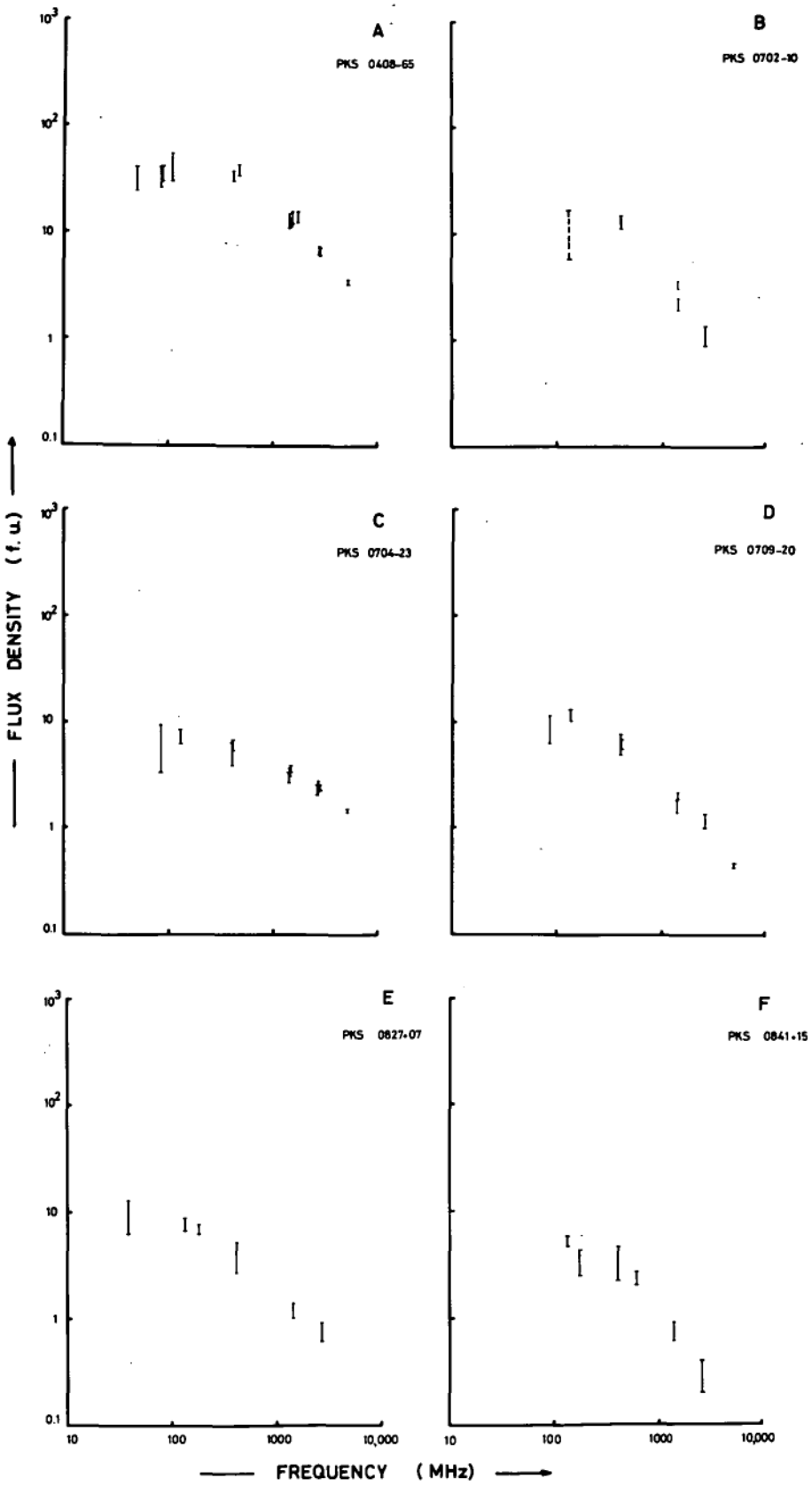
A
PKS 0408-65
B
PKS 0702-10
C
PKS 0704-23
D
PKS 0709-20
E
PKS 0827-07
F
PKS 0841+15
FLUX DENSITY (f.u.)
FREQUENCY (MHz)
10
100
1000
10,000
0.1
1
10
10^2
10^3

FIGURE 3.16.

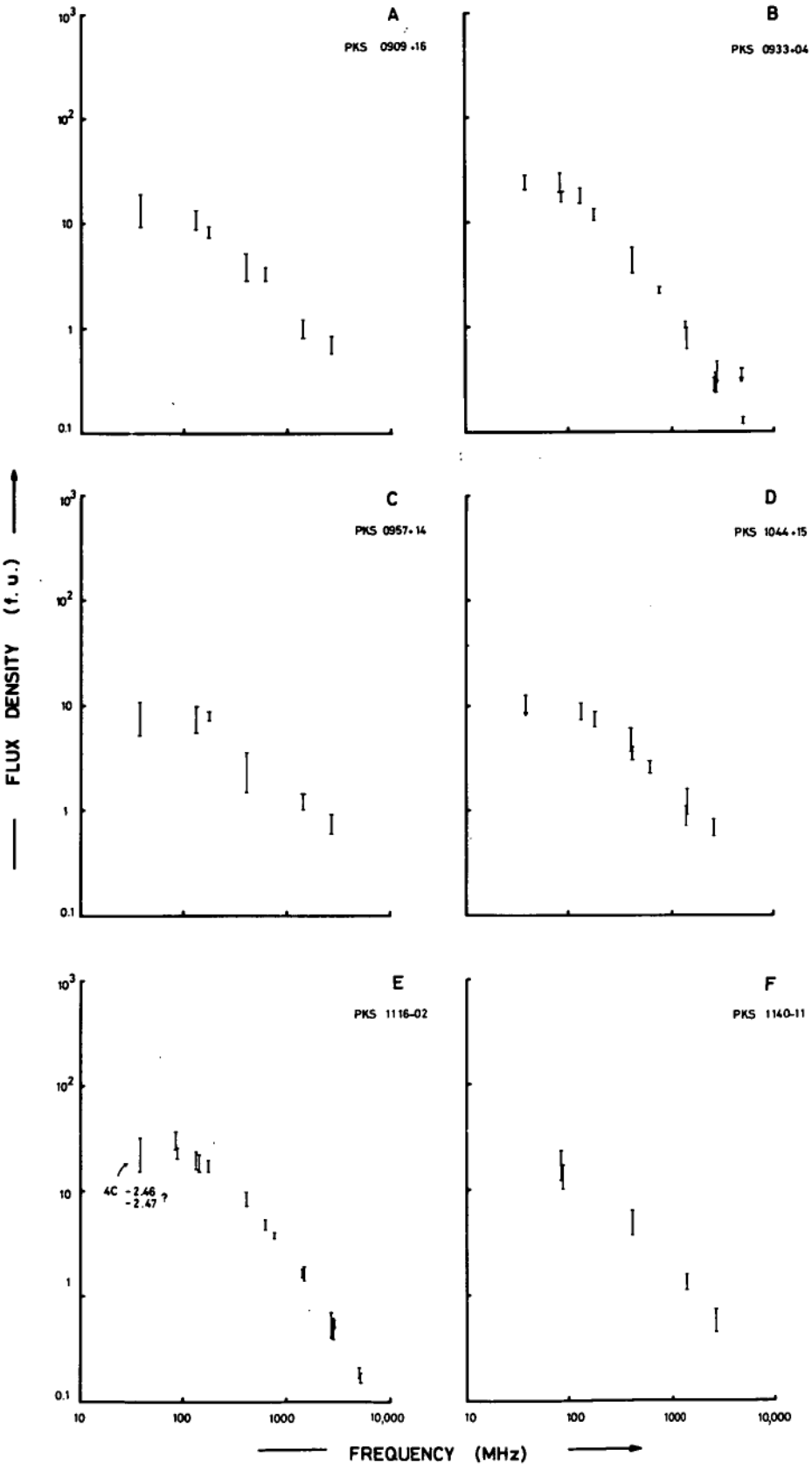
A
PKS 0909+16
B
PKS 0933+04
C
PKS 0957+14
D
PKS 1044+15
E
PKS 1116-02
4C -2.46
-2.47 ?
F
PKS 1140-11
FLUX DENSITY (f.u.)
FREQUENCY (MHz)
10
100
1000
10,000
0.1
1
10
10^2
10^3

FIGURE 3.17.

115

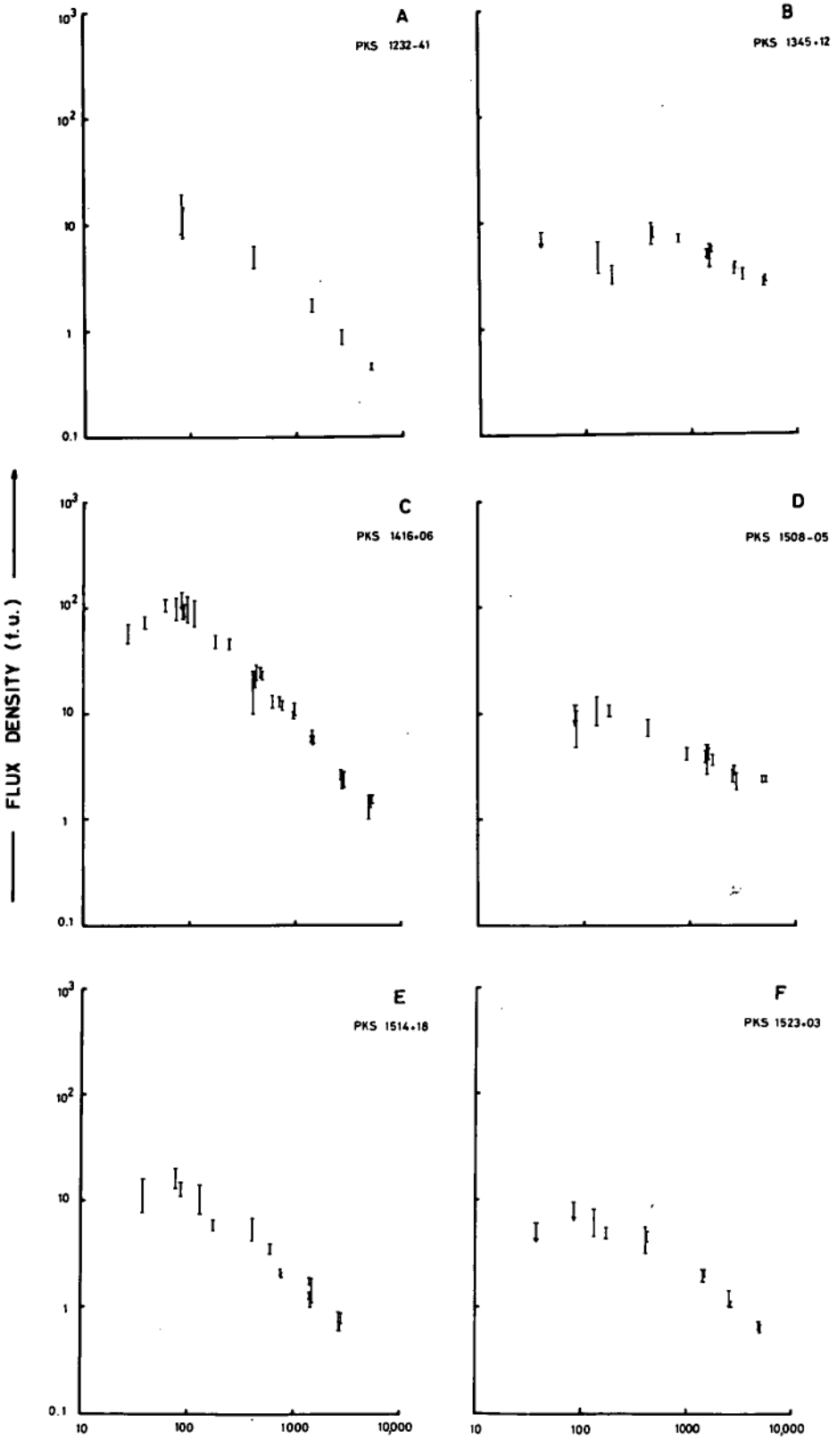

FIGURE 3.18

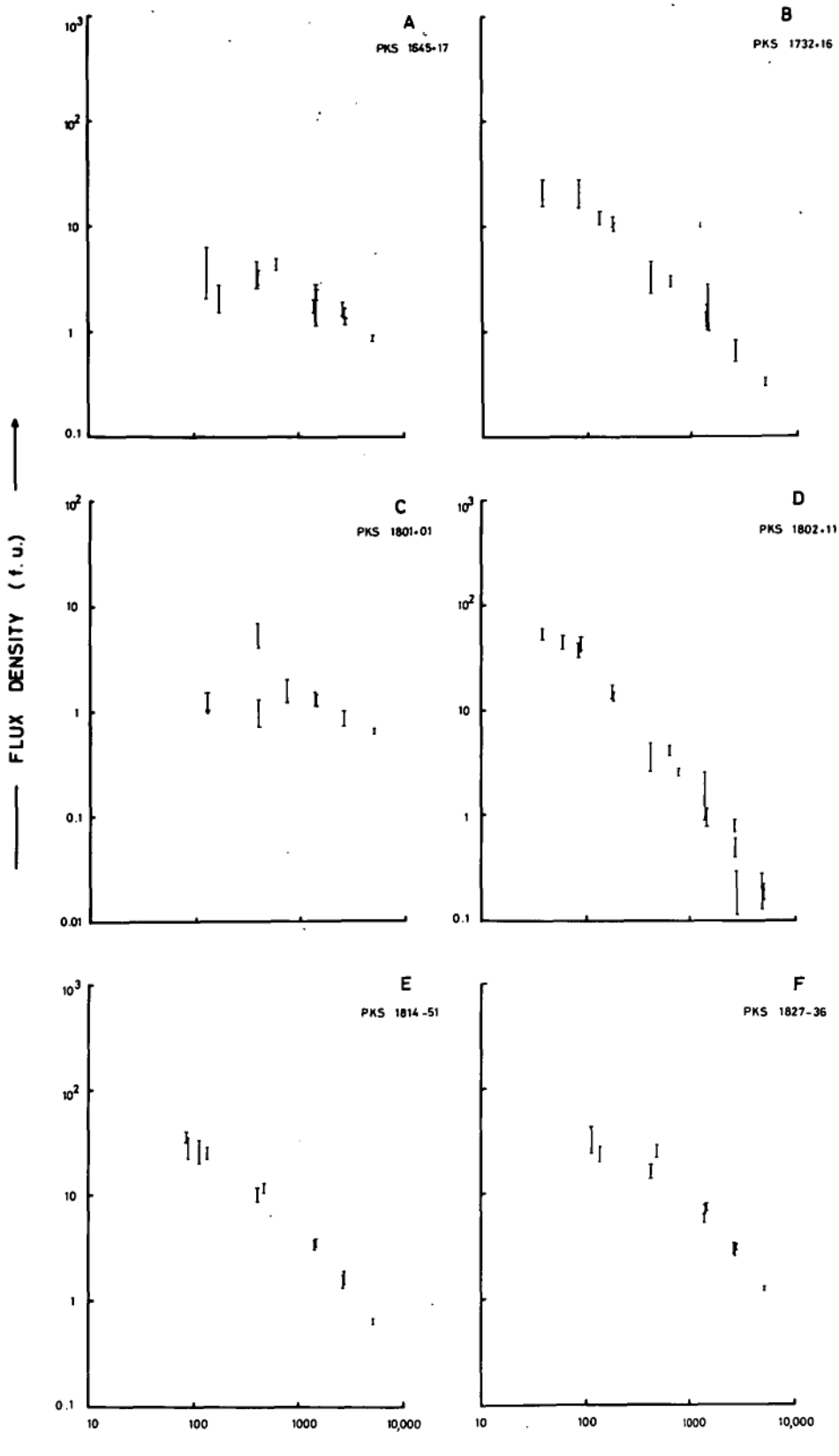
A
PKS 1645-17
B
PKS 1732-16
C
PKS 1801-01
D
PKS 1802-11
E
PKS 1814-51
F
PKS 1827-36
FLUX DENSITY (f.u.)
FREQUENCY (MHz)
10
100
1000
10,000

FIGURE 3.19.

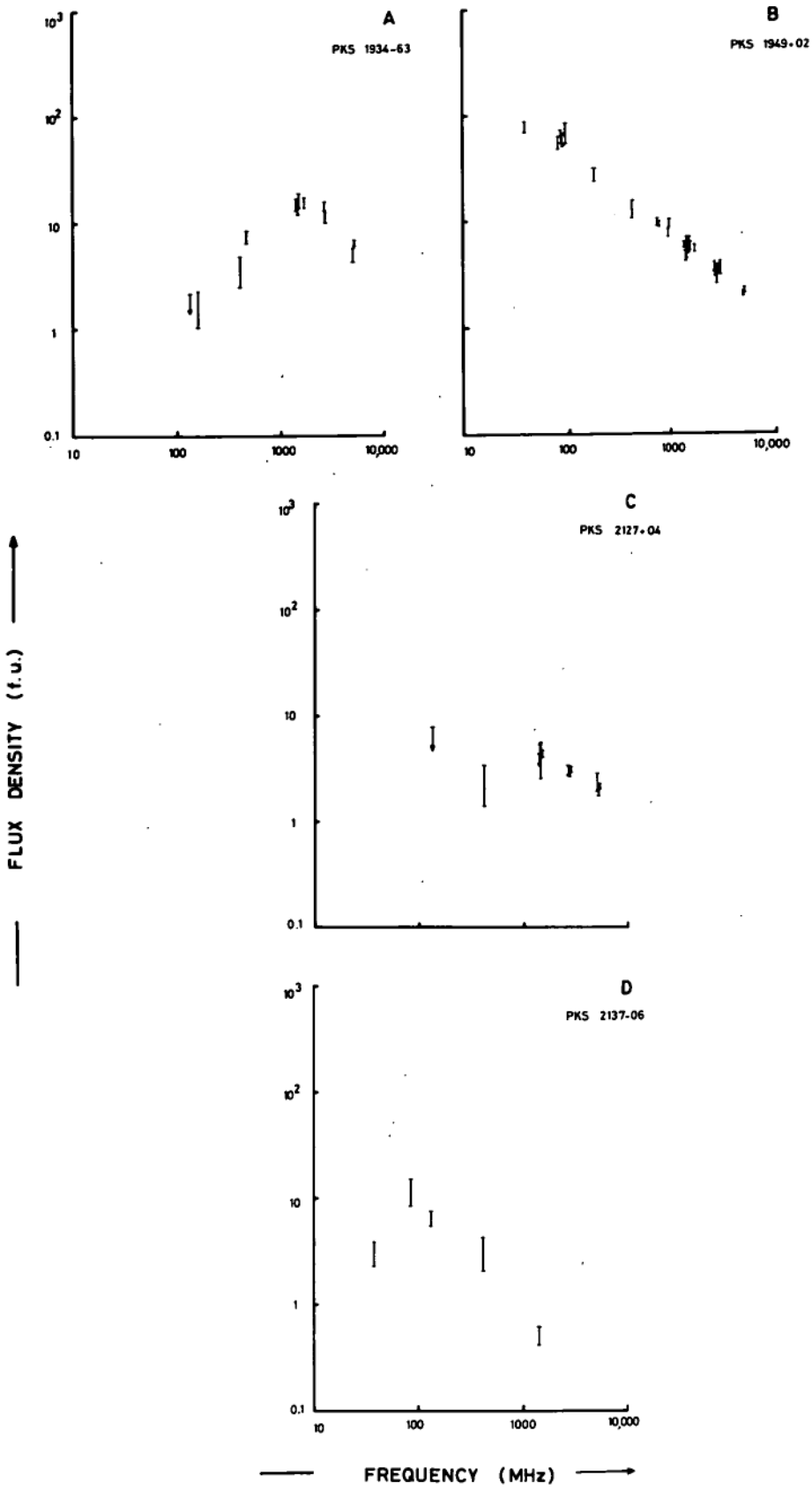
A
PKS 1934-63
B
PKS 1949+02
C
PKS 2127+04
D
PKS 2137-06
FLUX DENSITY (f.u.)
FREQUENCY (MHz)
10
100
1000
10,000
0.1
1
10
10^2
10^3

FIGURE 3.20

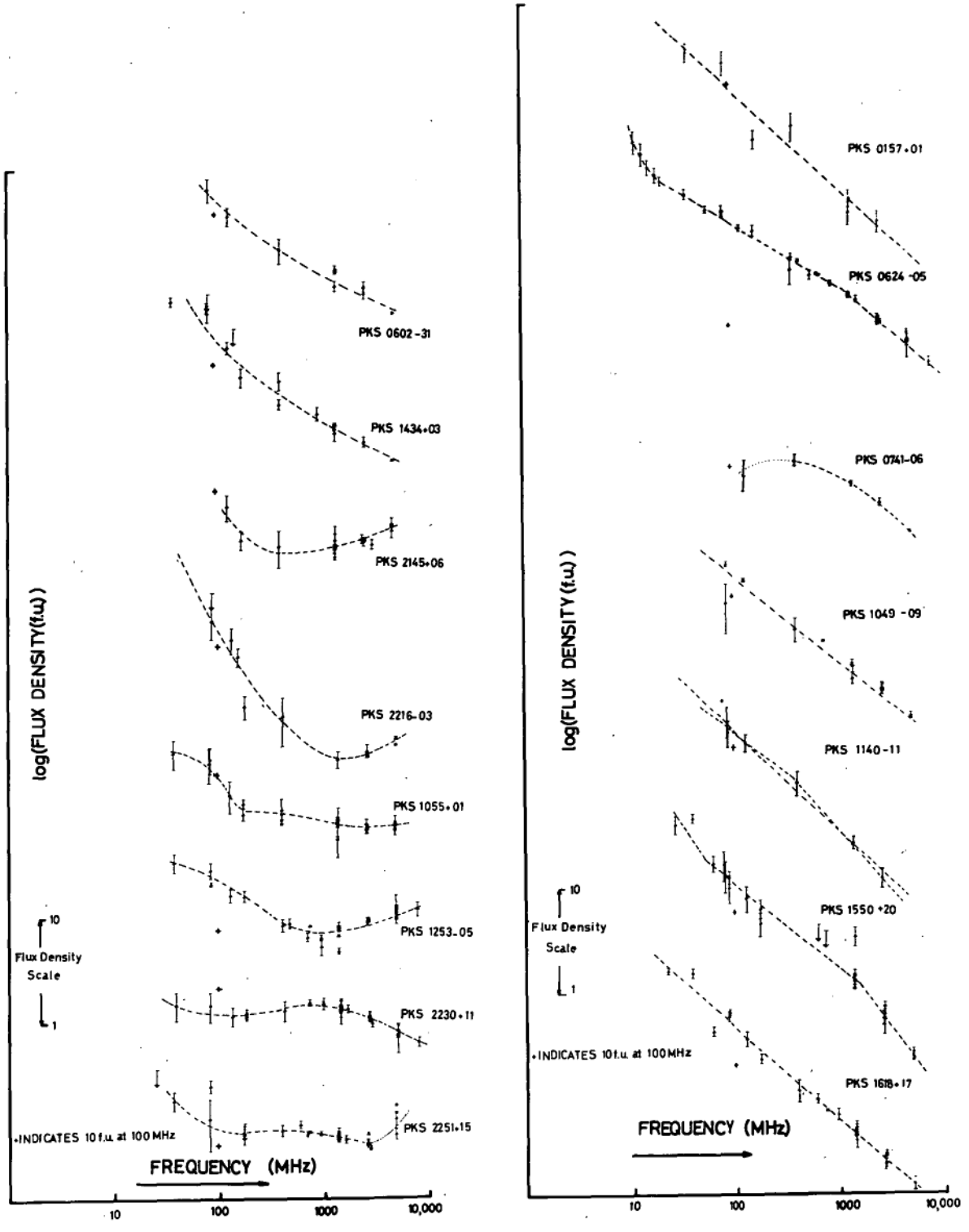
log(FLUX DENSITY(f.u.))
PKS 0602-31
PKS 1434+03
PKS 2145+06
PKS 2216-03
PKS 1055+01
PKS 1253-05
PKS 2230+11
PKS 2251+15
10
Flux Density
Scale
1
*INDICATES 10 f.u. at 100 MHz
FREQUENCY (MHz)
10
100
1000
10,000
log(FLUX DENSITY(f.u.))
PKS 0157+01
PKS 0624-05
PKS 0741-06
PKS 1049-09
PKS 1140-11
PKS 1550+20
PKS 1618+17
10
Flux Density
Scale
1
*INDICATES 10 f.u. at 100 MHz
FREQUENCY (MHz)
10
100
1000
10,000

FIGURE 3.21.

F. Conclusion.

The low frequency source measurements presented in this chapter have provided useful data for some 350 sources visible from the southern hemisphere. These results will be used in the source spectra analysis in the next section.

ADDENDUM TO CHAPTER 3.

The following discussion should be read prior to the conclusions to chapter 3 on page 119.

F. Confusion Effects:

In the discussion of the source measurements above little has been said about the problems of source confusion. The study of discrete sources at low frequencies is seriously affected by this problem, especially with instruments with a low resolving power. Certain corrections for confusion can be made using the catalogues of known sources (see appendix 3). However, integrated emission from numerous weak, unresolved sources in the telescope beam is the most important contribution to the confusion background. In this part of chapter 3 we estimate these effects for each of the surveys discussed above using methods outlined by Mills and Slee (1957), Bennett (1961) and others.

Mills and Slee (1957) have shown that if the distribution of sources in space is uniform and isotropic then an expression can be found relating the minimum reliably observable flux density, S_r, of a survey to S_o, the flux density of the strongest "average" source. If the root mean square deviation of the output due to all sources with flux density less than S_r in the beam is smaller than $(1/3)S_r$ then:

$$S_r = 9(\Omega/4\pi)^{2/3} S_o$$

where for a uniformly illuminated aperture of area, A,

$$\Omega = \tfrac{1}{2} \frac{\lambda^2}{A}$$

To estimate S_r for a survey we therefore need to estimate a value for S_o at the observing wavelength, λ.

The only comprehensive survey that has been completed below 408 MHz in the southern hemisphere is that at 85 MHz by Mills, Slee and Hill (1958). To estimate S_o for each set of observations discussed in this chapter we have two alternative methods available. We can use a published source survey and log N ~ log S * curve (for example

* N is the number of sources per steradian observed with flux density greater than S.

by: Mills and Slee, 1957; Gower, 1966; or Pooley and Ryle, 1968) which we extrapolate to $N = 1$ to find S_o at the frequency of the published survey. We then use a value for the mean spectral index of radio sources to try and estimate S_o at our observing frequency from S_o found at the survey frequency. Alternatively, an approximation to S_o is obtained by averaging our observed flux densities for the strongest sources in the sky. The estimation of S_o is thus rather subjective but the two methods appear to give comparable results.

We have used the above equations to calculate the r.m.s. confusion level of each source survey reported earlier in this chapter. Values of S_r at various observing frequencies are listed below.

Survey Freq:	Telescope:	S_r (flux units)
10.2 MHz Background	Rectangular Array	1.4×10^3
153 MHz Background	Parkes 210 ft dish	13.0
Total Power Source Measurements 70 MHz	Parkes 210 ft dish	62.0

Interferometer Source Measurements 159 MHz	Parkes 210, 60 ft dishes	10.5
Interferometer Source Measurements 132 MHz	"	17.0
Interferometer Source Measurements 84 MHz	"	41.0

As a result of these calculations the following points should be noted.

(a) The errors quoted for the 10.02 MHz source measurements include errors due to source confusion and background irregularities. (See table 3.3 - page 80).

(b) The new source flux densities at 153 MHz given in table 3.4 which are less than 13 flux units should be treated with caution. These are less than the r.m.s. confusion level. Also, the confusion error given above should be included with the other errors discussed on page 86 when assessing the significance of the 153 MHz results.

(c) Results for some of the sources listed in table 3.8 should also be treated with caution. In particular the results for the sources:

PKS: 0002+12, 0036+03, 0157+01, 0252-71, 0358+00, 0602-31, 0702-10, 0704-23, 0709-20, 0741-06, 0827+07, 0841+15, 0909+16, 0957+14, 1044+15, 1055+01, 1140-11, 1302-49, 1330+02, 1345+12, 1414+11, 1449-13, 1514+18, 1523+03, 1550+20, 1617-04, 1645+17, 1732+16, 1801+01, 1934-63, 2127+04, 2137-06, 2145+06, 2216-03, 2230+11, and 2251+15.

are within the r.m.s. confusion limits. To assess the significance of the results (given in table 3.8) the reader should include the confusion errors (given above) with the other types of error, given in the table of results (column 10).

It is immediately apparent from these calculations that the upper limit to the flux density of the source PKS 1934-63 for instance, is much less than the r.m.s. confusion level. The flux density given in table 3.8 is therefore not meaningful.

G. Conclusions

The low frequency .....

(continued on page 119).

ERRATA

Page 56: line 18 ~~ff~~ jj should read:

... survey frequency of 408 MHz. In this thesis results taken from the Parkes Catalogue are all from the revised catalogue edited by J. Ekers (1969). The source flux densities are therefore all based on the revised C.K.L. scale discussed by Kellermann (1964a). Only passing reference will be made to the original Parkes Catalogues by Bolton et al. (1964), Day et al. (1966), Price and Milne (1965) and Shimmins et al. (1966).

Page 59: Part B should read:

B. Sources used as Survey References

The measurements reported in this chapter were all calibrated by a relative intensity method using one or more of the sources PKS: 0915-11, 1226+02, 1648+05 or 1711-00 as primary calibration sources. The low frequency spectrum of each standard source was determined from the flux density scales of Conway, Kellermann and Long (1963) and Kellermann (1964a). The receivers used for the Parkes measurements were checked for stability periodically by scanning the telescopes in declination through regions of the sky

centred on six other sources. (PKS: 0106+13, 1120+05, 1330+02, 1932-46, 2152-69, 2310+05). Note that because of problems of source confusion the spectra of these six sources were not used as calibration standards. However, for reference we show the spectra of all of the sources mentioned above in figures 3.1 to 3.5. The data shown was obtained from articles listed in table 1 of appendix 2. We have fitted a power-law spectrum to the data of each ... (page 60)

page 79: line 21 ff should read:

...

fluctuations on the records. An upper limit to the error of each measurement is indicated as a percentage of the flux density in the table of results.

page 86: line 2 ff should read:

An upper limit to the errors in the 153 MHz source flux densities is 10% ± 14 flux units. The errors result from noise fluctuations on the records, from the calibration technique used and from the effects of confusion with weak, unresolved sources in the beam of the telescope.

page 86: lines 19 and 20 should read:

The confusion effects are discussed in the addendum to this chapter (part F).

facing page 87:

Insert:

Notes to Table 3.4

Since the compilation of table 3.4 we have found that a number of alterations are required for accuracy. A number of the sources listed in this table lie within one beamwidth of one another (beamwidth = 2.18° at 153 MHz). Such sources should be grouped in column 1 and the flux density observed is the sum of the radiation from each source in the beam. The following sources in the table are of this category and the total observed flux density is as shown below rather than the value shown in column 5 of the table.

Parkes Cat. No.	Total Flux Density (f.u.)	Parkes Cat. No.	Total Flux Density (f.u.)
0036+03	(59)	0456-30	(65)
0037+04		0503-28	
		0511-30	
0053-01	(88)		
0055-01		0800-09	(33)
		0806-10	
0056-17	(31)		
0056-18		0850-20	(27)
		0855-19	
0109+02	(30)		
0115+02		0851-14	(57)
0118+03		0859-14	
0146+00	(39)	0949+00	(81)
0150+00		0950+00	
		0957+00	
0235+09	(16)		
0237+09		1005+07	(46)
		1008+06	
0331-01	(63)		
0336-01		1122-37	(27)
		1123-35	
0446-20	(36)		
0453-20		1131-17	(29)
		1131-19	

Parkes Cat. No.	Total Flux Density (f.u.)	Parkes Cat. No.	Total Flux Density (f.u.)
1134+01	(33)	1635-14	(36)
1138+01		1640-15	
1146+05	(21)	2101-49	(16)
1152+04		2105-48	
1245-19	(33)	2119-16	(32)
1247-19		2120-16	
1246+09	(16)	2149-20	(33)
1249+09		2154-18	
1332-33	(78.3)	2207-45	(30)
1333-33		2213-45	
1334-33			
		2216-03	(27)
1348-12	(42)	2221-02	
1358-11			
		2218-50	(14)
1424+03	(21)	2220-50	
1425+04			
		2219-15	(60)
1547-79	(53)	2220-15	
1549-79			
		2252-53	(50)
		2253-52	

Parkes Cat. No.	Total Flux Density (f.u.)	Parkes Cat. No.	Total Flux Density (f.u.)
2258+09	(40)	2323-40	(33)
2307+10		2331-41	
2309+09			
		2335+03	(19)
2305-41	(22)	2338+04	
2310-41		2338+03	

Page 87:

The sources PKS: 0000+00, 2357+00 and 0003+00 should be deleted from the beginning of table 3.4.

Page 92: line 2 *ff* should read:

... 153 MHz in table 3.4. Note, however, that 4 of these sources (namely PKS: 0055-01, 0331-01, 0806-10, 1008+06) are close to other sources and the 153 MHz flux densities may be uncertain.

Page 93: line 7 ff should read:

... catalogue. Note, however that the 153 MHz flux densities for 4 of these sources may be uncertain due to confusion with nearby sources also in the beam of the telescope.

Page 101: line 11 ff should read:

An upper limit to the errors in the total power measurements is shown in table 3.7. The errors result from variations in the noise diode signal, fluctuations in the records and errors in determining the flux density of Hydra A. Sources obviously confused with nearby sources were not measured using total power receivers. The Parkes Catalogue was used to locate such confusion sources. The r.m.s. confusion errors are calculated in the addendum to this chapter (part F).

Page 101, line 19 ff should read:

... records and from confusion effects. An upper limit to each type of error involved in the interferometer measurements was found as follows. The method ....

Page 103: line 2 ff should read:

... the errors due to confusion effects is discussed in appendix 3 and in the addendum to this chapter.

Page 103 lines 3,4 should be deleted.

Pages 242-247

The following references should be included in the Bibliography.

Bennett, A.S. (1961): - "Some Studies of Galactic Radio Sources of Large Angular Extent" Ph.D. Thesis. Univ. of Cambridge, Cambridge.

Gower, J.F.R. (1966) - Mon. Not. R. astr. Soc., 133, 151.

Mills, B.Y. and Slee, O.B. - (1957) Aust. J. Phys., 10, 162

Pooley, G.G. and Ryle, M. (1968) - Mon. Not. R. astr. Soc., 139, 515.

SECTION 3

SOURCE SPECTRA ANALYSIS

CHAPTER 4

Curvature in Source Spectra.

A. Introduction:

With the data at present available many extragalactic sources appear to have spectra of the form*: $S_\nu \propto \nu^\alpha$ where S_ν is the source flux density, ν, is the frequency and α the spectral index. However, a significant number of sources have spectra that differ from this (see, for example Kellermann and Pauliny-Toth, 1969) in which case the spectra are said to be curved. In this chapter we consider the different types of curved spectra and summarize the theories that have been proposed to account for them.

For further discussions the reader is referred to articles by Hornby and Williams (1966), Williams (1966), Slish (1963), Bridle (1967), and Scheuer and Williams (1968).

B. Classification of Curved Spectra.

Curved spectra are classified according to the changes that occur in the spectral index, α, with frequency. If the spectral index $\alpha(\nu_1, \nu_2)$ between the frequencies ν_1 and ν_2 *decreases* with increasing frequency, the source spectrum is said to be *convex* (positive curvature). The spectrum is *concave* if the spectral index *increases* with increasing frequency (negative curvature). The spectra of some sources

---

* The spectrum is straight on a plot of $\log(S_\nu)$ against $\log(\nu)$.

are more complicated than either of these two types. If a spectrum is a combination of *concave* and *convex* segments, it is referred to as a *complex* spectrum.

C. Convex Spectra:

(i) Low Frequency Turnovers in Spectra.

Low frequency turnovers (cut-offs) result either from the effects of enhanced absorption or from decreased source emissivity at low frequencies. Many sources with low frequency cut-offs have a high surface brightness temperature [see Williams, 1966; Slish, 1963]. The maximum temperature is less than or equal to 10^{12} degK. [Kellermann and Pauliny-Toth, 1969], since, for higher values, inverse Compton scattering becomes very important. Losses by this process quickly reduce the temperature into the range 10^{10} to 10^{11} degK, where electron energy losses by the inverse Compton process are about equal to losses by synchrotron radiation. A high surface brightness temperature is a necessary condition for synchrotron self-absorption to occur and hence this mechanism is believed to be responsible for the *convex* spectra of many sources although other mechanisms cannot be ignored. An electron distribution cut-off, thermal absorption and the Tsytovich effect can also cause low frequency cut-offs. These above processes were discussed in chapter 1.

There are a number of effects not mentioned previously

in chapter 1 which should be considered.

Electron Distribution Cut-offs.

Decreased emissivity may result from a direct electron distribution cut-off at low energies. If the number of electrons with energy ε in the range ε to $\varepsilon + d\varepsilon$ is $N(\varepsilon)\, d\varepsilon$ then:

$$N(\varepsilon)\, d\varepsilon = Ke^{-\gamma}\, d\varepsilon \quad \text{for } \varepsilon \geq \varepsilon_1$$
$$= 0 \qquad \text{for } \varepsilon < \varepsilon_1 \qquad \ldots.(4.1)$$

where ε_1 is the cut-off energy. The synchrotron spectrum emitted by this electron distribution will be

$$S(\nu) \propto \nu^{\frac{1}{2}(1-\gamma)} \qquad \ldots.(4.2)$$

[c.f. equation 1.18]

at frequencies above the characteristic frequency

$$\nu_c = 16.1\ B_\perp [\mu\text{-gauss}]\ \varepsilon_1^2\ [\text{GeV}]\ \text{MHz} \qquad \ldots.(4.3)$$

[c.f. equation 1.5]

Here: $S(\nu)$ is the flux density emitted at frequency ν;
ε is the electron energy;
$B_\perp$ is the component of the magnetic field perpendicular to the direction of motion of the electron;

and: Ke and γ are constants.

The synchrotron radiation from a single electron rises as $\nu^{1/3}$ for frequencies well below the cut-off frequency given by equation (4.3). Thus, the spectrum emitted by a distribution of electrons all radiating below their cut-off frequencies will be

$$S(\nu) \propto \nu^{1/3} \quad \text{for } \nu \ll \nu_c \qquad \ldots.(4.4)$$

We note from equation (4.4) that if the spectral index of the radiation is more positive than $+1/3$ below the turnover in the source's spectrum, then an electron energy cut-off cannot alone account for the radiation.

An approximation for finding the electron distribution cut-off in the source is to assume that all the emission at a frequency ν_1 originates from electrons with energy ε_1 such that:

$$\nu_1 = 0.29\ [16.1\ B_\perp\ \varepsilon_1^2]\ \text{MHz} \qquad \ldots.(4.5)$$

[see equations 1.5, 1.8]

where: ε_1 is the cut-off energy (in GeV) in the electron distribution;

ν_1 (MHz) is the observed low frequency spectrum cut-off;

and: $B_\perp$ is in μ-gauss.

A more accurate estimate of the cut-off energy ε_1 (for values of $\gamma \geq 1.5$) has been given by Ginzburg and Syrovatskii

(1965), namely:

$$\frac{\nu_1\,[\mathrm{MHz}]}{k_1(\gamma)} \simeq 16\ B_\perp\ [\mu\text{-gauss}] \times \varepsilon_1^2\ [\mathrm{GeV}] \qquad \ldots.(4.6)$$

where: $k_1(\gamma)$ is a numerical factor depending on gamma.

Values for k_1 are given in the table below:

γ	1	1.5	2.0	2.5	3.0	4.0
$k_1(\gamma)$	0.8	1.3	1.8	2.2	2.7	3.4

The Tsytovich Effect and Thermal Absorption.

If a source contains free electrons then the Tsytovich effect and thermal absorption can change the low frequency spectrum of the source. Hornby and Williams (1966) have shown that polarization data enables the relative importance of each of these effects to be determined. The percentage polarization, P, of the radiation from the source at infinite frequency is related to the magnetic field within the source:

$$\frac{P}{100} = \frac{|B_\parallel|}{|B_\perp|} \qquad \ldots.(4.7)$$

As the waves pass through the ionized medium the plane of polarization is rotated. The rotation measure is given by: (see equation 1.64):

$$\mathrm{R.M.} = 8.1 \times 10^8\ N\ B_\parallel\ L \text{ radian } m^{-2} \qquad \ldots.(4.8)$$

where we have assumed that all the Faraday rotation occurs within the source of diameter L (kiloparsecs) and the density of free electrons N (cm^{-3}) is constant throughout the source. The symbols, $B_{\parallel}$, $B_{\perp}$, are the components of the magnetic field, (assumed uniform) within the source (in gauss). If the characteristic frequency of the thermal absorption within the source is ν_{OH} (from equation 1.56) and ν_T is the Tsytovich cut-off frequency, then:

$$\frac{\nu_{OH}^2}{\nu_T} \simeq 1.7 \times 10^{12} \, P^{-1} \, (R.M.) \, Te^{-3/2} = k \qquad ....(4.9)$$

[Hornby and Williams, 1966]

where ν_{OH} and ν_T are in Hertz and Te is the temperature of the ionized medium in degK.

If k is greater than the observed cut-off frequency then the effects of the Tsytovich process are small compared with thermal absorption. If k is less than the observed cut-off frequency then the converse holds.

If the temperature of the ionized medium is known, then equation (4.9) can be used to find the relative importance of the Tsytovich process and thermal absorption in changing the spectrum of a source. The temperature in the ionized hydrogen medium is often taken in the literature to be 10^4 degK, but this particular value is debatable.

(ii) High Frequency Steepening:

A large number of sources have spectra that steepen at high frequencies. The curvature is not usually continuous since above and below the cut-off frequency the spectrum is straight (power-law). The cut-off frequency often occurs near 1000 MHz; however this may not be significant but may result from the observations at present available [see Kellermann and Pauliny-Toth, 1969].

The decreased emissivity at high frequencies results from a lack of energetic particles within the source either because of a direct electron distribution cut-off of the form:

$$N(\varepsilon)\, d\varepsilon = Ke\ \varepsilon^{-\gamma}\, d\varepsilon \quad \text{for } \varepsilon < \varepsilon_2$$

$$= 0 \qquad \text{for } \varepsilon > \varepsilon_2$$

where: ε is the energy of the electron, ε_2 is the cut-off energy,

and: Ke and γ are constants,

or because of electron energy loss processes. The latter have been discussed in chapter 1.

D. Concave and Complex Spectra.

High resolution interferometer studies have shown that sources with *concave* or *complex* spectra usually consist of more than one emission component [Fomalont, 1968; Bash, 1968; Clark et al., 1968 a,b]. The emission from the younger, more compact components may be self-absorbed

in the observed wavelength range [Kellermann and Pauliny-Toth, 1968].

(i) Concave Spectra:

Several mechanisms have been proposed to account for *concave* spectra.

High energy particles are injected into a source by catastrophic events within the source. The electrons will rapidly lose energy by inverse Compton interactions and synchrotron radiation (provided there is a magnetic field) during their early life. This type of process may lead to an excess of low energy electrons and hence to a steep low frequency emission spectrum from old and extended sources. The young components of a source usually have flat spectra, [Scheuer and Williams, 1968] and hence we might expect old sources with young emission components to have *concave* (or perhaps *complex*) spectra. Recent observations between 12 and 25 MHz by Braude et al. (1969 a,b) have shown that there are a significant number of sources with *concave* spectra at low frequencies. These spectra are adequately explained by assuming there are two "power-law" components, of the form described above, in each source.

A source which consists of a thermal and a nonthermal (synchrotron) component may have a *concave* spectrum. However the high frequency emission from many extragalactic sources is polarized [see, for example, Gardner et al., 1969 a]

and non-thermal radiation from these sources must therefore greatly exceed any possible thermal component. In general we believe there is little thermal emission from extragalactic radio sources.

The electron energy distribution within a source can be changed by synchrotron radiation losses from a power-law to one of the form: (c.f. equation 1.42)

$$N(\varepsilon,\theta,t)\, d\varepsilon = \frac{Ke\ \varepsilon^{-\gamma}\, d\varepsilon}{[1-aB_{\perp}^{2}\ \varepsilon\ t]^{2-\gamma}}$$

where: ε is the energy of the electron,

θ is the electron pitch angle,

t is the time,

Ke is a constant,

a is a constant,

$B_{\perp}$ is the component of the source magnetic field perpendicular to the direction of motion of the electron,

and: γ is the index of the electron distribution at the initial instant of time.

The energy losses cause a "bunching" of electrons with energy near $\varepsilon_s = \frac{1}{aB_{\perp}^{2}t}$ and a *concave* emission spectrum may result. However, new electrons are provided by explosive events within the source and hence there is no basis for assuming an abundance of electrons all with an energy ε_s,

and a pitch angle θ. Some emission might be expected from extragalactic sources by this process if coherent streaming of electrons along the magnetic field lines occurred. (see also the model discussed on page 40).

The theory that best explains *concave* curvature is one of power-law emission from two components of the source.

(ii) Complex Spectra:

Kellermann and Pauliny-Toth (1968 and 1969) have shown that sources with *complex* spectra usually consist of more than one radiation component. They suggest that a *complex* spectrum may be explained adequately by the summation of *power-law* and *self-absorbed* radiation from the different parts of the source.

E. Conclusion.

In this chapter we have briefly discussed different types of curved spectra and the theories proposed to account for the curvature. A number of other theories have been advanced [See, for example, Scheuer and Williams, 1968] to account for part of the emission from some sources with unusual spectra but these probably relate to only a small minority and will therefore not be considered here.

The theories discussed above will be used in the next chapter to explain the curvature in the spectra of sources visible from the southern hemisphere.

CHAPTER 5

ANALYSIS OF CURVED SPECTRA.

A. Introduction.

In this chapter we discuss the curvature in the spectra of sources visible from the southern hemisphere. Many of the sources to be considered had been measured at only one or two frequencies below 408 MHz prior to the observations discussed in chapter 3. An analysis of the spectra was impossible with the data then available. The new results now permit such a discussion.

The sources to be analysed, the models used to explain the curvature and the method of fitting theoretical spectra to the source data are discussed in the first section of this chapter (parts B and C). The parameters of the models for each source are given in part D. Finally, the results of the curve fitting are discussed in detail in part E taking account of any polarization, angular size and identification data that is available.

B. Sources to be Analysed.

The sources to be considered are all those south of declination $+27^{o}$ that have well defined *low frequency convex* spectra, *concave* spectra, or *complex* spectra. There is apparently no way to differentiate between the electron energy loss processes proposed to account for high frequency steepening in a spectrum (see page 25) and hence sources with this type of spectrum have not been considered here. The spectral data used in the analysis is from the new results presented in chapter 3 and from the references listed in table 1 of appendix 2. A number of the sources considered were not measured by the author, but they are included in the analysis for completeness since they have well defined spectra.

The results of the most extensive source survey completed in the southern hemisphere are given in the "Parkes Catalogue of Radio Sources" [S 32 - table 1, appendix 2]. Some 40 sources have been classified in this catalogue as having curved spectra. Of these, 23 have proved unsuitable for analysis for the reasons listed in table 5.1. When the new low frequency data (Chapter 3) is combined with data from the articles listed in table 1 of appendix 2 a further 53 sources appear to have curved spectra. Thus a total of 70 source spectra are discussed in this chapter.

TABLE 5.1

SOURCES UNSUITABLE FOR ANALYSIS.

Sources. [PKS]	Comments. [H.F. CUT-OFF: indicates that the spectrum of the source has a high frequency cut-off (convex curvature)]
0008-42	Spectrum uncertain - new data (chapter 3) suggests that the source has a H.F. CUT-OFF.
0049-43	H.F. CUT-OFF.
0319-45	Spectrum uncertain.
0336-01	Perhaps a *complex* spectrum - spectrum is uncertain.
0410-75	Perhaps a *convex* spectrum at low frequencies - spectrum is uncertain.
0537-75	Insufficient data for analysis - *convex* at high frequencies.
0735+17	Insufficient data for analysis.
1151-34	Spectrum uncertain - *convex* or *complex*.

Table 5.1 (cont.)

Sources. [PKS]	Comments.
1226+02	This source has been discussed extensively elsewhere.
1252+11	Spectrum uncertain - possibly *concave*.
1414+11	H.F. CUT-OFF.
1514+07	H.F. CUT-OFF.
1712-03	Spectrum uncertain - possibly H.F. CUT-OFF.
1754-59	H.F. CUT-OFF.
1802+11	Spectrum uncertain - possibly *convex*.
1814-63	Spectrum not curved (see new data page 119)
2012+23	H.F. CUT-OFF.
2048-57	Spectrum uncertain - possibly a H.F. CUT-OFF.
2144+15	H.F. CUT-OFF.
2154-18	Steep H.F. CUT-OFF.
2211-17	H.F. CUT-OFF.
2318-16	H.F. CUT-OFF.
2328+10	Insufficient data for analysis - probably a *complex* spectrum.

C. METHODS OF ANALYSIS.

The models that have been proposed to account for curved source spectra have been discussed in chapters 1 and 4. The theoretical spectral curves appropriate to these models can be fitted to the observed source spectra. The accuracy with which the curves can be fitted will then indicate the adequacy of the models in explaining the radiation.

(i) Summary of the Models and their parameters.

The models are summarized below in a suitable form for fitting to the source data.

Low Frequency Convex Spectra.

In the following analysis we have assumed that there is a *power-law* distribution of electrons within each source. The radiation is taken to be synchrotron emission from the relativistic electrons within the source.

Electron Distribution Cut-Off at Low Energies.

The source flux density at a frequency, ν(Hz) is given by: (see equation 1.14)

$$S^*(\nu) = A \int_{\varepsilon_1}^{\infty} \varepsilon^{-\gamma} F\{\frac{\nu}{\nu_c}\} d\varepsilon \quad W\ m^{-2}\ Hz^{-1} \quad ...(5.1)$$

where: ε is the energy of the electron;

$\gamma = 1 - 2\alpha$ where α is the spectral index;

ε_1 is the cut-off energy of the electron distribution;

and: ν_c is the characteristic frequency of the emission from a single electron (see equations 1.4, 1.5).

The parameters of the model are A, ε_1, α and ν_c. However, it is convenient to group ε_1 and ν_c together and to consider the parameters to be A, α and $\varepsilon_1^2 B_\perp$ (see equation 1.5), where $B_\perp$ is the component of the source magnetic field strength perpendicular to the direction of radiation.

Absorption in Ionized Hydrogen uniformly mixed with a synchrotron source.

The source flux density at a frequency, ν(Hz) is given by: (see equation 1.59)

$$S^*(\nu) = \frac{A\ \nu^{\alpha+2}}{\nu_o^2} \{ 1 - \exp [-\nu_o^2/\nu^2] \} \text{ Watt m}^{-2} \text{ Hz}^{-1} \quad \ldots(5.2)$$

where: A is a constant; α is the spectral index; and ν_o is the *characteristic* frequency or frequency at which the optical depth of the absorber is unity (Hz).

The parameters of the model are A, α, ν_o .

Absorption in Ionized Hydrogen which surrounds a synchrotron source.

The source flux density at a frequency, ν(Hz) is given by: (see equation 1.58)

$$S^*(\nu) = A\ \nu^{\alpha}\ \exp [-\nu_o^2/\nu^2] \text{ Watt m}^{-2} \text{ Hz}^{-1} \quad \ldots(5.3)$$

where: A is a constant; α is the spectral index and ν_o is the *characteristic* frequency of the ionized hydrogen medium (Hz).

The parameters of the model are A, α, and ν_o.

Synchrotron Self-Absorption.

The source flux density at a frequency, ν(Hz) is given by:

(see equation 1.30)

$$S^*(\nu) = A\ \nu^{2.5}\ \{1 - \exp\ [\ -\ [\ \frac{\nu}{\nu_1}\ ]^{\alpha-2.5}\ ]\ \}\ \text{Watt m}^{-2}\text{Hz}^{-1} \quad \ldots(5.4)$$

where: A is a constant, α is the spectral index and ν_1 is the *characteristic* frequency or the frequency at which the optical depth of the self-absorbing medium becomes unity (Hz).

The parameters of the model are A, α and ν_1. Note that in this model we have assumed that the size of the source is independent of the frequency

The Tsytovich-Razin Effect.

The source flux density at frequency, ν(Hz) is given by:

(see equation 1.22)

$$S^*(\nu) = A \int_{\varepsilon} \varepsilon^{-\gamma}\ \{\ 1 + (1-n^2)\ [\frac{\varepsilon}{m\ c^2}]^2\ \}^{-\frac{1}{2}}\ F(\nu/\nu_c^*)\ d\varepsilon$$

$$\text{Watt m}^{-2}\ \text{Hz}^{-1} \quad \ldots(5.5)$$

where: n is the refractive index of the medium in the vicinity of emission and: $n^2 = 1 - \frac{e^2 Ne}{\pi m \nu^2}$;

$$\nu_c^* = \nu_c \{1 + (1-n^2) [\frac{\epsilon}{m c^2}]^2 \}^{-3/2} \quad ;$$

c is the velocity of light;

e,m are the electronic charge and mass respectively;

ϵ is the energy of the electron;

ν_c is the *characteristic* frequency of emission from an electron (see equations 1.4, 1.5);

A is a constant; Ne= density of free electrons;

and: $\gamma = 1 - 2\alpha$ where α is the spectral index.

The unknowns in this model are A, α, ν_c, and n, although it is convenient to take the parameters of this model as A, α Ne and $B_\perp$ (see equation 1.5).

The function F(x) in the above relations is given by:

$$F(x) = x \int_x^\infty K_{5/3} (y)\, dy \quad ;$$

the calculation of this function is discussed in appendix 1.

Concave and Complex Curvature Spectra.

The radiation from sources with *concave* or *complex* spectra may be adequately described by the relation; (see chapter 4)

$$S^*(\nu) = \sum_m A_m \nu^{\alpha_m} + \sum_n B_n \nu^{2.5} \{ 1 - \exp [-(\frac{\nu}{\nu_{o_n}})^{\alpha_n - 2.5}] \}$$

Watt m^{-2} Hz^{-1} ...(5.6)

where: $S^*(\nu)$ is the source flux density at frequency, ν(Hz);

m,n are integers;

A_m, B_n are constants;

α_m, α_n are spectral indices;

and: ν_{o_n} is the frequency at which the optical depth of the self-absorbed source, n, becomes unity.

The first term in equation 5.6 represents the *power-law* components of the source and the second term the radiation from *self-absorbed* components of the source. Note that the angular diameter of the self-absorbed components is taken to be independent of the frequency. The values of m and n in the equation will depend on the structure of the radio source. For example a *concave* spectrum may be explained by taking m=2, n=0 provided the spectral index is not greater than zero, whereas, for a *complex* spectrum m and n will, in general, both be greater than unity. This can be seen in the analysis given in part D of this chapter.

(ii) Solution of the Models:

The relations (5.1 to 5.6) define the theoretical spectral curves fitted to the observed curved spectra. The curves were fitted by minimizing the function:

$$F^* = \sum_{i=1}^{M} \{ \ln S^*(\nu_i) - \ln S(\nu_i) \}^2 \qquad \ldots(5.7)$$

with respect to the variables of the appropriate model.

Here: M is the number of experimental measurements of the source flux density available;

$S^*(\nu_i)$ is the flux density at frequency, ν_i, predicted by the source model;

and: $S(\nu_i)$ is the observed flux density at ν_i.

This "least-squares" fitting of the theoretical curve to the data is undertaken on a log-log scale to avoid giving excessive weight to the low frequency measurements. Note that a log(frequency) against log (flux density) graph is the normal method of presenting the observed spectrum.

The functions, $S^*(\nu_i)$, are, in general, non-linear under any transformation of the appropriate variables and the minimum of the function, F^*, has to be found by an iterative process. The process used in this investigation was that of Fletcher and Powell (1963 and 1965). The algorithm published by Fletcher and Powell (1965) was modified so that a local minimum of the function, F^*, was found with the variables of the model being constrained to have physically meaningful values. The implementation of the minimizing procedure is discussed further in appendix 4.

D. RESULTS OF THE MODEL ANALYSIS.

The parameters of the different models consistent with the observed source spectra are given in this part of chapter 5. The theoretical spectral curves are also shown together with the data used in the analysis.

(i) Sources with Low Frequency Convex Spectra.

Fourty-nine of the sources being considered in this chapter have low frequency *convex* spectra. Five models have been proposed to account for this type of curvature in a source spectrum. The problem is to determine which model or models is appropriate to the source. If the cut-off mechanism is known then by fitting the appropriate curve (see equation 5.1 to 5.5) to the observed spectrum we may obtain information about the nature of the source (or surrounding medium if absorption in ionized hydrogen causes the cut-off). However, if the mechanism is unknown the parameters of these models give only upper limits to the properties of the source (or surrounding medium).

We consider first the spectra of the sources, PKS: 1322-42, 1343-60, 1549-56, 1711-38 and 1934-63 since it is possible to specify more exactly the mechanism producing the curvature in each case.

PKS: 1322-42, 1343-60, 1549-56, 1711-38.

Curvature in the spectra of these sources probably results from absorption in ionized hydrogen in the galaxy [see for example, Ellis and Hamilton, 1966 a]. The data available at 4.7 MHz [Ellis and Hamilton, 1966] and now at 10 MHz (see chapter 3) permits an analysis of the curvature. We have assumed that each of the sources has a power-law emission spectrum down to 4.7 MHz and have fitted the

theoretical spectrum defined by equation (5.3) to the data using the method discussed in part C (ii) above. The parameters of the model appropriate to each source are given in table 5.2. Figure 5.1 shows the theoretical spectral curves together with the data used in the analysis. The implications of the model fitting are discussed in E below.

PKS 1934-63.

This source has a broadly peaked spectrum with a maximum near 1400 MHz. It has been discussed by Shklovskii (1965) and in detail by Kellermann (1966 b). Kellermann fitted various theoretical spectra to the data and showed that a power-law spectrum modified by thermal absorption, self-absorption or the Tsytovich-Razin effect could be made to fit the measurements available. He found that the source is probably young (~ few hundred years) and apparently has a high magnetic field(~ 10^{-2} gauss) or alternatively that there was a large mass of ionized hydrogen associated with the source. Kellermann indicated the need for more spectral data near 200 MHz to determine which of the mechanisms caused the curvature in the spectrum.

PKS 1934-63 was measured during the interferometer observations reported in chapter 3. This source was only just strong enough to be observed since it has a flux density of 1.7 flux units at 159 MHz while the "sensitivity limit" of the interferometer was ~ 1.1 flux units at this frequency.

TABLE 5.2.

Model Fitting to the sources PKS 1322-42, 1343-60, 1549-56 and 1711-38.

1. SOURCE PKS	2. l^{II} (degrees)	3. b^{II} (degrees)	4. Spectral Index.	5. $\int \frac{n^2}{Te^{3/2}} dl$ (cm^{-6} parsec $degK^{-3/2}$)
1322-42	309	19	-0.71	27×10^{-6}
1343-60	310	+2.1	-0.58	94×10^{-6}
1549-56	326	-1.7	-0.69	31×10^{-6}
1711-38	349	+0.6	-0.60	49.6×10^{-6}

Column 1: Parkes Catalogue Number (or using the same notation as used in the catalogue).

Columns 2,3: Galactic Coordinates *(new)*.

Column 4: Spectral index determined from the observed high frequency spectrum.

Column 5: The quantity $\int \frac{n^2}{Te^{3/2}} dl$ deduced from the variable ν_o (see equation 1.56).

FIGURE 5.1 A.

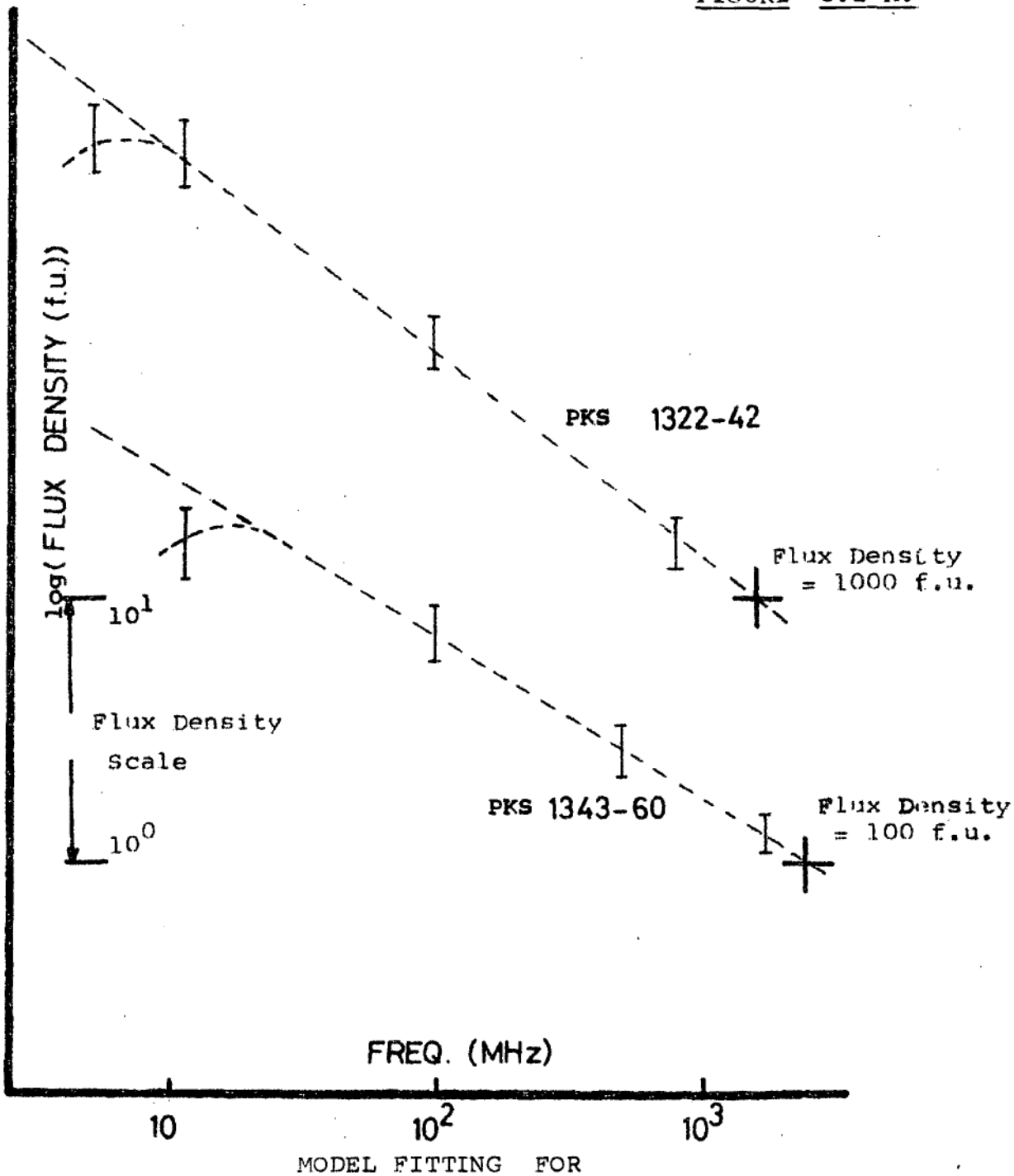

MODEL FITTING FOR

PKS: 1322-42, 1343-60.

FIGURE 5.1 B.

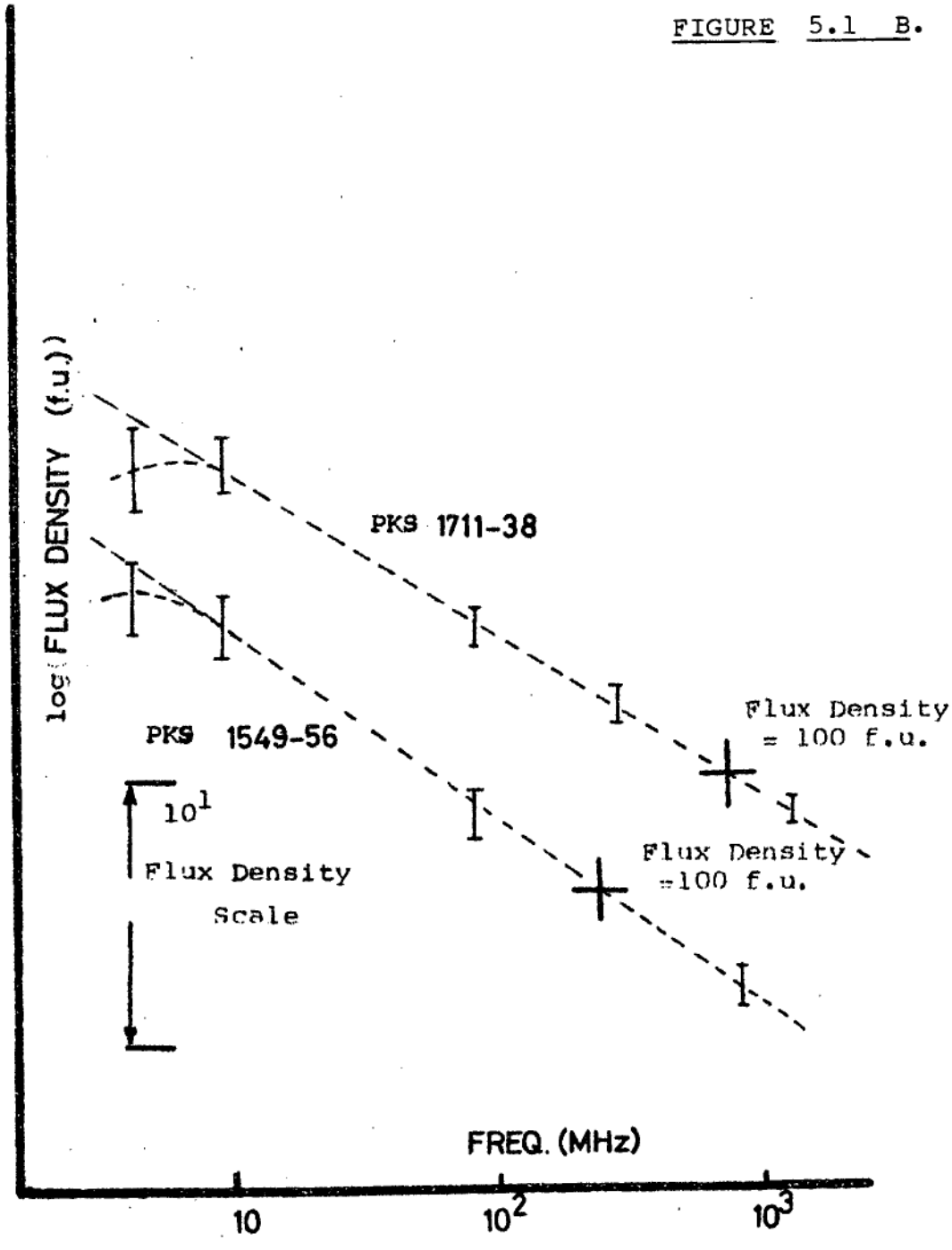

MODEL FITTING FOR

PKS: 1549-56, 1711-38 .

(facing page 145.)

Explanation of Figure 5.2

• Experimental data discussed by Kellermann (1966 b.)

I New results (see chapter 3) plus data from the Parkes Catalogue [S32 - table 1, appendix 2] and Ekers (1967) [S39-table 1, appendix 2]

Curves Fitted.

1. Absorption in ionized hydrogen uniformly mixed with a synchrotron source. [$\alpha = -0.97$, $\nu_\sigma = 1580$ MHz see equations 1.56 and 5.2]
2. Synchrotron self-absorption in a source with a uniform brightness temperature [$\alpha = -0.87$, $\nu_1 = 697$ MHz : - see equation 1.54]
3. Self-absorption in a source in which the surface brightness temperature varies across the source [B~10^{-1} to 10^{-3} gauss; total angular diameter ~ 0.003" but 50% of the radiation coming from a region ~ 0.0015" diameter : - model after Kellermann, 1966 b.]
4. Synchrotron radiation from a region where the Tsytovich-Razin effect is important and in which the density of thermal electrons is 4000 cm^{-3} [model after Kellermann, 1966 b.]
5. Absorption in ionized hydrogen which has an emission measure varying from $\frac{1}{2}Te^{3/2}$ to $8Te^{3/2}$ cm^{-6} parsec located between the source and the observer. [model after Kellermann, 1966 b]

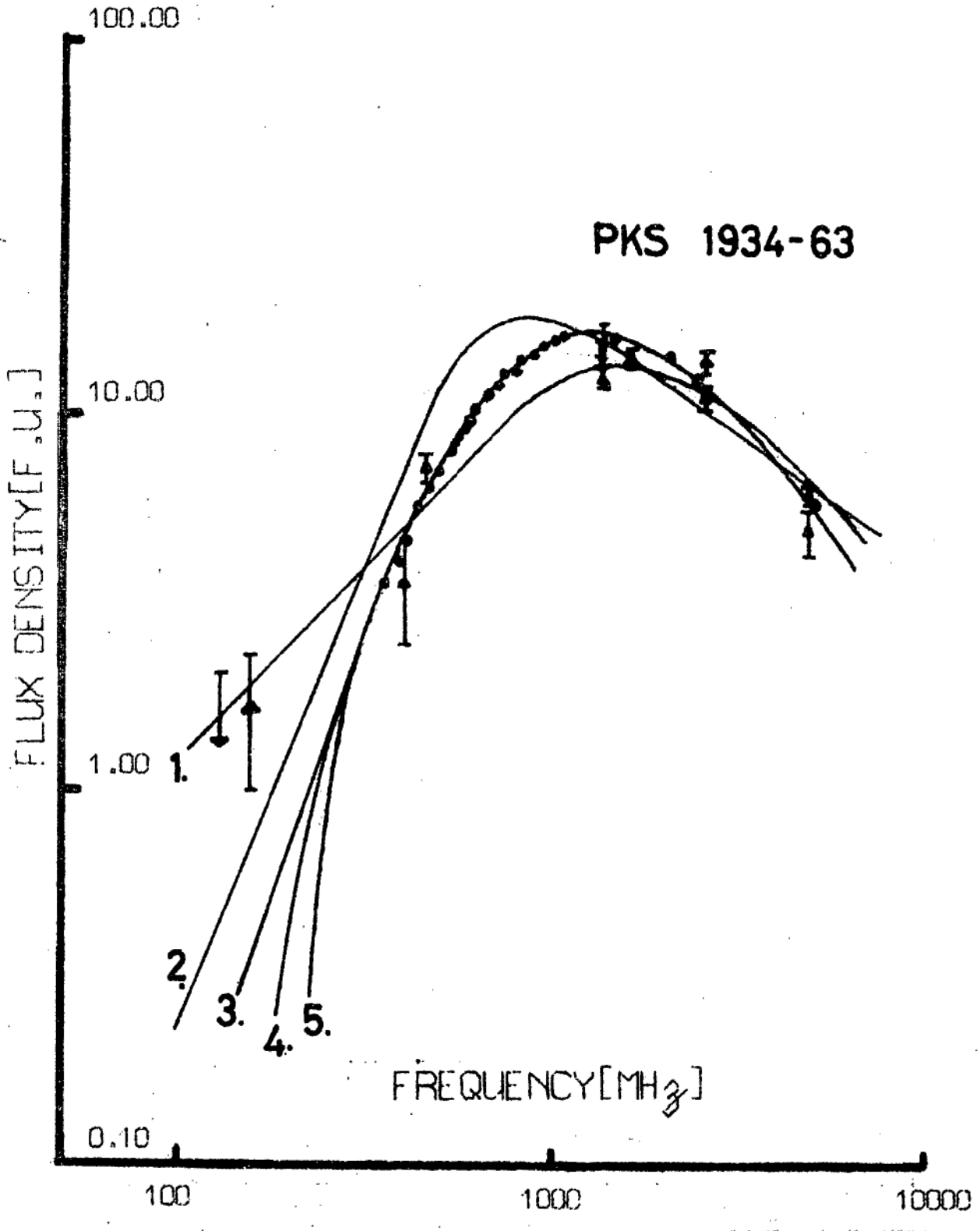
PKS 1934-63
100.00
10.00
1.00
0.10
FLUX DENSITY[F.U.]
1.
2.
3.
4.
5.
FREQUENCY[MHz]
100
1000
10000

FIGURE 5.2

The errors in the measurement are therefore rather large in relation to the source intensity; however the result is accurate to within the quoted error.

Figure 5.2 shows the spectral data now available together with the theoretical spectral curves proposed by Kellermann (1966 b). Other models fitted to the data by the author are also given. The new measurement at 159 MHz lies above the spectral curves discussed by Kellermann. Thus, observations are still needed between 200 and 300 MHz to determine unambiguously the mechanism causing the curvature.

Other Sources With Low Frequency Convex Spectra.

Five theoretical spectral curves (see equations 5.1 to 5.5) have been fitted to the *convex* spectra of a further 44 sources using the methods discussed in C (ii) above. Table 5.3 gives the parameters of each of the models and figures 5.3 to 5.11 show the theoretical spectra fitted to

EXPLANATION OF TABLE 5.3.

Parameters of the Models for Sources with Low Frequency Convex Spectra.

Symbols used in the table are:

B is the magnetic field strength in the source. (Note that the field is assumed to be uniform and that $B^2 = 1.5\ B_{\perp}^2$ [Ginzburg and Syrovatskii, 1965]);

α is the spectral index;

ν_o is the frequency at which the optical depth of the medium becomes equal to unity;

n is the density of free electrons in the ionized hydrogen regions;

θ is the angular diameter of the source;

z is the optical redshift of the source;

n_e is the density of free electrons in the region of emission of the radiation;

and: ε is the cut-off energy of the electron distribution.

TABLE DIRECTORY.

Column 1: Source Catalogue number from the "Parkes Catalogue of Radio Sources" [S32 - table 1, appendix 2]

Columns 2,3: Parameters of the model of absorption in ionized hydrogen uniformly mixed with the synchrotron source (equation 5.2).

Column 4: The emission measure corresponding to the parameter in column 3 (see equation 1.56).

Column 5: The value of the function F^* (see equation 5.7) for the best fit of the theoretical spectrum defined by equation 5.2 to the source data.

Columns 6,7: Parameters of the model of absorption in ionized hydrogen which surrounds the synchrotron source (equation 5.3)

Column 8: The emission measure corresponding to the parameter in column 7 (see equation 1.56)

Column 9: The value of the function F^* (see equation 5.7) for the best fit of the theoretical spectrum defined by equation 5.3 to the source data.

Columns 10,11: Parameters of the model of absorption in the source by the self-absorption process.

Column 12: The quantity $B\theta^{-4}(1+z)$ deduced from the self-absorption model (see equation 1.32).

Column 13: The value of the function F^* (see equation 5.7) for the best fit of the theoretical spectrum defined by equation 5.4 to the source data.

Column 14: The ratio $n_{e/B}$ deduced from fitting the theoretical spectrum defined by equation 5.5 to the source data.

Column 15: The quantity $\varepsilon^2 B$ deduced from fitting the theoretical spectrum defined by equation 5.1 to the source data.

Note: In fitting the electron distribution cut-off model (equation 5.1) and the Tsytovich-Razin effect model to the source data we assumed that the spectral index of the radiation (at high frequencies) was the average of the values given in columns 2, 6, and 10.

Note also that the error, F^*, given in columns 5, 9, 13 cannot be used to compare the models for different sources, but it does indicate the "goodness of fit" of the models described by equations (5.2 to 5.4) to the data of any one source.

TABLE 5.3 - Convex Spectra.

1	2	3	4	5	6	7	8	9	10	11	12	13	14	15
SOURCE (PKS No.)		H II IN SOURCE				H II AROUND SOURCE			SYNCHROTRON SELF ABSORPTION				TSYTOVICH EFFECT	ENERGY CUT-OFFS
	α	ν_o (MHz)	$\int n^2 d\ell$ (cm^{-6}kpsec)	ERROR	α	ν_o (MHz)	$\int n^2 d\ell$ (cm^{-6}kpsec)	ERROR	α	ν_o (MHz)	$B\theta^{-4}(1+z)$ [Gauss (sec arc)$^{-4}$]	ERROR	n_e/B [cm^{-3}/μGauss]	$\varepsilon^2 B$ [GeV$^2\mu$Gauss]
0019-00	-0.97	764.6	1473	0.005	-0.94	450.1	510	0.004	-0.88	549.1	5.75×10^{5}	0.004	13.9	21.4
0023-26	-0.60	129.9	43	0.15	-0.59	81.1	16.6	0.15	-0.57	106.3	2.918×10^{1}	0.18	2.16	5.84
0109+14	-0.99	66.3	11.1	0.04	-0.98	40.5	4.14	0.04	-0.94	49.6	1.71×10^{-1}	0.04	1.23	1.71
0252-71	-0.76	210.4	112	0.07	-0.71	110.6	30.8	0.08	-0.69	141.4	1.452×10^{2}	0.09	3.59	9.70
0316+16	-0.69	403.1	409	0.32	-0.63	212.5	113.8	0.41	-0.59	267.7	1.36×10^{4}	0.51	5.96	21.8
0320+05	-0.76	127.3	40.8	0.38	-0.72	59.1	8.8	0.28	-0.69	78.3	1.426×10^{1}	0.32	~2.2	5.92
0333+12	-0.74	107.1	28.9	0.36	-0.72	55.8	7.8	0.24	-0.69	72.0	1.306×10^{1}	0.23	1.8	Too steep for cut-off
0340+04	-0.90	44.2	4.93	0.20	-0.90	29.9	2.25	0.19	-0.87	36.6	1.14×10^{-2}	0.17	0.82	1.23
0358+00	-0.90	58.5	8.63	0.35	-0.90	37.5	3.54	0.33	-0.87	46.8	1.581×10^{-1}	0.31	1.06	1.53
0408-65	Considered separately													
0417+15	-0.88	48.3	5.89	0.06	-0.88	31.9	2.56	0.06	-0.88	43.8	2.255×10^{-1}	0.05	0.90	1.38
0439+01	-1.10	65.5	10.81	0.18	-1.09	40.6	4.16	0.16	-1.07	49.0	7.953×10^{-2}	0.15	1.22	1.37
0518+16	-0.58	85.9	18.59	0.17	-0.56	48.7	5.97	0.14	-0.55	63.5	1.319×10^{9}	0.15	1.59	Too steep for cut-off
0702-10	-1.56	483?	589	0.12	-1.45	202?	103	0.08	-1.34	224?	1.411×10^{2}	0.08	8.17	5.96 (Spectrum uncertain)
0704-23	-0.51	117.6	34.8	0.06	-0.50	75.4	14.3	0.06	-0.48	100.6	3.635×10^{2}	0.07	1.96	8.08 (Spectrum uncertain)
0709-20	-1.05	170.5	73.2	0.09	-1.02	99.0	24.7	0.10	-0.97	119.1	3.148×10^{1}	0.13	3.10	3.94
0827+07	-0.82	59.5	8.91	0.02	-0.81	37.2	3.49	0.02	-0.80	47.8	6.680×10^{-1}	0.03	1.14	1.73
0841+15	-1.56	389.1	399	0.22	-1.22	144.9	52.9	0.36	-1.09	163.6	7.623×10^{2}	0.48	4.90	3.70
0855+14	-0.90	62.2	9.75	0.68	-0.89	39.2	3.87	0.66	-0.87	48.1	8.70×10^{-2}	0.65	1.25	1.99
0909+16	-0.99	63.9	10.28	0.08	-0.97	39.3	3.89	0.08	-0.95	49.3	1.844×10^{-1}	0.09	1.06	1.33

TABLE 5.3 [cont.]

1.	2.	3.	4.	5.	6.	7.	8.	9.	10.	11.	12.	13.	14.	15.
0933+04	-1.35	83.0	17.4	0.21	-1.31	44.7	5.02	0.25	-1.25	51.8	3.994×10^{-2}	0.34	1.47	1.23
0957+14	-0.83	64.2	10.4	0.11	-0.82	39.7	3.97	0.10	-0.80	50.6	1.071×10^{0}	0.10	1.31	2.10
1005+07	-0.71	48.0	5.8	0.53	-0.68	26.0	1.70	0.62	-0.66	33.3	1.471×10^{-2}	0.74	0.82	2.04
1008+06	-1.00	61.7	9.58	0.38	-0.98	34.6	3.02	0.35	-0.94	42.2	1.519×10^{-2}	0.40	1.14	1.56
1031+11	-1.00	50.4	6.41	0.03	-1.00	32.8	2.72	0.03	-0.98	41.8	4.871×10^{-2}	0.04	0.98	1.13
1044+15	-0.94	70.7	12.6	0.16	-0.93	42.1	4.46	0.17	-0.90	52.3	5.243×10^{-1}	0.18	1.27	2.0
1116-02	-1.35	118.3	35.3	0.36	-1.23	49.8	6.24	0.55	-1.18	56.8	5.615×10^{-2}	0.74	1.63	1.53 (High frequency cut-off)
1117+14	-0.71	313.9	248	0.10	-0.68	186.7	87.8	0.11	-0.63	233.6	2.708×10^{4}	0.12	5.72	12.6
1232-41	-0.98	109.4	30.2	0.04	-0.98	71.2	12.8	0.04	-0.97	95.7	1.087×10^{1}	0.05	2.04	2.41
1241+16	-0.91	42.5	4.54	0.12	-0.91	28.8	2.09	0.12	-0.88	34.3	6.722×10^{-3}	0.14	0.69	1.23
1345+12	-0.51	290.2	212	0.34	-0.41	147.2	54.6	0.46	-0.39	199.9	2.174×10^{4}	0.50	4.25	Too steep for cut-off
1416+06	-1.15	82.6	17.2	0.34	-1.10	39.6	3.94	0.53	-1.07	51.1	3.890×10^{-3}	0.68	1.63	~1.37?
1508-05	-0.52	106.1	28.4	0.12	-0.52	71.2	12.8	0.11	-0.50	98.9	1.712×10^{2}	0.09	2.12	7.14
1514+18	-0.92	63.8	10.3	0.46	-0.91	39.6	3.95	0.46	-0.87	49.5	3.503×10^{-1}	0.45	1.14	1.59
1523+03	-0.66	73.9	13.7	0.20	-0.64	42.9	4.64	0.21	-0.61	54.4	8.142×10^{0}	0.25	1.22	3.44
1645+17	-0.59	215.6	117.1	0.57	-0.53	120.9	36.8	0.62	-0.49	155.6	2.304×10^{4}	0.68	~3.35	12.09
1732+16	-1.01	53.14	7.12	0.32	-1.00	34.4	2.98	0.32	-0.93	42.5	6.845×10^{-2}	0.62	0.98	1.32
1801+01	-0.72	765	1473	0.008	-0.68	447.9	505	0.001	-0.60	555	2.560×10^{7}	0.0	13.06	27.71
1814-51	-1.11	122.2	37.6	0.17	-1.09	74.7	14.1	0.18	-1.04	95.9	1.364×10^{0}	0.25	2.21	2.19
1827-36	-1.18	239.9	145.1	0.34	-1.11	129.0	41.9	0.40	-1.07	156.5	1.002×10^{1}	0.48	4.49	3.96
1934-63	Considered separately													
1949+02	-0.83	34.1	2.93	0.30	-0.83	23.5	1.39	0.30	-0.83	36.9	4.476×10^{-3}	0.27	0.63	0.99 (Spectrum uncertain)
2127+04	-0.63	801	1617	0.04	-0.59	462.9	539	0.04	-0.54	586.7	4.494×10^{6}	0.04	13.72	44.1
2137-06	-1.28	141.7	50.6	0.44	-1.25	63.2	10.1	0.17	-1.15	74.3	2.361×10^{0}	0.19	2.37	Too sharp for cut-off
2345+18	-0.85	46.3	5.4	0.54	-0.85	30.8	2.39	0.54	-0.83	42.6	1.616×10^{-1}	0.52	0.86	1.43

Addition to table 5.3.

Source:- 0408-65

Parameters of the models:

Ionized hydrogen uniformly distribution throughout the source:

$\alpha = -1.12 \qquad \nu_o = 244.9$ MHz

Ionized hydrogen around the source:

$\alpha = -0.94 \qquad \nu_o = 130$ MHz

Synchrotron self-absorption:

$\alpha = -0.94 \qquad \nu_o = 150$ MHz

Electron distribution cut-off:

$\gamma = 2.84 \qquad \varepsilon^2 B = 6.45$ GeV^2 μgauss

The Tsytovich-Razin effect:

$\gamma = 2.84 \qquad n_{e/B} = 3.02$ cm^{-3} μgauss^{-1}

FIGURE 5.3.

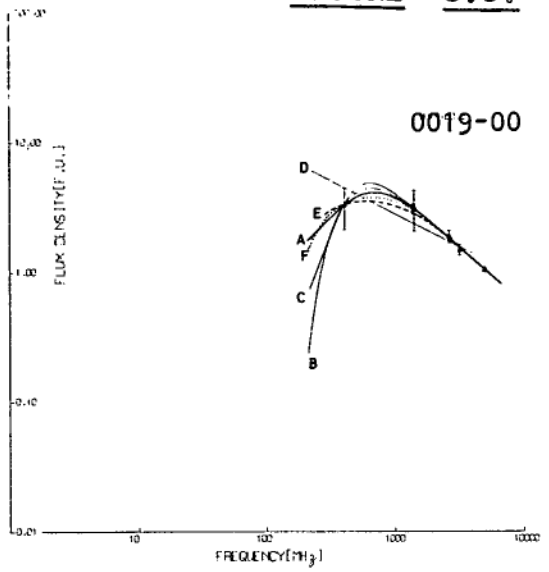
0019-00
FLUX DENSITY[F.U.]
FREQUENCY[MHz]
D
E
A
F
C
B

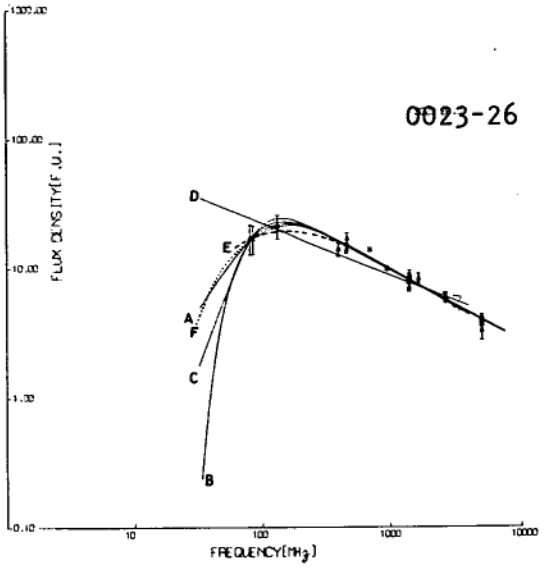
0023-26
FLUX DENSITY[F.U.]
FREQUENCY[MHz]
D
E
A
F
C
B

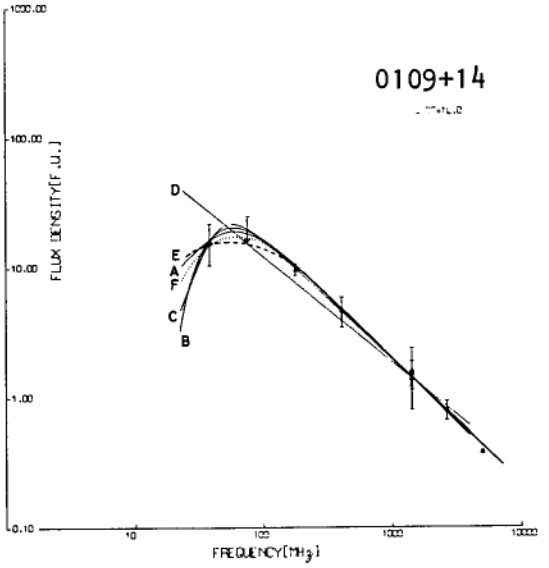
0109+14
FLUX DENSITY[F.U.]
FREQUENCY[MHz]
D
E
A
F
C
B

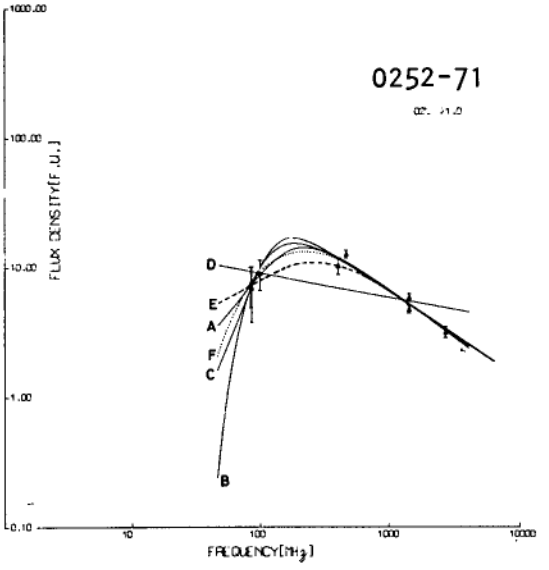
0252-71
FLUX DENSITY[F.U.]
FREQUENCY[MHz]
D
E
A
F
C
B

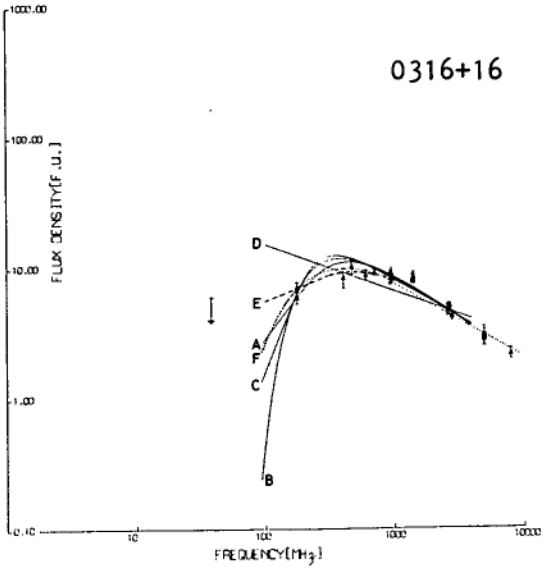
0316+16
FLUX DENSITY[F.U.]
FREQUENCY[MHz]
D
E
A
F
C
B

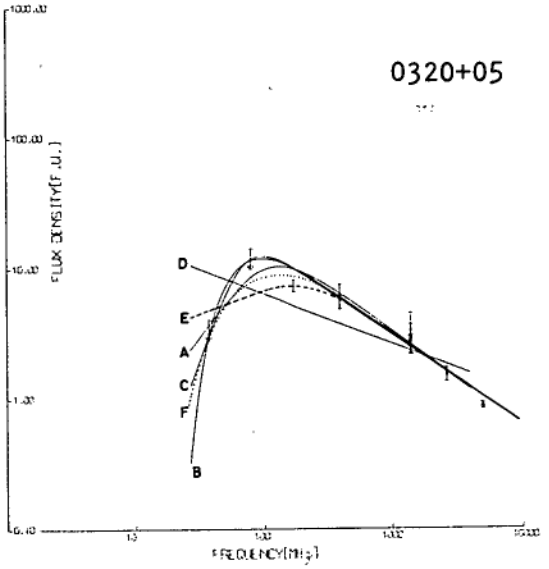
0320+05
FLUX DENSITY[F.U.]
FREQUENCY[MHz]
D
E
A
C
F
B

FIGURE 5.4.

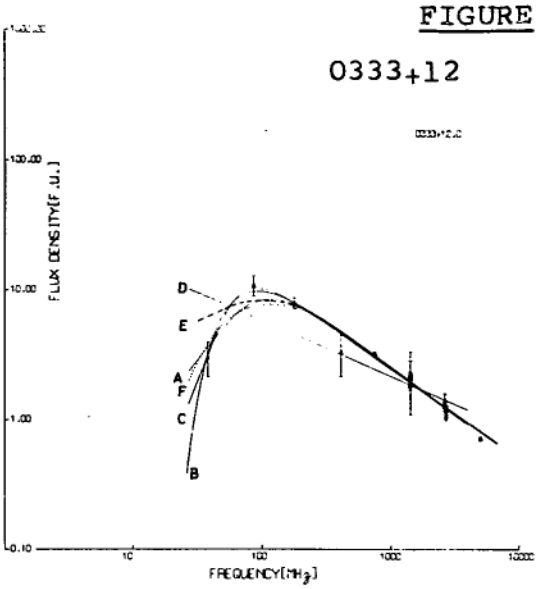
0333+12
FLUX DENSITY[F.U.]
FREQUENCY[MHz]
D
E
A
F
C
B

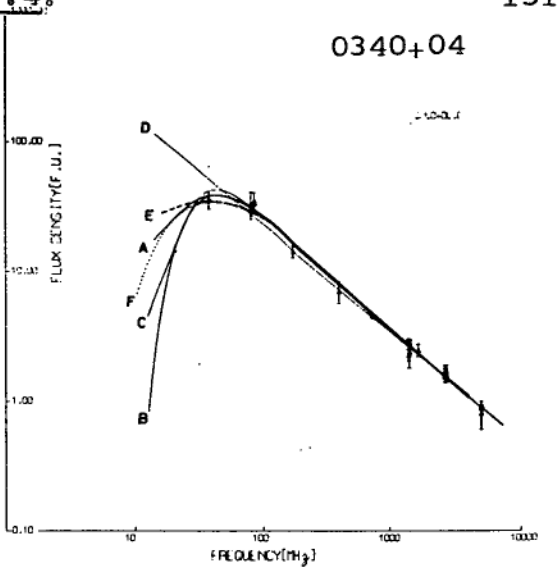
0340+04
FLUX DENSITY[F.U.]
FREQUENCY[MHz]
D
E
A
F
C
B

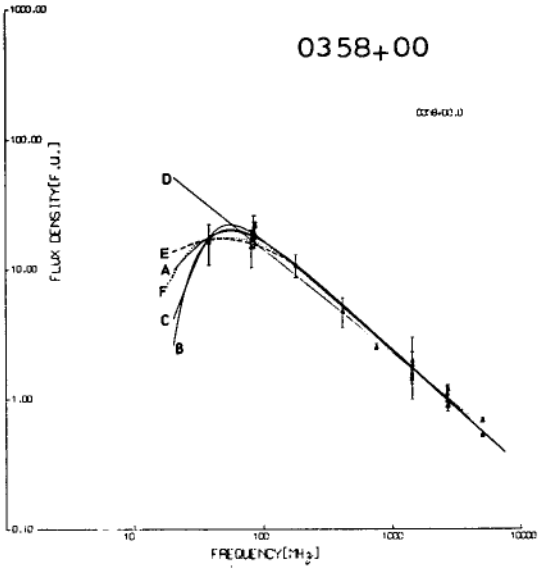
0358+00
FLUX DENSITY[F.U.]
FREQUENCY[MHz]
D
E
A
F
C
B

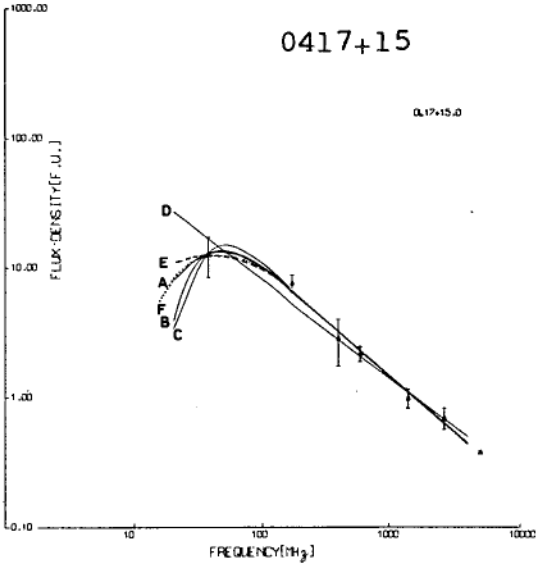
0417+15
FLUX DENSITY[F.U.]
FREQUENCY[MHz]
D
E
A
F
B
C

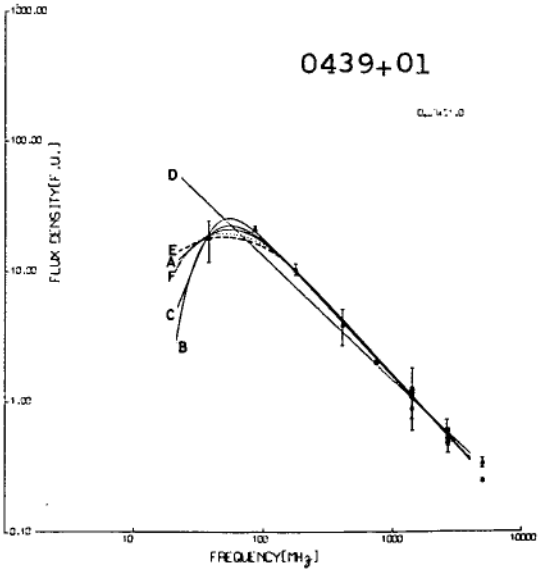
0439+01
FLUX DENSITY[F.U.]
FREQUENCY[MHz]
D
E
A
F
C
B

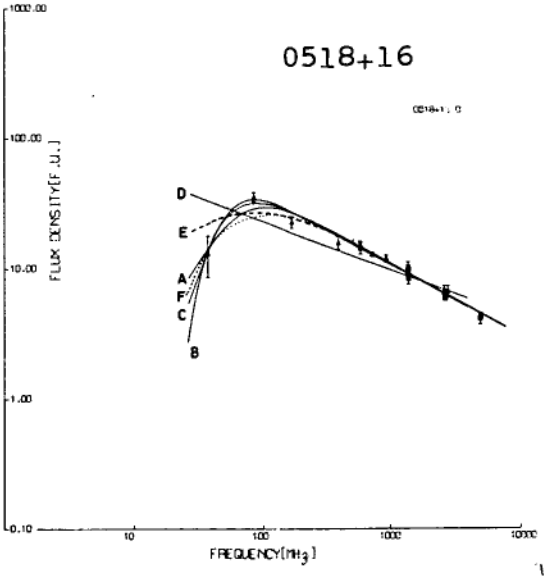
0518+16
FLUX DENSITY[F.U.]
FREQUENCY[MHz]
D
E
A
F
C
B

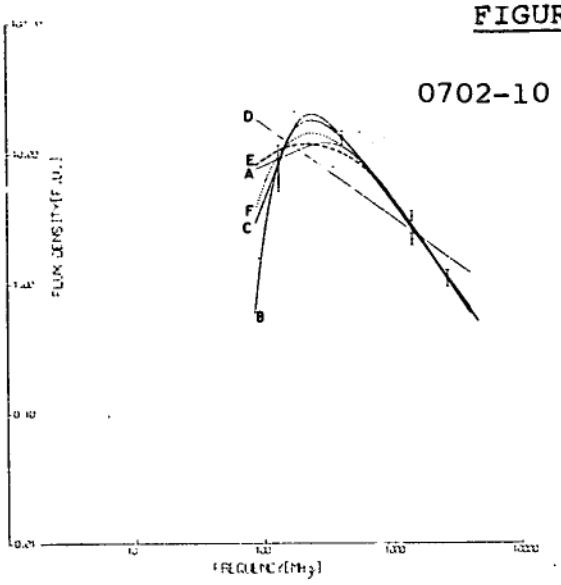
0702-10
FLUX DENSITY(F.U.)
FREQUENCY(MHz)
D
E
A
F
C
B

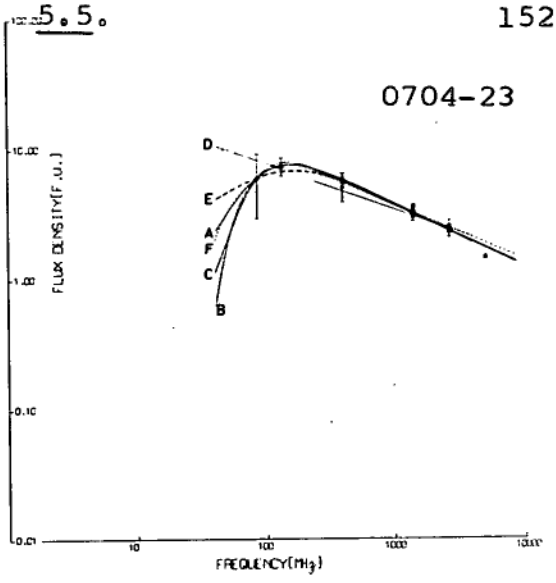
0704-23
FLUX DENSITY(F.U.)
FREQUENCY(MHz)
D
E
A
F
C
B

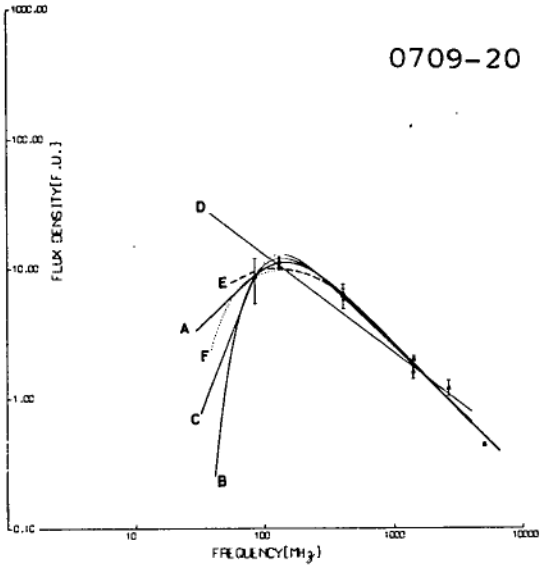
0709-20
FLUX DENSITY(F.U.)
FREQUENCY(MHz)
D
E
A
F
C
B

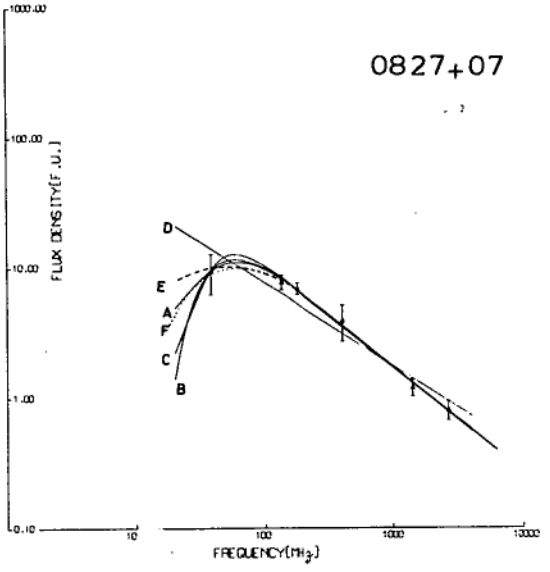
0827+07
FLUX DENSITY(F.U.)
FREQUENCY(MHz)
D
E
A
F
C
B

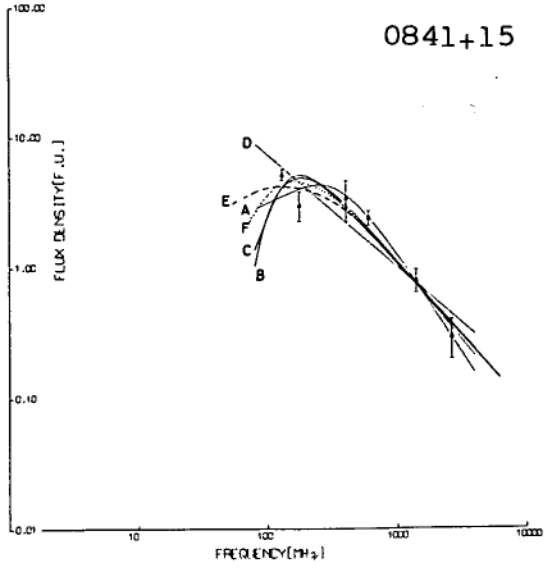
0841+15
FLUX DENSITY(F.U.)
FREQUENCY(MHz)
D
E
A
F
C
B

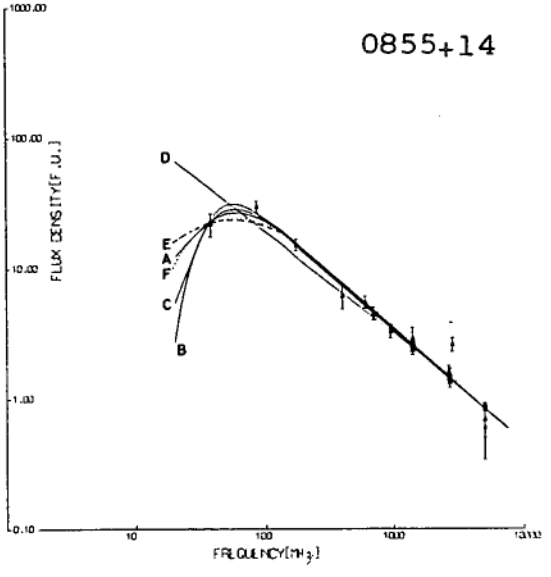
0855+14
FLUX DENSITY(F.U.)
FREQUENCY(MHz)
D
E
A
F
C
B

FIGURE 5.6.

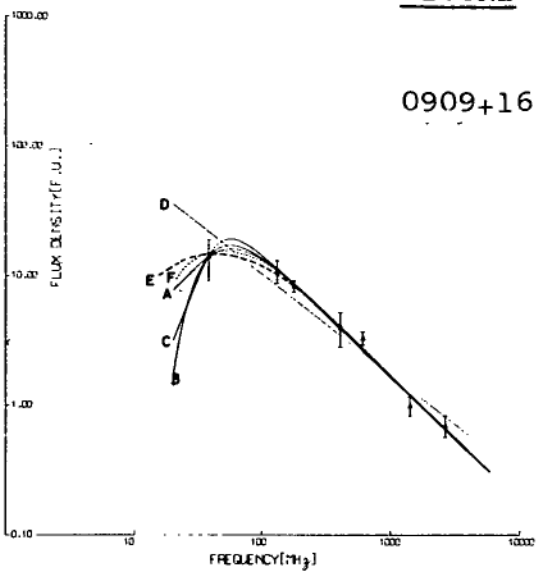
0909+16
FLUX DENSITY(F.U.)
FREQUENCY(MHz)
D
E
F
A
C
B

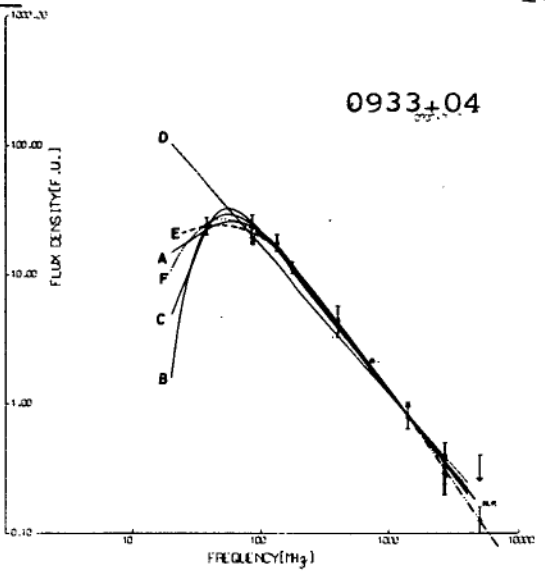
0933+04
FLUX DENSITY(F.U.)
FREQUENCY(MHz)
D
E
A
F
C
B

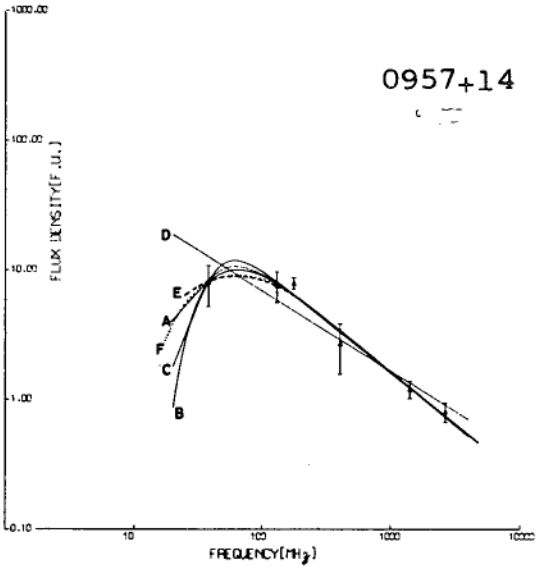
0957+14
FLUX DENSITY(F.U.)
FREQUENCY(MHz)
D
E
A
F
C
B

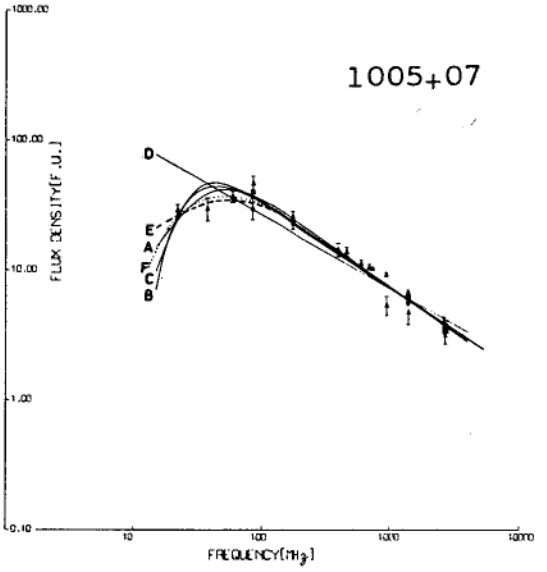
1005+07
FLUX DENSITY(F.U.)
FREQUENCY(MHz)
D
E
A
F
C
B

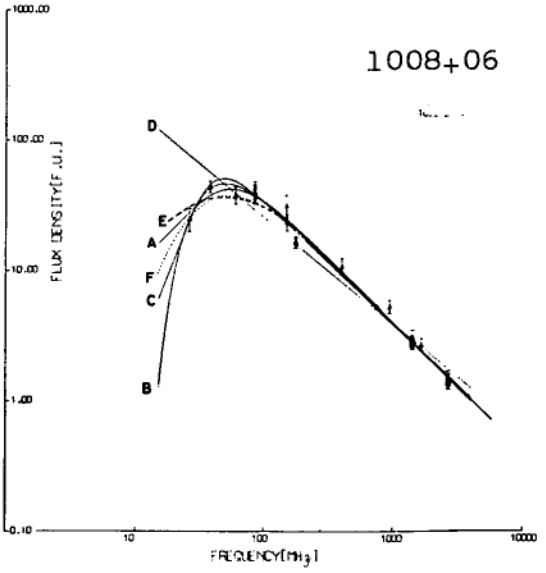
1008+06
FLUX DENSITY(F.U.)
FREQUENCY(MHz)
D
E
A
F
C
B

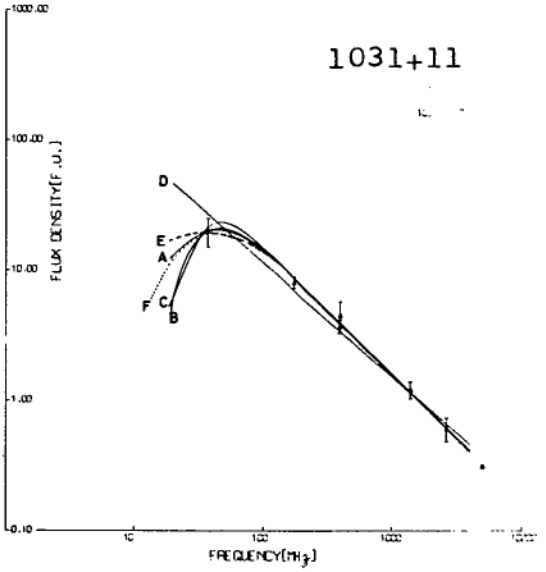
1031+11
FLUX DENSITY(F.U.)
FREQUENCY(MHz)
D
E
A
F
C
B

Figure 5.7

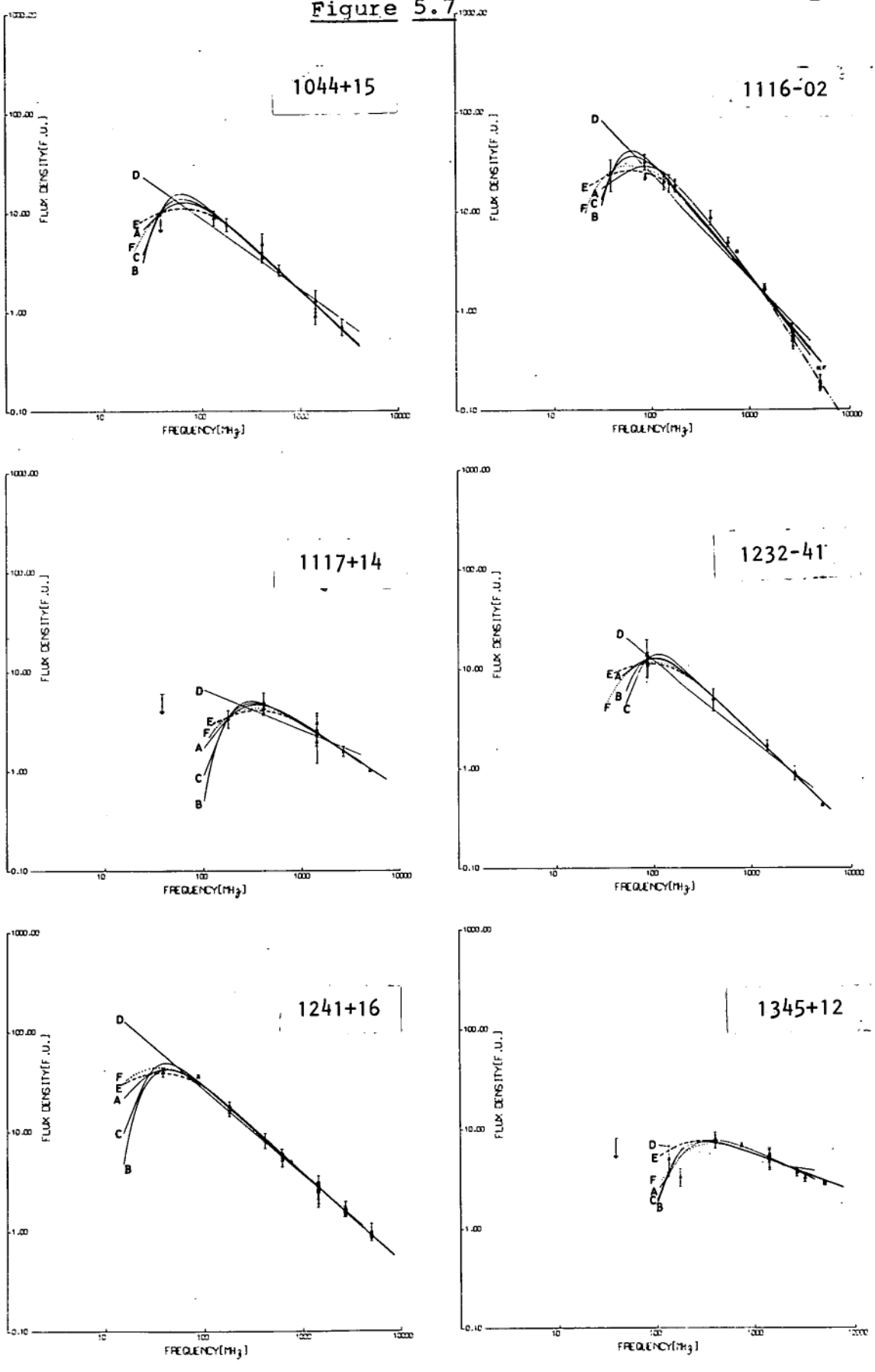
1044+15
1116-02
1117+14
1232-41
1241+16
1345+12
FLUX DENSITY[F.U.]
FREQUENCY[MHz]
A
B
C
D
E
F

FIGURE 5.8.

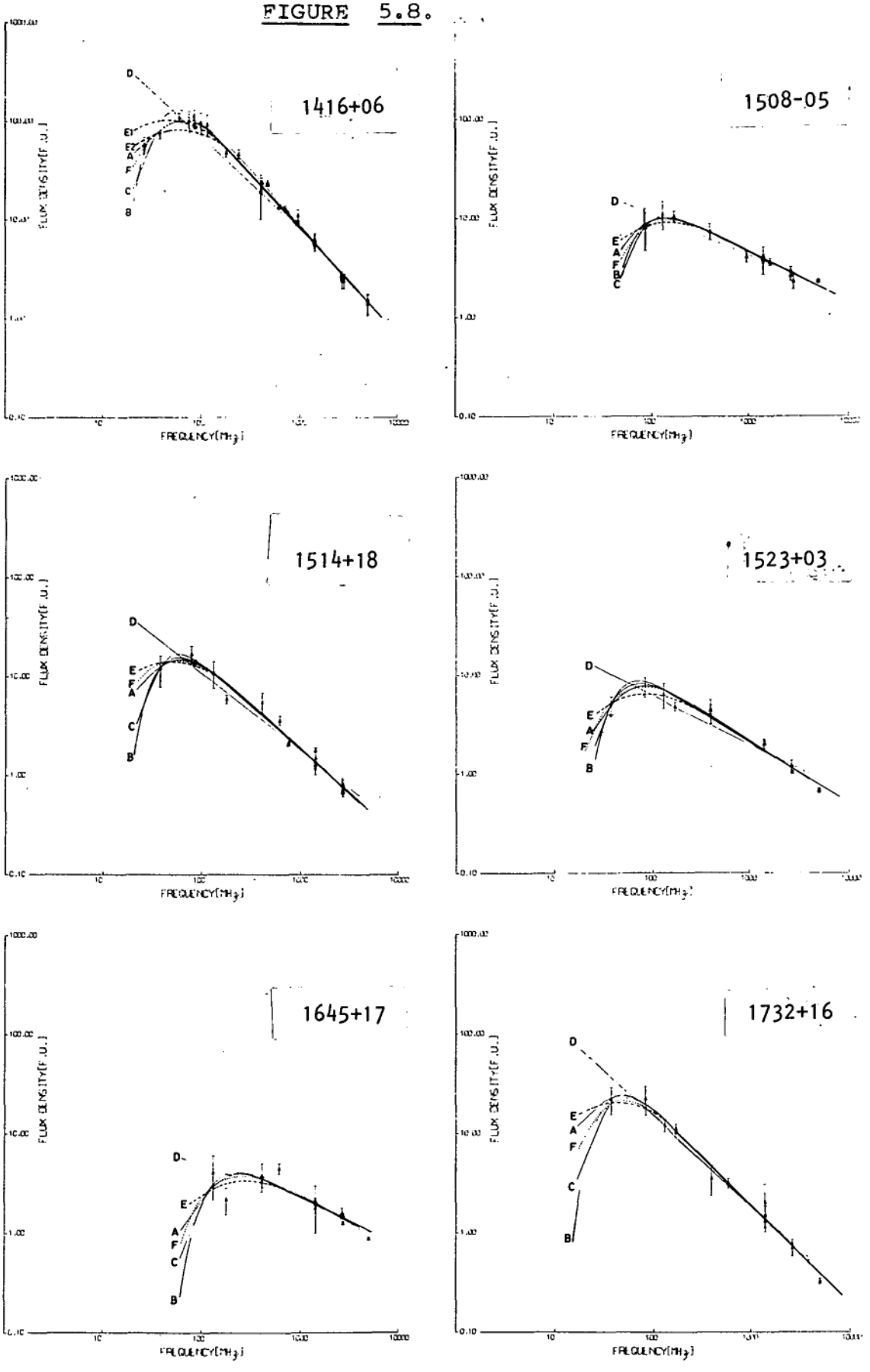
1416+06
1508-05
1514+18
1523+03
1645+17
1732+16
FLUX DENSITY(F.U.)
FREQUENCY(MHz)

FIGURE 5.9.

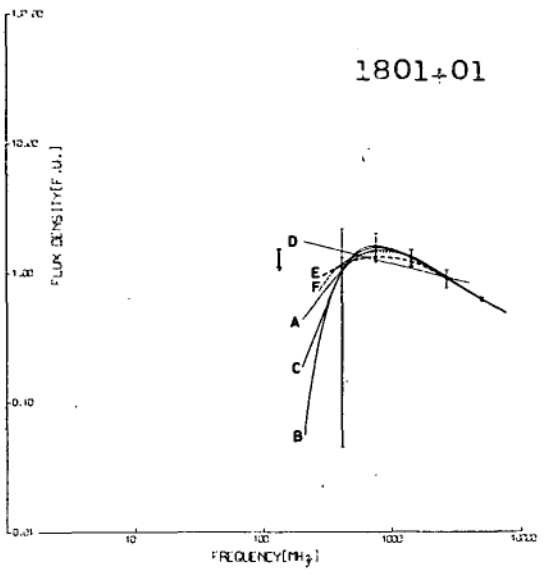
1801+01
FLUX DENSITY[F.U.]
FREQUENCY[MHz]
D
E
F
A
C
B

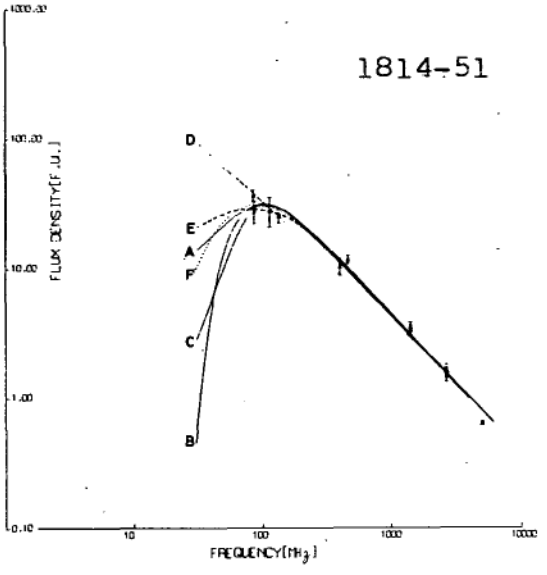
1814-51
FLUX DENSITY[F.U.]
FREQUENCY[MHz]
D
E
A
F
C
B

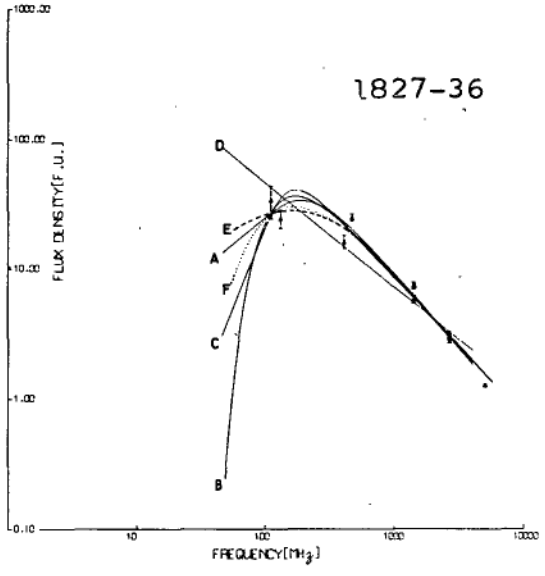
1827-36
FLUX DENSITY[F.U.]
FREQUENCY[MHz]
D
E
A
F
C
B

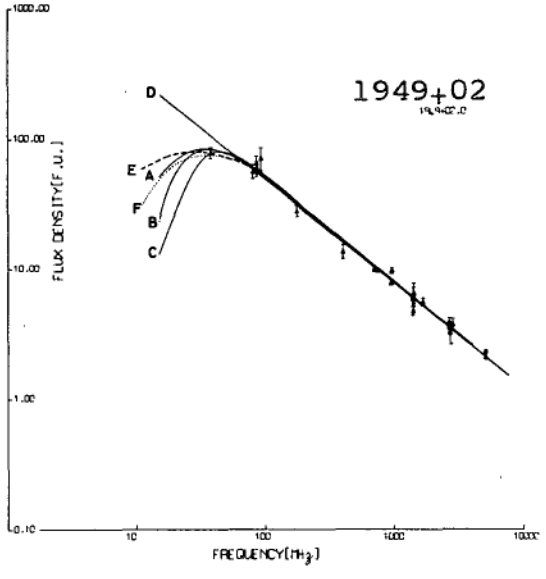
1949+02
FLUX DENSITY[F.U.]
FREQUENCY[MHz]
D
E
A
F
B
C

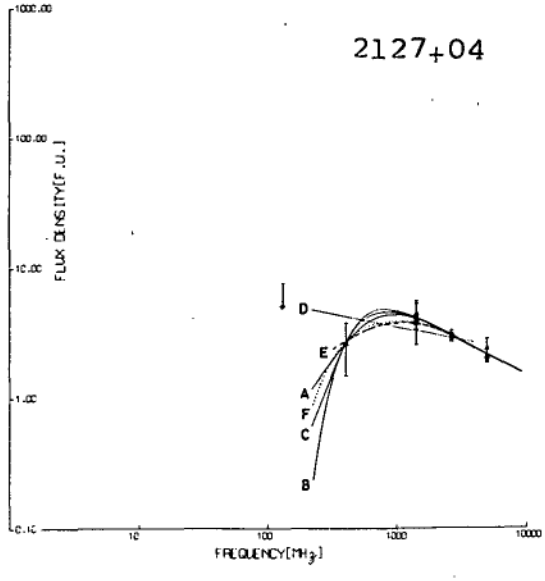
2127+04
FLUX DENSITY[F.U.]
FREQUENCY[MHz]
D
E
A
F
C
B

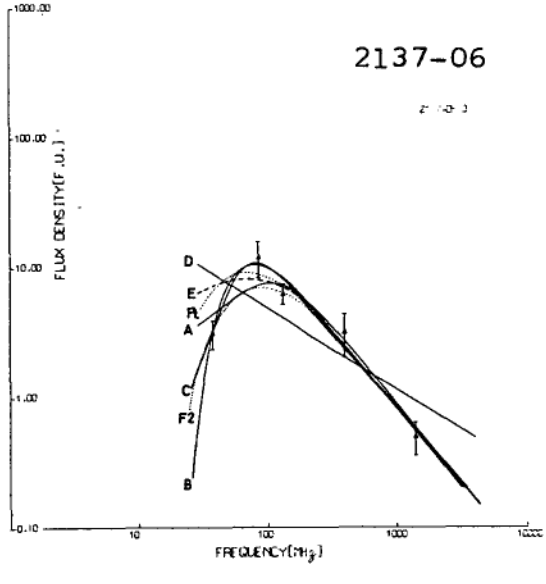
2137-06
FLUX DENSITY[F.U.]
FREQUENCY[MHz]
D
E
F
A
C
F2
B

FIGURE 5.10.

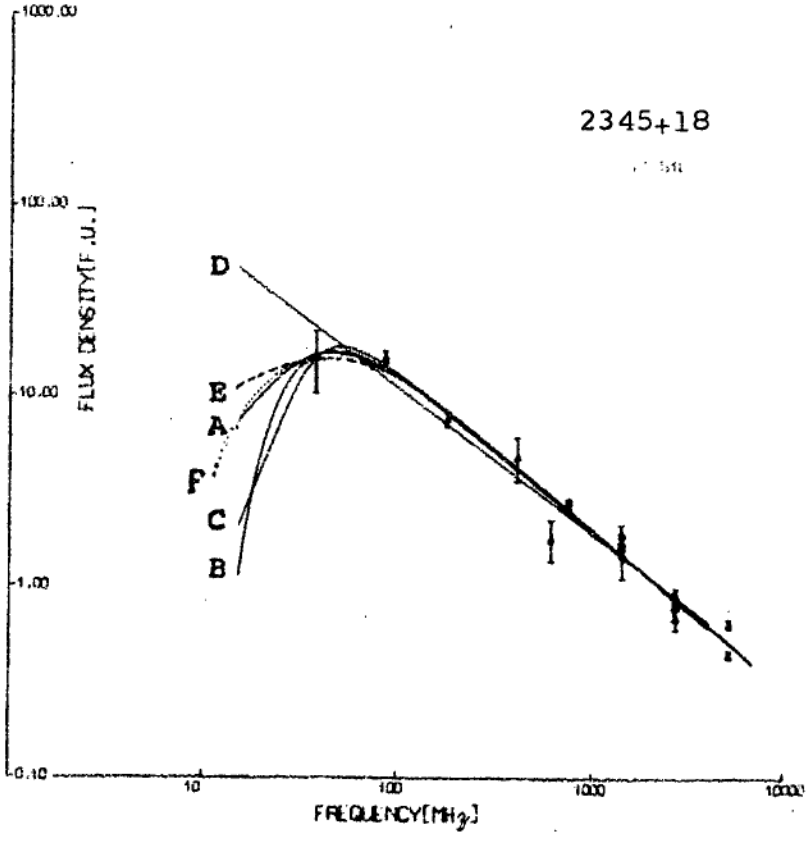
2345+18
1000.00
100.00
10.00
1.00
0.10
FLUX DENSITY[F.U.]
10
100
1000
10000
FREQUENCY[MHz]
D
E
A
F
C
B

FIGURE 5.11.

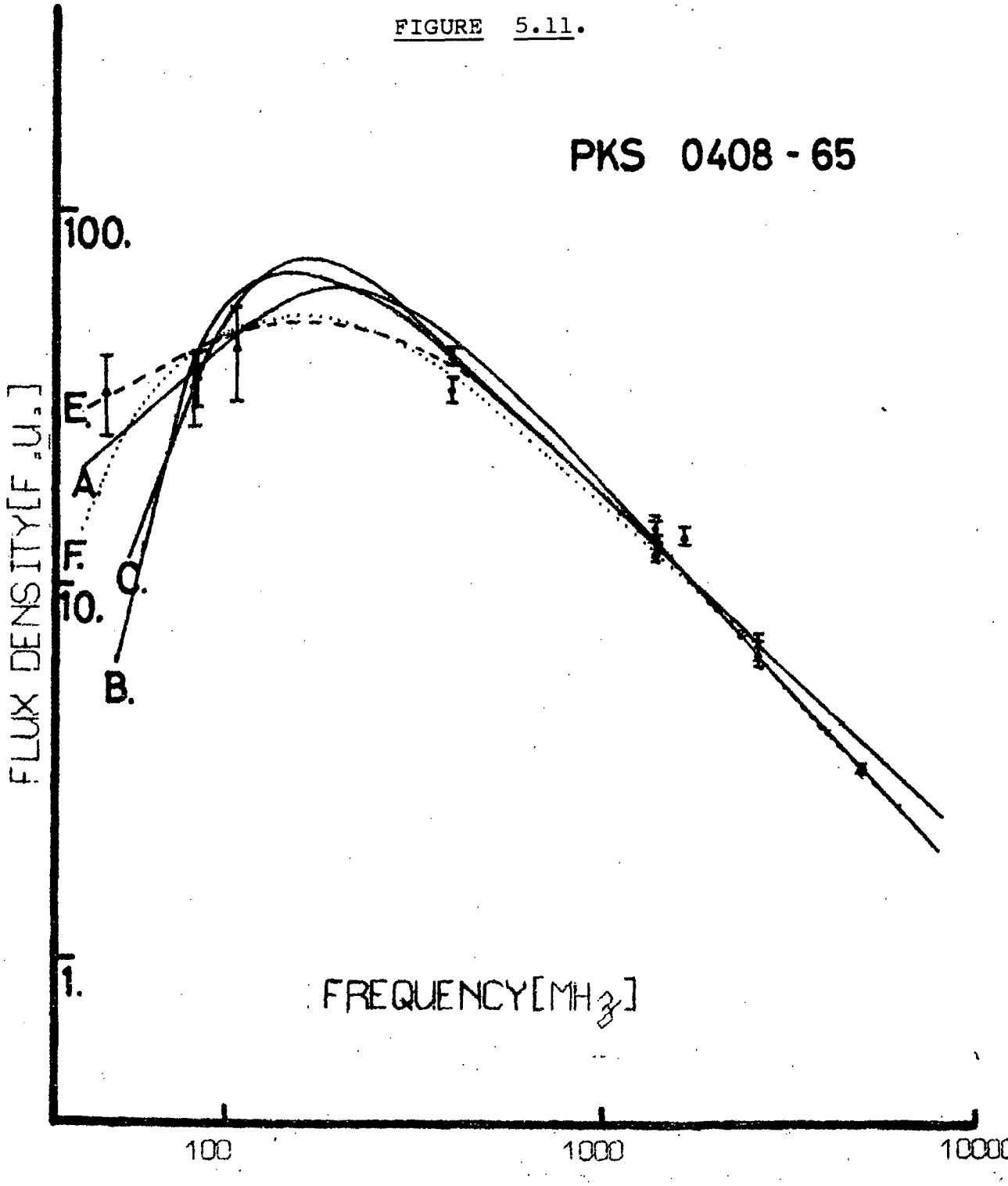
PKS 0408 - 65
100.
E.
A.
F.
C.
10.
B.
1.
FLUX DENSITY[F.U.]
FREQUENCY[MHz]
100
1000
10000

the data used in the analysis. The values of *emission measure* given in columns 4 and 8 were obtained by taking the temperature of the ionized hydrogen absorbing region to be $Te = 10^4$ degK.

It is important to note that an electron distribution cut-off at low energies cannot explain the curved spectra of the sources: PKS: 0333+12, 0518+16, 1345+12, and 2137-06, since the spectral index below the cut-off in these source spectra is more positive than $+1/3$ (see note page 123). Other implications of the curve fitting are discussed in E below.

(ii) Concave Spectra.

Thirteen sources which have *concave* spectra have been considered (see table 5.4). Two of the sources, PKS 2145+06 and 2216-03, have been discussed by Kellermann and Pauliny-Toth (1969) using results obtained from northern hemisphere surveys. These sources are however included in this discussion since they were recently observed by the author (see chapter 3).

An upper limit to the angular size of 7 of the 13 sources is known from interferometer measurements, but the internal structure of each source is not known. However, the sources PKS: 0413-21, 0624-05, 1116+12, 1434+03, 2145+06

scintillate and hence must contain components with an angular diameter of less than 1" arc [Hewish et al., 1964]. Since the structure of each source is unknown it is impossible to determine explicit values for m and n in the general relation [equation (5.6)] which may describe the radiation. The simplest model that may explain a *concave* spectrum is of the form: (m=2, n=0)

$$S^*(\nu) = A\nu^{\alpha} + B\nu^{\beta} \qquad \ldots(5.8)$$

where A,B are constants and α,β are spectral indices. This spectrum was fitted to the data available for each of the 13 sources using the method discussed in C(ii) above. The values of the variables α,β for each model are given in table 5.4 [see also figure 5.12].

Note that the source PKS 0624-05 has an unusual spectrum since above 900 MHz it is *convex* whereas below 30 MHz it is *concave* [see Braude et al., 1969a,b]. We have fitted a "double power-law" spectrum to the data below 850 MHz only.

The model defined by equation (5.8) adequately explains the observed spectra of 5 of the 13 sources [namely, PKS 0413-21, 0454-22, 0602-31, 0620-52 and 0624-05] (see figure 5.12). However, this model is probably not adequate to explain the spectra of the other 8 sources. For these we have fitted a model for which m=n=1. The low frequency part of the spectrum is thus determined by *power-law* radiation while

TABLE 5.4 : CONCAVE CURVATURE.

1.	2.	3.	4.	5.	6.	7.	8.
SOURCE	SIZE	SCINTILLATION	DOUBLE POWER-LAW		POWER-LAW + SELF-ABSORBED SOURCE		
[PKS]	[' arc]	DATA.	α	β	α	β	ν_o [MHz]
0358-48	*	*	-1.19	+1.04	-1.19	-0.66	~ 5200
0405-12	<0.25'[F.]	non-sc.	-1.03	-0.02	-1.12	-0.46	~ 600
0413-21	<0.25'[F.]	sc.	-2.56	-0.52	*	*	*
0454-22	*	*	-2.23	-0.39	*	*	*
0602-31	<0.25'[F.]	non-sc.	-2.90	-0.48	*	*	*
0605-08	*	*	-1.62	+0.38	-0.71	-0.52	~ 4500
0620-52	*	non-sc.	-1.47	-0.40	*	*	*
0624-05	<0.25'[F.]	sc.	-1.27	-0.48	*	*	*
0719-55	*	*	-1.48	-0.28	*	*	*
1116+12	<0.002'	sc.	-1.58	-0.28	*	*	*
1434+03	<0.25'[F.]	sc.	-1.10	-0.18	*	*	*
2145+06	<0.0008'	sc.	-1.10	+0.29	-0.80	-0.48	~ 5000
2216-03	*	*	-2.17	+0.17	-1.80	-0.50	~ 6000

Notes: Column 1: Source Catalogue number from the Parkes Catalogue [S32,table 1, appendix 2];

Column 2: Source size data from Fomalont(1968), [F.]; Miley et al. (1967) and Palmer et al. (1967);

Column 3: Scintillation data from Whiteoak (unpublished results) and Cohen et al. (1967);

Columns 4,5: Parameters of the "Double Power-Law" model;

Columns 6,7,8: Parameters of the "Power-Law + Self-Absorbed components" model.

[α: Low frequency power-law component; β, ν_o: High frequency self-absorbed component]

FIGURE 5.12.

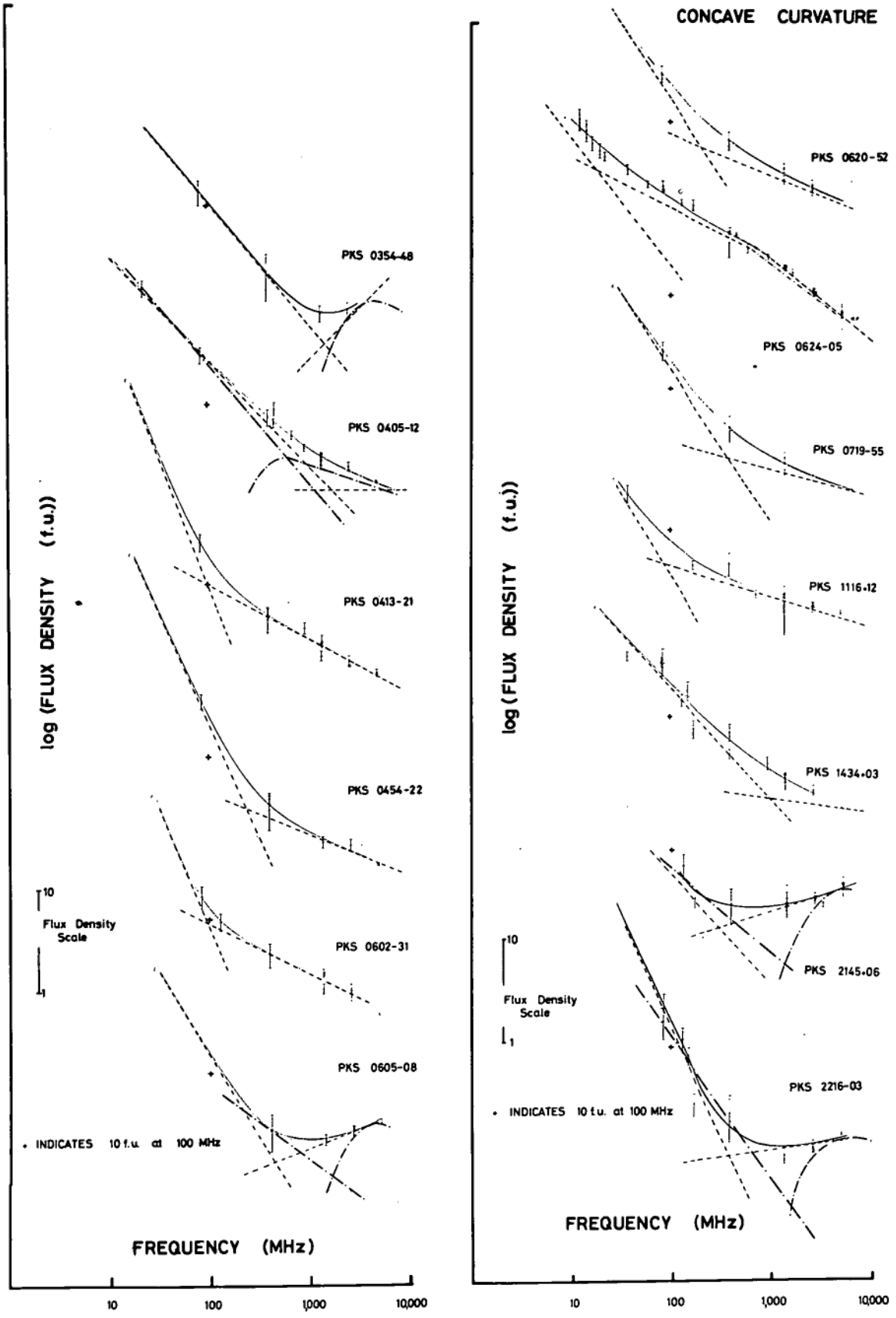
CONCAVE CURVATURE
PKS 0354-48
PKS 0405-12
PKS 0413-21
PKS 0454-22
PKS 0602-31
PKS 0605-08
PKS 0620-52
PKS 0624-05
PKS 0719-55
PKS 1116-12
PKS 1434-03
PKS 2145-06
PKS 2216-03
log (FLUX DENSITY (f.u.))
Flux Density Scale
10
1
• INDICATES 10 f.u. at 100 MHz
FREQUENCY (MHz)
10
100
1,000
10,000

the high frequency part results from radiation from a *self-absorbed* component of the source. Such a model is consistent with recent observations of sources which contain young, small components [Kellermann and Pauliny-Toth, 1968].

It is unfortunately impossible to determine the spectrum of the self-absorbed component uniquely and thus the models fitted (see table 5.4) are only tentative ones which satisfy the data that is at present available. It should be noted that as further measurements above 5000 MHz are made we may find that sources considered here as having *concave* spectra may have *complex* spectra at high frequencies.

(iii) Complex Spectra.

The data available suggests that fourteen sources visible from the southern hemisphere have *complex* spectra. Six of these are not considered here because they have been discussed by Kellermann and Pauliny-Toth (1969), [PKS: 0106+01, 0420-01, 2221-02, 2223 -05, 2328+10]; the spectrum of the source PKS 0428+20 is not well defined over a wide frequency range. The eight sources considered are listed in table 5.5 together with angular size data. Three of these sources [PKS: 1055+01, 1253-05 and 2251+15] were discussed by Kellermann and Pauliny-Toth (1969) however they are included in this analysis since they were recently measured by the author (see chapter 3).

TABLE 5.5 : COMPLEX CURVATURE

1. SOURCE [PKS]	2. SIZE [' arc]	3. SCINTILLATION DATA	4. COMP. 1 α_1	5. 6. COMP. 2 α_2	ν_{o_2} [MHz]	7. 8. COMP. 3 α_3	ν_{o_3} [MHz]	9. 10. COMP. 4 α_4	ν_{o_4} [MHz]
0430+05	≤0.0008'[2]	sc.	-0.76	-0.5	~ 7500	-0.61	~ 340	*	*
0438-43	<0.25'[F]	sc.?	-0.48	-0.52	~ 2500	*	*	*	*
1055+01	<0.0008'[2]	sc.	-0.83	-0.45	~ 4000	-0.50	~ 450	*	*
1253-05	<0.0003'[3]	sc.	-0.61	-0.48	~ 13000	-1.07	~3700	-1.25	~1600
2203-18	<0.0008'[2]	sc.	-0.60	-0.50	~ 1550	*	*	*	*
2230+11	<0.0002'[4]	sc.	?	?	?	?	?	?	?
2247+14	<0.25'[F]	non-sc.	-0.46	-0.50	~ 560	*	*	*	*
2251+15	<0.0004'[2]	sc.	-0.59	-0.63	~ 10100	-0.69	~700	*	*

Notes: Column 1: Parkes Catalogue Number; Column 2: Source size from Fomalont(1968),[F], Palmer et al.(1967), [2], Cohen and Gundermann (1967), [3] and Broten et al. (1967), [4];

Column 3: Scintillation data from Whiteoak (unpublished results) and Cohen et al. (1967);

Column 4: Spectral index of the low frequency power-law component of the spectrum;

Columns 5,6: Spectral index and *characteristic* frequency of the high frequency, self-absorbed component [see equation 5.6];

Columns 7,8 and 9,10: Spectral index and *characteristic* frequency of two other self-absorbed components of the source.

FIGURE 5.13.

COMPLEX CURVATURE

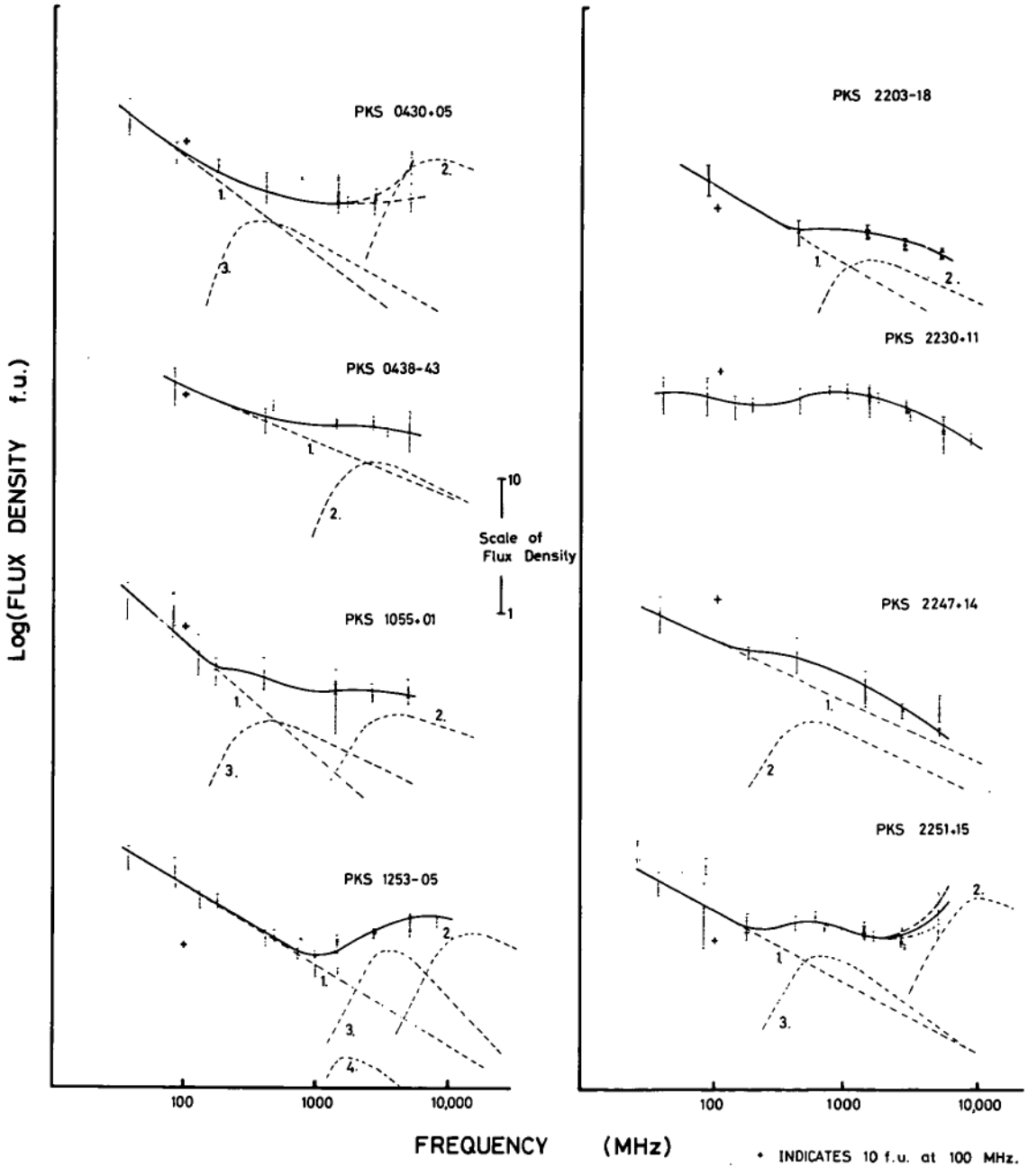

70/5-1212

High resolution interferometer studies have shown that the source PKS 2230+11 [C.T.A. 102] consists of a single, compact emission component [Broten et al., 1967; Kellermann and Pauliny-Toth, 1969]. The other 7 sources are either known or can be assumed to consist of more than one emission component (see chapter 4 for a discussion). We determined the number of components per source either from interferometer measurements (where available) or from the spectrum of the source itself. [n.b. Kellermann and Pauliny-Toth(1969) first noted that the number of emission components within a source can be reasonably accurately determined from the source spectrum.]

The theoretical spectrum defined by equation (5.6) was fitted to the data of the seven sources using the curve fitting methods discussed in C (ii) above. The variables m and n in equation (5.6) were chosen by successive model fitting, to have minimal integer values consistent with the total source spectrum. The results of the model fitting are given in table 5.5 and figure 5.13.

E. DISCUSSION AND CONCLUSIONS.

In this part of chapter 5 we consider the implications of the curve fitting analysis discussed above. Tables 5.7, 5.8, 5.9 and 5.10 list all the sources together with relevant optical identification and polarization data at present available [January, 1970]. Table 5.8 also gives scintillation or angular size data that is available for the sources with *convex* spectra.

(i) Sources with Low Frequency Convex Spectra.

It is not possible to determine the mechanism(s) causing the curved spectra of most of the 49 sources listed in tables 5.7 and 5.8 solely from the curve fitting analysis; recourse must be made to other data such as radio polarization and optical measurements. Even then it is not always possible to define the mechanism or mechanisms uniquely. However, the curve fitting analysis does indicate that the electron energy distribution cut-off within the sources: PKS: 0333+12, 0518+16, 1345+12 and 2137-06 cannot explain the observed spectra.

In this discussion we consider first the sources PKS 1322-42, 1343-60, 1549-56 and 1711-38 since their spectra can be explained adequately by a model of absorption in ionized hydrogen located within our own galaxy. Hamilton (1969) has recently shown, from an analysis of six high resolution surveys of the southern sky (see chapter 6), that ionized

hydrogen is distributed along the galactic plane such that

$$\int_0^L \frac{n^2 dl}{Te^{3/2}} \propto |\mathrm{cosec}(b^{II})| \text{ for } |b^{II}| \gtrsim 5^o \qquad ...(5.9)$$

where: n and Te are the electron density and temperature along the line-of-sight (length L) through the ionized hydrogen.

The integral in equation (5.9) takes a value of 9×10^{-6} cm^{-6} parsec $degK^{-3/2}$ for $b^{II} = 90^o$. Thus in the direction of the extragalactic source PKS 1322-42 ($b^{II} \simeq 19^o$) the left hand side of equation (5.9) has a value of 27.6×10^{-6} cm^{-6} parsec $degK^{-3/2}$. This is almost identical to the value obtained from the curve fitting analysis using model (5.3) (see table 5.2). The dashed line in figure (5.1 a) shows the spectrum of PKS 1322-42 after removing the effects of absorption. It follows that if there is no enhancement in the emission spectrum of this source at low frequencies above that expected from a power-law distribution of electrons then all the curvature in the spectrum can be accounted for by galactic absorption. In this case the electron distribution must be a power-law with index 2.4 (see equation 1.19).

The sources PKS 1343-60, 1549-56 and 1711-38 are all situated at galactic latitudes of 2.1 degrees or less and are probably galactic objects. Equation 5.9 is not valid for very low values of galactic latitude [see Hamilton,1969;

Ellis and Hamilton, 1966 a]. However, if the emission spectra of these sources are linear to 10 MHz and if the observed spectral curvature results from absorption in ionized hydrogen in the galactic plane then the integral $I = \int n^2 dl / Te^{3/2}$ can be determined for each source by curve fitting. The results of this process have been given in table 5.2. Now from the background analysis of Hamilton (1969) we have a value for the integral I in the direction, $b^{II} = 5^o$; namely:

$$I_5 = \int \frac{n^2 dl}{Te^{3/2}} \simeq 103 \times 10^{-6} \text{ cm}^{-6} \text{ parsec degK}^{-3/2} .$$

Thus the values of I determined by the curve fitting (see tables 5.2 or 5.11) are all less than I_5. It follows that *either* these sources are galactic objects *or* else the synchrotron emission from each source is enhanced at low frequencies above that expected from a power-law distribution of electrons. The values of I given in column 2 of table 5.11 can be used to determine the distance to each source provided the *mean* line-of-sight values of n and Te are known. However, the latter quantities cannot readily be determined; we have taken $Te \simeq 10^3$ degK [Radhakrishnan and Murray, 1969] and $n \simeq 0.03$ cm^{-3} [Hamilton, 1969] to calculate the distances given in column 4 of table 5.11. Milne (1969) has recently estimated the distances to these three sources using surface brightness temperature data and typical expansion rates for supernova remnants. These are shown, for comparison, in column 5 of table 5.11.

TABLE 5.7

CONVEX SPECTRA

THE SOURCES PKS: 1322-42, 1343-60, 1549-56, 1711-38.

1. SOURCE [PKS]	2. R. A. H. M. S.	3. Decl. o '	4. Size [min.arc]	5. Comments.
1322-42	13 22 24	-42 45	Extended	Integrated polarization at 1410MHz is 7%. This source is identified with the external galaxy Centaurus A (NGC 5128); MSH 13-42.
1343-60	13 42 42	-60 13.9	6.3 dia.	13 S 6A
	13 43 33	-60 08.3	7.1x5.4	
1549-56	15 48 26	-56 02.8	11x8.6	MSH 15-56
1711-38	17 11 12	-38 26.7	8.1x5.3	CTB 37
	17 10 47	-38 07.7	3.8x6	

Data on this page is taken from the Parkes Catalogue [S32, table 1, appendix 2] and from Milne (1969).

CONVEX SPECTRA

NOTES ON TABLE 5.8.

[References used to compile this table are not necessarily the original publications of the results.]

Column 1: Parkes Catalogue number [S32 - table 1, appendix 2]

Column 2: % polarization at 5 GHz from Gardner et al. (1969b)

Column 3: Rotation measure (R.M.). Note that this will be a liberal estimate of the source rotation measure since it includes rotation of the plane of polarization within the galaxy. The value of the R.M. was calculated from the results of Gardner et al. (1969 a) and Gardner et al. (1969 b) and Maltby et al. (1966).

Column 4: $K = 1.7 \times 10^{6} P^{-1} \times (R.M.)\ Te^{-3/2}$ MHz with $Te \simeq 10^{4}$ degK; (see equation 4.9);

P = % polarization at infinite frequency and R.M. = rotation measure. If k > cut-off frequency observed then the Tsytovich effects < H II absorption in the source. If k < cut-off frequency then H II absorption in the source < Tsytovich effects.

Column 5: Identification Data and estimated magnitude.

Abbreviations Used:

Q.S.O. - optically confirmed quasi-stellar object.

Q.S.O.? - possible quasi-stellar object.

E - elliptical galaxy.

N - compact galaxy.

SO - elliptical galaxy with a dust lane.

III region - no galaxies above the plate limit, and north of declination - 33^{o} no blue stars within the errors of the published source position.

IV region - optical field in the position of the radio source is heavily obscured.

Sources which have "unidentified" in brackets are only tentatively identified.

Numbers in square brackets indicate the publication from which the identification data was obtained. These are as follows:

Numbers prefixed by *I* indicate the publications from table 2 (appendix 2).

or [0] : From the "Parkes Catalogue of Radio Sources" [S32 - table I, Appendix 2].

[1] : J.G. Bolton - unpublished data.

[2] : E.M. Burbidge (1967 a,b).

[3] : Shimmins et al. (1966).

[4] : Wills and Bolton (1969)

[5] : Ekers [1967].

Column 6: Source Sizes quoted in minutes of arc. From the Parkes Catalogue [S32, table 1, appendix 2]; Gardner et al. (1969 a) and Fomalont (1968); (0.3 T indicates : 33% of the total emission).

Column 7: Scintillation data from : J.B. Whiteoak (unpublished data); Gardner et al. (1969 a), Ekers (1967) or Cohen et al. (1967).

Column 8: Redshift data from : Gardner et al. (1969 a) and the Parkes Catalogue [S32, table 1, appendix 2] together with results from J.G. Bolton (private communication).

Column 9: Estimated frequency of the peak emitted source flux density.

TABLE 5.8.

1	2	3	4	5	6	7	8	9
SOURCE (PKS)	% Pol. 5 GHz	R.M.	K. (MHz)	Identification	Size (' arc)	Scint.?	Red Shift Z.	f_{max} (MHz)
0019-00	0.1±0.4	*	*	III region	?	scint.	?	600-700
0023-26	0.3±0.2	+19	106	III region	<0.25	scint.	?	130-160
0109+14				III region				= 70
0252-71	0.6±0.3	+30 ?	85 ?	III region	<0.4	*	?	>150
0316+16	0.2±0.3	+27	220	III region	<0.0008	scint.	?	>300
0320+05	0.7±0.6	+40 ?	97 ?	20 m.gal.[I19]	<0.3	scint.	?	90-150
0333+12	1.7±0.7	*	*	18 m.QSO ?[1] unidentified?	<0.25	scint.	?	65-100
0340+04	7.7±0.5	+8	17	18.1 m.QSO[2]	0.3	non-sc.		30-50
0358+00	3.9±1.0	*	*	III region	?	scint.	?	≈60
0408-65	0.4±0.3	-28 ?	127 ?	QSO[1] U-V excess	<0.3	scint.		≈150
0417+15				III region				≈50
0439+01				19.5 m. E[1]		scint.		≈60
0518+16	10.9±0.5	-3	0.5	18 m.QSO[2]	0.003	scint.	0.754	80-100
0702-10	*	*	*	H II region[3] [extended]		non-sc.	*	≈250
0704-23	5.0±0.4	-110/+200 ?	37/68 ?	III region	<0.25	*		>120 i
0709-20	6.0±1.0	*	*	III region	<0.25	?		≈150
0827+07	*	*	*	?	?	?		≈60
0841+15	*	*	*	?	?	?		150-200
0855+14	3.3±0.6	+57 ?	29 ?	20.5 m.N[1]	0.05sep. 0.3	scint.		≈50 ? ii
0909+16	*	*	*	18.5 m.E[1]	?	?		≈56
0933+04	*	*	*	III region	?	scint.	?	55-65
0957+14	*	*	*	III region	?	?	?	≈60
1005+07	2.5±0.3	+20	14.1	19.5 m.gal.[I05]	0.003	scint.		65-100
1008+06	2.2±0.7	+34	26	III region	0.3T in <0.003	scint.	?	≈60
1031+11	*	*	*	III region	Ext.in decl.	scint.	?	≈47
1044+15	*	*	*	III region	?	scint.	?	≈65
1116-02	*	*	*	III region	?	scint.	?	60-80
1117+14	1.1±0.5	*	*	III region	<0.25	scint.	?	≈300
1232-41	1.1±1.0	*	*	III region	?	scint.	?	90-150
1241+16	2.6±0.5	-18	11.8	19 m.QSO[2]	0.05	non-sc.	0.557	≈40
1345+12	0.2±0.2	+44/+60 ?	374/425 ?	17 m.SO[I19]	<0.003	scint.		≈370
1416+06	1.4±0.5	-42	51	16.8 m.QSO[2]	0.6T in <0.003	scint.	1.439	50-85 iii
1508-05	2.9±0.2	-26	15	III region	<0.0008	non-sc.	?	120-160
1514+18	*	*	*	III region	?	?	?	≈65
1523+03	0.6±0.7	*	*	19.5 m.E[1] unidentified ?	<0.25	scint.	?	65-95
1645+17	1.3±0.6	*	*	QSO 19.5 mag	<0.25	?		≈250
1732+16	*	*	*	18.5 m.QSO ?[4]	?	?	?	≈50
1801+01	1.7±0.7	*	*	QSO[0]	?	?	?	≈770
1814-51	0.1±0.7	-4/+71 ?	68/1200 ?	III region	0.4±0.1	scint.	?	≈100 j
1827-36	0.4±0.4	-40	140	IV region	<0.25	scint.	?	100-180
1934-63	0.1±0.1	*	*	18.4 m.gal.[5]	<0.3	?		≈1500
1949+02	6.1±0.3	-39	10.9	16.5 m.SO[I48]	D.0.6 sep.1.3	non-sc.		<40 ??
2127+04	0.3±0.2	-178/+162 ?	921/1010 ?	III region	<0.0008	scint.	?	≈1100 i
2137-06	*	*	*	?	?	?	?	80-120
2345+18	6.1±1.0	*	*	19.5 m.E[0]	?	?	?	≈50

ii pol.data for PKS 0855+14 not consistent between Maltby et al.(1966) and Gardner et al.(1969) a.
R.M. for this source deduced from Maltby's work together with the 6 cm results of Gardner et al. (1969) b.

iii pol.data for PKS 1416+02 is not consistent between southern results and northern results.
The R.M. for this source found using the southern hemisphere results of Gardner et al.(1969a) and Gardner et al.(1969b) only.

i Lack of sufficient data makes it impossible to determine a unique value for the R.M. in the sources
PKS 0704-23, 1814-51, 2127+04. Changes of 180° in position angle give the two values of R.M. shown.
Values of R.M. given with a query are approximate or averaged results.

TABLE 5.9.

SOURCES WITH CONCAVE SPECTRA.

1. SOURCE [PKS NO.]	2. IDENTIFICATION Object	3. RED SHIFT	4. PERCENTAGE POLARIZATION 11 cm.	5. POLARIZATION 6 cm.
0354-48	*	*	*	*
0405-12	14.8 m. QSO [I 10]	0.574	1.2 ± 0.6	0.7 ± 0.3
0413-21	III region	*	*	3.0 ± 0.4
0454-22	III region	*	1.6 ± 0.5	1.6 ± 0.5
0602-31	III region	*	2.3 ± 0.9	1.5 ± 0.4
0605-08	III region	*	1.6 ± 0.5	1.0 ± 0.2
0620-52	*	*	2.7 ± 0.6	4.2 ± 0.4
0624-05	III region	*	10.1 ± 0.2	4.6 ± 0.1
0719-55	*	*	{0.7 ± 0.6 at 1410 MHz}	3.4 ± 0.7
1116+12	19.3 m. QSO [I 09]	2.118	2.6 ± 1.3	1.4 ± 0.3
1434+03	III region	*	1.7 ± 0.7	2.6 ± 0.4
2145+06	16.5 m. QSO [I 26]	0.367	0.4 ± 0.6	0.7 ± 0.2
2216-03	16.4 m. QSO [I 10]	0.901	*	0.7 ± 0.4

Column 2: Identification data; I 09, I 10, I 26: from table 2 appendix 2; III region: no galaxies above the plate limit within the quoted source position.

Column 3: Red shift data: from Gardner, Morris and Whiteoak, (1969) and the Parkes Catalogue. (S 32, table 1, appendix 2).

Columns 4 and 5: Polarization data: from Gardner, Morris and Whiteoak, (1969), and Gardner, Whiteoak and Morris (1969).

TABLE 5.10.

SOURCES WITH COMPLEX SPECTRA.

1. SOURCE [PKS NO.]	2. IDENTIFICATION Object	3. RED SHIFT	4. PERCENTAGE 11 cm.	5. POLARIZATION 6 cm.
0430+05	15 mag.Sey [B]	0.0333	5.1 ± 1.0	1.0 ± 0.2
0438-43	III region	*	0.7 ± 0.3	1.2 ± 0.2
1055+01	18.3 mag.QSO [I 10]	*	3.8 ± 1.0	6.2 ± 0.2
1253-05	17.8 mag.QSO [I 37]	0.538	3.2 ± 0.2	2.7 ± 0.2
2203-18	19.5 mag.QSO [I 26]	*	0.5 ± 0.4	2.9 ± 0.2
2230+11 (CTA 102)	17.3 mag.QSO [I 47]	1.037	5.3 ± 0.6	6.9 ± 0.2
2247+14	III region	*	2.2 ± 1.0	2.1 ± 0.5
2251+15	16.1 mag.QSO [B]	0.859	5.6 ± 0.2	2.8 ± 0.2

Column 2: Identification Data from: Burbidge (1967 a,b) [B]. Numbers prefixed by *I* indicate data from references listed in table 2, Appendix 2.

Column 3: Redshift data from: Gardner, Morris and Whiteoak (1969) and the Parkes Catalogue (S 32, table 1, appendix 2).

Columns 4,5: Polarization data from: Gardner, Morris and Whiteoak (1969), and Gardner, Whiteoak and Morris (1969).

TABLE 5.11

SOURCE DISTANCE CALCULATIONS

1. SOURCE [PKS]	2. $\int \frac{n^2\,dl}{Te^{3/2}}$ [cm^{-6} parsec $degK^{-3/2}$]	3. $\int n^2\,dl$ [cm^{-6} parsec]	4. DISTANCE [parsec]	5. DIAMETER [parsec]	6. DISTANCE [parsec]
1343-60	94×10^{-6}	2.96	3.1×10^{3}	8.4	4.7×10^{3}
1549-56	31×10^{-6}	0.98	1.03×10^{3}	9	3.2×10^{3}
1711-38	49.6×10^{-6}	1.57	1.63×10^{3}	8.6	4.5×10^{3}

Column 1: Source Catalogue number based on the Parkes system of cataloguing.

Column 2: The integral $\int (n^2 dl / Te^{3/2})$ from the curve fitting results (table 5.2).

Column 3: The emission measure corresponding to the results in column 2. The temperature, Te, is taken to be 10^3 degK (see text).

Column 4: Distance to each source calculated from column 3; with the mean electron density along the line-of-sight taken to be 0.03 cm^{-3} (see text).

Columns 5,6: Source Diameter and distance respectively [from results of Milne, 1969]

Other Sources with Low Frequency Convex Spectra.

All five models (equations 5.1 to 5.5) proposed to account for low frequency *convex* spectra may adequately explain the data of many of the sources listed in table 5.8. The parameters of the five models will thus only determine upper limits to the magnetic field strength and/or free electron density within each source. Provided the observed spectrum is known accurately the model fitting analysis will indicate whether or not the Tsytovich effect or an electron distribution cut-off model can account for the observations. For instance we have already noted that an electron distribution cut-off cannot explain the spectra of the sources PKS: 0333+12, 0518+16, 1345+12 and 2137-06. Unfortunately, the data available does not preclude the Tsytovich effect as an explanation of the curved spectra. The data also does not permit a more complex assumption than that of a uniform distribution of electrons within the source (or absorber). Thus the absorption models (equations 5.2, 5.3, 5.4) cannot be excluded even if they do not fit the data precisely, since we have not taken account of irregularities in the electron distribution.

Where radio polarization measurements are available it may be possible to determine the relative importance of two of the models, namely absorption in ionized hydrogen which is uniformly mixed with the synchrotron source and the Tsytovich-Razin effect [see chapter 4 for a discussion]. We know the

value of rotation measure [column 3, table 5.8] for 16 of the sources listed in table 5.8. It follows (from the results in column 9, table 5.8 and equation 4.9) that thermal absorption within the sources:

PKS: 0023-26, 0252-71, 0316+16, 0340+04, 0518+16
0704-23, 1005+07, 1008+06, 1241+16 and 1508-05

cannot account for the observed spectral curvature. This may also be the case for PKS: 0408-65 and 0855+14 but the data [see columns 4, 9 - table 5.8] is uncertain. Thermal absorption effects *may* exceed those due to the Tsytovich effect within only one source, PKS 1345+12, however, the data is again uncertain. Note that the results in column 4 of table 5.8 are dependent on the value assumed for the temperature within the ionized hydrogen in the source. We have taken Te to be 10^4 degK.

To determine the source magnetic field strength and electron density from the results in table 5.3 we require the distance and diameter of the source. Estimates of these quantities will depend on the assumed cosmology of the universe. The angular diameter, θ, of a source in an isotropic world model universe is: (see appendix 5)

$$\theta = \frac{L(1+z)}{R_o[T_k(\omega)]} \qquad \ldots(5.10)$$

where: L is the linear size(diameter) of the source;
z denotes the optical redshift of the source;

k is the curvature of the universe;

$T_k(\omega) = \sin(\omega),\ \omega,\ \sinh(\omega)$ for $k = +1,\ 0,\ -1$

respectively;

$$= \frac{c}{R_o H_o} \int_1^y \frac{dy}{y\sqrt{f(y)}} \qquad \ldots(5.11)$$

$y = (1+z)^{-1}$;

$f(y) = \frac{2\sigma_o}{y} + (q_o + 1 - 3\sigma_o) + (\sigma_o - q_o)y^2$;

σ_o is the universe density parameter;

q_o is the deceleration parameter;

c is the velocity of light;

H_o is the Hubble constant at the present epoch;

and: R_o is the radius of curvature of space at the present epoch.

In a steady state, Euclidean universe [$q_o = -1$, $\sigma_o = 0$, $k = 0$] the angular diameter is given by: (using the above relationships)

$$\theta = \frac{L\, H_o (1+z)}{cz} \qquad \ldots(5.12)$$

where for large values of the redshift, the angular diameter of the source tends to LH_o/c . The angular diameter of the source in an evolving universe in which q_o=+1 (for example) is given by:

$$\theta = \frac{L\, H_o}{c} \frac{[1+z]^2}{z} \qquad \ldots(5.13)$$

In the following discussion of the *convex* spectra we use these two relations (5.12, 5.13), (as example cosmologies),

to compute the linear diameter and distance of each source.

Most source size measurements have been made at frequencies above 1000 MHz [eg. Bridle, 1967]. However, we require the angular diameter of the sources at the turnover frequency (of the *convex* spectra) and high frequency measurements can only be used in the analysis provided the size is independent of the frequency. Very little work has been done in determining the variation of source size with emission frequency. An estimate of the size of the source (or components thereof) at low frequencies may be obtained from scintillation data. Column 7 (table 5.8) lists which of the sources being considered are scintillators [from Whiteoak - unpublished data and from Cohen et al. (1967)]. Sources which scintillate contain components not exceeding 1" arc in angular diameter [Hewish, Scott and Wills (1964)]; in fact those of the sources in table 5.8 which scintillate at a wavelength of 2 metres emit 30% or more of their radiation from a region not exceeding 0.3" arc [eg. Gardner and Whiteoak, 1969]. In this discussion we have assumed that a scintillating source has components with an angular diameter of approximately 0.5" arc.

An upper limit for the angular diameter of 33 of the 45 sources listed in table 5.8 is known from the data given in columns 6,7 of the same table. Size measurements are not available for the other 12 sources and hence no further

analysis is possible for these. The diameter of the source PKS 1508-05 at 11 cm. wavelength is less than 0.0008' arc [Palmer et al., 1967], but at 2 metres wavelength this source was observed to be a non-scintillator [Whiteoak - unpublished data]. This apparent inconsistency may however be a result of using a receiver with too great a bandwidth compared with the decorrelation bandwidth of the source. A similar effect has recently been observed with the pulsar PSR 0833-45 [Ables, Hamilton and Komesaroff - private communication]. We have taken the size of PKS 1508-05 to be 0.0008' in the following analysis.

The source magnetic field strength (given in column 7 of table 5.12)) can be determined from the parameters of the self-absorption model (column 12, table 5.3) fitted to the source spectrum in part D of this chapter provided the angular diameter of the source is known reliably. These calculations are of course only valid if the self-absorption model explains the observed spectral curvature. Note that the estimate of the magnetic field strength is extremely large for those sources with an angular diameter of 15" arc or more. Such fields are unlikely in cosmic radio sources [eg. Kellermann and Pauliny-Toth, 1969]. There are therefore two alternatives: either synchrotron self-absorption does not cause the low frequency *convex* curvature or else the estimate of the size of the source is wrong. Further

1.	2.	3.	4.	5.	6.	7.	8.	9.		10.	11.
SOURCE (PKS)	ANG. SIZE (" arc.)	Z	LIN.SIZE (parsecs) q_0=1	HUBBLE DISTANCE (Mparsec) q_o=-1	VOLUME (cm^3) q_o=1	ESTIMATES OF MAG. FIELD (gauss) q_o=-1	ρ_1 (cm^{-3})	ρ_2 Upper (cm^{-3}) a	Lower b	MAGNETIC ENERGY DENSITY (eV cm^{-3})	ELECTRON EN. DENSITY (eV cm^{-3}) q_o=-1
0019-00	0.5(sc.)	0.2	1009-1211	6×10^2	$1.6\text{-}27\times10^{64}$	2.99×10^4?	*	36.4	22.4	*	*
		1.0	1817-3633	3×10^3	$9.2\text{-}74\times10^{64}$	1.80×10^4?	*	23.2	13.7	*	*
0023-26	0.5(sc.)	0.2	1009-1211	6×10^2	$1.6\text{-}2.7\times10^{64}$	1.52×10^0?	3.28×10^6	6.2	$3.86^{\#\#}$	5.7×10^{10}	$1.6\text{-}2.7\times10^4$
		1.0	1817-3633	3×10^3	$9.2\text{-}74\times10^{64}$	9.12×10^{-1}?	3.28×10^5	4.0	$2.46^{\#\#}$	2.1×10^{10}	$0.3\text{-}2.6\times10^5$
0252-71	20 (?)	0.2	$4\text{-}4.8\times10^4$	6×10^2	$1.1\text{-}1.8\times10^{69}$	1.94×10^7 ?	*	1.6	0.84	*	*
		1.0	$0.7\text{-}1.5\times10^5$	3×10^3	$5.9\text{-}47\times10^{69}$	1.2×10^7 ?	*	1.0	0.53	*	*
0316+16	0.048	0.2	97-116	6×10^2	$1.4\text{-}2.4\times10^{61}$	6.1×10^{-2}	3.6×10^5	61.8	$32.6^{\#\#}$	9×10^7	$1.4\text{-}2.4\times10^9$
		1.0	174-349	3×10^3	$0.8\text{-}6.5\times10^{62}$	3.6×10^{-2}	2.14×10^5	39.6	$20.8^{\#\#}$	3.2×10^7	$0.3\text{-}2.4\times10^{10}$
0320+05	0.5(sc.)	$0.2^{\dagger}$	1009-1211	6×10^2	$1.6\text{-}2.7\times10^{64}$	7.43×10^{-1}	1.63×10^6	6.1	2.02	1.3×10^{10}	$2.8\text{-}4.8\times10^3$
		$0.8^{\dagger}$	1794-3230	2×10^3	$0.9\text{-}5.2\times10^{65}$	4.95×10^{-1}	1.09×10^6	4.1	1.87	0.6×10^{10}	$0.48\text{-}2.8\times10^4$
0333+12	$0.3^{\#}$(sc.)	0.2	605-727	6×10^2	$3.4\text{-}5.9\times10^{63}$	8.82×10^{-2}	1.59×10^5	6.6	3.42	1.9×10^8	$4.6\text{-}7.9\times10^5$
		1.0	1090-2180	3×10^3	$2.0\text{-}16\times10^{64}$	5.29×10^{-2}	9.5×10^4	4.2	2.18	7.0×10^7	$1.0\text{-}8.2\times10^6$
0340+04	1.0(n-sc.)	$0.4^{\dagger}$	2966-4152	1.2×10^3	$0.4\text{-}1.1\times10^{66}$	8.14×10^{-3}	6.6×10^3	1.2	0.8	1.65×10^6	$0.5\text{-}1.3\times10^6$
		$1.0^{\dagger}$	3633-7267	3.0×10^3	$0.7\text{-}5.9\times10^{66}$	5.7×10^{-3}	4.7×10^3	0.95	0.64	8.1×10^5	$1.0\text{-}8.6\times10^6$

TABLE 5.12.

1.	2.	3.	4.	5.	6.	7.	8.	9.		10.	11.
0358+00	0.5(sc.)	0.2†	1009-1211	6×10^{2}	$1.6\text{-}2.7\times10^{64}$	8.23×10^{-3}	8.7×10^{3}	2.8	1.78	1.7×10^{6}	$2.8\text{-}4.9\times10^{6}$
		0.6†	1703-2725	1.8×10^{3}	$0.8\text{-}3.1\times10^{65}$	6.18×10^{-3}	6.6×10^{3}	2.0	1.26	9.5×10^{5}	$0.4\text{-}1.6\times10^{7}$
0408-65	0.5(sc.)	0.6	1703-2725	1.8×10^{3}	$0.8\text{-}3.1\times10^{65}$	2.45×10^{-1}	7.3×10^{5}	8.3	4.4	1.5×10^{9}	$2.6\text{-}11\times10^{4}$
		1.0	1817-3633	3.0×10^{3}	$0.9\text{-}7.4\times10^{65}$	1.5×10^{-1}	4.5×10^{5}	7.6	3.9	5.6×10^{8}	$0.8\text{-}6.3\times10^{5}$
0439+01	0.5(sc.)	0.2†	1009-1211	6×10^{2}	$1.6\text{-}2.7\times10^{64}$	4.14×10^{-3}	5.1×10^{3}	3.1	1.94	4.3×10^{5}	$0.6\text{-}1.0\times10^{7}$
		0.6†	1703-2725	1.8×10^{3}	$0.8\text{-}3.1\times10^{65}$	3.1×10^{-3}	3.8×10^{3}	2.2	1.37	2.4×10^{5}	$0.9\text{-}3.6\times10^{7}$
0518+16	0.18	0.754	641-1125	2.26×10^{3}	$4.0\text{-}22\times10^{63}$	7.89×10^{-4}	1.25×10^{3}	4.6	2.6##	1.6×10^{4}	$3.5\text{-}6.4\times10^{11}$
0704-23	15.0	0.2	$3.0\text{-}3.6\times10^{4}$	6.0×10^{2}	$4.3\text{-}7.4\times10^{68}$	1.53×10^{7} ?	*	1.03	0.6##	*	*
		1.0	$5.5\text{-}11\times10^{4}$	3.0×10^{3}	$0.3\text{-}1.9\times10^{70}$	9.2×10^{6} ?	*	0.7	0.42##	*	*
0709-20	15.0	0.2	$3.0\text{-}3.6\times10^{4}$	6.0×10^{2}	$4.3\text{-}7.4\times10^{68}$	1.33×10^{6} ?	*	1.5	0.87	*	*
		1.0	$5.5\text{-}11\times10^{4}$	3.0×10^{3}	$2.5\text{-}20\times10^{69}$	7.9×10^{5} ?	*	0.95	0.55	*	*
0855+14	3.0$	0.56†	$1.0\text{-}1.6\times10^{4}$	1.68×10^{3}	*	4.5×10^{0}	*	0.87	0.55	*	*
		0.9†	$1.1\text{-}2.1\times10^{4}$	2.70×10^{3}	*	3.71×10^{0}	*	0.78	0.49	*	*
	0.5(sc.)	0.56†	1672-2609	1.68×10^{3}	$7.2\text{-}27\times10^{64}$	3.49×10^{-3}	4.4×10^{3}	2.2	1.34	3.04×10^{5}	$1.9\text{-}7.5\times10^{7}$
		0.9†	1811-3442	2.7×10^{3}	$0.9\text{-}6.3\times10^{65}$	2.86×10^{-3}	3.6×10^{3}	1.9	1.19	2.0×10^{5}	$0.3\text{-}2.2\times10^{8}$
0933+04	0.5(sc.)	0.2	1009-1211	6.0×10^{2}	$1.6\text{-}2.7\times10^{64}$	2.08×10^{-3}	3.4×10^{3}	3.96	2.12	1.7×10^{5}	$2.3\text{-}3.9\times10^{7}$
		1.0	1817-3633	3.0×10^{3}	$0.9\text{-}7.4\times10^{65}$	1.25×10^{-3}	1.8×10^{3}	2.5	1.36	3.9×10^{4}	$0.7\text{-}5.4\times10^{8}$
1005+07	0.18	0.39†	528-734	1.17×10^{3}	$2.3\text{-}6.1\times10^{63}$	1.11×10^{-5}	9.1	3.02	1.64##	3.06×10^{0}	$>10^{5}$
		0.56†	602-939	1.68×10^{3}	$0.3\text{-}1.3\times10^{63}$	9.89×10^{-6}	8.1	2.74	1.48##	2.43×10^{0}	$>10^{5}$
1008+06	0.18	0.2	363-436	6.0×10^{2}	$0.7\text{-}1.3\times10^{62}$	1.33×10^{-5}	15.0	4.9	2.74##	4.39×10^{0}	$>10^{5}$
		1.0	654-1308	3.0×10^{3}	$4.3\text{-}34\times10^{63}$	7.9×10^{-6}	9.1	3.14	1.76##	1.6×10^{0}	$>10^{5}$

TABLE 5.12 (cont.).

1.	2.	3.	4.	5.	6.	7.	8.	9.		10.	11.
1031+11	0.5(sc.)	0.2	1009-1211	6.0×10^{2}	$1.6\text{-}2.7\times10^{64}$	2.54×10^{-3}	2.5×10^{3}	2.4	1.57	1.6×10^{5}	$1.8\text{-}3.1\times10^{7}$
		1.0	1816-3633	3.0×10^{3}	$0.9\text{-}7.4\times10^{65}$	1.52×10^{-3}	1.5×10^{3}	1.53	1.0	5.7×10^{4}	$0.5\text{-}3.7\times10^{8}$
1044+15	0.5(sc.)	0.2	1009-1211	6.0×10^{2}	$1.6\text{-}2.7\times10^{64}$	2.73×10^{-2}	3.5×10^{4}	3.37	2.01	1.9×10^{7}	$1.9\text{-}3.2\times10^{5}$
		1.0	1816-3633	3.0×10^{3}	$0.9\text{-}7.4\times10^{65}$	1.64×10^{-2}	2.1×10^{4}	2.15	1.28	6.7×10^{6}	$0.5\text{-}3.6\times10^{6}$
1116-02	0.5(sc.)	0.2	1009-1211	6.0×10^{2}	$1.6\text{-}2.7\times10^{64}$	2.92×10^{-2}	4.8×10^{4}	5.64	2.37	2.1×10^{7}	$1.1\text{-}1.9\times10^{5}$
		1.0	1816-3633	3.0×10^{3}	$0.9\text{-}7.4\times10^{65}$	1.75×10^{-2}	2.9×10^{4}	3.6	1.51	7.6×10^{6}	$0.33\text{-}2.7\times10^{6}$
1117+14	0.5(sc.)	0.2	1009-1211	6.0×10^{2}	$1.6\text{-}2.7\times10^{64}$	1.41×10^{3} ?	*	14.9	8.9	*	*
		1.0	1816-3633	3.0×10^{3}	$0.9\text{-}7.4\times10^{65}$	8.46×10^{2} ?	*	9.55	5.67	*	*
1232-41	0.5(sc.)	0.2	1009-1211	6.0×10^{2}	$1.6\text{-}2.7\times10^{64}$	5.66×10^{-1}	1.2×10^{6}	5.22	3.4	8×10^{9}	$0.6\text{-}1.0\times10^{3}$
		1.0	1816-3633	3.0×10^{3}	$0.9\text{-}7.4\times10^{65}$	3.4×10^{-1}	6.9×10^{5}	3.33	2.16	2.9×10^{9}	$0.16\text{-}1.3\times10^{4}$
1241+16	3.0(n-sc.)	0.577	$1.1\text{-}1.6\times10^{4}$	1.73×10^{3}	$1.6\text{-}6.3\times10^{67}$	3.45×10^{-1}	2.4×10^{5}	0.58	0.39##	2.9×10^{9}	$\sim 6\times10^{3}$
1345+12	0.18	0.15†	296-341	4.5×10^{2}	$4.0\text{-}6.1\times10^{62}$	1.99×10^{1} ?	*	25.8	13.1	*	*
		0.3†	464-603	8.99×10^{12}	$1.5\text{-}3.4\times10^{63}$	1.76×10^{1} ?	*	19.9	10.1	*	*
1416+06	0.18	1.439	632-1543	4.31×10^{3}	$3.9\text{-}57\times10^{63}$	1.67×10^{-6}	2.72	3.97	1.9	6.9×10^{-2}	$>10^{8}$
1508-05	0.048	0.1	57-63	3.0×10^{2}	$3.0\text{-}3.9\times10^{60}$	8.26×10^{-4}	1.8×10^{3}	21.8	14.6##	1.7×10^{4}	$>10^{8}$
		1.0	174-349	3.0×10^{3}	$0.8\text{-}6.5\times10^{62}$	4.54×10^{-4}	9.7×10^{2}	10.4	6.99##	5.1×10^{3}	$>10^{8}$
1523+03	0.5(sc.)	0.2†	1009-1211	6.0×10^{2}	$1.6\text{-}2.7\times10^{64}$	4.24×10^{-1}	5.2×10^{5}	3.51	2.04	4.4×10^{9}	$1.1\text{-}2.0\times10^{4}$
		0.6†	1703-2725	1.8×10^{3}	$0.8\text{-}3.1\times10^{65}$	3.18×10^{-1}	39×10^{5}	2.48	1.45	2.5×10^{9}	$1.5\text{-}6.0\times10^{4}$
1645+17	15.0	0.6†	$5.1\text{-}8.2\times10^{4}$	1.8×10^{3}	$2.1\text{-}8.4\times10^{69}$	7.29×10^{8} ?	*	1.33	0.74	*	*
		1.0†	$5.5\text{-}11\times10^{4}$	3.0×10^{3}	$0.3\text{-}1.9\times10^{70}$	5.83×10^{8} ?	*	1.19	0.67	*	*

TABLE 5.12 (cont)

1.	2.	3.	4.	5.	6.	7.	8.	9.		10.	11.
1814-51	0.3# (sc.)	0.1	360-396	3.0×10^{2}	$7.2\text{-}9.6\times10^{62}$	1.0×10^{-2}	2.2×10^{4}	9.97	6.11	2.5×10^{6}	$2.2\text{-}2.9\times10^{7}$
		1.0	1090-2180	3.0×10^{3}	$0.2\text{-}1.6\times10^{65}$	5.52×10^{-3}	1.2×10^{4}	4.78	2.94	7.6×10^{5}	$0.5\text{-}3.7\times10^{8}$
1827-36	0.3# (sc.)	0.1	360-396	3.0×10^{2}	$7.2\text{-}9.6\times10^{62}$	7.38×10^{-2}	3.3×10^{5}	19.6	10.5	1.4×10^{8}	$5.5\text{-}7.3\times10^{5}$
		1.0	1090-2180	3.0×10^{3}	$0.2\text{-}1.6\times10^{65}$	4.06×10^{-2}	1.8×10^{5}	9.41	5.06	4.1×10^{7}	$1.2\text{-}9.4\times10^{6}$
1949+02	36.0	0.12†	$5.0\text{-}5.6\times10^{4}$	3.6×10^{2}	$1.9\text{-}2.7\times10^{69}$	6.71×10^{3} ?	*	0.23	0.16	*	*
		0.3†	$9.3\text{-}12\times10^{4}$	8.9×10^{2}	$1.2\text{-}2.7\times10^{70}$	5.78×10^{3} ?	*	0.17	0.11	*	*
2127+04	0.048	0.1	58-63	3.0×10^{2}	$2.9\text{-}3.9\times10^{60}$	2.17×10^{1} ?	*	163.5	94.5	*	*
		1.0	174-349	3.0×10^{3}	$0.8\text{-}6.5\times10^{62}$	1.19×10^{1} ?	*	78.6	45.4	*	*

NOTES:

† Red shift values derived from the results of Sandage(1961).

Scintillation of the emissions from a source indicate that 30% of the source radiation is emitted from a region not larger than 0.3" arc in angular diameter.

Model in which *absorption in ionized hydrogen within the source* does not hold.

$ Total source size (but small components within the source are indicated by scintillation results)

TABLE 5.12. (cont.).

measurements of the angular diameter of the sources PKS: 0252-71, 0704-23, 0709-20 and 1645+17 are needed.

If absorption in ionized hydrogen causes the spectral curvature and if the linear diameter of this absorber is known then the mean electron density along the line-of sight through the absorber can be determined (given in columns 9 a and b) from the parameters given in columns 4 and 8 of table 5.3. The linear diameter can be found from equations 5.12 and 5.13 provided the angular diameter and redshift of the source is known. Redshift data is available for only three of the sources, PKS: 0518+16, 1241+16, 1416+06, listed in table 5.8. Calculations for the other sources (see table 5.12) have been undertaken by assuming values of redshift appropriate for normal galaxies [$z \sim 0.1$ or 0.2] and for quasi-stellar sources [$z \sim 1.0$]. Note that when optical magnitude data is available for the identified radio sources [see column 5, table 5.8], approximate values of redshift can be obtained using the method of Sandage (1961). The values of redshift determined in this way are indicated in column 3 of table 5.12 by the symbol †. The Hubble distance to each source, given by cz/H_o (c = velocity of light and H_o is the Hubble cosmological constant = 10^5 m sec^{-1} $Mparsec^{-1}$). is given in column 5 of table 5.12. The electron densities given in column 9 (a,b) were obtained from the ionized hydrogen absorption models by assuming that the linear diameter

of the absorbing medium is the average of the two values given in column 4 of table 5.12. The results in column 9 (a) were then determined from the emission measures given in column 4 (table 5.3) and those in column 9 (b) from the emission measures in column 8 (table 5.3).

The parameters of the Tsytovich-Razin effect model (column 14, table 5.3) may be used together with the estimate of magnetic field strength (column 7, table 5.12) to give an *approximate* upper limit estimate to n_e, the free electron density within the emitting region (see column 8, table 5.12).

A basic assumption often made is that the energy stored in the magnetic field of a radio source is approximately equal to the total energy of relativistic particles within the source [eg. Ginzburg and Syrovatskii, 1964]. Radio observations can be used to obtain an estimate of the energy of the relativistic electrons within the source (see below), however, to obtain the *total* particle energy we need to know the proportion of relativistic electrons to heavier particles. In our own galaxy, the energy of relativistic electrons, E_e, and the total energy of all cosmic ray particles, E_p, are related by:

$$E_p \simeq 100\ E_e \qquad \ldots(5.14)$$

[Ginzburg and Syrovatskii, 1965]

At present there is no way of determining if equation (5.14)

also applies for extragalactic sources however.

The energy contained in the magnetic field of a source is:

$$E_B = \frac{1}{8\pi} \int_v B^2 \, dv \qquad \ldots(5.15)$$

and the energy of relativistic electrons is:

$$E_e = \int_v \int_{\varepsilon_1}^{\varepsilon_2} N(\varepsilon) \, \varepsilon \, d\varepsilon \, dv \qquad \ldots(5.16)$$

where: B is the magnetic field strength is the source (field assumed to be uniform);

ε is the energy of the electron;

v the volume of the source $= \frac{\pi L^3}{6}$;

L is the linear diameter of the source;

$N(\varepsilon) \, d\varepsilon$ is the number of electrons with energy, ε, in the range ε to $\varepsilon + d\varepsilon$ per unit volume;

and ε_1, ε_2 are the cut-off energies of the electron distribution.

If the electron distribution within the source is a power-law of the form: $N(\varepsilon) \, d\varepsilon = Ke \, \varepsilon^{-\gamma} \, d\varepsilon$; where Ke, γ, are constants, then equation (5.16) becomes:

$$E_e = Ke \int_v \int_{\varepsilon_1}^{\varepsilon_2} \varepsilon^{-\gamma+1} \, d\varepsilon \, dv \qquad \ldots(5.17)$$

Thus, E_e can be determined from the source spectrum provided

Ke, ε_1 and ε_2 and the source size and distance are known. The quantity Ke can be determined by rearranging equation (1.15), (see page 11), and substituting for the source intensity measured at a (high) frequency where the spectrum of the source is a power-law. The electron densities given in column 11 (table 5.12) were obtained using equations (5.17) and (1.15) and by assuming that the lower cut-off energy of the electron distributions occurred at 0.1 GeV; the distribution had no upper energy cut-off.

The magnetic field energy density, $E_B^* = B^2/8\pi$ (c.f. equation 5.15) can be determined for each source from the values of magnetic field strength given in column 7 of table 5.12; the results are given in column 10 of table 5.12). The total energy density, E_p^*, (calculated from the results of column 11, table 5.12 and equation 5.14) exceeds the magnetic field energy density, E_B^*, in 70% of the sources listed in table 5.12. Thus *equipartition* may not exist within most of these sources. This result should be treated as tentative however, since the angular size data used in the calculations is somewhat uncertain. Note that Kellermann and Pauliny-Toth (1969) have pointed out that E_{e/E_B} depends on approximately the twentieth power of the cut-off frequency (of the spectrum) and source angular size. Thus departures from *equipartition* are difficult to detect.

In the analysis above we have fitted five theoretical

models to the observed data of 49 sources which have low frequency *convex* spectra. Data from the references listed in table 1 of appendix 2 and from the surveys reported in chapter 3 show that the sources have curved spectra and it has been possible to determine the parameters of each of the models using this information. Further measurements between 40 and 408 MHz, particularly of the sources:

PKS: 0109+14, 0252-71, 0320+05, 0408-65, 0417+15
0702-10, 0841+15, 1005+07, 1031+11, 1044+15,
1241+16, 1345+12, 1523+03, 1645+17, 1814-51,
1827-36, 1949+02,

would be useful for obtaining a more accurate estimate of the cut-off frequency of each *convex* spectrum. However, new results should not significantly alter the model parameters obtained above. Measurements below 40 MHz would perhaps determine the importance of the Tsytovich effect in each of the sources; observations in this frequency range may soon be made with the new low frequency telescope at present under construction in Tasmania.

The calculations and results summarized in table 5.12 depend strongly on the source angular diameters and redshifts. Redshift data is known for only three of the sources, PKS: 0518+16, 1241+16, 1416+06, and only two of the sources have been measured with an angular resolution of better than 0.1" arc (see table 5.8). The calculations in table 5.12

are therefore mainly based on assumed values for source red-shift and on values of source "size" determined from scintillation data, [The fact that a source scintillates only indicates that it contains components with an angular diameter of less than 1" arc (Hewish et al., 1964)]. The values of magnetic field strength (column 7, table 5.12) are in general greater than those thought to exist in most extra-galactic radio sources [Scheuer and Williams, 1968]. This may be a result of the probable over-estimation of source size. High resolution measurements of discrete sources are needed to determine the magnetic fields more accurately from the *self-absorption model* (assuming that it explains the curvature).

(ii) Sources with Concave or Complex Spectra.

All the sources with *concave* or *complex* spectra considered in part D above, which have been identified, are either quasi-stellar objects or Seyfert galaxies and hence have a high surface brightness temperature. The fact that many of these sources also scintillate [except PKS: 0405-12, 0602-31, 0620-52, 2247+14] indicates that they may also contain small components, some of which are perhaps self-absorbed. The model-fitting analysis made allowance for the scintillation data.

Little can be added to the comments made above in part D for the *concave* spectra. There is no doubt that as more measurements become available we shall find that some of

the sources have *complex* rather than *concave* spectra. Data near 10 or 20 MHz would help to define accurately the low frequency components of each spectrum; such measurements may also be made in Tasmania with the new telescope. Observations above 5000 MHz are needed to determine which of the spectra are *complex*. It may be some time before these are obtained however, mainly because of the lack of a solid-surface paraboloid in the southern hemisphere.

The analysis for the *complex* specta given above is useful since it reliably indicates the number of components within a given source (here we assume that the source components are self-absorbed in the observed wave-length range). The spectrum of each component is, however, somewhat uncertain since this is determined from the model described by equation 5.6 by curve-fitting only. Note that model 5.6 was not fitted to the spectrum of the source PKS 2230+11 since this seems to consist of a single, compact component [Pauliny-Toth and Kellermann, 1968] . It is possible that there is an unusual electron energy distribution within this particular source or else an alternative emission mechanism to the synchrotron process is causing the radiation [see page 41]. Further spectral measurements of each source should help to define more accurately the spectra of each source component.

SECTION 4.

GALACTIC RADIATION

AT

10.02 MHz and 153 MHz.

CHAPTER 6

HIGH RESOLUTION SURVEYS OF THE SOUTHERN SKY At 10.02 and 153 MHz.

A. Introduction.

In this chapter we present the results of two background surveys of the southern sky at 10.02 MHz and 153 MHz. Source flux density measurements obtained during these surveys have already been discussed in chapter 3.

The 10 MHz and 153 MHz surveys were undertaken as part of a more extensive series of measurements of galactic radiation recently completed by workers in Tasmania. High resolution surveys of the southern sky have now been completed at 2.1 MHz [Reber, 1968], 4.7 MHz [Ellis et al., 1963; Ellis and Hamilton, 1966], 10.02 MHz [Hamilton and Haynes, 1968], 30 MHz [Mathewson et al., 1965], 85 MHz [Yates et al., 1967], 153 MHz [Hamilton and Haynes, 1969] and 408 MHz [Komesaroff, 1966]. Hamilton (1969) has used these surveys (except the 408 MHz survey) in an analysis of the distribution of ionized hydrogen in the galaxy.

B. The 10.02 MHz Survey.

The equipment used to obtain the 10 MHz survey results has already been discussed in chapter 3 (page 72.). Data was obtained in the form of right ascension scans at fixed declinations between -2.4° and -64°. The method of

obtaining the final profile at each declination was discussed on page 78 .

The distribution of sky brightness at 10.02 MHz has been determined from the right ascension scans and is shown in figure 6.1. The map is in *new* galactic coordinates on a Hammer equal area projection. The sky survey was calibrated by setting the temperature in the direction of the south galactic pole equal to 6.3×10^5 degK (see Higgins and Shain, 1954; Ellis, 1965) determined from low resolution observations. The contour interval shown in figure 6.1 is equal to 2×10^5 degK.

C. The 153 MHz Survey.

The 153 MHz survey was undertaken using the 210 ft. paraboloid at Parkes in 1966 and early 1967. The equipment and the observing method used during the observations have already been discussed in chapter 3 (page 83). The sky survey map is based on declination scans 30^o long and 12 minutes apart in right ascension. These scans were calibrated by reference to the south *celestial* pole which was used as a standard for the entire survey. The equivalent temperature of this region of the sky was determined to be 280 (± 15) degK using a thermal load.

Repeated scans of different parts of the sky showed that the relative error of the survey is not greater than 5 percent.

FIGURE 6.2.

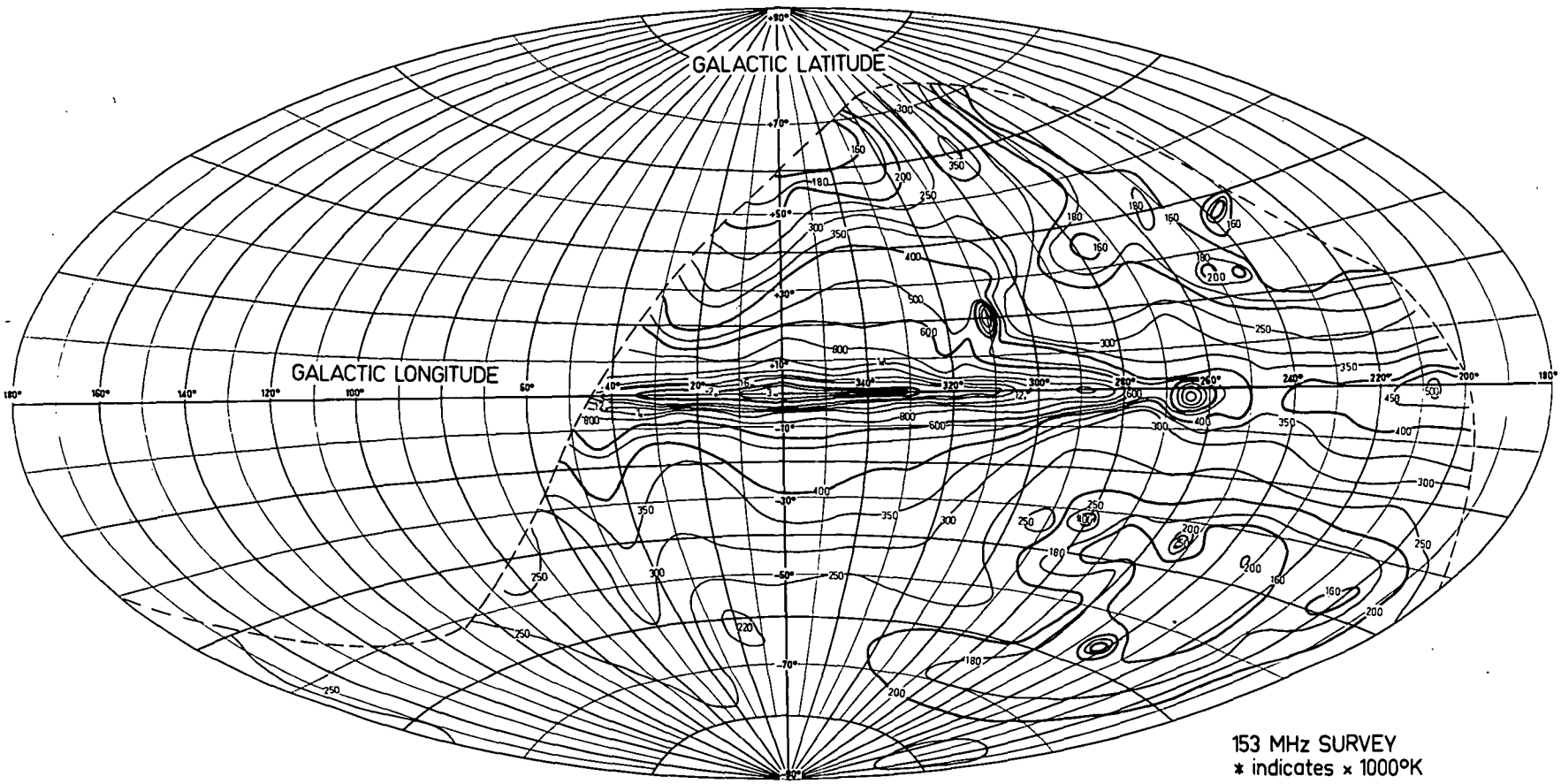

Galactic Background Radiation at 153 MHz.

Figure 6.2 shows the distribution of sky brightness at 153 MHz in *new* galactic coordinates on a Hammer equal area projection grid. The contours are marked in units of effective aerial temperature (degK). The dashed line shows the limit of the survey.

D. Discussion.

The low frequency, high resolution surveys of the southern sky now completed at 2.1 MHz, 4.7 MHz and 10.02 MHz show the galactic plane as a region of low brightness due to absorption in ionized hydrogen. The absorption coefficient is inversely proportional to ν^2 [ν = wave frequency], and since this is a rapidly varying function of the frequency, only broad features may be seen as common to the low frequency surveys. There is a deep absorption trough in the direction of the galactic centre on the 2.1 MHz survey by Reber (1968) and the 4.7 MHz survey of Ellis and Hamilton (1966 a). This trough is not as pronounced in the new survey at 10.02 MHz, although there are strong absorption features in the directions $l^{II} = 20^o$, $b^{II} = 0^o$ and $l^{II} = 346^o$, $b^{II} = 0^o$ (l^{II}, b^{II} represent the *new* galactic longitude and latitude respectively) with some sign of a link between them. These same features are evident on the 19.7 MHz survey map by Shain et al. (1961). An overlay in figure 6.1 of the known (optical) H II regions [after Rogers et al., 1960] indicates the correlation between

the two absorption troughs already mentioned and the distribution of H II regions (optical) along the galactic plane.

The ionized hydrogen absorption regions become transparent in the surveys above 20 MHz. Hamilton (1969), from his analysis of the high resolution surveys, suggests that a resolution of better than or equal to 1 degree would be required at 30 MHz to see the galactic plane in absorption. The spectrum of the galactic non-thermal radiation can be determined in the absence of absorption effects; the emission is probably a result of synchrotron radiation from cosmic ray electrons in the metre and decimetre wavelength band [eg. Ginzburg and Syrovatskii, 1964].

The 153 MHz map given in figure 6.2 agrees well with an 85 MHz survey map by Yates et al. (1967) and with the 178 MHz northern hemisphere survey map of Turtle and Baldwin (1962) in the region common to the surveys. The most notable feature of the 153 MHz map is the large cold region centred on $l^{II} = 240^{o}$, $b^{II} = -40^{o}$. The same feature can be seen in the 30 MHz survey of Mathewson et al. (1965) and 85 MHz survey of Yates et al. (1967). In the northern galactic hemisphere there is a corresponding cold region at $l^{II} = 240^{o}$, $b^{II} = +35^{o}$; however, the northern feature is not as pronounced as is the southern feature, especially at 30 MHz.

Steps in Emission along the galactic plane.

Mills (1959) first noted, from the results of a southern

sky survey at 85 MHz, that there existed pronounced steps in the intensity of non-thermal radiation along the galactic plane, particularly in the direction $l^{II} = 308^{o}$ and 327^{o}. Wielebinski et al. (1968) noted that there were also similar steps at $l^{II} = 14^{o}$, 35^{o}, and 345^{o}. The new 153 MHz survey map agrees well with these previous observations, showing definite steps in emission at about 306^{o} and 328^{o} galactic longitude. Mills suggested, from results of 21 cm. H-line studies, that the steps in emission correspond to line-of-sight directions tangential to the spiral arm directions.

Galactic Spurs.

High resolution surveys of the galactic non-thermal radiation at frequencies above 20 MHz have led to the discovery and detailed mapping of spur- or ridge-like features in the cosmic background radiation. Three major spur features are known:

The North Pole Spur [see, Davies, 1964];

The Cetus Arc Spur [Quigley and Haslam, 1965];

and The Loop III Arc [Seeger et al., 1965; Quigley and Haslam, 1965]

Yates (1968) has combined the 85 MHz survey map of Yates et al. (1967) with northern hemisphere survey maps to produce a complete sky map in order to study these spurs. The northern hemisphere surveys he used were: the 81.5 MHz survey (beam-width: $15^{o}x2^{o}$) of Baldwin (1955); the 178 MHz survey

(beamwidth: 4^{o}x13') by Turtle and Baldwin (1962) and the 404 MHz survey of Pauliny-Toth and Shakeshaft (1962). Yates gives a maximum relative error for his combined map of 10% between directions in opposite hemispheres. Figure 6.3 shows a reconstruction of Yates' map on a Hammer equal area projection grid, (the same grid used for the 153 MHz map).

If we compare the results of the 153 MHz survey with figure 6.3, we can see that the part of the North Pole Spur near $l^{II} = 35^{o}$, $b^{II} = 20^{o}$ is recognizable on the 153 MHz map. The feature near $l^{II} = 290^{o}$, $b^{II} = 70^{o}$ may well be a continuation of this spur [eg. Quigley and Haslam, 1965]. Until recently there was a lack of reliable, high resolution surveys in the southern hemisphere and spurs could not be tracked near the galactic plane. Although we now have surveys at 85 MHz [Yates et al., 1967] and 153 MHz available, there is still some debate as to whether or not the spurs discovered in northern hemisphere surveys cross the galactic plane. Bingham (1967) notes that the spurs appear to intersect the galactic plane at right angles, but he suggests that they do not cross the plane.

Observations of the North Pole Spur show that it has a steep outer edge near $l^{II} = 35^{o}$, $b^{II} = 30^{o}$ which supports the theory that this feature is an incomplete shell of emission of an old supernova. To test the theory that all

FIGURE 6.3.

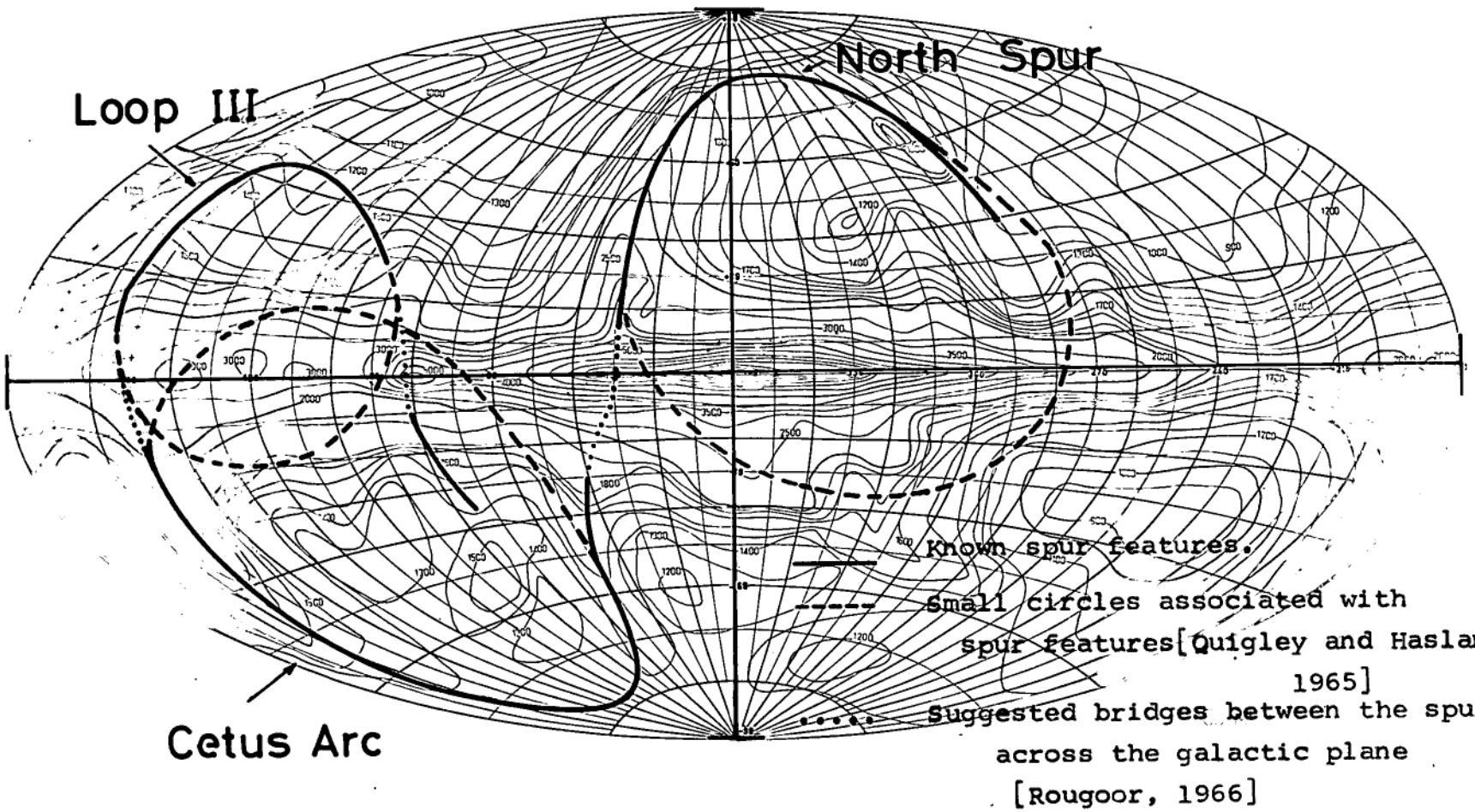

Galactic Background Radiation at 85 MHz.

the spurs are supernova remnants, Quigley and Haslam (1965) plotted the shape of the known spurs on the celestial sphere; all the large spurs appear to lie along *small* circles. The overlay of figure 6.3 shows the suggested positions of the spur circles.

Two spur features can be clearly identified in the 153 MHz survey in the southern galactic hemisphere. There is a strong feature running from $l^{II} = 45^{o}$, $b^{II} = -20^{o}$ towards the south galactic pole. The same feature is visible near $l^{II} = 170^{o}$, $b^{II} = -50^{o}$ and is part of the extensive spur discussed by Quigley and Haslam (1965), known as the Cetus Arc. Another important feature is a spur from near the galactic centre to the point $l^{II} = 300^{o}$, $b^{II} = -50^{o}$ extending into the cold region near $l^{II} = 240^{o}$, $b^{II} = -40^{o}$. This spur was also observed by Yates et al. (1967) at 85 MHz (see figure 6.3). It lies very close to the *small* circle of the North Pole Spur over about 60^{o} of the sky. This coincidence of a southern spur close to the North Spur circle adds support for the supernova theory of spurs. It may also show that the spurs can be traced across the galactic plane. However, comparisons of optical and radio polarization data [Bingham, 1967] give an estimated distance to the North Spur of 100 ± 20 parsecs and a linear diameter 300 parsecs. This is an order of magnitude larger than for the known supernova remnants [Seaquist, 1968].

A number of other theories have been suggested to explain the spurs. Oda and Hasegawa (1962) suggested that the magnetic field of a spur was parallel to the ridge of maximum brightness. Relativistic electrons introduced into this field near the galactic plane may radiate by the synchrotron process and explain the spur emission. Note that Bingham (1967) has shown that the field of the North Spur is parallel to the ridge of maximum brightness. Rougoor (1967) has suggested that all the spurs are part of a single, large scale helical structure with axis in the direction $l^{II} = 110^{o}$, $b^{II} = 0^{o}$ which is associated with the local spiral arm of the galaxy. Rougoor's feature is shown in the overlay of figure 6.3.

E. Note

The two high resolution low frequency surveys presented here provide data that was needed for a comprehensive analysis of the distribution of ionized hydrogen in the galaxy. The analysis was beyond the scope of this thesis, but has been discussed elsewhere by Hamilton (1969).

APPENDIX 1.

Calculation of the Function: $F(\nu/\nu_c)$

The function:

$$F(\nu/\nu_c) = \frac{\nu}{\nu_c} \int_{\nu/\nu_c}^{\infty} K_{5/3}(x)\, dx \qquad \ldots.(1)$$

characterizes the synchrotron emission from a single electron *in vacuo*. Here ν_c is the *characteristic* frequency (see equation 1.4), $K_{5/3}(x)$ is a modified Bessel function of order $5/3$ and ν is the frequency of emission. To determine the intensity of the synchrotron radiation from a distribution of electrons, the function given by equation (1) has to be evaluated repeatedly (see equations 1.7 and 1.11). However, the computation of $F(\nu/\nu_c)$ from the appropriate Bessel function is complex. It is convenient to fit a set of Chebycheff Polynomials to the rapidly changing regions of the function and to use approximations to the function in the other regions. The behaviour of the function for large and small values of ν/ν_c has been discussed by Ginzburg and Syrovatskii (1965).

The calculations of equations 1.7 and 1.11 needed during the source spectral analysis of section 3 were made using an Elliott 503 digital computer. The procedure developed by the author to calculate the function $F(\nu/\nu_c)$

is given below for reference. The procedure is given in Elliott Algol. Note that some of the symbols used in this computing *language* differ from those used in Algol 60; they are listed below:

SYMBOLS.

Elliott 503 Algol.	Algol 60.
and	∧
or	∨
£ or $	'
?	,
div	÷
*	x
not	¬

Algorithm to Calculate the value of the function: $F(\nu/\nu_c)$

```
real procedure XINTK53(x);  value x;  real x;
begin real x2, x3, sum;
if x ≤ 0.401 then
 begin x2: = x*0.5;  x3: = x2 ↑ 0.33333333;
 sum:=2.70823602*x3*(1.0-0.5*2.6789385347*x3*x3+0.75*x2*x2
                              -0.225*2.6789385347*x3/0.90274529295)
 end
else if x < 1.0 then
 sum:=-1.6737204+x*(23.211799+x*(-83.585460+x*(155.68180
                  +x*(-160.48338+x*(86.515141-19.011542*x)))))
```

```
else if x ≤ 3.0 then
 sum:=0.73841307+x*(0.89747496+x*(-1.8945853+x*(1.2710539
                    +x*(-0.42328743+x*(0.06995919-0.00450117*x)))))
else if x ≤ 5.0 then
 sum:=1.4649655+x*(-1.0293666+x*(0.29929996+x*(-0.04173333
                                 +x*0.00230000)))
else begin x2:=sqrt(x)*exp(-x);  x3:=1.0/x ;
 sum:=1.253314137316*x2*(1.0+x3*(55.0/72.0-10151.0*x3/10368.0));
   end;
XINTK53:=sum;     comment sum = value of the function F(ν/νc);
end XINTK53;
```

APPENDIX 2.

Flux density measurements and Optical data for Sources south of declination $+27^{\circ}$.

In this appendix we summarize published articles which deal with flux density measurements and optical identification studies of discrete radio sources south of declination $+27^{\circ}$. Since the literature contains many such measurements we have restricted the summary to those articles which describe the more extensive surveys. Table 1 summarizes the articles dealing with source flux density measurements. The information is listed in (approximate) order of increasing frequency. Table 2 summarizes the optical studies of identified radio sources. Articles are listed in alphabetical order of the first author.

TABLE 1.

RADIO SOURCE SURVEYS

(A summary of published results of radio source surveys contributing to the known data of radio sources visible from Southern Hemisphere Observatories [August 1969])

Survey No.	Frequencies (MHz)	Author and Publication
S00	4.7	Ellis,G.R.A. & Hamilton,P.A. (1966) Astrophys.J. 143(1), 227
S01	10.02	Hamilton,P.A. & Haynes,R.F. (1968) Aust.J.Phys. 21, 895
S02	10.03	Bridle,A.H.& Purton,C.R. (1968) Astron.J. 73(8), 717
S03	12.6 to 25	Braude,S.Ya., Lebedeva et al.(1969) Mon.Not.Roy.astr.Soc. 143, 289
S04	12.6 to 25	Braude,S.Ya., Zhuk,I.N. et al.(1968) Soviet Phys.,Doklady 13(6), 512
S05	20 to 40	Guidice,D.A. (1966) Nature 211(5044), 57
S06	26.3	Erickson,W.C. & Cronyn,W.M. (1965) Astrophys.J. 142, 1156
S07A	38	Williams,P.J., Kenderdine,S. et al.(1966) Mem.Roy.astr.Soc. 70(3), 53
S07B	38,178,617, 1417	Long,R.J., Smith,M.A. et al (1966) Mon.Not.Roy.astr.Soc. 134(4), 371
S08	38	Slee,O.B. & Wraith,P.K. (1967) Nature 214(5092), 971
S09	38,178,1410,2650	Williams,P.J.,Collins,R.A. et al.(1968) Mon.Not.Roy.astr.Soc. 139, 289
S10	38,86	Artyukh,V.S., Vitkevich,V.V. & Dagkesamanskii,R.D. (1968) Soviet Astron.- AJ 11(5), 792
S11	40 to 130	Haynes,R.F. & Hamilton,P.A. (1968) Aust.J.Phys. 21, 87
S12	55	Haynes,R.F., Hamilton,P.A. & McCulloch,P.M. (1968) Aust.J.Phys.21(4), 539
S13	60	Aslanyan,A.M., Dagkesamanskii,R.D. et al.(1968) Astrofizika 4(1), 129
S14	85.5	Mills,B.Y. & Slee,O.B. (1957) Aust.J.Phys. 10, 162
S15	85.5	Mills,B.Y., Slee,O.B.& Hill,E.R. (The MHS Catalogue) 1958: Aust.J.Phys. 11, 360 1960: Aust.J.Phys. 13, 676 1961: Aust.J.Phys. 14, 497
S16	86	Artyukh,V.S., Vitkevich,V.V., Dagkesamanskii,R.D. et al. (1968) (a): Soviet Phys.,Doklady 13(2), 80
S17	86	(1969) (b): Soviet Astron.,AJ 12(4), 567
S18	153	Hamilton,P.A. & Haynes,R.F. (1967) Aust.J.Phys. 20(6), 697
S19	159	Edge,D.O., Shakeshaft,J.R. et al. (1959) Mem.Roy.astr.Soc. 68, 37
S20	178	Bennett,A.S. (a): (1962) Mon.Not.Roy.astr.Soc. 125, 75
S21	178	Bennett,A.S. (b): (1962) Mem.Roy.astr.Soc. 68, 163
S22	178	Bennett,A.S. (1963) Mon.Not.Roy.astr.Soc. 127(1), 3
S23	178	Pilkington,J.D. & Scott,P.F. (1965) Mem.Roy.astr.Soc. 69(5), 183
S24	178	Crowther,J.H. & Clarke,R.W. (1966) Mon.Not.Roy.astr.Soc. 132, 405
S25	178	Gower,J.F., Scott,P.F. & Wills, D.(1967) Mem.Roy.astr.Soc. 71(2), 49
S26	240 & 412	Conway,R.G. & Moran,M. (1964) Mon.Not.Roy.astr.Soc. 127(5), 377
S27	400	Davis,M.M., Gelato-Volders,L. & Westerhout,G. (1965) Bull.Astron.Inst.Netherlands 18(1), 42
S28	408,1410,2650	Bolton,J.G., Gardner,F.F. & Mackey,M.B. (1964) Aust.J.Phys. 17, 340
S29	408,1410,2650	Day,G.A., Shimmins,A.J., Ekers,R.D. & Cole,D.J. (1966) Aust.J.Phys. 19, 35
S30	408,1410,2650	Price,R.M. & Milne,D.K. (1965) Aust.J.Phys. 18, 329
S31	408,1410,2650	Shimmins,A.J., Day,G.A., Ekers,R.D. & Cole,D.J. (1966) Aust.J.Phys. 19(6), 837
S32	408,1410,2650	"The Parkes Catalogue of Radio Sources: Declination +20° to -90° Zone". Edited by J.A.Ekers (1969) Aust.J.Phys. Astrophys.Suppl.No.7, p.1-75
S33	408	Braccesi,A., Ceccarelli,M., Fanti,R. et al.(1965) Nuovo Cimento Ser.10 B 40(1), 267
S34	408	Kesteven,M.J.L. (1968) Aust.J.Phys. 21(3), 369
S35	408	Komesaroff,M.M. (1966) Aust.J.Phys. 19(1), 75

TABLE 1 (cont.).

S36	408	Large,M.T., Mathewson,D.S. & Haslam,C.G. (1961) Mon.Not.Roy.astr.Soc. 123(2), 113
S37	408	Murdoch,H.S. & Large,M.I. (1968) Mon.Not.Roy.astr.Soc. 141(4), 377
S38	408	Schilizzi,R.T. & McAdam,W.B.(1969) Proc.A.S.A. 1(5), 228
S39	468,1403	Ekers,R.D. (1967) "The Structure of Southern Radio Sources" Ph.D.Thesis. Aust.Nat.Univ.,Canberra
S40	468,1403	Ekers,R.D. (1969) Aust.J.Phys. Astrophys.Suppl. No.6, 3
S41	468,1403	Wall,J.V., Cole,D.J. & Milne,D.K. (1968) Proc.A.S.A. 1(3), 98
S42	610.5	Dickel,J.R., Yang,K.S. et al.(1967) Astron.J. 72(6), 757
S43	610.5	Fang,C.C. & Dickel,J.R. (1968) Astron.J. 73(2PT2), S12
S44	612,1400	Conway,R.G., Daintree,E.J. & Long,R.J. (1965) Mon.Not.Roy.astr.Soc. 131, 159
S45	635,1410,2650	Shimmins,A.J. & Day,G.A. (1968) Aust.J.Phys. 21(3), 377
S46	750,1410	Höglund,B.(1967) Acta Polytech.Scandinavica Phys. Including Nucleonics Ser. No. 48, 1 - 74
S47	750 to 15000	Kellermann,K.I. & Pauliny-Toth,I.I.K. (1968) Astrophys.J. 152(2PT1), 639
S48	750,1400	Pauliny-Toth,I.I.K.,Wade,C.M. & Heeschen,D.S. (1966) Astrophys.J.Supp.Ser. 13(116), 65
S49	960	Harris,D.E. & Roberts,J.A. (1960) Publications of the Ast.Soc.Pac. 72, 237
S50	1410,1660,2650	Gardner,F.F., Morris,D. & Whiteoak,J.B. (1969) Aust.J.Phys. 22(1), 79
S51	1415	Dixon,R.S. & Kraus,J.D. (1968) Astron.J. 73, 381
S52	1415	Fitch,L.T., Dixon,R.S. & Kraus,J.D. (1969) Astron.J. 74(5), 612
S53	1417	Davis,M.M. (1967) Bull.Astron.Inst.Netherlands 19, 201
S54	1420	Galt,J.A. & Kennedy,J.E.D. (1968) Astron.J. 73(3), 135
S55	1420	Galt,J.A. & Kennedy,J.E.D. (1968) Astron.J. 73(5:2):S93
S56	1425	Fomalont,E.B. (1968) Astrophys.J.Suppl.Ser. 15(138), 203
S57	1425	Fomalont,E.B. (1967) Astron.J. 72(3), 299
S58	1440	Mathewson,D.S., Healey,J.R. & Rome,J.M. (1962) Aust.J.Phys. 15, 354
S59	2695,4995	Horton,P.W., Conway,R.G. & Daintree,E.J. (1969) Mon.Not.Roy.astr.Soc. 143(3), 245
S60	2695	Kellermann,K.I., Pauliny-Toth,I.I.K. & Tyler,W.C. (1968) Astron.J. 73(5PT1), 298
S61	2695	Ristow,D. (1968) Beitr.Radioastron. 1(3), 65
S62	5000	Blum,E.J. & Davis,M.M. (1968) Astrophys.Letters 2(1), 41
S63	5000	Broten,N.W., Cooper,B.F.C., Gardner,F.F. et al. (1965) Aust.J.Phys. 18, 85
S64	5000	Kellermann,K.I. (1966) Aust.J.Phys. 19, 577
S65	5000	Maxwell,A. & Rinehart,R. (1966)Astron.J. 71(9), 927
S66	5000	Morris,D. & Whiteoak,J.B. (1968) Aust.J.Phys. 21, 493
S67	5000	Pauliny-Toth,I.I.K. & Kellermann,K.I. (1968) Astron.J. 73(10PT1), 953
S68	5009	Shimmins,A.J., Manchester,R.N. & Harris,B.J. (1969) Aust.J.Phys. Astrophys.Suppl.No. 8 (June)
S69	8000	Dent,W.A. & Haddock,F.T. (1966) Astrophys.J. 144(2), 568
S70	10000	Medd,W.J., Locke,J.L., Andrew,B.H. et al. (1968) Astron.J. 73(5PT1), 293
S71	10000	Doherty,L.H., Macleod,J.M., Purton,C.R. (1968) Bull.Radio Elect.Engng.Div.N.R.C. Canada 18, 43
Note Added:		
S72	38,178,750,1400, 2650,5000	Kellermann,K.I., Pauliny-Toth,I.I.K. et al. (1969) Astrophys.J. 157, 1

Note added:

S73 22.25MHz Roger, R.S., Costain, C.H. and Lacey, J.D., (1959), Astron J. 74 (3), 366.

TABLE 2.

IDENTIFICATIONS OF RADIO SOURCES

(A Summary of the more extensive identification studies undertaken for radio sources in the Southern Hemisphere. This includes the sky in the declination range 0° to +27°.)

Survey No.	Region	Author and Publication
I00	14 3C & Parkes Sources	Appenzeller,I., Hiltner,W.A. (1967) Astrophys.J. 149(1PT2),L17
I01	Catalogue of 103 Q.S.O's	Barbieri,C., Battistini,P., Nasi,E. (1967) Pubbl.Oss.Astron.Univ.,Bologna 9(13),1
I02	7 4C sources	Barbon,R., Braccesi,A., Fanti,R.(1967) Nuovo Cimento Ser.10 852, 262
I03	Parkes Sources -20° to -44° decl	Bolton,J.G.,Clarke,M.E. & Ekers,R.D.(1965) Aust.J.Phys. 18, 627
I04	Parkes Sources -20° to -30° decl	Bolton,J.G. & Ekers,J.(1966) Aust.J.Phys. 19(2), 275
I05	Parkes Sources 0° to +20° decl	Bolton,J.G., & Ekers,J.(1966) Aust.J.Phys. 19(3), 471
I06	Parkes Sources 0° to -20° decl	Bolton,J.G. & Ekers,J.(1966) Aust.J.Phys. 19, 559
I07	Parkes,Sources 0° to -20° decl	Bolton,J.G. & Ekers,J.(1966) Aust.J.Phys. 19, 713
I08	12 Parkes Sources +19° to -24° decl	Bolton,J.G. & Kinman,T.D.(1966) Astrophys.J.145, 951
I09	Parkes Sources +1° to +14° decl	Bolton,J.G.,Clarke,M.E.,Sandage,A.,Vérnon,P.(1965)Astrophys.J.142,1289 (1966)Astrophys J.144,860
I10	15 Parkes Sources +13° to -14° decl	Bolton,J.G.,Shimmins,A.J.et al (1966) Astrophys.J.144(3),1229
I11	Parkes Sources 0° to -20° decl	Bolton,J.G. & Ekers,J.(1967) Aust.J.Phys. 20(1),109
I12	Parkes Sources +27° to -30° decl	Bolton,J.G.,Shimmins,A.J. & Merkelijn,J.(1968) Aust.J.Phys. 21(1), 81
I13	12 Parkes Sources +26° to -2° decl	Bolton,J.G.,Kinman,T.D. & Wall,J.V.(1968) Astrophys.J.154, L105
I14	Parkes Sources:- 78 in all	Bolton,J.G.(1968) Publ.Astron.Soc.Pacific 80(472), 5
I15	12 3C & Parkes Sources	Burbidge,E.M. & Kinman,T.D.(1966) Astrophys.J.145, 654
I16	-10° to +27° decl	Burbidge,E.M. (1968) Astrophys.J. 154, L109
I17	Summary of Red Shift Data	Burbidge,G.M. & Burbidge,E.M. (1969) Nature 222, May 24, 735
I18	100 Sources in 4C Catalogue	Caswell,J.L. & Wills,D.(1967) Mon.Not.Roy.Astr.Soc. 135, 231
I19	138 Parkes Sources 0° to +20° decl	Clarke,M.E., Bolton,J.G. & Shimmins,A.J. (1966) Aust.J.Phys. 19(3), 375
I20	Red Shifts of gals. -39° to +71° decl	De Vaucouleurs,A. & De Vaucouleurs,G.(1967) Astron.J. 72(6), 730
I21	13 Parkes Sources	Fairall,A.P.(1966) Mon.Not.Astr.Soc.Sth.Afr. 25(8), 79
I22	Parkes Sources South of -45° decl	Fairall,A.P. (1966) pp105, Cape Town, Univ.Cape Town,Department Astron.
I23	Review of Optical Work	Fowler,W.A.(1965) Rend.Scuola Int.Fis."Enrico Fermi" 35, 313
I24	Galaxies South of +20° decl	Glanfield,J.R. & Cameron,M.J. (1967) Aust.J.Phys. 20(5), 613
I25	8 3C and MSH Sources	Hazard,C., Mackey,M.B. & Nicholson,N.(1964) Nature 202(4929),April 18, p.227
I26	16 Parkes Sources	Kinman,T.D., Bolton,J.G., Clarke,R.W. & Sandage,A.(1967) Astrophys.J. 147, 848
I27	4C & Parkes Sources	Kinman,T.D. & Burbidge,E.M. (1967) Astrophys.J. 148(2), L59
I28	3C, CTA* & Parkes Sources	Lü,P.K. & Frederick,L.W. (1967) Astrophys.J.150(2PT2),L71 [*California Institute of Technology Catalogue]
I29	26 (Primarily) Parkes Sources	Lü,P.K. & Fredrick,L.W.(1968) Astrophys.J. 151(2PT2),L75

TABLE 2 (cont.).

I30	3C & Parkes Sources	Lynds,C.R., Stockton,A.N. & Livingston,W.C.(1965) Astrophys.J. 142, 1667
I31	3C, 4C & Parkes Sources	Lynds,C.R., Hill,S.J. et al.(1966) Astrophys.J. 144(3), 1244
I32	Parkes Sources +20° to +27° decl	Merkelijn,J.K.,Shimmins,A.J. & Bolton,J.G. (1968) Aust.J.Phys. 21(4), 523
I33	Parkes Sources +20° to +27° decl	Merkelijn,J.K.(1968) Aust.J.Phys. 21(6), 903
I34	Parkes Sources +20° to -33° decl	Merkelijn,J.K. (1969) Aust.J.Phys. 22(2), 237
I35	3C, MSH, Parkes Sources	Peach,J.V.(1969) Nature 222(5192), 439
I36	9 Sources from 3C, CTA & Parkes Cats.	Sandage,A.R. & Wyndham,J.D.(1965) Astrophys.J. 141, 328
I37	10 3C Sources	Sandage,A.R.,Véron,P. & Wyndham,J.D.(1965) Astrophys.J. 142, 1307
I38	59 Sources from 3C,MSH,Parkes Cats.	Sandage,A.R.(1966) Astrophys.J. 146, 13
I39	11 3C Sources	Sandage,A.R.(1966) Astrophys.J. 144, 1234
I40	9 3C Sources	Sandage,A.R. (1967) Astrophys.J. 150, L145
I41	10 4C Sources	Scheuer,P.A. & Wills,D.(1966) Astrophys.J. 143, 274
I42	23 3C & MSH Sources	Schmidt,M.(1965) Astrophys.J. 141, 1
I43	5 3C & CTA Sources	Schmidt,M.(1965) Astrophys.J. 141, 1295
I44	14 3C, MSH & C.T.D.* Sources	Schmidt,M.(1966),Astrophys.J. 144, 443 [*Cal.Inst.Tech.list D]
I45	15 Parkes Sources	Searle,L.,Bolton,J.G.(1968) Astrophys.J. 154(3PT2), L101
I46	Ohio Sources with Peculiar Spectra	Thompson,J.R., Kraus,J.D. & Andrew,B.H. (1968) Astrophys.J. 154(1PT2), L1
I47	8 3C & CTA Sources	Véron,P.(1965) Astrophys.J. 141, Letters to the Editor, 332
I48	3C Catalogue Sources	Véron,P.(1966) Astrophys.J. 144, 861
I49	Catalogue of Galaxies -9° to -33° decl	Vorontsov-Vel'Yaminov,V.A., Arkhipova,V.P. (1968) Trudy Gosud,Astron.Inst.Im.P.K. Shternberga 38, 1
I50	Parkes Sources -33° to -77° decl	Westerlund,B.E. & Smith,L.F.(1966) Aust.J.Phys. 19(2), 181
I51	64 4C Sources +20° to +80° decl	Wills,D.(1967) Mon.Not.Roy.astr.Soc. 135, 339
I52	Revised 3C Cat.	Wyndham,J.D.(1966) Astrophys.J. 144, 459

In addition to the publications above, some identifications of radio sources are given in the following catalogues.

(a)	MSH Catalogue	Mills,B.Y.,Slee,P.B. & Hill,E.R. (1958) Aust.J.Phys. 11, 360 (1960) Aust.J.Phys. 13, 676 (1961) Aust.J.Phys. 14, 497
(b)	Parkes Catalogue	Editor: J.A.Ekers(1969) Aust.J.Phys. Supp. 7
(c)	Parkes Catalogue +20° to +27° decl	Shimmins,A.J.,Day,G.A.(1968) Aust.J.Phys. 21, 377

APPENDIX 3

Discussion of Experimental Equipment.

A. Summary.

In part B of this appendix we summarize the properties of the feed systems used during the low frequency source observations at Parkes. Photographs of one of the focus package boxes which contained the main part of the interferometer receivers constructed by the author are also included.

The layout of the Parkes interferometer and the relations describing the interferometer response are given in part C.

Finally we discuss (in part D) the method of determining the errors in the interferometer measurements which result from confusing sources within one beamwidth of the required source.

B. Broad-band Feed Systems.

The properties of the aerial feed systems used during the source observations are:

(i). Pair of broad band dipoles: (see figure 1)

[total-power measurements]

Length of dipoles = 6 feet.

Maximum diameter of one dipole = 19 inches.

Separation of dipoles = 4.5 feet.

Characteristic impedance of the total feed 100 ohm.

(facing pages 211, 212)

Figures 1,2 :

Broad-band feed systems used for source observations at the Parkes Observatory.

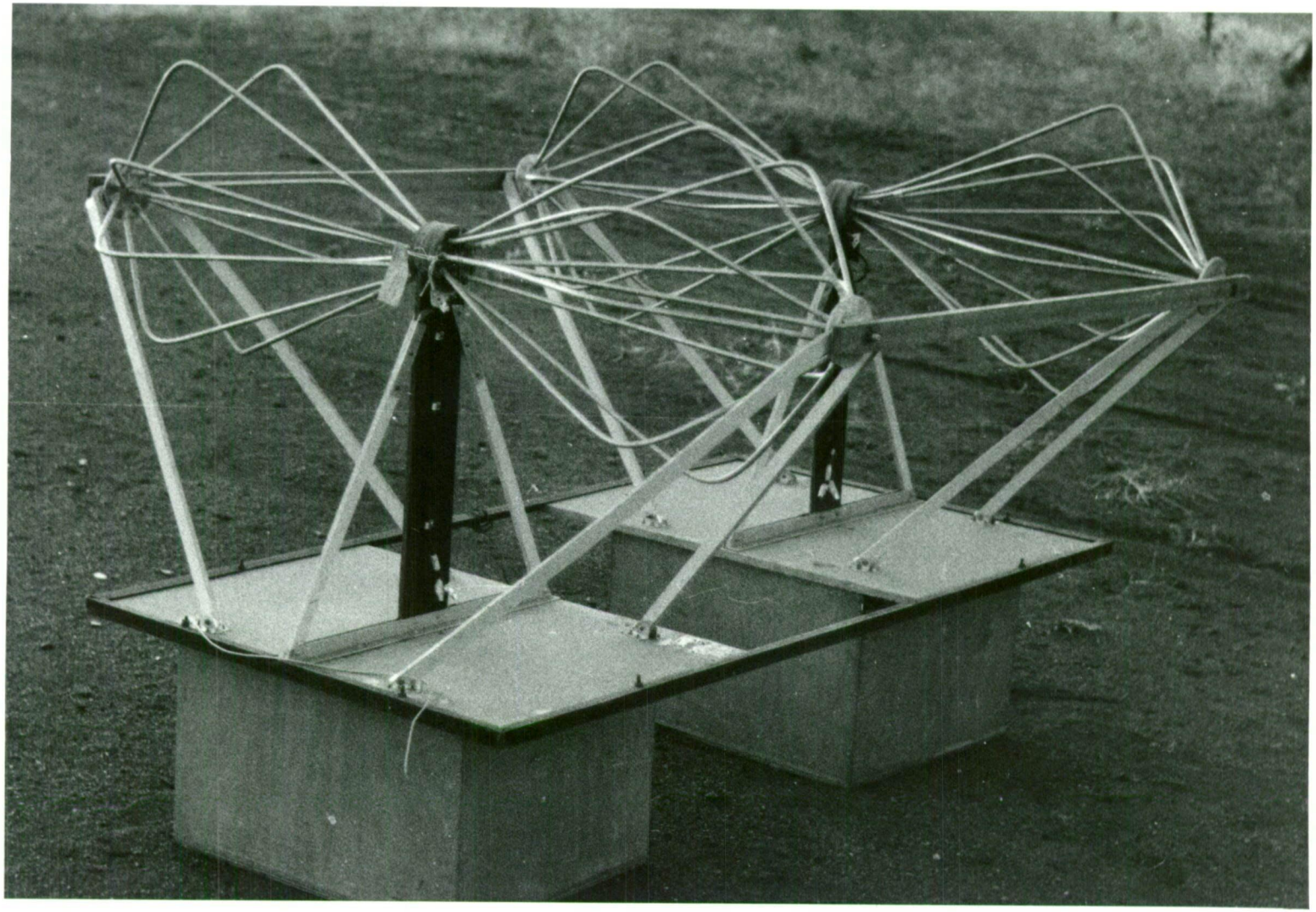

FIGURE 1.

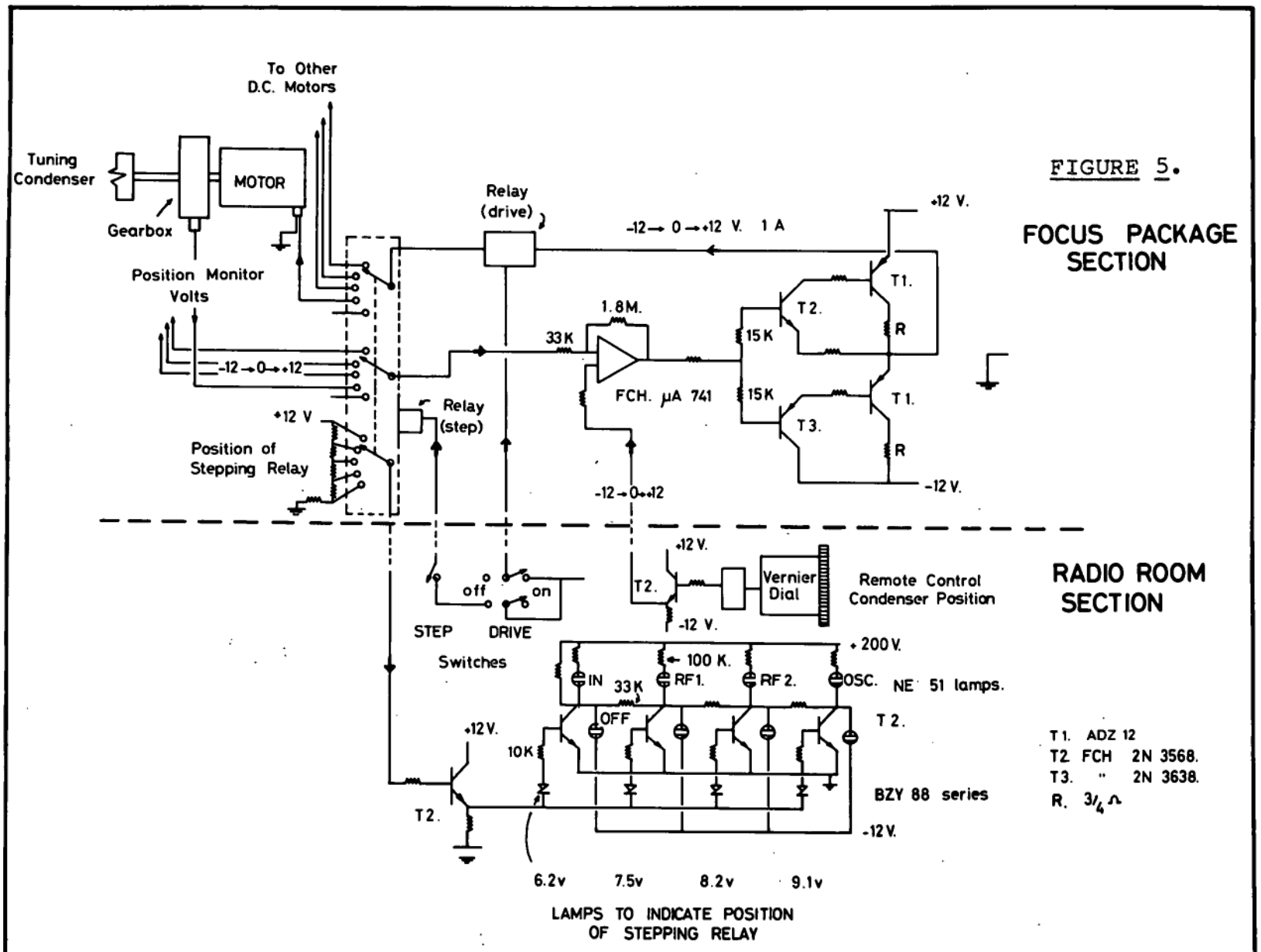
To Other
D.C. Motors
Tuning
Condenser
MOTOR
Gearbox
Position Monitor
Volts
-12→0→+12
+12 V
Position of
Stepping Relay
Relay
(drive)
-12→ 0 →+12 V. 1 A
+12 V.
T1.
T2.
R
1.8M.
33K
15K
FCH. μA 741
15K
T1.
T3.
R
-12 V.
Relay
(step)
-12→0→+12
FOCUS PACKAGE
SECTION
RADIO ROOM
SECTION
off
on
STEP
DRIVE
Switches
+12 V.
T2.
-12 V.
Vernier
Dial
Remote Control
Condenser Position
+200V.
100 K.
IN
33K
RF1.
RF 2.
OSC.
NE 51 lamps.
OFF
T2.
+12V.
10K
T2.
BZY 88 series
-12V.
6.2v
7.5v
8.2v
9.1v
LAMPS TO INDICATE POSITION
OF STEPPING RELAY
T1. ADZ 12
T2. FCH 2N 3568.
T3. " 2N 3638.
R. 3/4 Ω

FIGURE 5.

The feed was matched into 50 ohm coaxial cable with an auto-transformer (broad-band). With this form of matching the aerial was more than 50% efficient from 41 to 160 MHz.

(ii). Helix.

[total-power measurements]

Length = 8 feet, diameter = 20 inches.

The helix had two windings (1½ turns with pitch angle = 35°).

Characteristic impedance = 300 ohm.

The two windings were fed 180° out of phase and an auto-transformer (broad-band) was used to match the helix to 50 ohm coaxial cable.

Bandwidth = 45 to 75 MHz.

(iii). Variable length folded dipoles. (see figure 2)

[interferometer measurements]

Characteristic impedance 400 ohm.

Tuning range = 74 to 150 MHz.

The aerial was matched to 50 ohm cable using a broad-band auto-transformer.

FOCUS PACKAGES AND REMOTE TUNING:

Figures 3 and 4 show the layout of the components in the focus package boxes used for the interferometer observations. Figure 5 shows the circuit diagram of the servo system used for remote tuning.

C. The Parkes Interferometer.

The two-telescope interferometer at the Parkes Observatory has been described in detail by Ekers (1967). Here we outline the important features of the instrument and discuss the relations defining the radiation response of the system.

The Parkes interferometer consists of one fixed element (210 ft. telescope) and one movable element (60 ft. telescope). The layout of the instrument is shown in figure 6. The 60 ft. telescope moves along a system of rails (gauge 35ft.) in either a north-south or east-west direction. The separation between the two telescopes can be continuously varied from 400 to 1360 feet in each direction. The 60 ft. telescope can be driven along the tracks at rates of from 5 to 120 feet per minute. The difference in height between the 60 ft. and 210 ft. telescope pivot points is given by:

$$\Delta h_{\substack{N-S \\ E-W}} = 33 \pm [\frac{d}{400} - 1] \quad \text{feet} \qquad \ldots.(1).$$

[Ekers, 1967]

The plus/minus sign in equation (1) results from the different slopes of the north-south and east-west tracks. Both telescopes move on *alt-azimuth* mountings and during observations the 60 ft. telescope is *slaved* to the position of the 210 ft. telescope (tracking error < 10 minutes of arc).

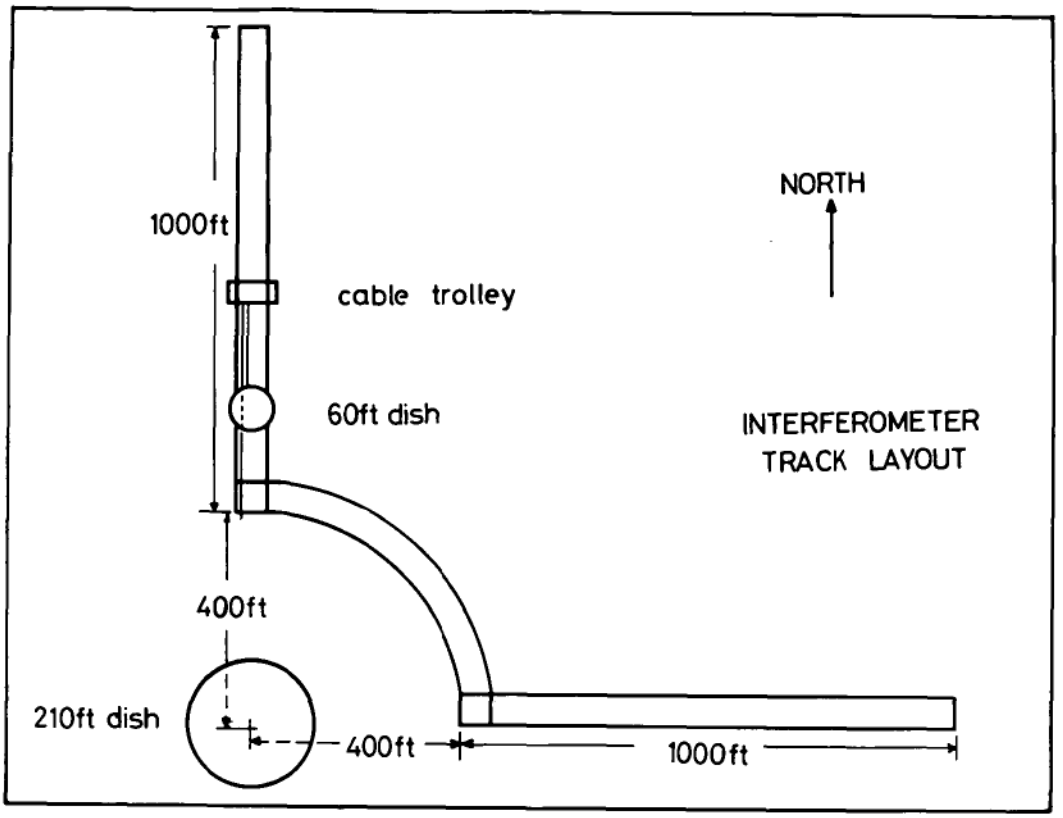
1000ft
cable trolley
60ft dish
400ft
210ft dish
400ft
1000ft
NORTH
INTERFEROMETER
TRACK LAYOUT

FIGURE 6.

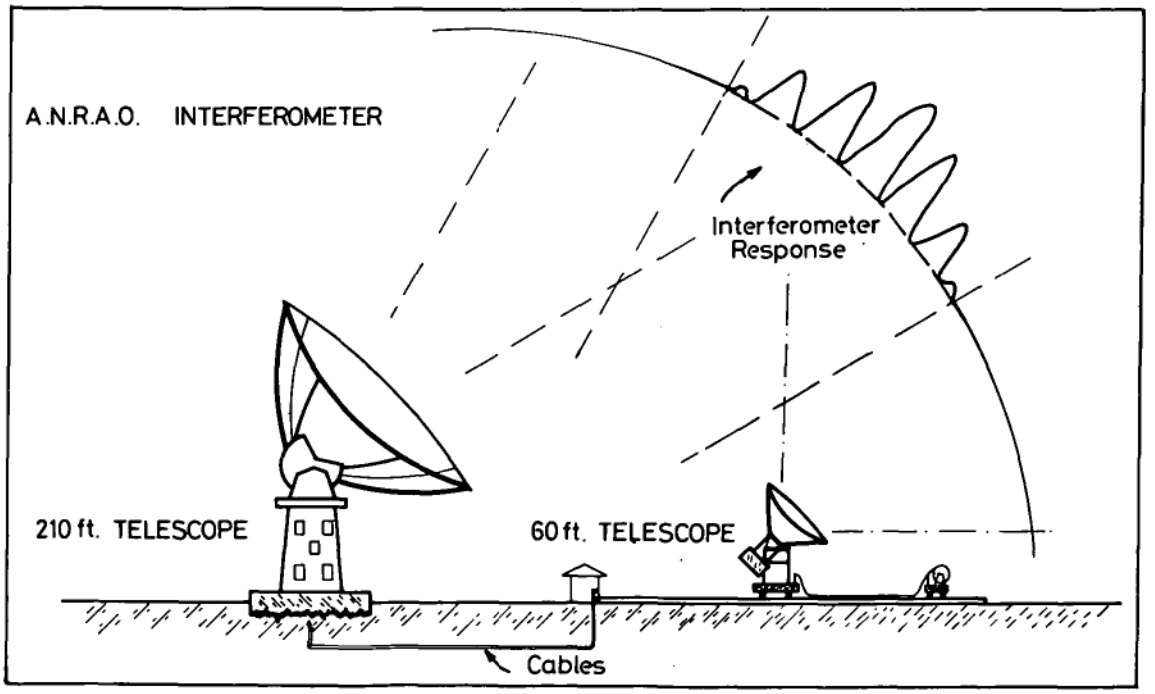
A.N.R.A.O. INTERFEROMETER
Interferometer
Response
210 ft. TELESCOPE
60 ft. TELESCOPE
Cables

Cable Compensation and the Computer.

A switched or multiplying interferometer uses the principle of phase coherence between two observing stations. The path length travelled by the signals from the two observing stations must therefore be kept almost equal. The path difference of the signals from the foci of the two Parkes telescopes is given by:

$$\Delta l = d \cos(Az-b) \sin(Zn) - \Delta h \cos(Zn) + \Delta r \quad ....(2).$$

[Cole, D.J. - private communication; Ekers, 1969]

where: d = separation of the two telescopes

Az = azimuth angle of the telescope position,

Zn = zenith angle of the telescope position,

b = azimuth of the baseline direction,

Δh = difference in height of the two telescope pivot points (equation 1)

and: Δr = 47.3 ft. = difference in focal length of the two telescopes.

The path difference is calculated by an analogue computer which also inserts cable to compensate for the variable path length component of equation (2) as the telescopes move. The cable is switched in steps of 2.5 feet from one i.f. channel (eg. from the 210 ft. telescope receiver) to the other

(from the 60 ft. telescope receiver) [Ekers, 1969]. This method of cable switching keeps the level of the product output from the multiplier of the interferometer constant.

The effective projected baseline, d', of the interferometer is:

$$d' = [d^2+\Delta h^2) - [d \cos(Az-b) \sin(Zn) - \Delta h \cos(Zn)]^2]^{\frac{1}{2}} \quad ...(3)$$

[Ekers, 1967]

Here all the symbols have been defined already.

D. Confusion Errors in Source Measurements with the Parkes Interferometer.

Moffet (1962) has discussed the relations which define the fringe pattern of a two-element (equal antenna) interferometer system. Here we outline the method of applying Moffet's results to the Parkes interferometer which consists of two unequal telescopes.

If the response pattern of a radio telescope is (circular) Gaussian then the observed flux density, S, of a radio source of true flux density, S_0 is:

$$S = S_0 \exp\left[\frac{-\theta^2}{K\emptyset^2}\right] \quad ...(4)$$

where: $\emptyset$ is the beamwidth of the telescope, k is a constant and where the telescope is pointed at an angle θ to the direction of the radio source. For small displacements from the true position of the source, equation (4) can be expressed

in terms of Cartesian coordinates (x,y) on the celestial sphere:

$$R(x,y) = A \exp \left[\frac{-(x^2+y^2)}{k^* \phi^2} \right] \qquad \ldots.(5)$$

where A depends on the collecting area of the telescope, k^* is a constant, and R(x,y) is the telescope response on the celestial sphere. Moffet derived the relations describing the response of an interferometer which consisted of two *equal* antennas. If the telescopes differ (collecting areas: A_1, A_2 and beamwidths: ϕ_1, ϕ_2 respectively) then Moffet's relations can still be used provided the interferometer is assumed to consist of two *equivalent* telescopes having collecting area $[A_1 \times A_2]^{\frac{1}{2}}$ and beamwidth:

$$\left[\frac{2}{[\frac{1}{\phi_1^2} + \frac{1}{\phi_2^2}]} \right]^{\frac{1}{2}} \qquad \ldots.(6).$$

For example, the half-power beamwidth of the 60 ft. Parkes telescope at 132 MHz is 8.8 degrees, and for the 210 ft. telescope the beamwidth is 2.5 degrees. The beamwidth of the *equivalent* telescopes at 132 MHz would be 3.4 degrees.

If there is more than one source in the beam of the 210 ft. telescope, interferometer observations at Parkes may be affected by confusion. The confusion error was calculated for each interferometer scan made at Parkes as follows:-

step (1): The Parkes Catalogue of sources [S32-table 1, appendix 2] was used to locate sources within 8 degrees of the position of the source measured at Parkes.

step (2): The flux density of each of these confusing sources was determined (at the observing frequency) from the data available in the catalogues listed in table 1, appendix 2. The calculation of the confusion error relies on having good estimates of these flux densities. Thus the results of the interferometer measurements of a particular source were given in chapter 3(table 3.8) provided the *background radiation* due to confusing sources was small (and known accurately) in relation to the intensity of the required source. The intensity of the *background* due to confusing sources was found by simulating the actual interferometer source scan made at Parkes as follows:-

step (3): The aerial response pattern of a two-element interferometer when the telescopes are stationary is given by:

$$F(x,y,t) = G_1G_2\ [A_1(x,y)\ A_2(x,y)]^{\frac{1}{2}}\ S_i\ \cos\{2\pi[s_x(x-\Omega t)+s_yY]+\psi\}$$

Moffet (1962) ....(8).

where:

there is a source, i, of flux density S_i in the interferometer response;

x,y, are coordinates of the Celestial sphere (hour angle and declination);

Ω is the sidereal rate; t is the sidereal time;

$s_x = \frac{d'}{\lambda} \sin(p)$; $s_Y = \frac{d'}{\lambda} \cos(p)$;

λ is the observing wavelength;

d' is the effective projected baseline separation of the two telescopes (see equation 3);

p is the position angle of resolution (given below);

ψ is a phase constant;

and: G_1, $A_1(x,y)$ and G_2, $A_2(x,y)$ represent the gain and collecting areas of the two telescopes.

Each of the telescopes at Parkes has a Gaussian response at the frequencies we are interested in and hence:

$$[A_1(x,y)\ A_2(x,y)] = (a_1 a_2)^{\frac{1}{2}} \exp\left[-\tfrac{1}{2}(x^2+y^2)\left\{ \frac{1}{\phi_1^2} + \frac{1}{\phi_2^2} \right\} \right]$$

(from equation 6) ....(9)

where:

a_1, a_2 are the collecting areas of the two telescopes

and:

ϕ_1, ϕ_2 are the beamwidths at wavelength, λ.

If there is more than one source in the fringe pattern of the interferometer, the effect of these sources is found by summing equation 8 over different values of i. The effective baseline, d', and the position angle, p, of a certain source can be

determined from the azimuth and the zenith coordinates of that source with respect to the interferometer. The values of the azimuth and zenith can in turn be determined (at the time of observation) from the position data given in the Parkes Catalogue. At time, t we have:

$$\tan(p) = \frac{AA}{BB} \qquad \ldots.(10)$$

where:

$$AA = \sin(Az)\cos(HA) - \cos(Az)\sin(\emptyset)\sin(HA)$$

$$BB = \sin(Az)\sin(Dec)\sin(HA) + \cos(Az)[\cos(\emptyset)\cos(Dec) + \sin(\emptyset)\sin(Dec)\cos(HA)]$$

and: Az = azimuth of the baseline of the interferometer measured from north through east;

$\emptyset$ = geographic latitude of the interferometer;

HA = hour angle of the source (positive after transit);

Dec. = source declination

and d' is found from equation (3).

[Moffet, 1962].

The equations 1 to 10 above were used to plot theoretical source scans consistent with the actual scans undertaken at the Parkes observatory. The possible confusion error in the flux density measurement of a source was then obtained by comparing the computed scans with the actual observations. The calculations and plotting of the scans was undertaken in an Elliott 503 digital computer. Figures 7 and 8 show sample scans calculated for six sources. Sources in figure 8 are confused.

(facing pages 225, 226)

Figures 7,8

Theoretically calculated source scans consistent with actual scans undertaken with the low frequency Parkes interferometer.

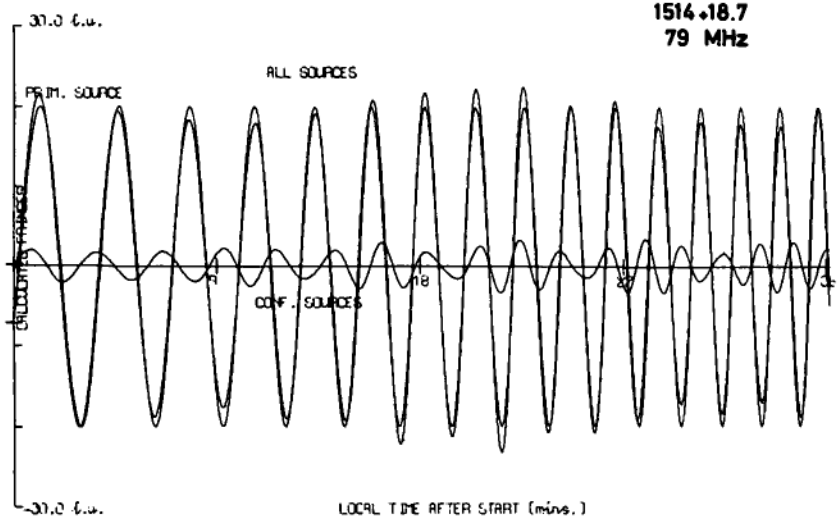
1514+18.7
79 MHz
30.0 f.u.
ALL SOURCES
PRIM. SOURCE
CONF. SOURCES
-30.0 f.u.
LOCAL TIME AFTER START (mins.)

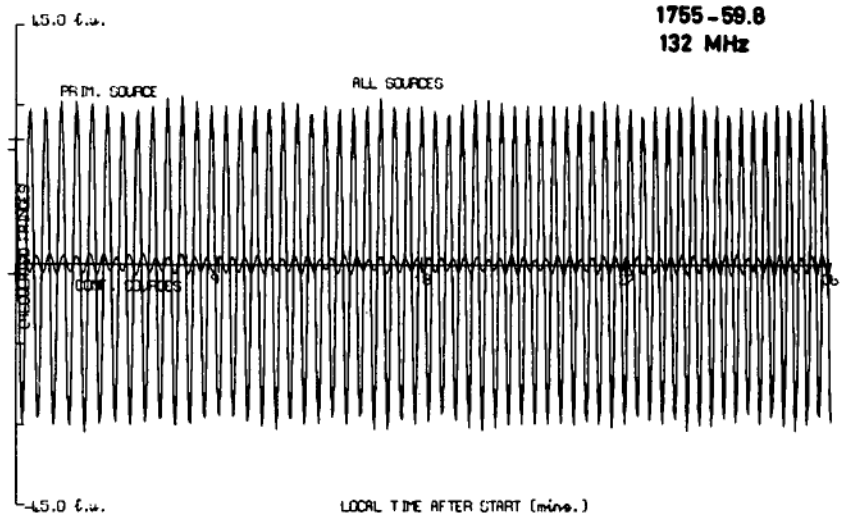
1755-59.8
132 MHz
45.0 f.u.
PRIM. SOURCE
ALL SOURCES
CONF. SOURCES
-45.0 f.u.
LOCAL TIME AFTER START (mins.)

FIGURE 7.

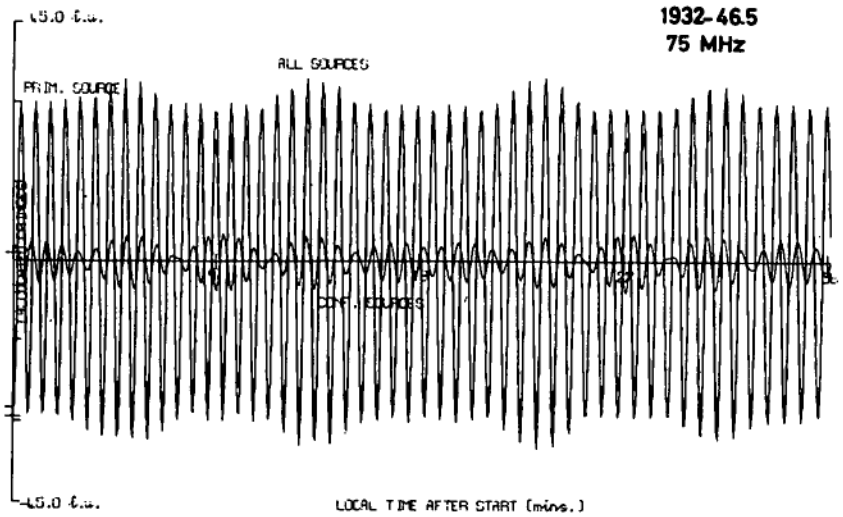
1932-46.5
75 MHz
45.0 f.u.
ALL SOURCES
PRIM. SOURCE
CONF. SOURCES
-45.0 f.u.
LOCAL TIME AFTER START (mins.)

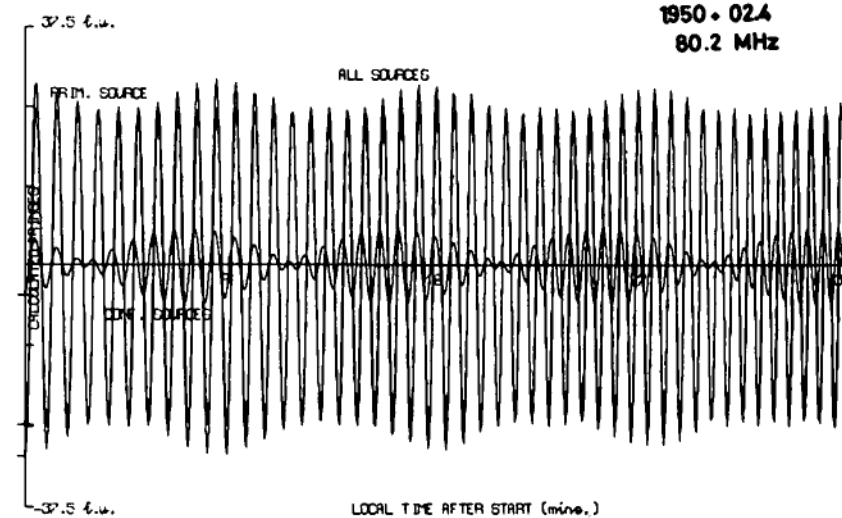
1950+02.4
80.2 MHz
37.5 f.u.
ALL SOURCES
PRIM. SOURCE
CONF. SOURCES
-37.5 f.u.
LOCAL TIME AFTER START (mins.)

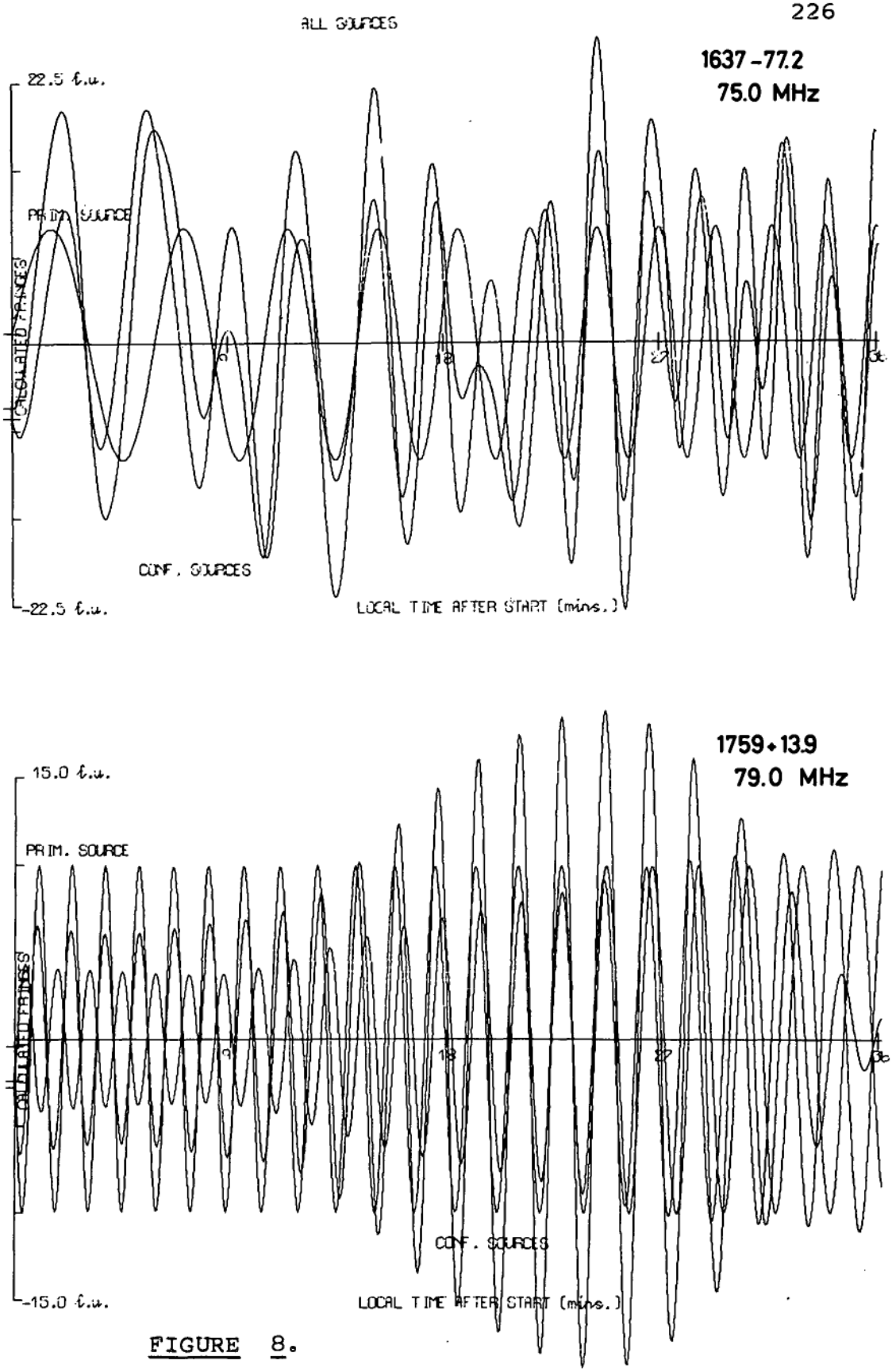
ALL SOURCES
1637-77.2
75.0 MHz
22.5 f.u.
PRIM. SOURCE
CALCULATED FRINGES
CONF. SOURCES
-22.5 f.u.
LOCAL TIME AFTER START (mins.)
1759+13.9
79.0 MHz
15.0 f.u.
PRIM. SOURCE
CALCULATED FRINGES
CONF. SOURCES
-15.0 f.u.
LOCAL TIME AFTER START (mins.)

FIGURE 8.

APPENDIX 4.

Curve Fitting.

A major part of the analysis in section 3 of this thesis involves fitting theoretical models to the observed spectral data of discrete radio sources and hence, for reference, we include in this appendix the curve fitting programme developed by the author. Various minimization processes that have been published were comprehensively tested to find one suitable for minimizing the function, F^* (equation 5.7), for any of the models described by equations (5.1 to 5.6). The best method available [see Fletcher and Powell (1965)] had to be extensively modified since truncation errors in the floating-point arithmetic used in the computer [Elliott 503] made the original algorithm by Fletcher and Powell numerically unstable.

The curve fitting programme (in its basic form) is given below in Elliott 503 Algol.

```
THEORETICAL SPECTRAL FITTING;
begin integer count,NOCOUNT,type,loops,Iterations,repeat,mmm,
      set,shift,lcount,insynch,specfitno,limit,M,n,i,j,k,t,
        variables,K;
real eps,f1,f2,ASTAR,aa,bb,x1real,w, f,Y, Z,ALPHA,AA, spare;
integer array A[1:50];
switch ssw:=REPEAT,LAST;
boolean conv, START, synch,ONCE;
real array x,g,X,G[1:15];

comment This programme determines,for a given source model,
  the best theoretical spectral curve that can be fitted to
  the observed spectrum of the source. The curve is fitted
  by minimising the function:
```

$$F = \sum_{i=0}^{M} [\ S_1(\nu_i) - S(\nu_i)\ ]^2$$

where: $S(\nu_i)$ is the observed source flux density at frequency, : $S_1(\nu_i)$ is the flux density predicted from the source model at frequency, ν_i : M is the number of measurements of the flux density available.

The minimisation process is based on the method discussed by Fletcher and Powell(1965). However, we have modified their published algorith to find the minimum of the function,F, such that the variables of the model are constrained to physically meaningful values.

The variables of the source model are held in the array x[i] throughout and the experimental data is held in the two arrays freq[0:M], flux[0:M];

```
procedure LINFIT(N,x,y,a0,a1); value N; integer N;
  real a0,a1;     real array x,y;
comment The procedure fits a straight line of the form
     y= a1*x +a0 to the data stored in x,y[0:N];
   begin real n,xi,yi,sx,sy,sxx,sxy; integer i;
         n:=N+1.0; sx:=sy:=sxx:=sxy:=0.0;
         for i:=0 step 1 until N do
            begin xi:=x[i]; yi:=y[i];  sx:=sx+xi;  sy:=sy+yi;
                  sxx:=sxx+xi*xi;  sxy:=sxy+xi*yi
            end;
         a1:=(n*sxy-sx*sy)/(n*sxx-sx*sx);  a0:=(sy-a1*sx)/n
   end LINFIT;
```

```
      procedure SYNCH(observ,freq,flux,A,alpha); value observ;
      integer observ; real A,alpha; real array freq,flux;
      comment This procedure fits a power-law spectrum of
        the form S_ν = A ν^α to the source spectral data
          stored in the arrays freq,flux[0:observ];
        begin integer i;   real factor;
              real array Lfreq,Lflux[0:observ];
              factor:= 1.00/0.434294482;
              for i:=0 step 1 until observ do
               begin Lfreq[i]:=ln(freq[i])+6.00*factor;
                     Lflux[i]:=ln(flux[i])-26.00*factor;
                end;
             LINFIT(observ,Lfreq,Lflux,A,alpha);  A:= exp(A);
        end SYNCH;

      sameline;    leadzero($?); scaled(9);   digits(3);
      ONCE:= true;    NOCOUNT:= 0; repeat:= 1;   count:= 20;
      Iterations:= 3;   eps:= 1.0_10-6;
      comment eps is an exit parameter from the minimising
        procedure: it specifies  to what accuracy the minimum of
        the function is required;

      read  insynch;
      comment  if repeat = 1 then repeat program to compute a new
                 theoretical spectrum;
      synch:= if insynch = 1 then true else false;
      comment if synch is true then a power-law spectrum is fitted
         to part of the observed source spectrum;

      read n;    comment n is the number of unknowns  in the model;
      constraints:= 2*n;
      comment Number of constraints on the variables = 2 x n;

REPEAT: read M;
      if M<0 then goto LAST;
      top of form;
      if synch then read specfitno;
      comment Number of spectral data points to which the
        power-law spectrum is to be fitted;

      mmm:=1;   print $$1t4??;  instring[A,mmm];
      mmm:=1;  outstring[A,mmm];

       begin real array  freq,flux[0:M], fitfreq,fitflux[0:specfitno];
             integer array NEXT[0:n];   switch sw:= BACK;
```

```
integer procedure nexti;
  comment This procedure keeps track of the parameters
    of the model that are being treated as variables
    in this particular minimisation. Note that this
    programme allows us to minimise with respect to
    only some of the n variables at any one time;
      begin t:= if t> variables then 0 else t+1;
            nexti:= NEXT[t];
       end nexti;

real procedure Mfunc( n,M,freq,flux,x,g);
    value n,M; integer n,M; real array freq,flux,x,g;
comment The value of the function,F, is computed
 at the point x[1:n] and the procedure itself
 takes the value of F. The partial derivatives:

      g[i] = ∂Mfunc
             ∂x[i]

 are also computed during the call of this
 procedure. As an example form for this procedure
 we give below the calculations required for fitting the
 theoretical spectrum defined by a self-absorption model
 (equation 5.4) to the observational spectrum. Note that
 the number of variables in this model is 3, (namely.... A,
    α , ν1 );
  begin real xalpha, xAtheta2, xfo, q, a,b,c,d, v1,
    Z, logf,t, u, v2,p,w,z,f;
    integer i,j;  switch sss:= selfabsorb;
    goto selfabsorb;
selfabsorb: xalpha:= x[1]; xAtheta2:= x[2]; xfo:= x[3];
    q:= xalpha-2.5;  a:= b:= c:= d:= 0.0;
    for i:= 0 step 1 until M do
       begin v1:= 1.0₁₀6*freq[i]; Z:= 1.0₁₀-26*flux[i];
             comment freq[i], flux[i] are in MHz and flux
                 units respectively;
             logf:= ln(v1);  t:= logf-xfo; u:= t*q;
             v2:= exp(u);  p:= exp(-v2);  w:= 1-p;
             z:= xAtheta2+2.5*logf + ln(w) - ln(Z);
             a:= a + z*z;  z:= 2.0*z;  w:= 1.0/w;
             v1:= v2*p*w;  b:= b+ z*t*v1;
             c:= c+z;    d:= d- z*q*v1
        end;
  f:= Mfunc:= a;  g[1]:= b;  g[2]:= c;  g[3]:= d;
end Mfunc;
```

```
        procedure output(f); value f; real f;
         comment This procedure outputs the results of the
                      minimization process;
           begin integer k;   print $$12??,scaled(9),f,$ ?;
                 for k:= 1 step 1 until n do
                    print  leadzero($?), scaled(6),x[k];
                 if conv then print $   true ? else print $ false?;
                 comment conv true or false indicates  whether
                     or not a minimum has been located;
                 for k:= nexti while k>0 do
                    print $ ?,leadzero($ ?), digits(1),k;
                 comment Prints out which of the n unknowns
                   of the model are being treated as variables
                        in the minimization;
                 print $     ?,digits(3),leadzero($ ?),limit;
                 comment  Prints the number of iterative loops needed
                    within the minimizing procedure to achieve
                        the minimum;
           end output;

       real procedure CONSTRAINT(K,X,G); value K; integer K; array X,G;
       comment This procedure  specifies the constraints placed
         on the  variables of the model. As an example form for
         this procedure we give below the constraint equations
         used to fit the self-absorption model to the data;
          begin real FF;  switch CON:= C1,C2,C3,C4,C5,C6,EXIT;
                comment Number of constraints = 6;
               goto CON[K];
C1:            FF:= -X[1]+0.60;   G[1]:= -1;     goto EXIT;
C2:            FF:=3.0+X[1];      G[2]:= 1;      goto EXIT;
               comment 3.0>-X[1]>-0.6;
C3:            FF:= 21.484-X[3];     G[3]:= -1;    goto EXIT;
C4:            FF:= X[3]-13.81;      G[4]:= +1;    goto EXIT;
               comment  21.484>X[3]>13.81;
C5:            FF:= -X[2]+4.0;       G[5]:= -1;    goto EXIT;
C6:            FF:= X[2] + 113.2;    G[6]:= +1;    goto EXIT;
               comment  4.0>X[2]>-113.2;
 EXIT:        CONSTRAINT:= FF
       end CONSTRAINT;
```

```
real procedure MINIMUM(Mfunc,x,g,n,totalv,nexti,eps,
        loops,conv,CONSTRAINT,X,Gdash,K,constraints);
value n,eps,totalv,constraints;  real  eps,CONSTRAINT,Mfunc;
integer n,K,loops,totalv,nexti,constraints;
real array x,g,X,Gdash;  boolean conv;
comment This procedure finds a local minimum of the function,
 Mfunc, with respect to the variables x[i].  The minimization
 process is based on the method discussed by Fletcher and Powell(1965)
  although their algorith has been modified so that the procedure
  locates a local minimum consistent with certain constraints on the
        variables x[i];
  begin real G,holdf,max step,f,fa,fb,oldf,ga,gb,step,Gdash s,GGdash,
         ss,sg,test eps,ghg;
        integer C number,inlim,count,i,j,k,temp;
       real array s,holdx,sigma,gamma[1:totalv],H[1:((totalv*(totalv+1))div
                                                        2)];
        boolean restricted,moved,found,update H;
        switch SSS:=try this one, change s, new H, new s,more, hop,
              test, exit, downhill, finish;

        real procedure dot(a,b);  array a,b;
         begin integer i;  real s;
               s:=0.0;
               for i:=nexti while i>0 do s:=s+a[i]*b[i];
               dot:=s
         end dot product of a and b;

        integer procedure subscr(i,j);  value i,j;  integer i,j;
         begin   integer temp;
                 if i-j>0 then begin temp:= i;   i:= j; j:= temp  end;
                 i:= i-1;  j:= j- ((i-1)*i)div 2;
                 subcr  := j:= j+((totalv-1)*i);
           end subscr;

        real procedure up dot H(b,i);  value i;  integer i;  array b;
          begin integer j;  real s;
               s:=0.0;
               for j:=nexti while j>0 do s:=s + b[j]*H[subscr(i,j)];
              up dot H:=s
           end up dot H;

        procedure test constraints along s;
         begin real p,q;  integer i;
               switch SS:=next test,exit,try again,loop,there;
```

```
            real procedure value at(p);  value p;  real p;
               begin for i:=nexti while i>0 do  X[i]:=x[i] + p*s[i];
                     value at:=CONSTRAINT
               end getting value at p;

            restricted:=false;
            for K:=1 step 1 until constraints do
               begin if value at(1.0)>0.0 then goto next test;
                     if value at(0.0)<0.0 then
                       print $$12?OVER THE WALL OF CONSTRAINT NO?,
                         digits(12),leadzero($?),K,$ WITH VALUE?,
                         special(2),scaled(8),value at(0.0),stop;
   try again:        q:=p:=0.5;
                     for q:=q/2.0 while abs(q)>10-7 do
                       p:=p + (if value at(p)>0.0 then q else -q);
                     if p<5.010-6 then
                     begin if dot(s,s)<test eps then
                             begin p:=0.0;  goto there  end;

                           step:=step/4.0;  max step:=1.1;
                           for i:=nexti while i>0 do s[i]:=s[i]*5.010-6;
                           goto try again
                     end;
   loop:             if value at(p)<0.0 then
                      begin p:=p*(1.0-2.010-7);  goto loop  end;
   there:            if not restricted then
                      begin restricted:=true; C number:=K;  max step:=p
                       end
                     else if max step>p then
                      begin max step:=p;  C number:=K  end;
                    if max step=0.0 then goto exit;
   next test:  end;
   exit: end testing constraints along s;

   procedure search along s;
    begin real w,z,lambda;  integer i;
          switch SSS:=interp,extrap,exit;
          moved:=false;  fb:=f;  gb:=dot(g,s);
          if abs(gb)<10-30 then begin found:=true;  goto exit  end;
          if gb>0.0 then
            begin for i:=nexti while i>0 do s[i]:=-s[i];
                  gb:=-gb
               end reversing direction of s;

extrap:   test constraints along s;
          if restricted then
           begin if max step=0.0 then
                  begin found:=false; goto exit  end;
```

```
                for i:=nexti while i>0 do s[i]:=s[i]*max step
            end;
          fa:=fb;  ga:=gb;
          for i:=nexti while i>0 do
            begin z:=x[i];  ss:=z+s[i];
                  if z≠ss then begin moved:=true; x[i]:=ss  end
             end;
          fb:= Mfunc;  gb:=dot(g,s);
          if gb<0.0 and fb<fa then
            begin if restricted then
                    begin found:=false;  f:=fb;  goto exit  end;
                  for i:=nexti while i>0 do s[i]:=s[i]*4.0;
                  step:=step*4.0;  goto extrapolate
              end;

interp: z:=3.0*(fa-fb)+ga+gb;  w:=sqrt(z*z-ga*gb);
           lambda:=(gb+w-z)/(gb-ga+w+w);
         for i:=nexti while i>0 do X[i]:=x[i] - lambda*s[i];
         for K:=1 step 1 until constraints do
             if CONSTRAINT<0.0 then
               begin found:=false;
                     if fb>fa then for i:=nexti while i>0 do x[i]:=x[i]-s[i];
                 f:= Mfunc;  goto exit
             end;

         for i:=nexti while i>0 do x[i]:=x[i]-lambda*s[i];
         f:= Mfunc;
        if f≠fa and f≠fb and (f>fa or f>fb) then
          begin step:=step/4.0;
                if fb<fa then
                 begin for i:=nexti while i>0 do
                           x[i]:=x[i]+lambda*s[i];
                       f:=fb
                  end
                else  begin gb:=dot(g,s);
                            if gb<0.0 and step<10-6 then
                              begin found:=false;  goto exit  end;
                            fb:=f;  lambda:=abs(1.0-lambda);
                            for i:=nexti while i>0 do s[i]:=s[i]*lambda;
                            goto interpolate
                      end
            end;
        found:=true;
exit: end searching for minimum along s;

 conv:=true;  inlim:=loops;  step:=0.3819660112500;
  test eps:=eps*eps;
  for i:=1 step 1 until totalv do
  for j:=i step 1 until totalv do
    H[subscr(i,j)]:=if i=j then 1.0 else 0.0;
```

```
  f:= Mfunc;

  for count:=1, count+1 while oldf>f do
    begin oldf:=holdf:=f;  update H:=true;
downhill: for i:=1 step 1 until totalv do
            begin sigma[i]:=holdx[i]:=x[i];  gamma[i]:=g[i];
                  s[i]:= -up dot H(g,i)*step
             end;

try this one: search along s;
          if found then goto (if moved then new s else finish)
            else if moved then goto new H;
 change s:   update H:=false;
          for i:=nexti while i>0 do X[i]:=x[i];
          K:=C number;  G:=CONSTRAINT;
          Gdash s:=dot(Gdash,s); GGdash:=dot(Gdash,Gdash);
          for i:=nexti while i>0 do s[i]:=Gdash s*Gdash[i] - GGdash*s[i];
          search along s;
          if found then goto (if moved then new s else finish)
            else if moved then goto new H;
          for i:=nexti while i>0 do X[i]:=x[i];
          K:=C number;  G:=CONSTRAINT;
          for i:=nexti while i>0 do s[i]:=Gdash[i];
          if dot(Gdash,g)<0.0 then goto try this one;
          test constraints along s;
          if restricted then
            begin if max step=0.0 then
                    goto finish;  max step:=max step*0.5
             end
          else max step:=if step>1.0 then 1.0 else step;

           if holdf<f then
              begin for i:=1 step 1 until totalv do x[i]:=holdx[i];
                    f:= Mfunc;  goto test
               end;
          for i:=1 step 1 until totalv do holdx[i]:=x[i];  holdf:=f;
          for i:=nexti while i>0 do x[i]:=x[i]+max step*Gdash[i];
 new H:   update H:=false;
          for i:=1 step 1 until totalv do
          for j:=i step 1 until totalv do H[subscr(i,j)]:=if i=j then
                step else 0.0;
          goto downhill;
  new s:   update H:=true;
  test:    for i:=nexti while i>0 do
            begin sigma[i]:=x[i]-sigma[i];
                  gamma[i]:=g[i]-gamma[i]
             end;
```

```
          if count>n then
            begin if dot(s,s)<test eps and dot(sigma,sigma)<test eps
                  then goto finish
              end;
          if update H then
            begin for i:=1 step 1 until totalv do
                    s[i]:=up dot H(gamma,i);
                  ghg:=dot(s,gamma);  sg:=dot(sigma,gamma);
                  if abs(sg)>10-50 and abs(ghg)>10-50 then
                  begin goto hop;
      more:             temp:=0;
                        for temp:=temp while temp≠i do temp:=nexti;
      hop:              i:=nexti;
                        if i>0 then
                         begin for j:=i, nexti while j>0 do
                                 begin k:=subscr(i,j);
                                       H[k]:=H[k]+sigma[i]*sigma[j]/sg-
                                         s[i]*s[j]/ghg
                                 end;
                               goto more
                          end
                  end
              end;
           if count>inlim then goto exit
          end of iteration loop;

         goto finish;
exit:    conv:=false;
finish:  loops:=count;  MINIMUM:= Mfunc
       end MINIMUM with linear search;

    for i:=0 step 1until M do read freq[i],flux[i;
    comment input spectral data of a source;

    if synch then
      begin for i:=0 step 1 until specfitno do read fitfreq[i];
            comment Input frequencies on the spectrum  to
             which a power-law spectrum is to be fitted;
            for j:= 0 step 1 until specfitno do
              for i:= 0 step 1 until M do
                begin if abs( fitfreq[j]-freq[i])<0.0001 then
                        begin fitflux[j]:=flux[i];  i:=M  end
                  end;
          SYNCH(specfitno,fitfreq,fitflux,AA,ALPHA);
          print $$1?POWER-LAW SPECTRUM FITTED TO THE SOURCE SPECTRUM?,
              $$1? alpha=?,  aligned(1,5),alpha, scaled(6), AA;
      end synch call;
```

```
        for i:= 1 step 1 until n do read x[i];
        comment Set up the initial values of the parameters of the
           model prior to minimization.  For the self-absorption model
           x[1] and x[2] can be initialized to alpha and AA respectively;
        for i:= 1 step 1 until n do X[i]:= x[i];
BACK:   variables:=0;  NEXT[0]:=-1;  read t;
        for i:=0 while t>0 do
          begin variables:=variables+1;  NEXT[variables]:=t;
                read t
          end;
      t:= 0;    limit:= count;
      comment Have now read in which of the parameters of the model
          are to be treated as variables in the minimization;

      for i:=1 step 1 until Iterations do
        f:=MINIMUM(Mfunc(n,M,freq,flux,x g),x,g,variables,n,nexti,
             eps,limit,conv,CONSTRAINT(K,X,G),X,G,K,constraints);

      output(Mfunc(n,M,freq,flux,x,g));
      if ng(10) then begin print $$1?PROGRAM TERMINATED?,punch(3),
                             $$1?PROGRAM TERMINATED?;
                           goto LAST
                     end;
      read shift;
      if shift>0 then
           begin top of form;
                 print $$1?CHANGE VARIABLES:?;
                 goto BACK
             end;
         if repeat=1 then goto REPEAT;
        end inner block;
    LAST:  print punch(3),$$12?Thank you?;
    end of program;
     h
```

APPENDIX 5

Angular Diameters of Radio Sources

In a world model universe, the interval ds between two events in the four dimensional continuum is defined by the space-time Robertson-Walker metric:

$$ds^2 = dt^2 - \frac{R^2(t)}{c^2}\left[\frac{dr^2 + r^2(d\theta^2+\sin^2\theta\, d\emptyset^2)}{(1 + \frac{1}{4}kr^2)^2}\right] \quad ..1.$$

where $(r,\theta,\emptyset)$ are three dimensional co-moving radial coordinates; c is the velocity of light; t the universal time; R the radius of curvature of space; and k is the curvature index with values +1, 0 or -1 depending on whether the universe is *closed, flat* or *open.* McVittie (1965) introduces the relations:

$$w = \int \frac{dr}{1+\frac{1}{4}kr^2} \qquad T_k(w) = \frac{r}{1+\frac{1}{4}kr^2} \quad ..2.$$

to obtain a solution of equation (1). From relation (2), for the three types of universes specified by k we have:

$$T_k(w) = \sin(w),\ w,\ \sinh(w) \text{ for } k = +1,\ 0,\ -1 \text{ respectively.} \quad ..3.$$

When ds = 0 [null-geodesic], the light path in the universe is specified by:

$$\frac{dr}{dt} = \frac{-c}{R(t)}\left[1 + \frac{1}{4}kr^2\right] \quad ..4.$$

where R is the radius of curvature of space.

Then, using the Einstein field relations, the metric (1) can be solved to give a general relation describing the universe:

$$w = \frac{c}{R_o H_o} \int_1^y \frac{dy}{y\,[f(y)]^{\frac{1}{2}}} \qquad \ldots 5.$$

where the subscript zero denotes the value of the quantity at the present epoch and where:

$$z = \frac{d\lambda}{\lambda_o} = \frac{R(t_o)}{R(t)} - 1 = \text{optical red shift.}$$

$$y = (1+z)^{-1} = \frac{R}{R_o} \qquad \ldots 6.$$

$$f(y) = \frac{2\sigma_o}{y} + (q_o + 1 - 3\sigma_o) + (\sigma_o - q_o)y^2 \qquad \ldots 7.$$

$$H_o = \frac{\dot{R}_o}{R_o} = \text{Hubble expansion parameter}$$

$$q_o = \frac{-\ddot{R}_o}{R_o H_o^2} = \text{deceleration parameter}$$

$$\sigma_o = \frac{4\pi G\,\zeta_o}{3\,H_o^2} = \text{density parameter of the universe}$$

and: ζ_o is the mean density of matter in the universe and

G is the universal gravitation constant

[Sandage, 1961; McVittie, 1965]

Using the results from work by Sandage (1961) we find that the observed diameter of a source is given by:

$$\theta = L/R\ T_k(w) = \frac{L(1+z)}{R_o[T_k(w)]} \qquad \ldots 8.$$

(from equations 6,7)

where L is the linear diameter of the source.

The luminosity distance, D, to a source has also been given by McVittie (1965) as:

$$D = \frac{R_o^2 \, r}{R[1+\frac{1}{4}kr^2]}$$

and hence by substitution with the above relations this becomes

$$D = \frac{R_o^2}{R} \; T_k(w) = \frac{R_o}{y} \; T_k(w) \qquad \ldots 9.$$

From equations (8,9)we obtain the important relation

$$\theta = \frac{L}{D} (1 + z)^2 \qquad \ldots 10.$$

Equation (10) is a general relation for all world-model universes.

Steady State-Euclidean Universe. [q_o=-1, σ_o = 0, k = 0]
(de Sitter model)

Substitution of the values particular to this model into relation (8) shows that in a steady state universe:

$$\theta = \frac{L \, H_o}{c \, z} \; [1 + z] \qquad \ldots 11.$$

and the angular size of a source tends towards an asymptotic limit of $\frac{L \, H_o}{c}$ as the redshift approaches infinity.

Evolving $q_o \geq 0$: Relativistic Universes.

In a relativistic expanding universe, the angular size of the source is given by: [Sandage, 1961]

$$\theta = \frac{\text{constant x } (1+z)^2}{A} \qquad \ldots 12.$$

where A is a function of the red shift, z. It follows, for example [from equation (12)], that for $q_o = +1$,

$$\theta = \frac{L\, H_o\, [1 + z]^2}{c\, z} \qquad \ldots 13.$$

and in general it can be shown [eg. McVittie, 1965; Sandage, 1961] that for explosive cosmologies, θ will approach a minimum value at redshifts of the order of unity and increases as z is further increased.

Where appropriate these relations are referred to in the body of chapter 5.

BIBLIOGRAPHY.

Baldwin, J.E. (1955). - Mon.Not.R.astr.Soc.115, 684.

Bash, F.N. (1968). - Astrophys.J.Suppl. Ser. No. 16 (149), 373.

Bingham, R.G. (1967) - Mon.Not.R.astr.Soc. 137 (2), 157.

Blum, E.J. (1959) - Ann.d'Ast. 22, 140.

Braude, S.Ya, Lebedeva, O.M., Megn, A.V., Ryabov, B.P. and Zhouck, I.N.(1969 a) - Mon.Not.R.astr.Soc. 143, 289.

Braude, S.Ya., Lebedeva, O.M., Megn, A.V., Ryabov, B.P. and Zhouck, I.N.(1969 b) - Mon.Not.R.astr.Soc. 143, 301.

Bridle, A.H. (1967). - Observatory, 87, 263.

Broten, N.W.,Clarke, R.W., Legg, T.H. et.al. (1967). - Nature, 216, 44.

Burbidge, E.M. (1967 a). - Ann.Rev.Astron.Astrophys. 5, 399.

Burbidge, E.M. (1967 b). - Astrophys. J. 149, L51.

Clark, B.G., Kellermann, K.I., Bare, C.C., Cohen, M.H., and Jauncey, D.L. (1968 a) - Astrophys.J. 153, 705.

Clark, B.G., Kellermann, K.I., Bare, C.C., Cohen, M.H., and Jauncey, D.L. (1968 b) - Astrophys.J. (Letters), 153, L67.

Cohen, M.H. and Gundermann, E.J. (1967) - Astrophys.J. 148, L49.

Cohen, M.H. et al. (1967) - Astrophys. J. 150, 767.

Conway, R.G., Kellermann, K.I. and Long, R.J. (1963) - Mon.Not. R.astr.Soc. 125, 261.

Davies, R.D. (1964) - Mon.Not.R.astr.Soc. 128, 173.

Dent, W.A. and Haddock, F.T. (1966) - Astrophys, J. 144 (2), 568.

Doherty, L.H., Macleod, J.M. and Purton, C.R. (1968) - Bull. Radio Elect.Engng. Div. NRC Canada, 18 (3), 43.

Ekers, R.D. (1967) - "The Structure of Southern Radio Sources", Ph.D. Thesis, Australian National University, Canberra.

Ekers, R.D. (1969) - Aust.J.Phys. Astrophys. Suppl. No. 6, 3.

Ellis, G.R.A. (1960) - Proc.Inst.Radio Engrs. 48, 1650.

Ellis, G.R.A. (1963) - Aust.J.Phys. 16, 411.

Ellis, G.R.A. (1965) - Mon.Not.R.astr.Soc. 130, 429.

Ellis, G.R.A., Green, R.J. and Hamilton, P.A. (1963) - Aust.J. Phys. 16, 545.

Ellis, G.R.A. and Hamilton, P.A. (1966) - Astrophys.J. 143, 227.

Ellis, G.R.A. and Hamilton, P.A. (1966 a) - Astrophys.J.146, 78.

Findlay, J.W. (1966) - Ann.Rev.Astron.Astrophys. 4, 77.

Fletcher, R. and Powell, M.J.D. (1963) - The Computer Journal, 6, 163.

Fletcher, R. and Powell, M.J.D. (1965) - The Computer Journal, 7, 308.

Fomalont, E.B. (1968) - Astrophys. J. Suppl.Ser. 15, 203.

Gardner, F.F. and Davies, R.D. (1966) - Aust.J.Phys. 19, 441.

Gardner, F.F., Morris, D. and Whiteoak, J.B. (1969 a) - Aust. J.Phys. 22, 79.

Gardner, F.F. and Whiteoak, J.B. (1963) - Nature, 197, 1162.

Gardner, F.F. and Whiteoak, J.B. (1966) - Ann.Rev.Astron. Astrophys. 4, 245.

Gardner, F.F. and Whiteoak, J.B. (1969) - Aust.J.Phys. 22, 107.

Gardner, F.F., Whiteoak, J.B. and Morris, D. (1969 b) - Aust. J.Phys. 22, 821.

Ginzburg, V.L. (1957) - Uspekhi fiz. nauk. 62, 37.

Ginzburg, V.L. (1961) - Propagation of Electromagnetic Waves in a Plasma, New York.

Ginzburg, V.L. and Ozernoy, L.M. (1966) - Astrophys.J. 144 (2), 599.

Ginzburg, V.L. and Syrovatskii, S.I. (1964) - The Origin of Cosmic Rays, Oxford.

Ginzburg, V.L. and Syrovatskii, S.I. (1965) - Ann.Rev. Astron. Astrophys. 3, 297.

Hamilton, P.A. (1968) - Proc.Instn.Radio Elect.Engrs.Aust. 29, 56.

Hamilton, P.A. (1969) - "Low Frequency Radio Emissions from the Galaxy", Ph.D. Thesis, University of Tasmania.

Hamilton, P.A. and Haynes, R.F. (1968) - Aust.J.Phys. 21, 895.

Hamilton, P.A. and Haynes, R.F. (1969) - Aust.J.Phys. 22(6),839.

Haynes, R.F. (1966) - "High Resolution Ionospheric Sounding at 2.1 MHz", Honours Thesis, University of Tasmania.

Haynes, R.F. and Hamilton, P.A. (1968) - Aust.J.Phys. 21(1),87.

Hewish, A., Scott, P.F. and Wills, D. (1964) - Nature, 203, 1214.

Higgins, C.S. and Shain, C.A. (1954) - Aust.J.Phys. 7, 460.

Hornby, J.M. and Williams, P.J.S. (1966) - Mon.Not.R.astr.Soc. 131, 237.

Howard, W.E. and Maran, S.P. (1965) - Astrophys.J.Supp.No. 93 10, 1.

Hoyle, F. and Ellis, G.R.A. (1963) - Aust.J.Phys. 16, 1.

Jukes, J.D. (1967) - Nature, 216, 461.

Kardashev, N.S. (1962) - Soviet Astron, 6, 317.

Kellermann, K.I. (1964) - Astrophys. J. 140, 969.

Kellermann, K.I. (1964 a) - Astronom.J. 69 (2), 205.

Kellermann, K.I. (1966) - Astrophys. J. 146 (3), 621.

Kellermann, K.I. (1966 a) - Aust.J.Phys. 19, 577.

Kellermann, K.I. (1966 b) - Aust.J.Phys. 19, 195.

Kellermann, K.I. and Pauliny-Toth, I.I.K.(1968) - Ann.Rev. Astron.Astrophys., 6, 417.

Kellermann, K.I. and Pauliny-Toth, I.I.K. (1969) - Astrophys.J., 155, L71.

Komesaroff, M.M. (1966) - Aust.J.Phys. 19 (1), 75.

Kraus, J.D. (1966) - Radio Astronomy. New York.

Le Roux, E. (1961) - Ann.d'Astrophys. 24, 71.

Maltby, P. and Seielstad, G.A. (1966) - Astrophys.J.144, 216.

Mathewson, D.S., Broten, N.W. and Cole, D.J. (1965) - Aust. J.Phys. 18, 665.

McCray, R. (1966) - Science, 154, 1320.

McVittie, G.C. (1965) - General Relativity and Cosmology, London.

Medd, W.J., Locke, J.L., Andrew, B.H. and Van den Bergh, S. (1968), - Astronom.J. 73 (5 pt.1)293.

Miley, G.K., Rickett, B.J. and Gent, H. (1967) - Nature, 216, 974.

Milne, D.K. (1969) preprint - "Non-thermal Galactic Radio Sources" (in press)

Mills, B.Y. (1959) - Publ. Astron. Soc. Pac., 71, 267.

M.S.H. Catalogue [85.5 MHz]

Mills, B.Y., Slee, O.B. and Hill, E.R. Published in three parts:
(1958) - Aust.J.Phys., 11, 360
(1960) - Aust.J.Phys., 13, 676
(1961) - Aust.J.Phys., 14, 497

Moffet, A.T. (1962) - Astrophys.J.Suppl.No. 67, 93

Murdoch, H.S. and Large, M.I. (1968) - Mon.Not.R.astr.Soc. 141, (4), 377

Oda, M. and Hasegawa, H. (1962) - Phys. Letters (Neth.), 1 (6), 239

Oort, J.H. and Walraven, T. (1956) - Bull.Astr.Inst.Neth.,12, 285

Palmer, H.P. et al. (1967) - Nature, 213, 789

Parkes Catalogue of Radio Sources +20° to -90°: [408, 1410, 2650 MHz]

Bolton, J.G., Gardner, F.F. and Mackey, M.B. (1964) - Aust.J.Phys., 17, 340

Day, G.A., Shimmins, A.J., Ekers, R.D. and Cole, D.J. (1966) - Aust.J.Phys., 19, 35

Price, R.M. and Milne, D.K. (1965) - Aust.J.Phys., 18, 329

Shimmins, A.J., Day, G.A., Ekers, R.D. and Cole, D.J. (1966) - Aust.J.Phys., 19 (6) 837

Complete Catalogue (ed.) Ekers, J.A. (1969) - Aust.J.Phys., Astrophys. Suppl. No. 7, 1

Pauliny-Toth, I.I.K. and Kellermann, K.I. (1968) - Astrophys.J. (letters), 152, L169

Pauliny-Toth, I.I.K. and Shakeshaft, J.R. (1962) - Mon.Not.R. astr.Soc., 124 61

Quigley, M.J.S. and Haslam, C.G.T. (1965) - Nature, 208, 741

Radhakrishnan, V. and Murray, J.D. (1969) - Proc.Astr.Soc.Aust., 1, 215

Razin, V.A. (1960) - Radiofizika, 3, 584

Read, R.B. (1963) - Trans.Inst.Rad.Engrs. AP-9, 31

Reber, G. (1968) - Journal of the Franklin Inst., 285,(1),1

Rees, M.J. (1967) - Mon.Not.R.astr.Soc., 137, 429

Rees, M.J. and Simon, M. (1968) - Astrophys. J., 152, (3PT2), L145

Rougoor, G.W. (1966) - Astrophys. J., 144, (2), 852

Rodgers, A.W., Campbell, C.T., Whiteoak, J.B., Bailey, H.H. and Hunt, V.O. (1960) - "An Atlas of Hα emission in the Southern Milky Way", Australian National Univ., Canberra.

Ryle, M. (1963) - Comm. V, XIV General Assembly of the U.R.S.I., Tokyo

Ryle, M. and Longair, M.S. (1967) - Mon.Not.R.astr.Soc., 136,123

Sandage, A. (1961) - Astrophys. J., 133, (2), 355

Scheuer, P.A.G. (1965) - Quasi-Stellar Sources and Gravitational Collapse, Chicago

Scheuer, P.A.G. and Williams, P.J.S. (1968) - Ann.Rev.Astron. Astrophys., 6, 321

Seaquist, E.R. (1968) - Observatory, 88, 269

Seeger, Ch.L., Westerhout, G., Conway, R.G. and Hoekema, T. (1965) - Bull.Astron.Inst. Neth., 18 (1), 11

Shain, C.A., Komesaroff, M.M. and Higgins, C.S. (1961) - Aust.J. Phys., 14, 508

Shakeshaft, J.R. (1967) - Draft Report I.A.U., 13 th. General Assembly, (Prague), Commission 40, p.886

Shimmins, A.J., Clarke, M.E. and Ekers, R.D. (1966) - Aust.J. Phys., 19, 649

Shimmins, A.J. and Day, G.A. (1968) - Aust.J.Phys., 21,(3),377

Shimmins, A.J., Manchester, R.N. and Harris, B.J. (1969) - Aust.J.Phys. Astrophys.Suppl.No. 8, 3

Shklovskii, I.S. (1960) - Cosmic Radio Waves, Cambridge (Mass.)

Shklovskii, I.S. (1960a) - Soviet Astron., (AJ), 4, 243

Shklovskii, I.S. (1965) - Nature, 206, 176

Slish, V.I. (1963) - Nature, 199, 682

Syrovatskii, S.I. (1959) - Soviet Astron., 3, 22

Terrell, J. (1967) - Astrophys. J., 147, 827

Tsytovich, V.N. (1951) - Vestn.Mosk.gos.un-ta, 11, 27

Turtle, A.J. and Baldwin, J.E. (1962) - Mon.Not.R.astr.Soc., 124, 459

Twiss, R.Q. (1954) - Phil.Mag., 45, 249

Van der Laan, H. (1963) - Mon.Not.R.astr.Soc., 126, 519

Van der Laan, H. (1966) - Z.Astrophys., 64(1), 16

Westfold, K.C. (1959) - Astrophys. J., 130, 241

Wielebinski, R., Smith, D.J. and Cárdenas, X.G. (1968) - Aust.J.Phys., 21, 185

Wild, J.P., Smerd, S.F., and Weiss, A.A. (1963) - Ann.Rev. Astron.Astrophys., 1, 291

Williams, P.J.S. (1963) - Nature, 200, 56

Williams, P.J.S. (1966) - Nature, 210, (5033), 285

Williams, P.J.S., Kenderdine, S. and Baldwin, J.E. (1966) - Mem.Roy.Astron.Soc., 70 (3), 53

Wills, D., and Bolton, J.G. (1969) - Aust.J.Phys., 22, 775

Yates, K.W. (1968) - Aust.J.Phys., 21, 167

Yates, K.W., Wielebinski, R. and Landecker, T.L. (1967) - Aust.J.Phys., 20, 597

Zheleznyakov, V.V. (1967 a) - Soviet Astron.(AJ), 11, (1), 33

Zheleznyakov, V.V. (1967 b) - Soviet Phys.(JETP), 24(2), 381